SARS-CoV-2 replication and antiviral responses in bat cells

Sophie-Marie Aicher

Université Paris Cité

École doctorale Bio Sorbonne Paris Cité (BioSPC) - ED 562

Institut Pasteur

Laboratoire Virologie - UMR 3569
Équipe Signalisation antivirale

SARS-CoV-2 replication and antiviral responses in bat cells

Par Sophie-Marie AICHER

Thèse de doctorat d'Infectiologie

Dirigée par Dr. Nolwenn Jouvenet

Présentée et soutenue publiquement le 6 Décembre 2022

Devant un jury composé de :

Nolwenn Jouvenet, DR	Institut Pasteur, Université Paris Cité	Directrice de thèse
Sylvie van der Werf, PU	Institut Pasteur, Université Paris Cité	Examinatrice
Lucie Etienne, CR-HDR	Ecole Normale Supérieure de Lyon	Rapportrice
Jonathan Luke Heeney, PU	University of Cambridge	Rapporteur
Jean-Claude Manuguerra, DR	Institut Pasteur, Université Paris Cité	Examinateur
Meriadeg Le Gouil, CR-HDR	Université de Normandie	Examinateur
Arinjay Banerjee, Professeur associé	University of Saskatchewan	Invité

Résumé - Réplication du SARS-CoV-2 et réponses antivirales dans les cellules de chauve-souris

Les chauves-souris sont des réservoirs naturels pour de nombreux virus zoonotiques émergents, dont l'ancêtre potentiel du SARS-CoV-2. Plusieurs caractéristiques du système immunitaire des chauves-souris facilitant les réponses antivirales et permettant une grande tolérance immunitaire pourraient contribuent à leur capacité à héberger des virus sans développer de maladies. L'acquisition de nouvelles connaissances concernant les interactions moléculaires entre les virus et les cellules de chauve-souris sont cependant limitées par le manque d'outils spécifiques. Il est donc nécessaire de développer des modèles cellulaires de chauve-souris pour comprendre le tropisme cellulaire, la réplication virale et les réponses cellulaires induites par le virus.

J'ai étudié la capacité de cellules primaires isolées d'espèces de *Rhinolophus* et de *Myotis,* ainsi que celle de lignées cellulaires établies et nouvelles de *Myotis myotis, Eptesicus serotinus, Tadarida brasiliensis* et *Nyctalus noctula*, à permettre la réplication du SARS-CoV-2. Aucune de ces cellules n'était permissive à l'infection, pas même celles exprimant des niveaux détectables de l'enzyme de conversion de l'angiotensine 2 (ACE2), qui sert de récepteur viral chez de nombreuses espèces de mammifères, y compris les humains. L'expression de l'ACE2 humain (hACE2) dans trois lignées cellulaires de chauves-souris a permis la réplication du virus, suggérant que la restriction à la réplication virale était due à une faible expression d'ACE2 endogène (bACE2) ou à l'absence de liaison entre l'enveloppe virale et bACE2 dans ces cellules. En revanche, de multiples restrictions à la réplication virale existent dans les trois lignées cellulaires de *N. noctula* puisque l'expression de hACE2 n'a pas permis l'infection. Des virions infectieux ont été produits mais non libérés par les cellules cérébrales de *M. myotis* exprimant hACE2. Les cellules cérébrales *d'E. serotinus* et les cellules épithéliales nasales de *M. myotis* exprimant hACE2 contrôlaient efficacement la réplication virale, ce qui corrélait avec l'induction d'une réponse à l'interféron. Ces données suggèrent l'existence de barrières moléculaires capables de bloquer la réplication du SRAS-CoV-2 et spécifiques à certaines espèces de chauve-souris. Les modèles cellulaires de chiroptères que nous avons développés seront utiles pour étudier l'interaction entre les virus apparentés à SRAS-CoV-2 et leur réservoir naturel, y compris l'identification des facteurs responsables de la restriction virale.

J'ai également réalisé une étude transcriptomique comparative de plusieurs lignées cellulaires de chauve-souris appartenant aux espèces *Myotis myotis, Rhinolophus ferrumequinum, Eptesicus fuscus, Eptesicus serotinus, Eidolon helvum* et *Nyctalus noctula*. Une lignée cellulaire humaine a été incluse dans l'analyse à titre de comparaison. Toutes les cellules ont été stimulées avec des ARN double brin synthétiques pour activer les voies immunitaires innées. Les données de séquençage ont identifié des centaines de gènes dont l'expression est modifiée par la présence d'ARNdb dans chaque lignée cellulaire. Un groupe de 83 gènes communs à toutes les lignées cellulaires de chauves-souris a pu être identifié ainsi que des gènes spécifiques à une famille ou une espèce de chauves-souris données. Parmi les 83 gènes communs identifiés, quelques-uns n'avaient pas encore été associés à la réponse antivirale. Ces gènes représentent des cibles prometteuses pour caractériser la réponse immunitaire innée chez les chauves-souris.

L'ensemble de mon travail a permis de mieux comprendre les interactions entre un virus zoonotique émergent et des cellules dérivées de chauves-souris, qui sont d'importants réservoirs animaux. Mon travail ouvre également de nouvelles voies de recherche pour caractériser les mécanismes moléculaires qui permettent aux cellules de chauve-souris de contrôler la réplication virale.

Mots clefs : SARS-COV-2, chauves-souris, immunité inné, espéces réservoirs, zoonos**es.**

Abstract - SARS-CoV-2 replication and antiviral responses in bat cells

Bats are natural reservoirs for numerous emerging zoonotic viruses, including the potential ancestor of SARS-CoV-2. Several immune features that facilitate antiviral responses and immune tolerance towards viral infections are believed to contribute to the ability of bats to harbor viruses without pathogenesis. Investigating the molecular interaction between viruses and bat cells is limited by the lack of bat-specific tools. There is thus a need to develop bat cellular models to understand cell tropism, viral replication and virus-induced cell responses.

First, I investigated the ability of primary cells from *Rhinolophus* and *Myotis* species, as well as of established and novel cell lines from *Myotis myotis*, *Eptesicus serotinus*, *Tadarida brasiliensis* and *Nyctalus noctula*, to support SARS-CoV-2 replication. None of these cells were permissive to infection, not even the ones expressing detectable levels of angiotensin-converting enzyme 2 (ACE2), which serves as the viral receptor in many mammalian species including humans. The resistance to infection was overcome by expression of human ACE2 (hACE2) in three cell lines, suggesting that the restriction to viral replication was due to a low expression of bat ACE2 (bACE2) or absence of bACE2 binding in these cells. By contrast, multiple restrictions to viral replication exist in the three *N. noctula* cell lines since hACE2 expression was not sufficient to permit infection. Infectious virions were produced but not released from hACE2-transduced *M. myotis* brain cells. *E. serotinus* brain cells and *M. myotis* nasal epithelial cells expressing hACE2 efficiently controlled viral replication, which correlated with a potent interferon response. These data highlight the existence of species-specific molecular barriers to SARS-CoV-2 replication in bat cells. Our newly developed chiropteran cellular models are useful tools to investigate the interplay between viruses belonging to the SARS-CoV-2 lineage and their natural reservoir, including the identification of factors responsible for viral restriction.

As follow-up studies, I performed a comparative RNA-Seq transcriptomic study in several bat cell lines belonging to the species *Myotis myotis, Rhinolophus ferrumequinum, Eptesicus fuscus, Eptesicus serotinus, Eidolon helvum* and *Nyctalus noctula*. A human cell line was included in the analysis for comparison. All cells were stimulated with synthetic dsRNAs to activate innate immune pathways. Hundreds of differentially expressed genes (DEGs) were identified in each cell line. All bat cell lines shared a core set of 83 common DEGs. Multiple bat family- and species-specific DEGs were also identified. Several of the common bat DEGs were not previously reported as innate immune genes. The newly identified genes represent promising targets to decipher bat-specific immune mechanisms and are potential potent antiviral effectors.

Together, these studies investigated the molecular interplay between an emerging zoonotic virus and cells derived from bats, which represent important animal reservoirs. This work reveals the diversity of innate immune mechanisms in place in bat cells and opens up new lines of research to characterize the molecular mechanisms by which bat cells control viral replication.

Keywords : SARS-CoV-2, bats, innate immunity, zoonosis, reservoir species.

Résumé substantiel

Les virus émergents constituent une menace pour la santé publique du fait des pathologies graves qu'ils provoquent généralement chez l'homme. Le passage d'un virus d'une espèce à une autre est appelé franchissement de la barrière d'espèces. Le terme de zoonose désigne la transmission d'un virus circulant chez une espèce animale vertébrée à l'homme. Plusieurs conditions doivent être réunies pour rendre possible le franchissement de barrière d'espèces, parmi lesquelles l'excrétion virale par le premier hôte infecté, la persistance virale dans l'environnement, ainsi que la susceptibilité de l'hôte receveur. Bien que la réunion de toutes ces conditions soit rare, la fréquence des émergences virales au cours des dernières années a dramatiquement augmenté du fait du réchauffement climatique, de l'augmentation des déplacements humains à l'échelle internationale, de la déforestation accrue et de l'exploitation intensive de terres sauvages. Ces phénomènes de franchissement de barrière d'espèces ont lieu en particulier dans des régions ou des populations humaines à forte densité vivent à proximité d'une grande diversité d'espèces animales. Les retards de détection ou de réponse aux virus émergents dans notre monde interconnecté peuvent entraîner une surmortalité généralisée et de vastes dommages économiques, comme l'illustre l'actuelle pandémie de COVID-19. Au cours des deux dernières décennies, plusieurs virus émergents ont eu un impact dévastateur sur la santé publique, comme le virus Zika (ZIKV) transmis par les moustiques, le virus Lassa (LASV) qui circule chez les rongeurs ou encore les virus Ebola (EBOV) et Marburg (MARV), qui ont pour origine les chauves-souris. Les coronavirus, tels que le coronavirus du syndrome respiratoire du Moyen-Orient (MERS-CoV), le coronavirus du syndrome respiratoire aigu sévère (SARS-CoV) et le coronavirus du syndrome respiratoire aigu sévère 2 (SARS-CoV-2) viennent s'ajouter à cette liste d'émergences récentes.

Pour s'établir de façon durable dans un réservoir, un virus doit nécessairement infecter et persister dans son hôte sans provoquer de symptômes sévères. On définit une espèce animale réservoir comme une population épidémiologiquement connectée dans laquelle le pathogène peut se maintenir et à partir de laquelle il peut être transmis à des populations secondaires. Plus de 10000 virus à potentiel zoonotique circulent chez les mammifères. Ils infectent en moyenne quatre espèces chacun, principalement des chauves-souris, des rongeurs, des primates et des ongulés. Les chauves-souris ont été identifiées comme étant les mammifères abritant la majorité des virus à potentiel zoonotique par rapport aux autres espèces de mammifères. Au regard des changements climatiques drastiques qui s'annoncent, les chauves-souris faciliteront probablement davantage d'émergences virales en raison de leur capacité de dispersion. Les chauves-souris présentent plusieurs traits biologiques uniques, notamment une longévité au-dessus de la moyenne pour des animaux de petite taille, un métabolisme altéré, des capacités de vol et d'écholocalisation, une faible susceptibilité aux tumeurs, un système efficace de réparation de l'ADN et une réponse accrue au stress oxydatif. Elles présentent également des caractéristiques immunitaires uniques qui les distinguent des autres mammifères.

Au sein du règne des mammifères, seuls les rongeurs sont plus nombreux que les chauves-souris, avec plus de 1300 espèces identifiées chez ces dernières. Cette vaste diversité d'espèces est cependant la plupart du temps sous-estimée et les découvertes applicables à une espèce sont trop souvent généralisées. En effet, la littérature fait régulièrement référence à des caractéristiques « spécifiques aux chauves-souris » alors que d'importantes différences peuvent être observées au sein d'une même famille de chauves-souris. Si certains mécanismes de défense antivirale peuvent être extrapolés à l'ensemble de l'ordre

des chiroptères, certaines stratégies promouvant les infections virales semblent être spécifiques à certaines espèces.

Lorsqu'un virus infecte un nouvel hôte, le système immunitaire inné constitue la première ligne de défense de l'hôte. La réponse immunitaire innée est immédiate, efficace et hautement conservée parmi les espèces. Cependant, une réponse immunitaire excessive peut conduire à une inflammation systémique pathologique chez l'homme suite à une infection virale. Une réponse antivirale efficace couplée à une tolérance accrue aux infections et à des processus inflammatoires atténués pourrait expliquer la capacité des chauves-souris à héberger de manière asymptomatique des virus qui sont pathogènes chez d'autres espèces de mammifères. Depuis l'identification de la rage, un virus du genre Lyssavirus, chez une chauve-souris vampire asymptomatique en 1911, les chauves-souris ont été associées à une multitude de virus émergents. Des milliers d'espèces virales associées aux chauves-souris ont été découvertes. Ces virus sont regoupés dans 28 familles virales, avec une forte proportion de coronavirus, de paramyxovirus et de rhabdovirus.

Les coronavirus ont un fort potentiel de franchissement de barrière d'espèces du fait de deux caractéristiques spécifiques. D'une part, au cours de la réplication, leur polymérase utilise un mécanisme unique de changement de matrice qui peut être à l'origine d'évènements de recombinaison, donnant ainsi naissance à de nouvelles espèces virales. D'autre part, leur génome est le plus grand de tous les virus à ARN, permettant une grande plasticité pour l'établissement de nouvelles mutations. Avant 2019, six coronavirus humains étaient connus, tous d'origine zoonotique : SARS-CoV, MERS-CoV, HCoV-NL63 et HCoV-229E sont dérivés de virus de chauves-souris, tandis que HCoV-OC43 et HKU proviennent probablement de virus de rongeurs. Les chauves-souris sont également très probablement le réservoir naturel du SARS-CoV-2 qui a emergé en décembre 2019 à Wuhan, en Chine. Un virus étroitement apparenté, le virus BANAL-20-52, qui présente une similitude de séquence nucléotidique de 96,8% avec le SARS-CoV-2, a été prélevé sur un écouvillon anal de chauves-souris *Rhinolophus malayanus* dans le district de Feuang de la province de Vientiane au Laos en 2020. En outre, plusieurs autres virus de chauve-souris étroitement apparentés à SARS-CoV-2 ont été identifiés chez des chauves-souris *Rhinolophus* dans plusieurs pays d'Asie du Sud-Est.

Compte-tenu de la relation entre les chauves-souris et les virus à potentiel zoonotique, il est essentiel de mieux comprendre les mécanismes de réplication virale chez ces espèces réservoirs. Cependant, les interactions entre les virus émergents, en particulier les coronavirus, et les cellules de chauves-souris sont encore mal décrites. Cela s'explique en partie par le nombre limité de modèles cellulaires et d'outils moléculaires disponibles pour étudier ces espèces. Il est donc nécessaire de développer de nouveaux modèles *in vitro* pour caractériser le tropisme cellulaire, la réplication virale et les réponses cellulaires induites par les virus chez les chiroptères. Au regard de la pandémie de SARS-CoV-2 et de son émergence suspectée à partir du réservoir naturel que constituent les chauves-souris, il apparait crucial d'établir des modèles d'infection de ces espèces hôtes. Ainsi, l'objectif général de ma thèse de doctorat était d'étudier la susceptibilité et la réponse immunitaire innée aux virus émergents dans de nouveaux modèles cellulaires de chauves-souris, en mettant l'accent sur le SARS-CoV-2.

Seule une poignée de modèles cellulaires sont disponibles pour étudier la réplication des bétacoronavirus dans les cellules de chauve-souris. La réplication virale du SARS-CoV-2 a été décrite dans les cellules pulmonaires et cérébrales de *Rhinolophus sinicus*, ainsi que

dans les cellules rénales de *Pipistrellus abramus*. Cependant, les titres viraux obtenus étaient très faibles. En revanche, le virus se réplique efficacement dans les organoïdes intestinaux de *R. sinicus*, confirmant la capacité des cellules de cette espèce à permettre la réplication virale. L'inoculation intranasale du SARS-CoV-2 chez *Rousettus aegypticus* a entraîné une infection transitoire de leurs voies respiratoires et une excrétion orale du virus, indiquant que les chauves-souris non-apparentées au genre *Rhinolophus* peuvent être infectées de manière productive par le virus. Cependant, l'élevage et la manipulation de chauve-souris, ainsi que la génération d'organoïdes dérivés de cellules de chauve-souris, sont fastidieux et peu accessibles. Il est donc nécessaire de développer des lignées cellulaires à partir de divers organes et espèces pour mieux comprendre la co-évolution du virus et des chauves-souris.

Ainsi, j'ai développé de nouveaux modèles cellulaires dérivés d'espèces de chauves-souris peu étudiées et circulant en Europe et en Asie. Nous avons étudié la capacité du SARS-CoV-2 à se répliquer dans des cellules primaires que nous avons générées à partir de biopsies d'espèces de *Rhinolophus* et de *Myotis*, ainsi que dans des lignées cellulaires établies et nouvelles de *Myotis myotis, Eptesicus serotinus, Tadarida brasiliensis* et *Nyctalus noctula*. Des techniques variées de virologie, de biologie moléculaire, de cytométrie, de microscopie optique et électronique ont mis en évidence une susceptibilité et une permissivité variables de ces cellules à l'infection par le SARS-CoV-2. Ces expériences ont également permis de découvrir des mécanismes de restriction virale spécifiques à certaines espèces et à certains types cellulaires de chauve-souris. Ces nouveaux modèles cellulaires de chiroptères sont des outils précieux pour étudier les interactions moléculaires entre les cellules de chauve-souris et les virus. Cette première partie de ma thèse a été publiée dans 'Journal of Virology' en juillet 2022.

Dans une seconde partie, je me suis concentrée sur les réponses immunitaires innées des chauves-souris en tant qu'espèces réservoirs. Pour établir avec succès une infection dans un nouvel hôte, un virus doit contourner ou contrer la réponse immunitaire innée. Même si cette réponse est très largement conservée parmi les espèces de vertébrés, de plus en plus de données suggèrent que les espèces réservoirs pourraient présenter des caractéristiques immunitaires particulières. De ce fait, répertorier les effecteurs de la réponse immunitaire innée des chauves-souris permettrait de mieux caractériser leur capacité à maintenir une infection virale. Nous avons émis l'hypothèse que certains gènes immunitaires non-caractérisés des chauves-souris, spécifiques à l'espèce et à la lignée, pourraient avoir des fonctions antivirales et ainsi contribuer à la capacité de ces animaux à contrôler les infections virales. Dans cette optique, j'ai utilisé une approche transcriptomique comparative pour répertorier les gènes de l'immunité innée de sept lignées cellulaires de chauves-souris réprésentant un large spectre d'espèces de l'ordre des chiroptères (*Eptesicus fuscus, Eptesicus serotinus, Eidolon helvum, Myotis myotis, Nyctalus noctula, Rhinolophus alcyone et Rhinolophus ferrumequinum*). Mon travail représente la première étude comparative de transcriptomes immunitaires innés d'espèces de chauves-souris non-apparentées. L'analyse transcriptionnelle de ces cellules stimulées par un ARN double brin synthétique bien caractérisé pour induire une réponse immunitaire innée a révélé des centaines de gènes exprimés différentiellement ('DEG' pour 'Differentially Expressed Genes' en anglais) dans chacune des lignées cellulaires, y compris des DEG spécifiques à la famille et à l'espèce, ainsi qu'un ensemble de 83 DEG communs. Plusieurs des DEG que nous avons identifiés n'étaient pas décrit comme des gènes de l'immunité innée chez d'autres espèces de vertébrés et pourraient ainsi représenter des gènes immunitaires spécifiques des chauves-souris. Nous allons poursuivre ces travaux par des études

fonctionnelles visant à caractériser la fonction de certains de ses gènes pendant l'infection par des flavivirus et coronavirus de chauve-souris.

En conclusion, nous avons généré et caractérisé de nouveaux modèles cellulaires de chauves-souris. Mes travaux ont fourni de nouvelles connaissances sur les interactions entre le SARS-CoV-2 et les cellules de chauves-souris ainsi que sur la réponse immunitaire innée de ces importants réservoirs viraux. De plus, cette étude pourrait permettre l'identification et la caractérisation de gènes antiviraux exprimés chez les chauves-souris et jusque-là non-caractérisés. Ces résultats apporteraient des éléments clés pour comprendre pourquoi les chauves-souris sont des réservoirs viraux uniques.

Acknowledgements

First and foremost, I would like to dedicate a special thank you to my supervisor, Dr. Nolwenn Jouvenet, for her invaluable support of my research for the past three years. I am extremely grateful for the opportunity to join such an amazing team! Nolwenn, thank you for the possibility and freedom to develop my own experimental ideas, for your catching enthusiasm about results and your way of putting them immediately into a bigger picture!

Secondly, I would like to thank the present and former members of the Virus Sensing and Signaling Unit. I would not be at this point today without the helping hands, support, encouragement, laughter, head shaking, eyebrow raising and cheering of my lab. Sego, Max, Vince, Felix, Flo, Elodie and Anvita, doing science without you in future will be very different! Sego, you are the sparkly, little unicorn that did not just make my French skills but literally the entire lab life brighter. Thank you for organizing my chaos, for always being there and for not just being a super colleague but an even better friend! Flo, thank you for taking me under your wing at the beginning and for making countless evening sessions in the P2+ more fun! I shall always hold your timer in honor! Elo, thanks for translating everything for me and making me feel welcome when I joined the lab, thanks for going through the highs and lows of lab life together and for your constant support and encouragement! Felix, thank you for all the helpful discussion between PhD fellows, for sharing worries, ideas, concerns and celebrate the little stage victories. Max, thanks for teaching me a ton of things and for always finding a solution to any problem, no matter if it is finding a misplaced order, fixing a questionable protocol, knowing what went wrong at which step or asking the right questions when coming up with new ideas for experiments. The lab ship with me on board would totally sink without you! Anvi, thanks for sharing your advice and wisdom on “how to phd”, for keeping the cool and calmly evaluating crisis situations and being an awesome lab mama. Vince, thank you for always having an open ear and a smile on your face, for helping with any kind of troubles and for wearing the coolest T-Shirts ever! Even though I can’t wait to stop having “lunch” at 11.30 am, I will miss all of you a lot!

I would also like to thank the members of my jury, Prof. Sylvie van der Werf, Prof. Jean-Claude Manuguerra, Dr. Meriadeg Le Gouil, Dr Arinjay Banerjee and especially the reviewers, Dr. Lucie Etienne and Prof. Jonathan Luke Heeney for their time and commitment to evaluate my manuscript. I thank the members of my thesis advisory committee, Dr. Sylvie Lecollinet, Dr. Aaron Irving and Dr. Marcel Müller for their support, guidance, help and new ideas when discussing the progress of my thesis projects.

To my tutors, Dr. Valérie Caro and Dr. Timothée Bruel, thank you for being available at any time for questions and advice, for your time and encouragement, your kindness and guidance in more difficult times.

Thank you to the Institut Pasteur Community and the PPU doctoral program for three unforgettable PhD years!

For the study presented in Chapter II, I would like to thank Noémie Aurine (SBRI, U1208 INSERM, France) for her help designing RT-qPCR primers for bat samples; Ondine Filippi-Codaccioni and Marc López-Roig (Université Lyon 1, France) for their precious help in bat sampling; the French National Reference Centre for Respiratory Viruses hosted by Institut Pasteur Paris and headed by Prof. Sylvie van der Werf for providing the

historical viral strains; Hugo Mouquet and Cyril Planchais for providing anti-S antibodies; Françoise Porrot for lentiviral production; Florence Guivel-Benhassine for help in titration assays and Matthias Lenk (Friedrich-Loeffler-Institut, Germany) for providing the *Eptesicus serotinus* and *Tadarida brasiliensis* cell lines.

For the study presented in Chapter III, I would like to thank Juliana Pipoli da Fonseca and Etienne Kornobis for their help with preforming the RNA sequencing, analyzing and representing the data. I thank Dr. Marcel Müller (Charité – Universitätsmedizin Berlin, Germany) for providing us with *Rhinolophus* and *Eidolon* cell lines, for many constructive discussions and invaluable insights about experimental design. I would like to thank Niklas Endres and Ivan Nombela Diaz (Charité – Universitätsmedizin Berlin, Germany) for their help with data processing, analysis and graphic representation.

I am always grateful to Prof. François Jean, Dr. Christopher Netherton and Dr. Wayne Mitchell for being the mentors that inspired and guided my academic path from the first time I pipetted a virus dilution until now. Everything you taught me and your believe in me was fundamental for the completion of this work.

Finally, a huge thank you to goes out to my family and friends. Mum, dad, Korbi and Bene without your constant and unshakable love, support and encouragement over the years, I would have never come this far. You are my anchors in difficult times and fallback level I know I can always count on, thank you from the bottom of my heart! Chiara and Mariana, you went with me through all the ups and downs the PhD brought and made life in Paris truly special. I know I did not just find friends in you but family. K and Anna, you are my partners in crime, my go-to-persons for all worries. We complain, cry and scream but also laugh until we snort, cheer and celebrate all successes together. I am forever grateful to have met you during our Masters! Ella, Maggi, Flo, Toni and Lisa, I know you since forever and even though science keeps me busy, I know you are always there, ready to catch up right where we left off. Thank you for all these years of friendship! Joey, you had no idea what you got into when you met me just before writing up, but you stood by my side patiently. Thank you for the love and support!

This work is dedicated to all of you.

Table of Contents

Abbreviations

AA: Amino acid
AB: Antibody
ACE2: Angiotensin-converting enzyme 2
ACP3: Acid phosphatase 3
ADAR1: Adenosine deaminase acting on RNA 1
AIM2: Absent in melanoma 2
ALR: AIM2 like receptor
AOX1: Aldehyde oxidase 1
AP1: Activator protein 1
APAF1: Apoptotic peptidase activating factor 1
APOBEC3G: Apolipoprotein B mRNA editing enzyme, catalytic subunit 3G
ASO: Antisense RNA oligonucleotide
ATM: Ataxia Telangiectasia mutated
ATP: Adenosine triphosphate
bACE2: bat ACE2
bp: base pair
BRCA1/2: Breast cancer type 1/2 susceptibility protein
BST2: Bone marrow stromal cell antigen 2
CARD: Caspase activation and recruitment domains
Cas9: CRISPR-associated protein 9
CASP2: Caspase 2
CCHFV: Crimean-Congo hemorrhagic fever virus
cDC: conventional DC
cDNA: complementary DNA
cGAMP: 2'3' cyclic GMP-AMP
cGAS: cyclic GMP-AMP synthase
CH25H: Cholesterol 25-hydroxylase
CHAC1: ChaC glutathione specific gamma-glutamylcyclotransferase 1
CHIKV: Chikungunya virus
CLR: C-type lectin receptor
CM: Convoluted membranes
CoV: Coronavirus
CPE: Cytopathic effect
CREB: cAMP response element-binding protein
CRISPR: Clustered regularly interspaced short palindromic repeats
CSF: Colony-stimulating factor
CTD: C-terminal domain
CTSL: Cathepsin L
DAMP: Danger-associated molecular pattern
DAZAP2: DAZ Associated Protein 2
DBD: DNA-binding domain
DC: Dendritic cell
DDPP: Departmental Direction of Population Protection
DDX: DEAD-box helicase
DEG: Differentially expressed gene
DENV: Dengue virus
DF: Dengue Fever
DHX: DExH-Box Helicase
DMEM: Dulbecco's Modified Eagle Medium
DMS: Double-membrane spherules
DMV: Double-membrane vesicles
DNA: Deoxyribonucleic acid
DPP4: Dipeptidyl peptidase-4
E: Envelope protein
EBOV: ebola virus
EBP: Emopamil binding protein
EBV: Epstein–Barr virus
eIF2a: Eukaryotic translation initiation factor 2 subunit alpha
ELISA: Enzyme-linked immunosorbent assay
EMC2: ER Membrane Protein Complex Subunit 2
EMCV: Encephalomyocarditis virus
ENDOV: Endonuclease V
ENTV: Entebbe bat virus
ER: Endoplasmic reticulum
ERGIC: ER-Golgi intermediate compartment
ESIP1: Epithelial-stromal interaction protein 1
EVA: European virus archive
EVD: Ebola virus disease
FBS: Fetal bovine serum
FDR: False discovery rate
FILIP1: Filamin A interacting protein 1
FMO2: Flavin containing dimethylaniline monoxygenase 2
FOXS1: Forkhead box S1
GAF: Gamma-activated factor
GAPDH: Glyceraldehyde-3-phosphate dehydrogenase
GAS: Aamma-activation sequence
GFP: Green fluorescent protein
GP2: Glycoprotein 2
gRNA: genomic RNA

hACE2: human ACE2
HBV: Hepatitis B virus
HCoV: Human coronavirus
HCV: Hepatitis C virus
HDV: Hepatitis D virus
HEK: Human embryonic kidney
HeV: Hendra virus
HIV: Human immunodeficiency virus
HLA: Human leukocyte antigen
HMOX1: Heme oxygenase 1
hpi: Hours post infection
HS: Herpes simplex virus
HSP: Heat shock protein
HSV: Herpes simplex virus
IAV: Influenza A virus
IBV: Influenza B virus
ICAM4: Intercellular adhesion molecule 4
ICTV: International committee on taxonomy of viruses
IFI16: IFNg-inducible protein 16
IFITM: Interferon-induced transmembrane
IFN-I/II/III: Type I/II/III IFN
IFN: Interferon
IFNAR1/2: IFN-a receptor 1 and 2
IFNGR: IFN-g receptor
IFNLR: IFN-l receptor
IKK a/b/ε: IκB kinase a/b/ε
IL: Interleukin
IMDM: Iscove's modified dulbecco's medium
INAVA: Innate immunity activator
iPSC: Induced pluripotent stem cell
IRAK: IL-1R-associated kinases
IRES: Interferon-sensitive response element
IRF: Interferon regulatory factor
ISG: Interferon-stimulated gene
ISGF3: ISG factor 3
JAK: Janus kinase
JEV: Japanese encephalitis virus
KIR: Killer-cell immunoglobulin like receptor
KLR: Killer cell lectin-like receptor
KO: Knockout
LASV: Lassa virus
LCN2: Lipocalin 2
LF: Lassa fever
LMW: Low molecular weight
LPG2: Laboratory of genetics and physiology 2
LRR: Leucine-rich repeat
LY6E: Lymphocyte antigen 6 family member E
M: Membrane protein
MAPK: Mitogen-activated protein kinase
MARV: Marburg virus
MAVS: Mitochondrial antiviral-signaling protein
MCOLN2: Mucolipin-2
MDA5: Melanoma differentiation association gene 5
MDM2: Mouse double minute 2 homolog
MERS-CoV: Middle East respiratory syndrome coronavirus
MERS: Middle East respiratory syndrome
MHC: Major Histocompatibility Complex
MHCX1: MHC class I heavy chain
miRNA: microRNA
MOI: Multiplicity of infection
MORC3: MORC Family CW-Type zinc finger 3
MPXV: Monkeypox virus
mRNA: messenger RNA
MTHFD1: Methylenetetrahydrofolate dehydrogenase 1
MuV: Mumps virus
MVD: Marburg virus disease
MX: Myxoma resistance protein
MyD88: Myeloid differentiation primary response protein 88
N: Nucleocapsid protein
NA: Nucleic acid
NDV: Newcastle disease virus
NEMO: NFkB essential regulator
NEURL: Neuralized E3 Ubiquitin Protein Ligase
NFkB: Nuclear factor kappa B
NHP: Non-human primates
NIK: NFkB-inducing kinase
NiV: Nipah virus
NK: Natural killer cell
NLR: NOD-like receptor
NLRP3: NLR family pyrin domain containing 3
NO: Nitric oxide
NOD: Nucleotide-binding oligomerization domain
NS: Non-structural
nsp: Non-structural protein

NT: Nucleotide
OAS: 2'-5'-oligoadenylate synthetase
OASL: OAS-like protein
ONNV: O'nyong nyong virus
Orf: Open reading frame
OTOGL: Otogelin Like
OXPHOS: Oxidative phosphorylation
P/S: Penicillin/streptomycin
PACT: PKR-activating protein
PALM2: Paralemmin 2
PAMP: Pathogen-associated molecular pattern
PARP10: Poly(ADP-Ribose) Polymerase Family Member 10
PBS: Phosphate buffered saline
PCA: Principal component analysis
pCD: plasmacytoid DC
PDCovV: Porcine deltacoronavirus
PDE: Phosphodiesterase
PEDV: Porcine epidemic diarrhea virus
PEL: Primary effusion lymphoma
PFA: Paraformaldehyde
PFU: Plaque-forming units
PHEIC: Public health emergency of international concern
PKR: Protein kinase K
PLA1A: Phospholipase A1 member A
PM: Plasma membrane
Poly I:C: Polyinosinic:polycytidylic acid, dsRNA ligand
PPP1R15A: Protein phosphatase 1 regulatory subunit 15A
PRR: Pattern recognition receptor
PRV: Pteropine orthoreovirus
psg: Pseudogene
PSMA6: Proteasome 20S subunit alpha 6
PulV: Pulau virus
PYHIN: Pyrin and HIN domain-containing protein
RAB19: Ras-related protein 19
RAD50: RAD50 Double Strand Break Repair Protein
RANBP2: RAN binding protein 2
RBD: Receptor bindinding domaine
RdRp: RNA-dependent RNA polymerase
RIG-I: Retinoic acid-inducible gene I
RLR: RIG-I-like helicase
RNA: Ribonucleic acid
RNAi: RNA interference
RNASEL: Ribonuclease L
RNASeq: RNA sequencing
RND1: Rho Family GTPase 1
RNF: Ring finger protein
ROS: Reactive oxygen species
RSAD2: Radical S-adenosyl methionine domain containing 2
RT-qPCR: Reverse transcription quantitative real-time PCR
RT: Room temperature
RTP4: Receptor transporting protein 4
RVFV: Rift Valley fever virus
S: Spike protein
SADS-CoV: Swine acute diarrhea syndrome coronavirus
SAP30: SIN3A associated protein 30
SARS-CoV-1: Severe acute respiratory syndrome coronavirus 1
SARS-CoV-2: Severe acute respiratory syndrome coronavirus 2
SARS: Severe acute respiratory syndrome
SC1r-CoVs: SARS-CoV-1-related-CoV
SC2r-CoV: SARS-CoV-2-related-CoV
SERTAD1: SERTA domain-containing protein 1
SeV: Sendai virus
SFEPM: Société Française pour l'Etude et la Protection des Mammifères
sgRNA: subgenomic RNA
SINV: Sindbis virus
SLC: Solute Carrier Family
SNRNP200: Small nuclear ribonucleoprotein U5 subunit 200
SOCS1: Suppressor of cytokine signaling 1
STAT: Signal transducers and activators of transcription
STING: Stimulator of interferon genes
SUMO2: Small ubiquitin like modifier 2
SUN3: Sad1 and UNC84 domain containing 3
SV40T: Simian Virus 40 large T antigen
TAF: TBP-associated factors

TAF4B: TATA-Box binding protein associated factor 4b
TAOK: thousand and one amino acid kinase
TBK1: TANK-binding kinase 1
TBP: TATA-box binding protein
TCID50: 50% tissue culture infective dose
TEMEM156: Transmembrane protein 156
Th1: T helper cell type 1
THOV: Thogoto virus
TIR: Toll/IL-1 receptor
TiV: Tioman virus
TLR: Toll-like receptor
TMBIM1: Transmembrane BAX inhibitor motif containing 1
TMPRSS2: Transmembrane serine protease 2
TNF: Tumor necrosis factor
TRAF: TNF receptor-associate factor
TRAIL: Tumor necrosis factor-related apoptosis inducing ligand
TRANK1: Tetratricopeptide repeat and ankyrin repeat containing 1
TRIF: TIR-domain-containing adapter-inducing interferon-β
TRIM: Tripartite motif
TRS: Transcription-regulating sequence
TUT7: Terminal uridylyl transferase 7
TYK2: Tyrosine kinase 2
UBA7: Ubiquitin like modifier activating enzyme 7
USP18: Ubiquitin specific peptidase 18
UTR: Untranslated region
UVRAG: UV radiation resistance associated
VACV: Vaccinia virus
VARV: Variola virus
VLP: virus-like particle
VOC: Variant of concern
VSV: Vesicular stomatitis virus
WHO: World health organozation
WNF: West Nile fever
WNV: West Nile virus
WT: Wild type
YF: Yellow Fever
YFV: Yellow Fever virus
ZBP1: Z-DNA binding protein 1
ZIKV: Zika virus

Chapter I – Introduction

1. Emerging Viruses and Zoonosis

1.1 Viral zoonosis and spillover events

Viral emergences can have drastic impact on the health of humans and other animals, including livestock [1]. The jump of a virus from one species to another is called spillover and zoonosis describes the spillover event from a vertebrate animal species to humans. Spillovers are rare since they require the synchronization of several parameters. Viral shedding by the first infected host, environmental conditions of both hosts, viral persistence in environment and recipient host susceptibility are some of the crucial factors [2]. Intrinsic factors of hosts and pathogens combined with extrinsic factors linked to the human-wildlife contacts like urbanization, agriculture and socioeconomic standing, determine risk of viral emergence in the human population [3]. Thus, zoonotic viruses must overcome a series of hindering barriers to successfully establish infection in humans (Figure 1). These barriers can be roughly separated into three categories. The first barrier, called 'pathogen pressure', is dictated by the interaction between the virus and animal host. The distribution and density of the animal host, the virus prevalence in animals, the mode of viral transmission and dissemination, as well as the ability of the virus to survive in the environment, are influencing criteria [4]. The second barrier, called 'exposure', depends on the interaction between the animal host and humans. The behavior of both hosts, especially with a focus on likelihood, route, duration and nature of the exposure, decides the faith of the spillover. If the virus is sufficiently stable in the environment for a certain period, it can be dispersed beyond the primary host distribution via contaminated objects or natural transport like waste water or wind [4]. The migratory behavior of many animals is believed to enhance the global spread of pathogens and subsequent cross-species transmission. For instance, West Nile Virus (WNV) rapidly spread in North America along a major corridor for migrating birds departing from its point of origin in New York City [5]. A link between seasonal migration of fruit bats and human Ebola outbreaks in local villages of the Democratic Republic of Congo also exemplifies the role of migratory behavior of reservoir hosts towards virus dissemination [6]. The final 'within-host barrier' is comprised of the genetic, physical and immunological features of the novel host, human in case of a zoonotic spillover. The virus has to overcome physical barriers, such as skin, mucus or stomach acids, encounter a suitable receptor and evade innate immune defense mechanisms to

establish an efficient replication in humans [4]. Thus, the virus must be transmitted to other humans before the initial host controls infection or dies. This facilitates the evolutionary development of immune-evasion strategies of viruses [7]. The host competence for a given virus is defined as the rate at which an individual is exposed to a virus and transmits a resultant infection to a new host or vector. In brief, host competence = exposure x susceptibility x suitability x transmissibility. This definition applies for the reservoir as well as for the spillover host [8].

In summary, zoonotic viruses need to persist and propagate on multiple levels including cellular, individual and community levels, as well as in the environment [9]. Thus, the probability of successful transmission of a zoonotic virus to humans and the subsequent probability to successfully establishing infection within the human population are very low (Figure 1).

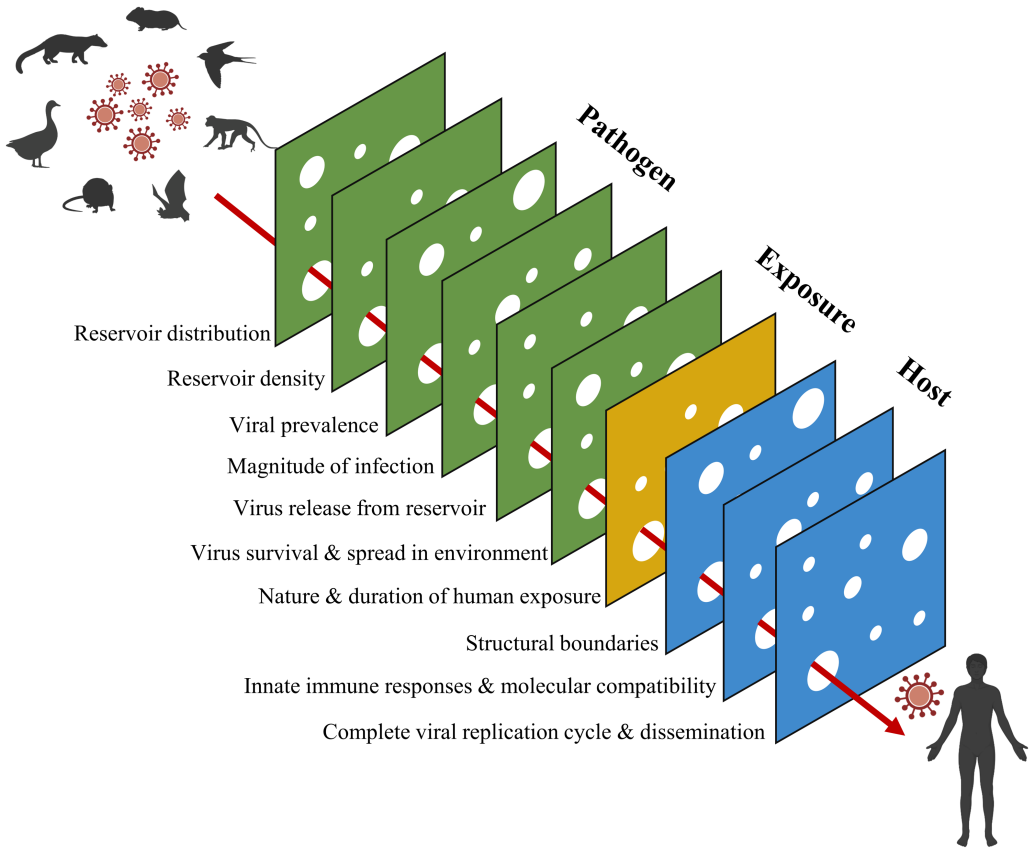

Fig. 1. Swiss Cheese Model representation of barriers for zoonotic virus spillover. Successful zoonosis events require the synchronization of several parameters. A virus must circumvent a multitude of hindering barriers to jump from a reservoir species into a novel host, like humans. The barriers are determined by the virus, the exposure circumstances and the spillover host. Only if all barriers can be overcome by the virus (depicted by alignment of holes in cheese slices), zoonotic spillover is possible (red arrow). Depending on the nature of virus and involved animal species, the window in space and time for correct alignment of all spillover conditions can be very narrow. Figure adapted from [4] and modified with biorender.com.

Some zoonotic viruses do not directly transmit from their reservoir host to humans but require amplification in an intermediate animal host or insect vector (Table 1) [4]. Ideal intermediate or amplifying hosts are animal species that interact closely with both the reservoir hosts and humans, for instance companion animals or domestic livestock, like pigs, horses or dromedary camels. Wild animals raised as exotic food sources, such as civet cats, can also serve as intermediate or amplifying hosts [10]. All zoonotic viruses are non or minimally pathogenic to their reservoir hosts while the human outcome can range from subclinical elimination of the virus to severe disease and death [7]. Viral transmission either ends in humans, which is called 'dead-end spillover infection', or is sustained and allows human-to-human transmission chains [4]. The transmission routes of emerging zoonotic viruses to humans are either foodborne, through consumption of contaminated animals or animal products, or via direct contact with wildlife or domestic animals [11]. The basic reproductive number or expected number of secondary infections caused by one infected individual in a susceptible population is represented as R0 value. Viruses with R0>1 can cause major epidemics through sustained transmission in human populations, whereas viruses with 0<R0<1 trigger self-limiting outbreaks and viruses with R0=0 are not transmitted between humans [4].

1.2 Emerging and re-emerging viruses in the past decades

Zoonoses emerging in human population are a significant threat to global health and security, as well as economic stability. They are steadily increasing in recent years. Detection or response delays to emerging viruses in our interconnected world can result in widespread mortality and vast economic damages, as illustrated by the on-going Coronavirus Disease (COVID-19) pandemic. The risk of zoonotic infectious disease emergence increases in regions with high human population density and extensive animal variety. Due to the high wildlife biodiversity, this risk is particularly heightened in tropical forested regions that are being perturbed by humans. Disruptions of these environments are more likely interlinked with spillover events (Figure 2A) [12]. Whereas most prediction models utilize 'total mammalian species richness' as criteria, the total number and species of zoonotic viruses are not evenly distributed amongst mammals. The geographic area with the highest amount of predicted future zoonotic events thus varies by host taxonomic order. South-east Africa is a predicted hotspot for outbreaks of viruses associated to carnivores and even-toed ungulates, South/Central America and parts of Asia for bat-borne viruses,

tropical regions in Central America, Africa and Southeast Asia for primate-associated viruses and the Americas as well as Central Africa for rodent-borne viruses (Figure 2B) [13].

Increased intrusion of humans into wildlife habitats and overcrowding of different animal species in farming or market environments favors interspecies transmission. Historically, agricultural development, forest clearing as well as animal domestication and more recently, international travel and trade, lead to the mixing of different animal species. This caused an alteration in virus ecology and facilitates rapid spread of viruses in new environments around the world [14]. Continuing in future, changes in climate and land use will constantly create opportunities for viral sharing among previously geographically isolated wildlife species and the subsequent emergence of new diseases [15].

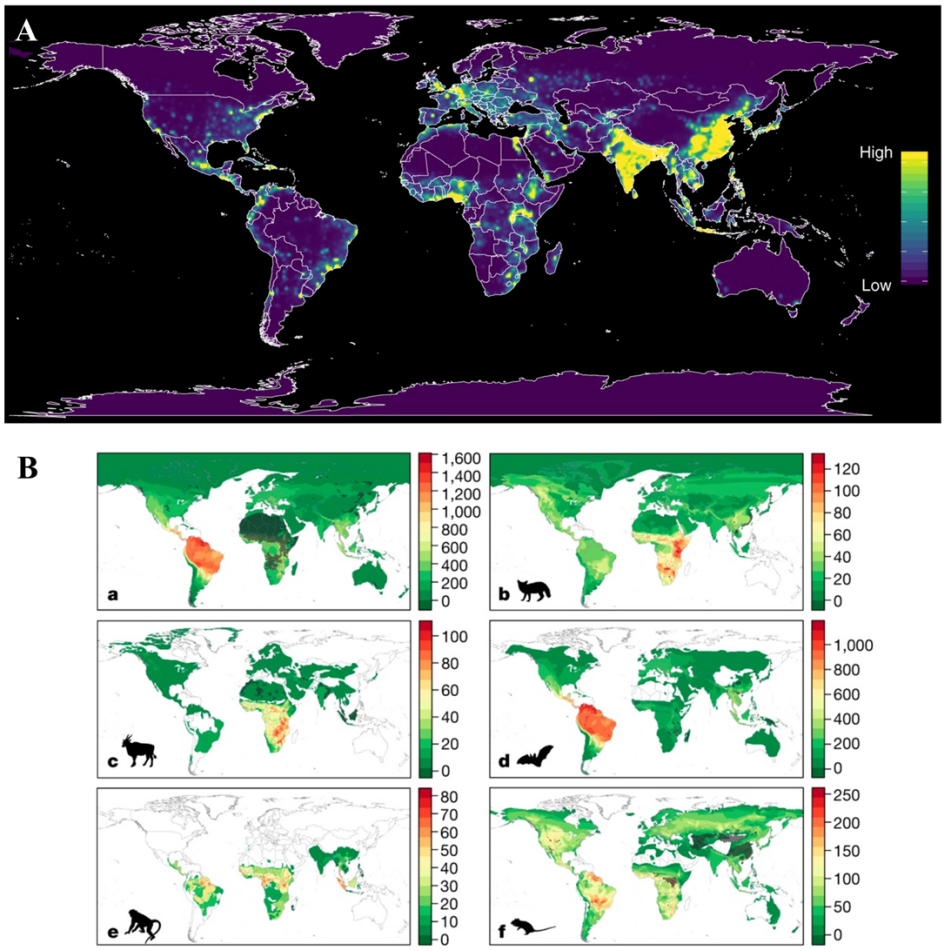

Fig. 2. Global distribution of hotspots for zoonotic spillover events. A, Global distribution of predicted emerging infectious disease risk areas, mapped globally. Main criteria influencing the risk after factoring out reporting effort are tropical rain forests, human population density, climate and mammalian biodiversity. Color code categorizes the risk in high and low. Panel from [12]. **B,** Global distribution of predicted zoonotic events of yet undiscovered viruses divided by reservoir species. Expected number of 'missing' zoonotic viruses per host species geographically projected to identify zoonosis hotspots. Total of 584 mammalian species were included in the model comprising 55 carnivores, 70 even-toed ungulates, 157 bats, 73 primates and 183 rodents. Panel from [13].

In the past two decades several zoonotic emerging viruses had a devastating impact on public health (Table 1 and Figure 3). Emerging infections are caused by novel viruses and re-emerging ones are due to viruses resurfacing after previous control or eradication. An epidemic describes the sudden increase in the frequency of a specific disease above normal expectation values in any given population. An epidemic that spread over several countries or continents at the same time and affects a large number of people is considered a pandemic [16]. Epidemic outbreaks from the past decades were often caused by flaviviruses transmitted by mosquito vectors, including WNV, Zika virus (ZIKV), Yellow Fever virus (YFV) and Dengue virus (DENV) [16]. Several viruses causing hemorrhagic fever and subsequent severe morbidity in human population have recently (re-)emerged, such as bat-borne Marburg virus (MARV) and Ebola viruses (EBOVs) as well as rodent-borne Lassa virus (LASV) [17–19]. Up until now, pandemics were most often caused by avian influenza A viruses (IAVs) with the swine flu emerged in 2009 being the latest out of four pandemics starting from 1918 [20,21]. Three bat-borne coronaviruses, Middle Eastern respiratory syndrome coronavirus (MERS-CoV), severe acute respiratory CoV (SARS-CoV) and SARS-CoV-2, emerged in the past 20 years resulting in devastating outbreaks and two new pandemics [22–24]. The most recent zoonotic outbreak, which affected over 50 countries with around 70 000 cases, was caused by monkeypox virus (MPXV) that was previously endemic in sub-Saharan Africa. So far, the animal reservoir remains unidentified and efficient human-to-human transmission was observed for the first time [25].

Table 1: Important emerging and re-emerging zoonotic viruses in the past 20 years [16,23,25]

Disease	Virus	Family/Genus	Reservoir/ Intermediate host	Transmission
West Nile fever (WNF)	WNV	*Flaviviridae/ Flavivirus*	Birds/Mosquitoes; Birds/horses, dogs,	Mosquitoes
Zika fever	ZIKV	*Flaviviridae/ Flavivirus*	Mosquitoes; NHPs; domestic	Mosquitoes; mother-to-child
Yellow fever (YF)	YFV	*Flaviviridae/ Flavivirus*	NHPs	Mosquitoes
Dengue fever (DF)	DENV	*Flaviviridae/ Flavivirus*	NHPs	Mosquitoes
Chikungunya fever	CHIKV	*Togaviridae/ Alphavirus*	NHPs	Mosquitoes
Lassa fever (LF)	LASV	*Arenaviridae/ Mammarenavirus*	Multimammate mice	Rodent-to-human
Ebola virus disease (EVD)	EBOV	*Filoviridae/ Ebolavirus*	Fruit bats/NHPs: antelopes	Human-to-human
Marburg virus disease (MVD)	MARV	*Filoviridae/ Marburgvirus*	Bats/NHPs; humans	Human-to-human
Swine flu	H1N1 IAV	*Orthomyxoviridae/ Influenzavirus A*	Pigs	Human-to-human
Severe acute respiratory syndrome (SARS)	SARS-CoV	*Coronaviridae/ Betacoronavirus*	Bats/palm civets	Human-to-human
Middle East respiratory syndrome (MERS)	MERS-CoV	*Coronaviridae/ Betacoronavirus*	Bats/dromedary camels	Human-to-human
Coronavirus disease 2019 (COVID-19)	SARS-CoV-2	*Coronaviridae/ Betacoronavirus*	Bats/ unknown (racoon dogs ?)	Human-to-human
Monkeypox disease	MPXV	*Poxviridae/ Orthopoxvirus*	Unknown (African rodents?)	Human-to-human

NHPs stands for non-human primates

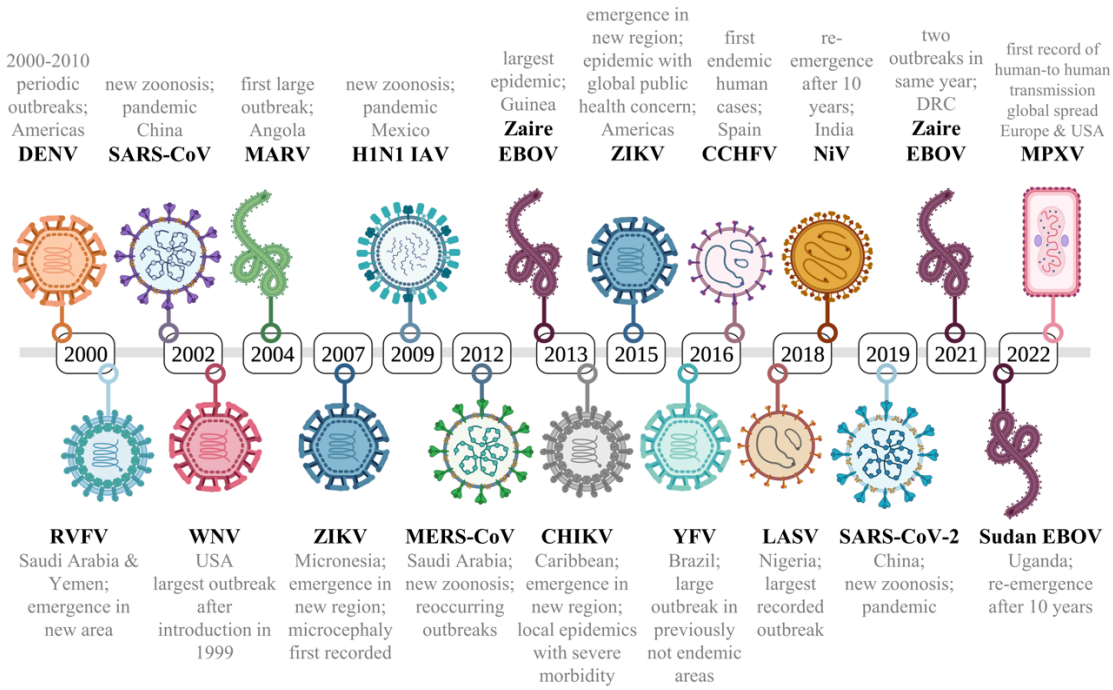

Fig. 3. Timeline of (re-)emergence of zoonotic viruses in the past 20 years. Main examples of spillover events of zoonotic viruses in human population from 2000 until present. Events indicate emergence or re-emergence of viruses in certain geographic areas or emergence of novel viruses. CCHFV stands for Crimean-Congo hemorrhagic fever virus, NiV for Nipah virus, CHIKV for Chikungunya virus and RVFV for Rift Valley fever virus. Figure adapted from [26,27] and created with biorender.com.

1.3 Host reservoirs for viral pathogens

To establish a successful reservoir-virus relationship, a virus must infect and persist in the host without causing substantial disease [7]. An animal reservoir species is defined as an epidemiological connected population in which the pathogen can be permanently maintained and from which infection is transmitted to target populations [28]. Persistence can be facilitated in two different ways. Either virus infections are acute and consequently cleared, but introduction of naïve individuals, such as juveniles, maintains the virus in the population [2]. Alternatively, individuals are able to maintain the virus in form of a persistent infection, as it is commonly seen in rodent reservoir with hanta- or arenaviruses [7].

Evolutionary divergent species from humans have more complex barriers to cross than closely related ones. This implies an elevated zoonotic risk from evolutionary similar animals, such as non-human primates. Nevertheless, zoonotic events have frequently been reported for viruses circulating within species divergent from humans, including bats, rodents and ungulates (Table 1) [29]. Different arrays of host species can be productively infected by a given virus. This characteristic is called host range and can vary dramatically between different viruses. For instance, the poxvirus family includes viruses that only infect one species, such as variola virus causing human smallpox, and others, like cowpox virus, which infects at least several dozen different mammalian species [30]. Mutational adaptation can change the host range as well as geographic distribution and cause a spillover event into new species often resulting in severe pathogenesis. For instance, while waterfowl are the natural hosts of IAVs, these viruses adapt to infect a broad range of host species, including other birds, pigs and humans [14]. A single point mutation in the CHIKV genome was responsible for the adaptation of the virus to a new vector species, *Ae. albopictus* mosquitoes. This is a plausible explanation how CHIKV caused the 2005–2006 Indian Ocean island epidemic, a region lacking the typical mosquito vector, *Aedes aegypti* [31].

Moreover, the overlap of natural habitats of potential host species determines the risk for zoonotic events in human population. For example, most wild carnivores have less direct contact with humans compared to other reservoir clades such as rodents or ungulates, which decreases the risk of direct zoonotic spillover from these animals. Domestic dogs and livestock species, however, have more frequent contact with wild carnivores providing an opportunity for human exposure through pets or farm animals [3].

More than 10000 viruses with zoonotic potential are circulating in mammals and share on average four mammalian hosts [32]. The pattern is not evenly distributed, since species like bats, rodents, primates and ungulates are disproportionally often involved in viral sharing over broad phylogenetic distances (Figure 4) [32]. Facing drastic climate changes in the upcoming years, bats will likely facilitate viral emergence due to their unique dispersal ability [15]. In general, while the total number of viruses sampled in each mammalian species was comparable, bats have been identified as the mammalian species harboring most zoonotic viruses [13].

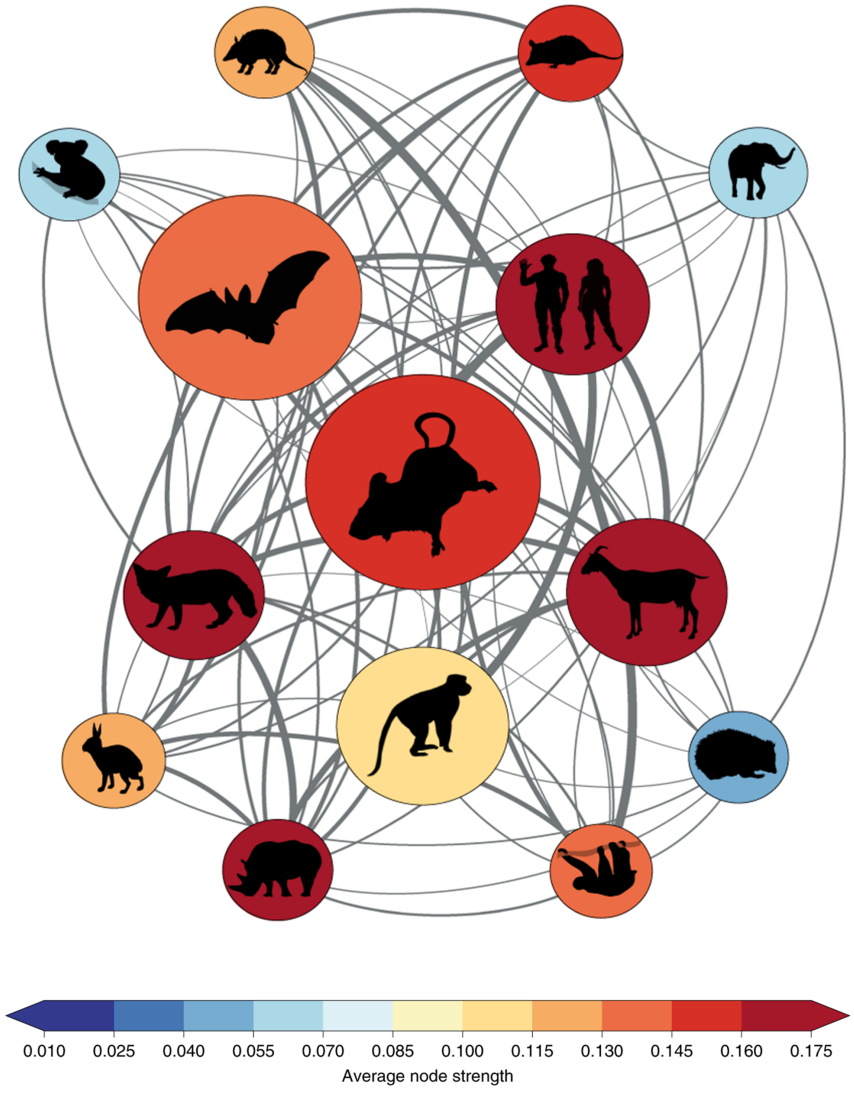

Fig. 4. Network of host sharing for predicted zoonotic viruses in mammals. System of host sharing of 10000 predicted zoonotic viruses in mammals. Unevenly distributed sharing pattern is biased towards bat, primate, ungulate, rodent and carnivore species. Links between nodes represent sharing events of viruses belonging to different orders between host species. Link width correlates to total amount of shared viruses between the two host species. Node size corresponds to total number of sampled viruses in each species. Node color depicts node strength based on number and with of links. Figure from [32].

2. Bats as Reservoir Species

2. Unique biological and anatomical features of bats

2.1.1 Phylogeny and classification

The mammalian order of Chiroptera (bats) includes over 1300 bat species and thus represents 20% of all existing mammals [33]. The golden-capped fruit bat (*Acerodon jubatus*) is the largest bat: it weighs one kilogram and has a wingspan of 1.5 m. The smallest bat, which weighs only two grams, is the echolocating bumblebee bat (*Craseonycteris thonglongyai*). Bats are the only mammals that developed the characteristic of self-powered flight and laryngeal echolocation. They are globally distributed, nocturnal animals and have a wide dietary range made up of insects, small mammals, fish, blood, nectar, fruit and pollen. This grants them an important role in diverse ecosystems, particularly on isolated islands on which they are the only native mammals and act as pollinators, seed-dispersers and crop pest managers [33]. Bats can be homo- or heterothermic. To preserve energy, they can use daily episodic torpor and hibernate during winter months [34]. Bats are known to roost in massive colonies ranging from 10000 to 200000 animals using environments which include caves, rock crevices, bird nests and tree cavities but also man-made structures like mines, tombs, buildings and bridges [14].

Bats have smaller genomes compared to non-flying mammals, with sizes fluctuating from 1.6 to 3.5 Gb. The development of flight capacity may have forced the loss of genomic redundancy and the rationalization of genomic structures [33]. Based on morphological characteristics, bats are split into two suborders: mega- and microbats. The four microbat superfamilies are *Rhinolophidea*, *Emballonuroidea*, *Noctilionoidae* and *Vespertilionoidae* [35]. Megabats only contain one superfamily, *Pteropodoidea*. Morphological data suggest a single origin of flight and laryngeal echolocation in mammals. By contrast, molecular data identified *rhinolophoid* microbats as closely related to megabats, suggesting either multiple origins of echolocation or a single origin but subsequent trait loss in megabats [35]. This resulted in a second sub ordering system which separates bats into Yinpterochiroptera including *Pteropodoidea* and *Rhinolophoidea* and Yangochiroptera with the remaining 3 microbat superfamilies (Figure 5) [35].

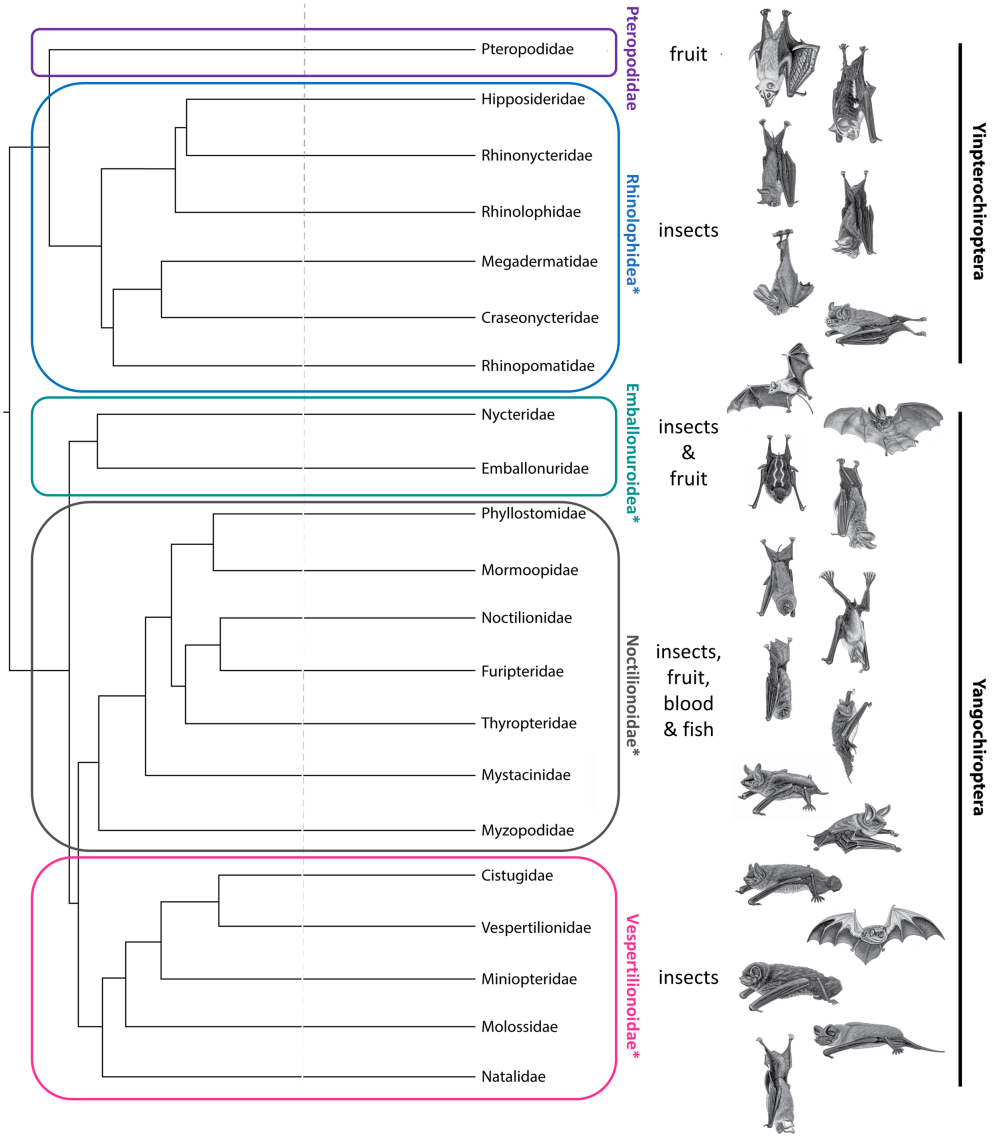

Fig. 5. Phylogenetic tree of the chiropteran order. Colors indicate the five superfamilies of bats and diet information is given for each family. Asterixis mark superfamilies belonging to the classification 'microbats'. Figure adapted from [33].

2.1.2 Extreme longevity

Bats display several unique biological features (Figure 6) including an above average longevity despite their small body size and altered metabolism. Their nocturnality and flight capacity, which result in a decreased number of predators, may contribute to this longevity. Eighteen-out of 19 mammal species that live longer than humans in proportion to their body mass are bats [33]. They live ten times longer than expected when compared to other similar sized mammals. The oldest wild-captured bat was a *Myotis brandtii* of 41 years weighing only seven grams [36]. Cave usage and hibernation as well as flexible thermoregulation have been identified as factors predicting longevity in *Desmodus*

rotundus bats [37]. Moreover, in *Myotis ricketti* and *Rhinolophus ferrumequinum* bats, unique activation of the phenylalanine and tyrosine catabolism pathway during hibernation as detoxification method for harmful nitrogen metabolites have been observed [38]. Non hibernating bat species, however, also display extended lifespans [37].

Some molecular processes that could contribute to bat longevity have been proposed. With increasing age, the excessive cell division will shorten the protective nucleotide repeats at the ends of chromosomes, called telomeres. This mechanism enhances cellular senescence and eventually restricts lifespan. As in other mammals, telomeres shorten with age in *Rhinolophus ferrumequinum* and *Miniopterus schreibersii*, but not in *Myotis* bats, as shown by quantitative real-time polymerase chain reaction (qPCR) assays of telomere length in wing tissue biopsies [39,40]. In a comparative multi-tissue transcriptomic analysis of *Myotis* and other mammalian transcriptomes, a set of 21 telomere maintenance genes were identified as upregulated in *Myotis* cells including 14 genes involved in DNA repair and five genes contributing to alternate telomere-lengthening pathways [40]. Fibroblasts of *Eptesicus fuscus*, *Nycticeius humeralis* and *Myotis spp.* resist extrinsic stressors like peroxisomes, heat, heavy metals, pesticides and starvation better than corresponding cells from short-lived mammals and depict a more equilibrated and dynamic regulation of the proteome [41–43]. Heat shock proteins (HSPs) bind and repair damaged proteins and safeguard protein homeostasis to limit prolonged cellular damage upon extrinsic stressors. Elevated levels of HSPs have been found across multiple tissues, like lung, liver, spleen, intestine and wing, in *Pteropus alecto* and *Eonycteris spelaea* [44]. Moreover, *P. alecto* kidney and lung cells as well as *E. spelaea* lung cells tolerate heat treatment better than other mammalian cells [44]. Autophagy is another cytoprotective mechanism that is believed to play a role in extending lifespan. In contrast to humans and mice, genes involved in autophagy mechanisms are upregulated with increasing age in *Myotis myotis* and *Pipistrellus kuhlii*. Twenty-six autophagy-associated genes are differentially expressed in cells from *Myotis* bats and ten of these genes showed conserved positive selection pattern in several bat lineages [45].

2.1.3 Tumorigenesis and oxidative stress

Contradicting their long lifespans, only very few studies report tumor cases in bats, for instance in *Rousettus aegyptiacus*. Multiple molecular mechanisms have been described potentially explaining this phenomenon [46]. Compared to other mammals, mitochondria from *Myotis* bats generate less oxidative byproducts per oxygen unit processed in aerobic respiration [47]. Liver proteins of *Tadarida brasiliensis* and *Myotis velifer* can withstand oxidative stress and urea-induced denaturation better than mice proteins [48]. A set of genes involved in DNA damage repair and protecting against oxidative damage, such as *ATM, RAD50, KU80* or *MDM2*, are under positive selection in *Myotis davidii* and *Pteropus alecto* [49]. Expression of *UVRAG*, which is linked to DNA repair, autophagy and tumor inhibition, is upregulated in *Myotis myotis* [50]. The enormous physical effort required for flight results in oxidative stress which is linked to DNA damage and release of self-DNA into the cytoplasm. Having protective DNA mechanisms in place is therefore key for survival of bats [28]. Moreover, highly expressed miRNA-155, which protects cells against oxidative damage, acts together with three other upregulated miRNAs (16, 101 and 143) and two coding genes (*BRCA* 1 and 2) as tumor suppressors. Importantly, miRNA-221, which is involved in promoting tumorigenesis, is downregulated in *Myotis* bats [50]. Fecal metabolomics studies in *Eptesicus fuscus* showed 41 metabolites with higher concentrations in elderly *versus* young bats. Some of these compounds are known to play key roles in cancer and inflammation pathways indicating elderly *Eptesicus* bats could be less susceptible to chronic inflammation and cancer [51].

2.1.4 Self-powered flight and metabolism

During flight, the metabolic rate of bats increases 15- to 16-times above the resting metabolism level which is comparatively much higher than the 7-fold increase of rodents running to exhaustion or the 2-fold increase of most flying birds [52]. Self-powered flight represents the most energy-demanding form of movement, thus bats needed to adapt towards increased metabolic capacity. Genes involved in the mitochondrial and nuclear energy metabolism, specifically in oxidative phosphorylation (OXPHOS) pathways and the production of adenosine triphosphate (ATP), which provides the majority of required energy for locomotion, are under positive selection in chiropteran species [53]. Maneuverability and energy expense during flight favored body mass reduction and thus shorter intestines in bats. To compensate, bats evolved special food processing and

digestive traits. Bats display an increased efficiency in digesting dry matter and depict the highest rates of nutrient absorption among mammalian species. An alternative paracellular transportation mechanism has been proposed for passive carbohydrate absorption in bat intestines [54,55]. Moreover, bats can tolerate blood glucose levels to a magnitude that would be pathogenic for other mammals. The glucose levels after food intake in fruit- or nectar-feeding bats are only downregulated after sustained flight. This suggests that they may not rely exclusively on the insulin-based glucose transport to avoid detrimental effects of hyperglycemia such as the formation of reactive oxygen species (ROS). In contrast to other mammals, bats might be capable of fueling their energetic demands during flight directly through recently ingested sugars [56,57].

Chiropteran microbiomes display a great variety due to the wide dietary ranges of different bat species. In-depth studies identifying microbial symbionts are still lacking. Recent findings, however, indicate that metabolites generated by gut microbes could counteract oxidative damages linked to flight in bats [58]. In *Myotis* bats, the anal microbiome remains stable with increasing age in contrast to shifts observed in other mammals. In bat metagenomes, pathways like metabolism, energy consumption, DNA repair and oxidative phosphorylation, were enriched indicating a beneficial relationship between a stable microbiome and the physiological needs of bats [59].

2.1.5 Echolocation and vocal communication

Bats are the only mammals to use laryngeal echolocation for hunting and orienting but this ability varies greatly amongst the 21 families of echolocating bats. The sense of vision remains a complement to ultrasonic echolocation in many bat species. Varying eye sizes and visual acuity could be correlated to differences in foraging techniques and migrating behavior among echolocating insectivorous bats. *Pteropodidae* fruit bats do not use laryngeal echolocation but instead have large sensitive eyes, specialized for nocturnal vision [60,61]. Echolocation might have evolved in the common bat ancestor and was subsequently lost in *Pteropodidae* bats. In cave-roosting *Rousettus* bats, echolocation might have evolved secondarily by tongue-clicking. It is also possible that echolocation has evolved independently in Yinpterochiroptera and Yangochiroptera [33,61]. Bats use ultrasounds and lower frequency sounds for communication and have evolved rich repertoires of social calls. Core component of spoken language is the ability to learn new

vocalizations. This ability is shared only between a few other species, including bats, birds, cetaceans, pinnipeds and elephants [33,61].

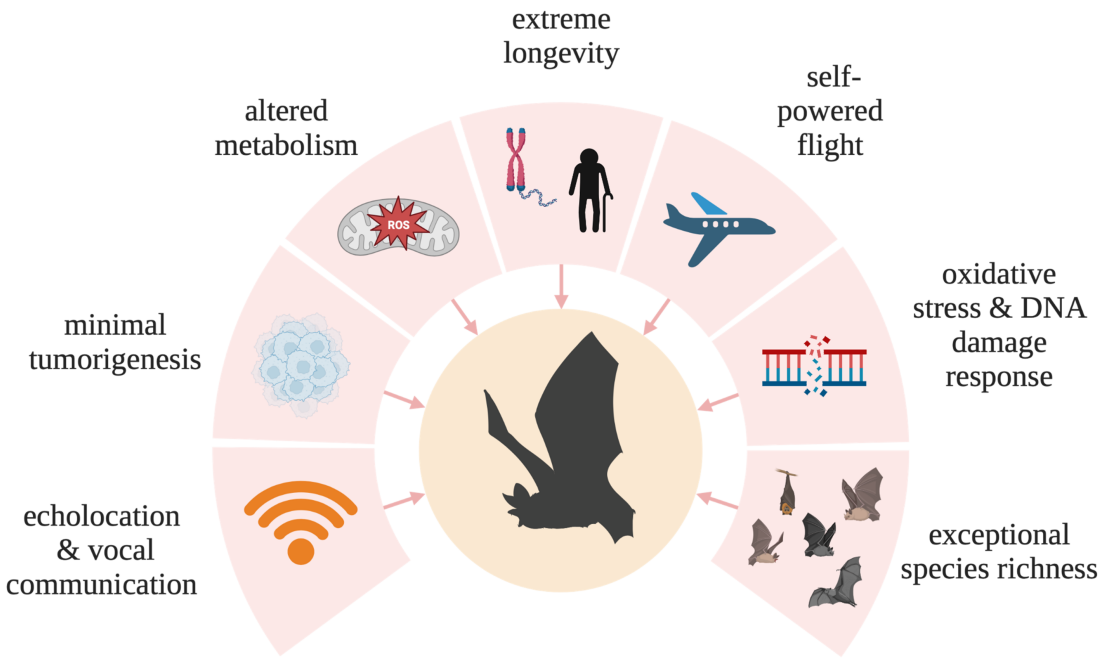

Fig. 6. Special biological features of chiropteran species. Graph summarizes the above-described characteristics and pathways found in bats. Figure created with biorender.com.

2.2 Relationship between bats and viruses

Since the identification of rabies, which belong to the Lyssavirus genus, in an asymptomatic vampire bat in 1911, bats have been linked to a multitude of emerging viruses [62]. Thousands of bat-associated viral species have been discovered from 28 diverse viral families with a high proportion of corona-, paramyxo- and rhabdoviruses (Figure 7) [63]. The diversity of bat species, their worldwide distribution and unique biological features (Figure 6) contribute to the biodiversity of viruses they carry [64]. Meta-analysis of 2800 host-virus interactions revealed that bats are more likely infected with viruses that can also infect human than other mammalian species [65]. Moreover, they harbor more viruses per species than any other mammal including rodents, the most species-rich mammalian clade on earth [66].

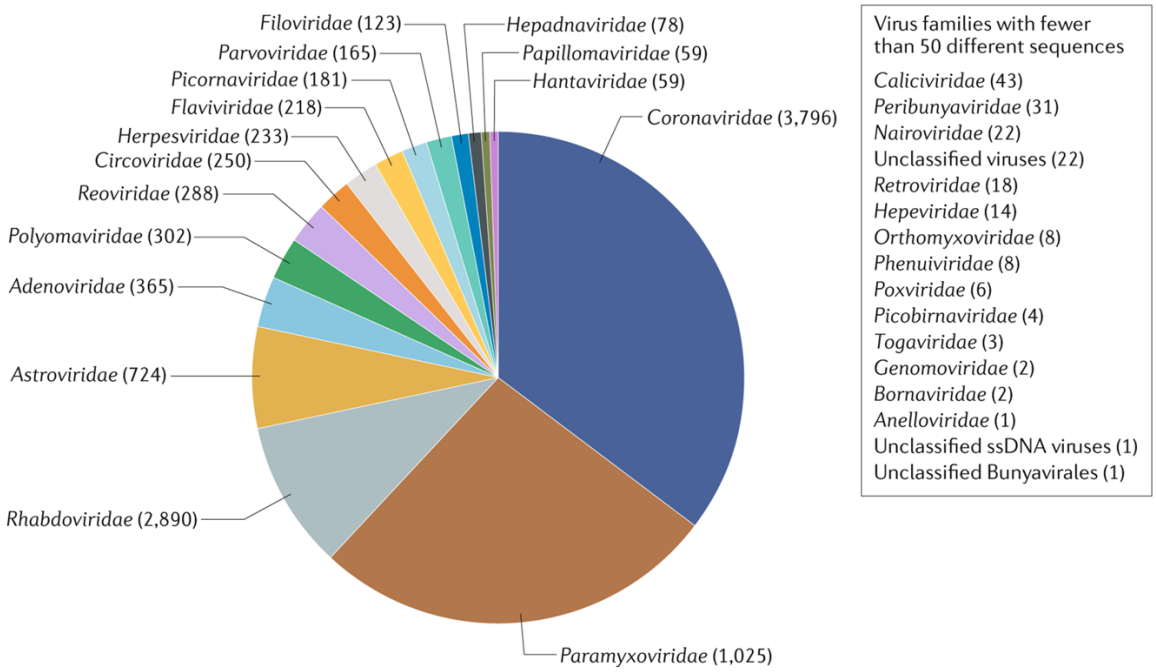

Fig. 7. Bat virome. Pie chart of pooled available sequencing data from the database DBatVir for all viruses sampled to date in different bat species. Display of viral families proportional to their abundance in bats. Figure from [63].

Bats have been identified as natural reservoir for numerous RNA viruses that cause severe disease in humans, such as rabies, MARV, Hendra virus (HeV), NiV and Sosuga virus via direct isolation. In addition, serological and genomic evidence strongly suggest that diverse bat species are the predicted reservoirs for EBOV, SARS-CoV and MERS-CoV (Table 2) [63]. Whereas bats are likely the ancestral origin of those viruses infecting humans, it cannot be ruled out that an intermediate host, in which viral mutations occurred and where virus reached significant prevalence, might have been necessary for zoonotic spillover rather than direct transmission from bats [28].

Understanding viral dynamics in a bat population is important for predicting spillover events. In some cases, cycles with increased cross-species transmission risk have been identified in bat colonies. For instance, surveillance of *Rousettus aegyptiacus* in the Kitaka cave in Uganda revealed biannual raise of MARV positive bats correlating with birth of pups in the colony and subsequently causing more human spillover events [67]. In certain tropical regions, direct contact between humans and bats is more frequent and thus potentially facilitates human infection. For example, this increased frequency of contacts can occur through the consumption of bats as bushmeat or via their use in traditional medicine [68]. Increased human-bat contacts can also be the result of agricultural

expansion which can lead to nutritional stress in bats. In the case of NiV, increased pig farming in Malaysia and subsequent deforestation caused overlapping habitats with bats. Farmed pigs fed on fruits contaminated with bat saliva leading to NiV outbreak in pigs and subsequent transmission to humans. In Bangladesh, bats fed on man-made date palm sap collection sites. Subsequent human consumption of contaminated sap likely caused the emergence of NiV in human population [63,69].

Table 2: Zoonotic bat-borne viruses responsible for severe pathology in human populations [7,70]

Disease	**Virus**	**Reservoir Host**
Rabies	Rabies virus and other lyssaviruses	Globally distributed multiple species *(Miniopterus, Myotis, Eptesicus, Rousettus, Pteropus, Eidolon, etc.)*
Marburg virus disease	Marburg virus	*Rousettus aegyptiacus*
Ebola virus disease	Ebolaviruses	*Hypsignathus monstrosus, Epomops franqueti, Myonycteris torquata*
Severe acute respiratory syndrome	SARS-CoV	*Rhinolophus spp. (Rhinolophus sinicus)*
Middle East respiratory syndrome	MERS-CoV	*Taphozous perforatus*
Encephalitis	Nipah virus	*Pteropus spp. (P. vampyrus and P. hypomelanus)*
Encephalitis	Hendra virus	*Pteropus spp. (P. alecto, P. poliocephalus, P. scapulatus, P. conspicillatus)*
Severe acute febrile disease	Sosuga virus	*Rousettus aegyptiacus*
Severe respiratory and enteric disease	Pteropine orthoreoviruses	*Pteropus spp. (P. vampyrus, P. poliocephalus, P. hypomelanus); Rousettus spp. (R. leschenaultii, R. amplexicaudatus); Eonycteris spelaea*

The intricate relationship between bats and viruses is ancient. Several endogenous viral elements (EVEs) which are incorporated in host genomes and represent ancient viral infections have been identified in bats [71]. Especially, EVEs of *Parvoviridae, Adenoviridae* and *Bornaviridae* have been found in several bat species and a partial filovirus EVE was identified in *Pipistrellus* and *Myotis* genomes, which suggest that vespertilionid bats have been exposed and survived filoviral infections [71]. Infection of *P. alecto* and *R. aegyptiacus* kidney cells with vesicular stomatitis virus (VSV) pseudotyped filoviruses resulted in a strong innate immune response and thus minimal cytopathic effect (CPE), but a rapidly spreading persistent infection [72]. Mathematical models fitted to these *in vitro* studies suggest that accelerated viral propagation with limited cellular morbidity might favor chronic subclinical infections in bats but acute infections in other hosts. These rapidly-reproducing viruses would likely generate extreme virulence upon spillover to hosts lacking similar immune capacities than bats [72]. While viruses like HeV, NiV, EBOV or MARV are highly pathogenic in humans and other mammals, experimental

studies and field observations have shown that bats rarely display clinical signs upon viral infection, even when high viral titers were detected in tissues and sera [73,74]. MARV experimental infection studies of *Rousettus aegyptiacus* showed that bats had prologued incubation periods, remained viremic and excreted viruses for three weeks [73]. Even lacking detectable virus in systemic circulation, one bat transmitted MARV after four months to another individual [73]. In this particular case, decreased antibody (AB) titers and a subsequent increase in systemic viral load possibly re-initiated viral shedding from a persistently infected organ [75]. Moreover, most of the bats experimentally infected with doses of henipaviruses that would be lethal to other mammals, did not show apparent clinical signs [76,77]. Similarly, upon infection with MERS-CoV, *Eptesicus* bats exhibited no or minimal signs of disease, even when high viral loads were detected in the sera or tissues [78]. There are few exceptions, however, since some viruses can indeed cause pathology in bats [7]. Depending on the route of infection, rabies viruses can cause clinical symptoms and even death in bats [79,80]. Tacaribe virus, a virus isolated from *Artibeus* bats in Trinidad, can cause rabies-like symptoms [81]. Lloviu virus infection has been linked to the death of *Miniopterus* bats in Spain, Portugal and France [82].

Several unique properties of bats are believed to render them particularly adapted to transmit viruses. Using echolocation or vocal communication, bats produce loud sounds which could generate droplets or small-particle aerosols of oropharyngeal fluids, mucus or saliva, enabling transmission of viruses between individuals in proximity. Airborne rabies virus transmission, for example, was documented in a large colony of Mexican free-tailed bats [64]. Fever in mammals is linked to high metabolic rates and anti-pathogenic immune mechanisms. During flight, a fever-like response is generated in bats, characterized by elevated metabolism and body temperature. This mechanism might help bats survive viral infections. It might also allow viruses to adapt towards greater tolerance of the fever response and thus to be more virulent in novel hosts, which mount fever as defense mechanism against infection [52,83]. The body temperature of bats rises as high as 40°C in flight and during daily torpor it can drop as low as 10°C with normal amplitudes between 20 and 37°C, which depicts an efficient energy saving method. This daily change in temperature is predicted to help bats coping with viral infections since it might reduce viral growth rate and thus viral concentrations [84]. Bats also exhibit unique immunological features that probably contribute their high tolerance towards viral disease. Finally, dampened inflammatory processes might aid supporting viral infections [85]. These bat-specific features will be described in chapter 1, subsection 4.

3. Innate immune Response in human cells

3.1 Host cellular defenses and immunity

All eukaryotes evolved a sophisticated biological system to combat pathogens, the immune system. In most organisms, it consists of two arms that interact with one another: innate and adaptive immunity. The innate immune system is the host's first line of defense to an invading microbe. The innate immune response is immediate, potent and highly conserved amongst species, but is unspecific and lacks memory capabilities. Moreover, it needs stringent regulatory mechanisms to not cause pathology itself. Innate immunity relies on the signaling of only few germ-line encoded receptors which recognize a limited set of conserved molecular patterns. Repeated exposure to the same pattern does not qualitatively or quantitatively ameliorate the response [86,87]. It consists of physical and molecular components that serve as barriers for the intruding pathogen, which need to be overcome to establish infection in the host. Elements of the innate immune system are innate immune cells, such as neutrophils, dendritic cells (DCs), natural killer (NK) cells, monocytes and macrophages, the complement system and proteins, including cytokines such as interferons (IFNs) and acute phase proteins [88].

The adaptive immune response is restricted to higher organisms, displays delayed kinetics but possesses effective recall responses in a pathogen-specific manner involving antigen-specific cells. It utilizes a large number of variable immune receptors to generate an extensive repertoire [86,87]. Antigens deriving from pathogens decorate antigen presenting cells like macrophages or DCs and are shown to antigen-specific T and B cells in secondary lymphoid tissues such as lymph nodes, spleen and mucosa-associated lymphoid tissues. Those T or B cells then get activated, proliferate and migrate to infection sites to combat invading microbes through antibody production and/or direct killing of the infected cells [89]. In the following paragraphs, the human innate immune system will be further described.

3.2 Sensing and signaling mechanisms

The innate immune response is initiated by the sensing of pathogen-associated molecular patterns (PAMPs) or danger-associated molecular patterns (DAMPs) by pattern recognition receptors (PRRs). Whereas DAMPs are stress-response cellular products, PAMPs are intrinsic structures of pathogens such as nucleic acids (NAs) or surface molecules. When PRRs encounter a PAMP, a signaling cascade is triggered and leads to the expression of

anti-pathogenic proteins called cytokines. IFNs represent a major subclass of cytokines and, once bound to their receptors, they activate a second signaling cascade that triggers the expression of hundreds of interferon-stimulated genes (ISGs) [90].

PRRs are constituted of four different types of germ-line encoded receptor families: transmembrane-bound Toll-like receptors (TLRs), C-type lectin receptor (CLRs), RIG-I like receptors (RLRs) and NOD-like receptor (NLRs). Whereas NLRs are specialized in recognizing peptidoglycan parts of the bacterial cell wall, the PAMPs interacting with CLRs are microbial carbohydrates, mostly of fungi. TLRs can sense a wide array of ligands ranging from surface structures of pathogens to NAs and RLRs sense mainly viral RNAs [91]. I will focus below on the pathways relevant for viral infection.

3.2.1 RIG-I-like receptor pathways

The three family members of RLRs, retinoic acid-inducible gene I (RIG-I), melanoma differentiation association gene 5 (MDA5) and laboratory of genetics and physiology 2 (LPG2), are ubiquitously expressed in almost all cell types. The ligands of the RLR family members are well characterized [90]. RIG-I interacts preferentially with short, blunt-ended dsRNA (10-300 bp) which contains a triphosphate motif on the 5'-terminus. Host RNAs only harbor a monophosphate or a cap motif on their 5'-end allowing the innate immune system to discriminate between self and not-self forms of RNA in the cytoplasm. Consequently, viral RNAs are sensed while host RNAs are tolerated [92]. MDA5, in contrast, binds to dsRNA with a minimal length of 2 kb. It does not rely on the 5'-terminal triphosphate motif for efficient interaction and rather binds to the phosphorylated backbone of web-like structured dsRNA molecules which can be found in stem-loop structured parts of ssRNA viral genomes [92]. Finally, LGP2 has been shown to interact with different sized dsRNAs unconnected to specific 5'-terminal motifs, which suggests that it can competitively bind to RNA molecules with RIG-I and act as its negative regulator. Additionally, LGP2 can also bind stem-looped ssRNA motifs and associate with MDA5, acting as its positive regulator [92].

Studies in diverse cellular models revealed differential involvement of MDA5 and RIG-I in the antiviral responses against certain viruses. During infection with VSV, paramyxoviruses, orthomyxoviruses, filoviruses (EBOV), Epstein–Barr virus (EBV), Hepatitis C virus (HCV), Japanese Encephalitis virus (JEV), ZIKV and DENV, viral PAMPs have been reported to be mainly sensed by RIG-I [93]. PAMPs of picornaviruses,

norovirus, encephalomyocarditis virus (EMCV), Hepatitis B virus (HBV), Herpes Simplex virus (HSV), avian IAV H5N1, Hepatitis D virus (HDV) and SARS-CoV-2 are rather recognized by MDA5 [94,95]. In some cases, such as flavivirus or reovirus infections, both RIG-I and MDA5 may act together to initiate innate immune signaling [96].

All three RLRs contain a central DEAD box helicase/ATPase domain, which is responsible for recognizing the viral NA motif, and a zinc-binding C-terminal domain (CTD). Only RIG-I and MDA5, but not LGP2, harbor two N-terminal caspase activation and recruitment domains (CARDs), which allow downstream signaling and induction of the innate immune response after binding to dsRNA. LGP2 acts as RIG-I or MDA5 regulator but is unable to induce interferon signaling due to the lack of CARD domains. In resting state, RIG-I and MDA5 are in a closed conformation, with the helicase domain and the CTD associating with the CARD. Upon binding to viral dsRNA, the CARD is released from the helicase and the CTD and is thus accessible to bind to mitochondrial antiviral-signaling protein (MAVS). MAVS thereafter assembles into aggregates which facilitates recruitment of two E3 ubiquitin ligases, tripartite motif containing 25 (TRIM25) as well as riplet, and the downstream effectors tumor necrosis factor (TNF) receptor-associate factor (TRAF) 2, 3 and 6. Two signal transduction cascades are subsequently activated. First, the MAVS signalosome associates with the kinases IKKα and IKKβ as well as with nuclear factor kappa-light-chain-enhancer of activated B cells (NFkB) essential regulator (NEMO), which trigger the nuclear translocation of NFkB and the induction of proinflammatory cytokine expression (Figure 8). The NFkB protein family has five members in humans: RelA (p65), RelB, c-Rel, NFkB1 (p50) and NFkB2 (p52). All members form homo- or heterodimers and are structurally similar. Bound to inhibitor of NFkB (IκB) proteins, these dimers are retained in an inactivated state in the cytoplasm [97].

Second, activated MAVS associates with TANK-binding kinase 1 (TBK1) and IKKε, which triggers the phosphorylation and nuclear translocation of interferon regulatory factor (IRF) 3 and 7 and induction of IFN expression [90,94] (Figure 8). The IFR family of transcription factors regulates the gene expression underlying IFN responses. Nine IRFs can be found in mammals. All IRFs share an amino-terminal DNA-binding domain (DBD) which allows the recognition of the IFN-sensitive response element (IRES), a DNA motif present in all promotors of IFN type I and III genes as well as ISGs [98]. Basal expression levels of IRF7 are high in plasmacytoid (p) DCs, thus primary IFN induction might be

largely reliant on IRF3. After the first round of IFN secretion, IFN-inducible IRF7 can contribute to exacerbate IFN responses [99].

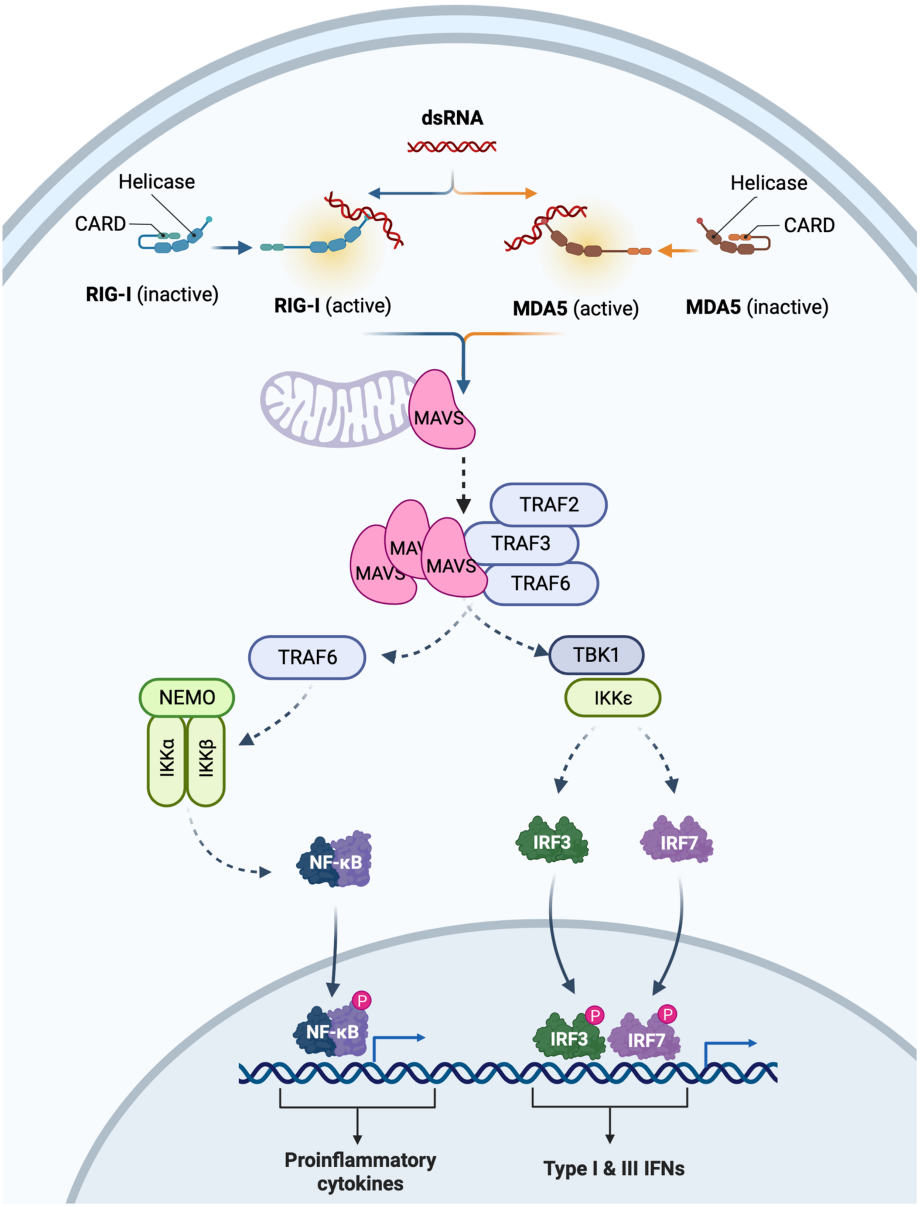

Fig. 8: RLR signaling pathway. dsRNA is sensed by RIG-I or MDA5, transferring them from their inactive to active states after NA binding. RLRs associate with mitochondria resident MAVS and subsequently two independent signaling cascades are stimulated. MAVS binds to TRAF6 and activates NFkB signaling cascade via NEMO and IKK-complex, leading to the nuclear translocation of NFkB and transcription initiation of proinflammatory cytokines. Via TBK1 and IKKε, a second signaling pathway leads to the activation of IRF3 and 7 which initiate transcription of IFNs after translocating into the nucleus. Figure created with biorender.com.

3.2.2 Toll-like receptor pathways

Most mammals encode ten different TLRs (TLR1–10). Additional TLRs have been described in other mammals such as rodents (TLR11, 12 and 13) [100]. Four TLRs (TLR3, 7, 8 and 9), that are highly conserved amongst all mammalian species, are responsible for NA sensing. TLR7 and 8 interact with ssRNA while TLR3 binds to dsRNA and TLR9 senses ssDNA with unmethylated CpG-motifs [101]. All NA-sensing TLRs are located in endosomes, which permits them to interact with the internalized genomes of pathogens (Figure 9). This location also compartmentalizes them to avoid stimulation with self-NA in a not-pathogenic context. TLRs play a crucial role in the early detection of viral NAs and initiation of antiviral innate immune responses, especially through high levels of IFN production in DCs [101]. TLR sensing of incoming viral genomes depends on the cellular tropism of each virus since they are not equally expressed in all cell types [92].

The distribution of TLRs is cell-type specific. TLR3 is present in all innate immune cells except neutrophils and pDCs. TLR7 can be found in pDCs, B lymphocytes and monocytes/macrophages. TLR8 is only expressed in monocytes, macrophages and cDCs. Finally, TLR9 is expressed in pDCs and B cells. Given their cell-specific distribution and the strong specialization of different immune cells, the pattern of induced anti-pathogenetic effectors upon TLR stimulation varies greatly [90,101].

TLRs are glycoprotein receptors with a N-terminal PAMP-binding domain, a central transmembrane domain which anchors the receptor either to the plasma membrane (PM) or endosomal membrane, and a C-terminal Toll/IL-1 receptor (TIR) domain that extrudes into the cytosol and facilitates downstream signaling. TLR7, TLR8 and TLR9 associate with MyD88 which itself binds IL-1R-associated kinases (IRAK) 1-4 as well as TRAF 3 and 6 (Figure 8). These interactions trigger subsequently two signaling cascades that lead to the activation of the NFkB pathway via the NEMO/IKK complex and IRF5 and IRF7 nuclear translocation for IFN-I/III production. TLR3, in contrast to the other TLRs, does not signal through MyD88 but via TIR-domain containing adaptor protein inducing IFN-beta (TRIF) as adaptor protein (Figure 8). TRIF then interacts with TRAF3 and 6, which induces in a shared cascade with the RLRs/IRF3 axis via TBK1 and IKKε as well as the NFkB pathway via the NEMO/IKK complex respectively (Figure 8) [90,91].

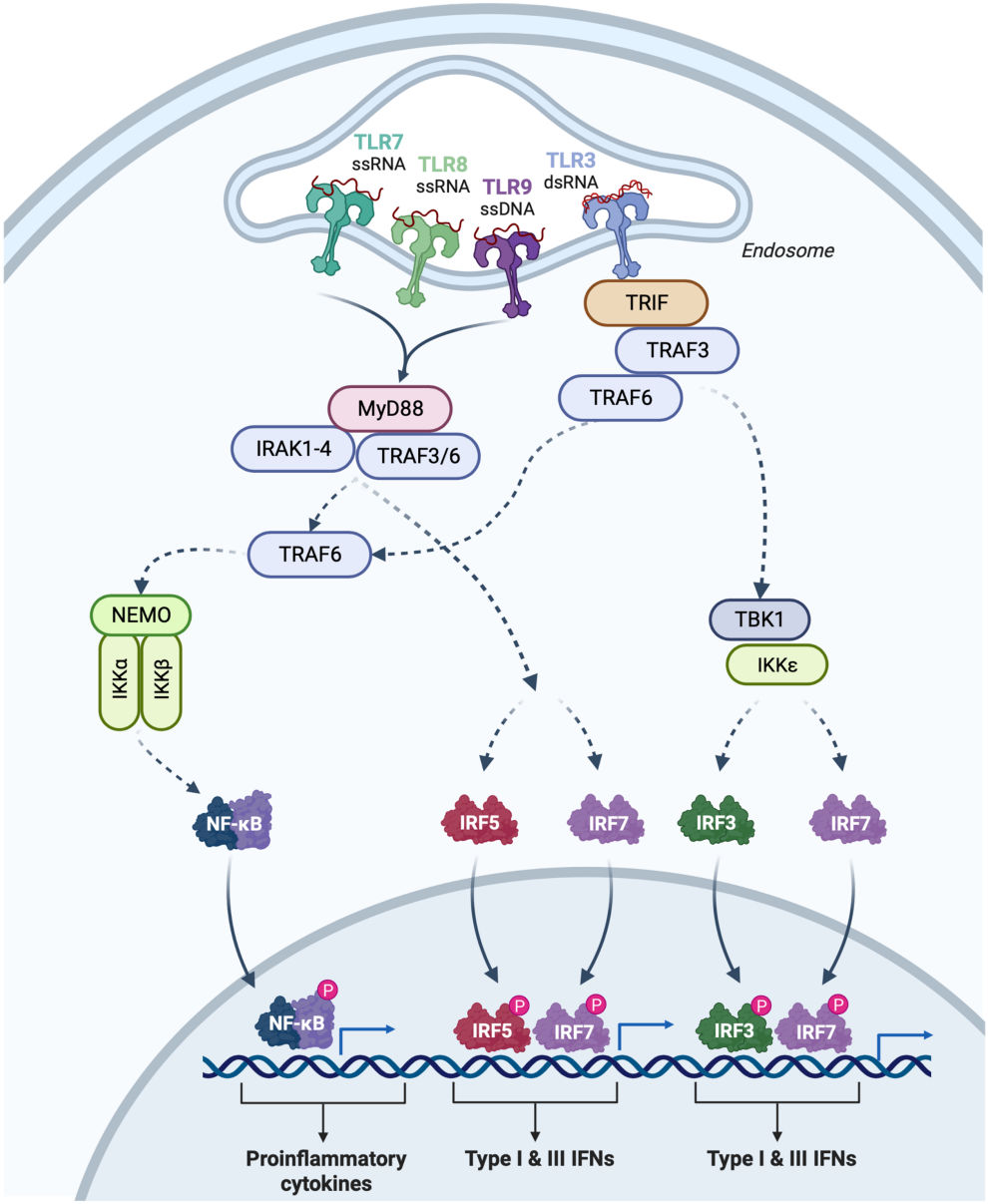

Fig. 9: TLR signaling pathway. NAs are sensed by different TLRs located in endosomes. TLR7-9 associate upon NA binding with MyD88 and subsequently IRAK1-4 and TRAF6. This leads to a downstream signaling cascade via NEMO and the IKK complex, resulting in the nuclear translocation of NFkB and transcription initiation of proinflammatory cytokines. Simultaneously, TRAF6 stimulates IRF5 and 7, leading to their translocation into the nucleus and stimulation of IFN transcription. TLR3 associates with TRIF and subsequently with TRAF3 and 6. As for TLR7-9, the TRAF6 signaling pathway via NEMO/IKK complex is subsequently stimulated. Additionally, TRAF3 facilitates signaling via TBK1 and IKKε leading to the nuclear translocation of IRF3 and 7 and transcription initiation of IFN-I/-III. Figure created with biorender.com.

3.2.3 cGAS/STING in DNA sensing and RNA virus infection

In a healthy cell, host DNA is sequestered in the nucleus and mitochondria, thus any free dsDNA in the cytoplasm indicates stress or injury. The cyclic GMP-AMP synthase (cGAS) and stimulator of interferon genes (STING) pathway is responsible for sensing any kind of dsDNA in the cytoplasm of all cell types, pathogenic or self, and subsequently initiates innate immune responses. cGAS binds to dsDNA, or less efficiently to DNA:RNA hybrid structures, leading to the generation of 2'3' cyclic GMP-AMP (cGAMP) molecules. cGAMP then interacts with STING which then dimerizes and binds TBK1. Once activated, TBK1 phosphorylates the transcription factors IRF3 and NFkB, which then translocate to the nucleus and initiate the expression of numerous genes, including *IFNs* [102,103]. STING itself can also bind DNA but the consequence of this direct interaction remains unclear. Intriguingly, recent studies have shown that the cGAS-STING pathway was efficiently inhibited during the replication of several RNA virus, such as DENV, ZIKV and CHIKV. It was later shown that during infection with these RNA viruses, DNA is released into the cytoplasm from damaged mitochondria, which stimulates cGAS [104]. To date it is unclear if the cGAS-STING pathway can also directly be activated by viral RNA and how conserved its inhibition is across different RNA virus families. Whereas cGAS does not seem to be capable of binding RNA, STING can directly interact with the RLR pathway by binding to MAVS and contributing to the initiation of IFN-I activation. It is thus not surprising that several RNA viruses spanning multiple families have evolved mechanisms to inhibit STING [102,103].

IFNγ-inducible protein 16 (IFI16) is another cytoplasmic DNA sensor that binds STING and thus activates IFN signaling [105]. IFI16 can also bind IAV and CHIKV viral RNA and inhibits ZIKV replication [106–108].

3.2.4 Additional cytoplasmic NA sensors

Besides RLRs, other cytoplasmic NA sensors exist. Eukaryotic translation initiation factor 2 alpha kinase 2 or protein kinase k (PKR) is a serine-threonine kinase that becomes activated by the presence of dsRNA [109]. PKR, which localizes mainly in the cytoplasm but can also found in the nucleus, self-activates via dimerization upon sensing dsRNA. This activation leads to the phosphorylation of eIF2α. Consequently, the initiation of translation, including the translation of viral mRNA, is blocked triggering apoptosis of infected cells and ultimately limiting the spread of infection. Moreover, PKR promotes NFkB activation

via NFkB-inducing kinase (NIK) and IKKβ binding and supports the IFN response by stabilizing IFN mRNA transcripts [110]. PKR can also be activated by the stress-response molecule PACT [99].

2'-5' oligoandenylate synthase (OAS) proteins are ISGs and cytosolic RNA-sensors that are activated by the interaction with dsRNA. The OAS protein family constitutes four IFN-regulated genes, OAS1-3 and the OAS-like protein (OASL). Upon interaction with dsRNA, OAS1-3 generate secondary messenger proteins, 2'-5' linked oligoadenylates, which consequently activate RNase L leading to its dimerization and the cleavage of ssRNA products. OAS signaling results in inhibition of protein synthesis and apoptosis as well as degradation of viral RNA. Additionally, RNA cleavage products might intensify RLR-mediated antiviral responses. OASL does not harbor synthetase activities but displays antiviral potential by acting as a positive regulator of the RIG-I signaling pathway [90,111].

Additional cellular sensors contributing to the innate immune response have been described for both viral DNA and RNA. For instance, DDX1, DDX3, DHX9, DHX15, DHX33, DDX60 and SNRNP200, which are members of the DEAD box helicases family, like the three RLRs, may play a role in innate immune signaling and antiviral mechanisms [90]. Recently, the family of thousand and one (TAO) kinases (TAOK1, 2 and 3) has been identified as dsRNA sensors with antiviral properties involved in the IFN-I induction in human THP-1 monocyte cells [112]. Also novel cytoplasmic DNA sensors, like Z-DNA binding protein 1 (ZBP1), have been identified in mouse (embryonic) fibroblasts and mice [113]. Additional to IFI16, another pyrin and HIN domain-containing protein (PYHIN) gene family member, absent in melanoma 2 (AIM2), was recognized as dsDNA sensor leading to inflammatory processes in bone-marrow-derived mouse macrophages [114]. Finally, Ku70, a component of a heterodimeric Ku protein, was shown to be a novel cytoplasmic dsDNA sensor inducing IFN in human HEK293 cells [115].

3.3 Cytokines and interferons in human

Cytokines are signaling molecules secreted by cells upon stress that can function in an autocrine, paracrine or endocrine way via binding to dedicated receptors. Many cytokines work in a cooperative manner and can stimulate multiple responses and signaling mechanisms. They represent the interface between innate and adaptive immune mechanisms. The five major classes of cytokines are interleukins (ILs), chemokines, colony-stimulating factors (CSFs), TNFs and IFNs (Table 3) [116].

Table 3: Cytokine groups

Group	Action	Ref
Interleukins	• Regulators of the innate immune system focusing on the differentiation and activation of immune cells • Involved in the host defense mechanisms upon microbial infection • Expressed by large set of cell types and often have a proinflammatory nature	[116]
Chemokines	• Largest class of cytokines, classified into four groups based on initial cysteine groups, namely CXC, CC, C and CXXXC • Chemotactic proteins that regulate migration of mostly immune cells such as their recruitment to sites of infection or disease • Implicated in embryogenesis, immune cell development and cancer metastasis	[117]
CSFs	• Control hematopoietic progenitor cell proliferation and differentiation • Linked to inflammation processes as amplifiers of the signaling cascades	[116]
TNFs	• Proinflammatory activities • Involved in multiple signaling cascades leading to apoptosis, cell proliferation, morphogenesis and differentiation • Name derives from the ability of the first discovered member to reduce tumor growth in mice • TNF-α is an essential part of the host response to many viral infections; produced by different immune cells but can act on any cells due to the ubiquitous expression of TNF-α receptor	[118]
IFNs	• Antiviral, proinflammatory and immunomodulatory activities • more details below	[98]

As key player in the host defense against viruses, I will focus on IFNs in the following sections. IFNs are cytokines with antiviral, proinflammatory and immunomodulatory potencies. Based on conserved structural features, they belong to the class II cytokine family also including IL10-like cytokines such as IL-10/19/20/22/24/26. Through sequence homology they can be categorized into three subclasses, type I, II and III IFNs. Discovered as secreted antiviral molecules, their name derives from their capacity to interfere with viral infections [88,98]. Emerged through gene duplication, the array of IFNs expressed in different vertebrates varies.

Type I IFNs comprise eight classes, IFN-α, β, δ, ε, κ, ω, τ and ζ (limitin), whereas IFN-δ is only found in some ungulates, primarily pigs, IFN-τ in ruminants and IFN-ζ in mice. With the exception of IFN-κ, all genes coding for IFN-I lack introns. INF-α has 13 subtypes in humans and 14 in mice, each of which exhibiting unique activities. Upon viral infection or stimulation with dsRNA, mostly IFN-α and β, as well as the less well defined IFN-ω, are activated. IFN-κ is selectively expressed in human keratinocytes and hormone-regulated. IFN-ε is not induced by PRR signaling but constitutively expressed and its activity is linked to the female reproductive system.

Type II IFN has one single member, IFN-γ, in all jawed vertebrate species. IFN-γ plays an important role in NK and T cell responses. It does not directly participate in the immediate response to viral infection but rather skews the adaptive immune system to promote a cell-mediated response effectively combating the infection. IFN-γ is produced by CD4+ T helper cell type 1 (Th1) lymphocytes, CD8+ cytotoxic lymphocytes and NK as well as NKT cells, B cells, DCs and macrophages [98,119]. Type III IFNs are IFN-λ_1 (IL-28A), IFN-λ_2 (IL-28B) and IFN-λ_3 (IL-29). Recently a fourth IFN-III, IFN-λ_4, has been identified as a pseudogene in human cells [120].

As a potent antiviral defense mechanism, the IFN system can control most viral infections but must also be tightly regulated to not cause pathology itself. Most cell types have the ability to produce IFNs, some immune cells such as pDCs and monocytes, however, secrete very high levels of IFNs after exposure to viruses. The composition and extend of the IFN response varies therefore depending on cell type and pathogens [120].

IFN-Is and IFN-IIIs are induced by similar PAMPs and elicit similar antiviral pathways (Figures 8 and 9). There is, however, a spatial segregation of the two signaling cascades and a difference in kinetics as well as magnitude [88]. In contrast to IFN-I receptors which are ubiquitously expressed by all nucleated cells, IFN-III receptor distribution is limited to epithelial cells, mainly in respiratory, gastrointestinal and reproductive tract. IFN-I response has high potency and is fast but also inflammatory, so it is downregulated rapidly after induction. The IFN-III response, however, is less potent, slower but less inflammatory and therefore causing a more sustained expression of IFN-III. Since epithelial surfaces are the first anatomic barrier encountered by most pathogens when infecting a host, IFN-III can be pictured as the first defense line. Only when the infection cannot be maintained, it is necessary to activate the systemic and more pathogenic IFN-I response. Recent studies show that also neutrophils are highly reactive to IFN-III. Despite similar transcriptomic activities to IFN-I in primary cells or certain tissues, some ISGs might be uniquely stimulated by IFN-III. These differences would, however, require more investigations in biological relevant models [88].

3.4 IFN signaling: the JAK/STAT pathway

All IFN-I signal through a shared heterodimeric receptor: IFN-α receptor 1 and 2 (IFNAR1/2). Two members of the Janus kinase family, tyrosine kinase 2 (TYK2) and Janus kinase 1 (JAK1), are associated to the cytoplasmic tail of IFNAR1 and IFNAR2, respectively (Figure 10) [121]. Interaction of IFN-I with IFNAR1/2 triggers the activation of TYK2, which phosphorylates IFNAR2 and creates a docking site for signal transducers and activators of transcription 2 (STAT2). After binding, STAT2 is also phosphorylated by TYK2 while JAK1 phosphorylates STAT1. Subsequently, the two STAT molecules form a stable heterodimer which interacts with IRF9, forming the ISG factor 3 (ISGF3) complex. ISGF3, whose components are themselves IFN-inducible, translocates to the nucleus, binds to ISRE and leads to the expression of hundreds of ISGs (Figure 10) [121].

IFN-III signal through the IFN-λ receptor (IFNLR), which is composed of IFNLR1 and IL10Rβ (Figure 10). The downstream signaling pathway is shared with IFN-Is, using JAK1 and TYK2 to phosphorylate STAT1 and STAT2, leading to the nuclear translocation of ISGF3 and ISRE activation. IFN-III can also activate JAK2 for phosphorylation [88,99].

IFN-γ binds to its heterodimeric receptor IFN-γ receptor (IFNGR) with its faintly linked parts IFNGR1 and 2. The receptor is associated with JAK1 and 2, but not with TYK2. Upon ligand binding, a phosphorylation cascade is initiated by the JAKs leading to IFNGR1 phosphorylation and subsequent STAT1 binding and phosphorylation. STAT1 disassociates as homodimer, shuttles to the nucleus as GAF and binds to GAS motifs. IFN-γ induction is independent of ISRE and IRF9 [88,99].

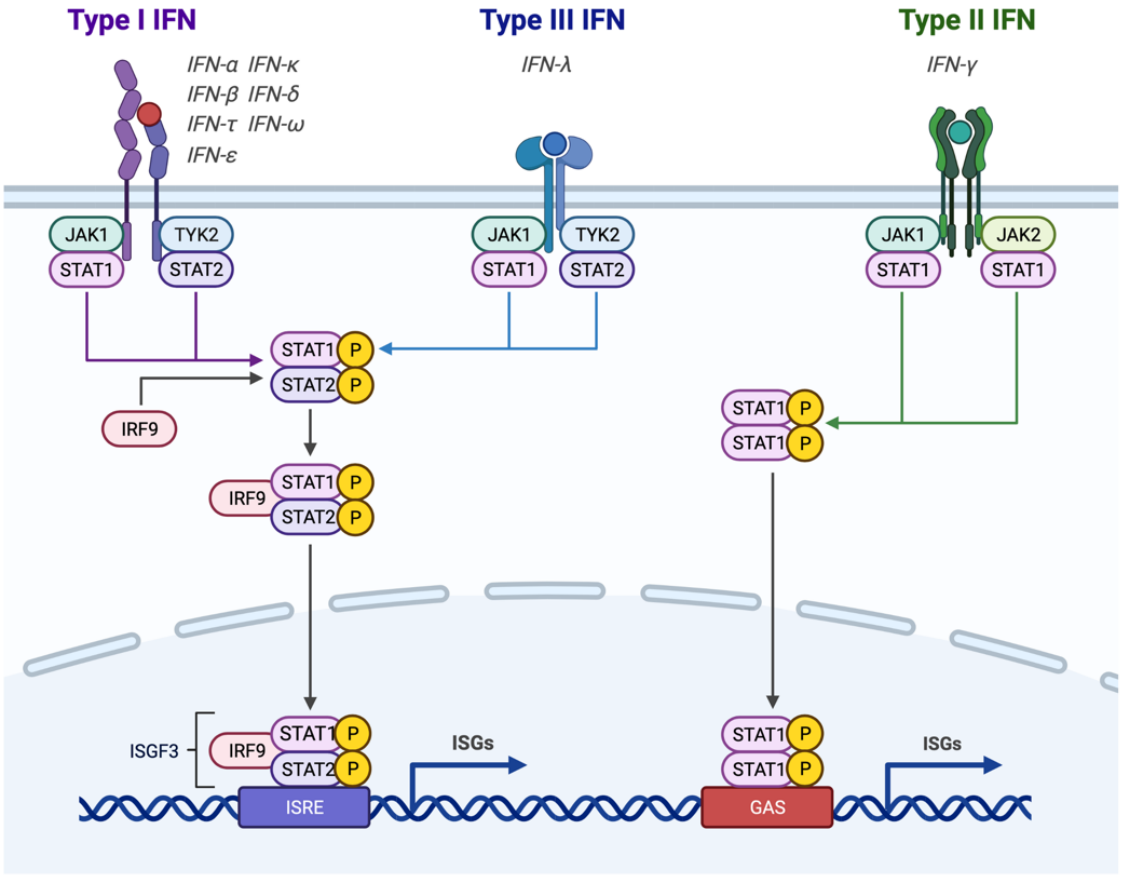

Fig. 10: JAK/STAT signaling pathway. Upon binding of IFN to the corresponding IFNRs, the signaling cascade is activated by heterodimerization and subsequent phosphorylation of STAT1/2 for IFN-I/III and/or homodimerization and phosphorylation of STAT1 for IFN-II. STAT1/2 heterodimer associates with IRF9 and translocated as ISGF3 into nucleus where it binds to IRES and facilitates ISG transcription. STAT1 homodimer translocates directly into the nucleus and binds GAS to activate ISG transcription. Figure created with biorender.com.

3.5 Antiviral interferon-stimulated genes

Following the classical definition of ISGs, this term describes genes which are expressed upon the activation of the JAK/STAT pathway (Figure 10). More recently it has been proposed that this definition could also include genes that are directly activated by ISGF3 or GAF but also genes, which are direct targets of IRFs, NFkB or IL-1 [122]. Some inducers are ISGs themselves, such as IRF1 and IRF7 [123,124]. The exact number of ISGs vary between cell types and depends on the nature of the IFNs. It is generally accepted that at least 300 genes are directly induced by IFNs, some estimations, however, range up to over 10% of the human genome. Moreover, some genes are downregulated upon IFN response [122]. As open-access overview, the database INTERFEROME gathers data of identified and potential ISGs in human and mice [125].

During viral infections, different ISGs target different aspects of the viral life cycle, either directly or through regulations of cell cycle or metabolism. Generally, negative-sense RNA virus replication is less impacted by ISG-mediated functions than positive-sense RNA viruses [122]. Some ISGs interfere with viral attachment and entry, uncoating, shuttling to site of viral replication, viral genome amplification, translation of viral genome, viral assembly and transport towards the cell membranes. While some ISGs are specific to a viral family, others are have broad-spectrum antiviral activities [122]. For example, IFN-induced transmembrane (IFITM) proteins inhibit the fusion between viral and endosomal membranes in the context of infection with numerous unrelated enveloped viruses [126]. During viral genome replication, radical S-adenosyl methionine domain containing 2 (RSAD2)/viperin can facilitate the incorporation of modified nucleotides into newly synthetized viral RNA, which act as chain terminator for viral RNA-dependent RNA polymerase in flaviviridae [127]. One prominent example of ISG that interfere with the budding of numerous enveloped viruses, like DENV, EBOV or human immunodeficiency virus (HIV), is the transmembrane protein bone marrow stromal cell antigen 2 (BST2)/tetherin [128].

A study comparing the transcriptomic changes triggered by IFN stimulation in nine mammalian and one avian species identified 60 conserved vertebrate and 90 conserved mammalian ISGs [129]. The functions of the core vertebrate ISG are linked to antiviral responses, antigen presentation, protein degradation, cell signaling and apoptosis. Few examples of mammalian-core ISGs are well-described antiviral proteins, such as viperin, myxoma resistance protein 1 (MX1), IFITM2/3 and OAS1 [129].

Some ISGs have evolved species-specific antiviral functions [130]. For instance, human MX2 interferes with HIV-1 replication in different human $CD4^+$ cells, whereas canine MX2 cannot [131,132].

Intriguingly, some ISGs exhibit pro-viral properties such as mucolipin-2 (MCOLN2) [133]. It directly aids the replication of several enveloped viruses including IVA, ZIKV and YFV by enhancing their transport within human U-2 OS and A549 cells. The existence of proviral ISGs suggest that some viruses have evolved to hijack these proteins to increase their infectivity [122,133]. Human and several mammalian orthologues of lymphocyte antigen 6 family member E (LY6E) enhance the replication of several RNA viruses form diverse families via increased uptake, uncoating or nuclear trafficking mechanisms [134]. The same protein, however, displays potent antiviral activities against many coronaviruses by inhibiting viral fusion [135].

3.6 Examples of viral evasion mechanisms against innate immune response

Viruses establish successful infection only if they can, at least partially, evade the host antiviral defenses. Co-evolution of viruses and hosts has allowed the formation of complex interaction patterns between host and viral factors that regulate and inhibit the IFN response. This phenomenon of host-pathogen co-evolution is called “molecular arms race”. An equilibrium, however, needs to exist between host and virus adaptations since complete blockage of the IFN system would lead to extinction of host and thereafter also of the virus. This arms race can be evidenced in host genomes and especially in ISGs since they stand under the constant selective pressure to outcompete pathogens. If the ratio of the number of nonsynonymous substitutions to the number of synonymous substitutions per genetic site is greater than one ($dN/dS > 1$), the gene stands by definition under positive selection. In mammalian genomes, certain ISGs depict signatures of positive selection, which evolutionary lead to mutations contributing to species-specific antiviral activities [120,130]. The opposite type of evolutionary pressure on a gene is the so-called purifying selection ($dN/dS << 1$), which conserves the amino acid composition of the encoded protein likely due to functional constrains and indispensable role for cellular mechanisms [136].

Viruses evolved different tactics to counteract the antiviral host defenses since no single strategy seems to be completely efficient. The ability of viruses to circumvent the IFN system contribute to their virulence. Viruses can globally shut-down host protein transcription or translation and certain components of the IFN induction. Additionally, signaling cascades are often targeted. Viruses are also hiding within their replication factories to become less accessible to the detection of PRRs [99,120]. Viral proteins are able to specifically block the activities of antiviral ISGs, interfere with viral RNA processing or dysregulate phosphorylation events by antagonizing host enzymes [120]. For instance, NSP2 of the alphaviruses SINV and CHIKV inhibit STAT signaling in Vero cells [137]. Coronavirus NSP16 exhibits a 2′-O-methyltransferase activity which can autonomously attach a 5′ cap structure to viral mRNAs, mimicking host mRNAs, and thus avoid RLR sensing [138]. Flaviviruses NS5 block STAT1 phosphorylation or target STAT2 for degradation [139]. Viral immune evasion mechanisms can furthermore be species-specific. For instance, the NS1 protein of Influenza B virus (IBV) binds human and non-human primate ISG15, but not mouse or canine orthologues [140]. ZIKV NS2B3 mediates cleavage of human but not mouse STING [141].

3.7 Inflammation and Inflammasome

Exaggerated immune responses leading to severe systemic inflammation are often observed upon viral infection [116]. Inflammation is stimulated when innate immune cells, like macrophages, fibroblasts, mast cells, DCs, monocytes and neutrophils, detect infection or injury through sensing of PAMPS and DAMPS, which lead to activation of NFkB, activator protein 1 (AP1), cAMP response element-binding protein (CREB), emopamil binding protein (c/EBP) and IRF transcription factors [142]. PAMPS and DAMPS sensing can be facilitated by classical PRRs, the inflammasome and/or additional NA sensors. Inflammasomes are large inflammation complexes that activate the protease caspase-1 which subsequently cleaves IL1β and IL18, stimulates cytokine expression and can trigger cell death through pyroptosis [142].

Acute inflammation aims to provide initial immune protection and stimulate the adaptive immune response. After activation, cells release inflammatory cytokines, chemokines as well as adhesion molecules and attract additional innate immune cells, such as leucocytes, which eliminate particles and debris [143,144]. Although the role of inflammation is to resolve infection and injury, increasing evidence indicates that chronic inflammation is a risk factor for cancer [143]. Excessive or uncontrolled release of proinflammatory cytokines and immune cell hyperactivation, which is also called ‘cytokine storm’, is a life-threatening systemic inflammation [116]. Cytokine storms are associated with a wide variety of diseases and can be triggered by various causes such as therapies, autoimmune conditions and viral infections. The exact trigger, clinical presentation and the extend of cytokine storms remain ambiguous and are highly patient- and disease-dependent [116,145].

Interferonopathies are another form of highly pathogenic inflammatory processes [146]. These inherited autoinflammatory diseases are caused by a lack of regulation of IFN signaling. To date, 40 distinct phenotypes have been observed with broadly ranging symptoms [146]. The exact molecular drivers, however, remain to be identified. Upon viral infection and subsequent stimulation of the innate immune system, regulatory processes that help the cells return to homeostasis are key for cell survival. Thus, viral infection of patients displaying an interferonopathy often result in death [146].

4. Bat Innate immune System

Recent findings suggest that a potent antiviral response coupled to an enhanced tolerance towards infection contribute to the ability of bats to asymptomatically host viruses that are pathogenic in other species [147,148].

At first glance, the innate immune system of bats seems similar to that of humans and other mammals since orthologues to many known players of innate immune pathways have been identified in several bat species [149]. For instance, *Pteropus* immunoglobulin heavy chains [150], *CD4* [151], *IFNA/B* [152,153], *IFNG* [154], *IFNL* [155], *STAT1* [156], *IL2, IL4, IL6, IL10, IL12, IL12B, TNFA* [157] and *TLR* genes [157,158] have a high level of sequence homology to their mammalian orthologues. Moreover, humans and bats express similar numbers of innate immune genes. In humans, around 7% of total genes are involved in immune mechanisms [159]. Whole genome studies in *Pteropus alecto, Artibeus jamaicensis* and *Rousettus aegyptiacus* identified around 500 immune genes, which corresponds to around 3% of all transcribed genes. These genes code for proteins involved in T and B cell activation, NK cell cytotoxicity, cytokine production, TLR signaling and antigen presentation [160–162].

Some subtle differences, which are described below, might, however, aid bats to sustain viral infections. Nonetheless, attention must be paid with generalizing the findings for all bat species since differences can be observed between single bat species, even within a family. Even though increasing effort into studying the immune responses of a broader variety of bat species have been made in the past years, results are still sparse and highly biased towards *pteropodid* bats. Thus, it is important to point out that different bat species have evolved various strategies to support viral infections and only some mechanisms can be extrapolated to the entire chiropteran order. Such specificities have been recently highlighted in a study describing the species-specific ability of PKR to counteract poxvirus K3 proteins in diverse bat species [163].

4.1 General characteristics of bat immune features

Comparative genomic analysis of six distantly related bat genomes from the species *Myotis myotis*, *Pipistrellus kuhlii*, *Rhinolophus ferrumequinum*, *Phyllostomus discolor*, *Rousettus aegyptiacus* and *Molossus molossus* suggest that certain immunomodulatory mechanisms had evolved in the genome of the last common chiropteran ancestor, before the order separated into families 60 million year ago, indicating an ancestral tolerance towards

pathogens [71]. Other genomic studies investigating the evolutionary adaptations of bats confirmed that positive selection of immune-related genes is a conserved pattern. Thirty-two *Artibeus jamaicensis* genes, which are mainly involved in transcriptional activation and regulation processes, are positively selected [161]. Evidence for positive selection could also be found within IFN response genes, including *TLR7, REL, TBK1, IFNG, ISG15* and *RIGI,* in *P. alecto* and *M. davidii* genomes [49]. Multiple immune genes under positive selection were identified in the ancestral bat genome, mainly involved in NFκB signaling (*INAVA, IL17D* or *IL1B*) and anti-pathogenic responses (*LCN2* and *GP2*). Moreover, these comparative genomics studies revealed that ten immune genes were inactivated in all six bat species, but not in most other mammals. Two of these genes (*LRRC70* and *IL36G*) relate to NFκB signaling, suggesting that altered NFκB pathways might contribute to immune-related adaptations in bats [71]. Finally, multiple lineage-specific expansions of *APOBEC3*-type genes, that encode IFN inducible NA editing enzymes implicated in viral restriction, were identified. For instance, 14 duplication events and the development of a second *APOBEC3* locus exists in *Myotis* bats [71].

Genomic integrations of diverse viruses were also revealed by these bat genomics studies [71], suggesting historical tolerance to viral infection in bats.

4.2 Bat IFNs and antiviral function

4.2.1 IFN genes and regulation of expression

While the most expanded IFN-I gene family is generally *IFNA* in mammals, in several bat species, especially *pteropodid* bats, this genomic locus seems to be contracted [152,164] [165] and even absent in *Myotis* bats [152,166]. No general rule can be drawn for *IFNB* genes in bats. In *Rhinolophus affinis* and *R. sinicus, IFNB* genes show high sequence similarity to human *IFNB* while *Rousettus leschenaultii IFNB* is most similar in sequence to the pig orthologue [153]. In contrast to *IFNA genes*, the *IFNW* family, which consist of one unique gene in humans, mice and pigs, is largely expanded in several bat species with up to 22 functional subtypes in *Rousettus aegyptiacus* bats [152,167]. Of note, only cattle is also known to also have a similar gene expansion in this locus since they encode 24 *IFNW* subtypes [168]. Similarly, the *IFND* gene family, which is absent in most mammals, is expanded in multiple bats species (Table 4) [152,164,167].

Various positions of IRF and NFκB binding elements in *IFNK* and *IFNW* promotor regions indicate that these IFNs might be differentially regulated in *E. serotinus* bats than in other

mammals [169]. Several *IFNA* and *IFND* pseudogenes found in several bat species indicate a contraction from a larger gene family in the ancestral bat genome [152,164,169].

Table 4: Numbers of IFN-I genes in bat species compared to human (psg stands for pseudogenes)

	IFNA	***IFNB***	***IFND***	***IFNE***	***IFNK***	***IFNW***
Human	13	1	0	1	1	1
Pteropus alecto [164]	3 (8 psg)	1	N/A	1	1	5
Pteropus vampyrus [152]	7	1	5 (7 psg)	1	1	18 (8 psg)
Rousettus aegyptiacus [167]	12	1	9	1	1	22
Dobsonia viridis [165]	8 (1 psg)	N/A	N/A	N/A	N/A	N/A
Myotis lucifungus [152]	0 (2 psg)	1	11 (3 psg)	2	2	12 (7 psg)
Myotis daubentoniid [166]	0	N/A	N/A	N/A	N/A	N/A
Eptesicus serotinus [169]	N/A	N/A	NA/	N/A	1	1
Eptesicus fuscus [170]	0	N/A	N/A	NA/	N/A	N/A

Besides the different composition of IFN-I genes in multiple bat species, several reports described an elevated basal expression of IFN-I and/or ISGs in tissues and cells of various bats (Table 5). This is especially true in the *Pteropodidae* family, for instance in kidney and fibroblast cells of *Pteropus spp*. bats. Both IFN mRNA and IFN-α protein basal levels were elevated in *Pteropus rodricensis* and *Pteropus lylei* serum samples [171]. IFN-α protein levels were elevated in *Rousettus aegyptiacus* serum samples but no basal mRNA expression was found in kidney cells [171].

Table 5: Constitutive expression of IFNs of ISGs in bat tissues and cells

Pteropus alecto	• IFN-α, most abundantly IFN-α3, constitutively expressed across tissues (wing, testes, thymus, spleen, small intestine, salivary gland, lymph node, lung, liver, kidney, heart, brain); mainly IFN-α3 and IFN-α2, IFN-α1 to a lesser extent [164] • Basal IFN-α expression in kidney cells regulates ISG-subset involved in antiviral activity, like BST2, MX1 and OAS3 [164] • Basal IFN-α expression in primary lung, liver, heart, kidney, small intestine, brain, fetus, salivary gland and muscle cells [164] • Basal IFN-β expression only found in testes, no other tissue [164] • Elevated basal ISG expression levels in kidney cells [172] • Basal IFN-I (particularly IFNω2) expressed in kidney cells [173] • Elevated ISG expression in spleen including WARS, SERPINE1, MT2A, SLC16A1, IFI6, TAP2, TMP1, IFITM3, SERPING1 and PNRC1 [173]
Pteropus rodricensis	• Elevated IFN-α protein levels in blood plasma and constitutive expression of IFN-α mRNA in whole blood [171]
Pteropus lylei	• Elevated IFN-α protein levels in blood plasma and constitutive expression of IFN-α mRNA in whole blood [171]
Pteropus vampyrus	• Elevated basal ISG expression levels in primary skin fibroblasts and kidney cells [174] [175]
Pteropus dasymallus	• Elevated basal expression of MDA5 and minimally TLR3 in kidney cells [176]
Rousettus leschenaultii	• Elevated IFN-α protein levels in blood plasma but no IFN-α mRNA expression found in whole blood [171] • Elevated basal expression of MDA5 and TLR3 in kidney cells [176]
Rousettus aegyptiacus	• No basal IFN-α expression in kidney nor primary kidney cells [177] [153] • Very low basal IFN-β expression across tissues (bone, brain, heart, kidney, liver, lung, lymph node, ovary, PBMC, spleen and testes) [162] • Basal OAS3 expression in kidney cells [178]
Cynopterus brachyotis	• IFN-α constitutively expressed across tissues (small intestine, brain, kidney, lung spleen) [164]
Myotis daubentonii	• No unusually high baseline levels of IFNs in kidney cells [166]
Myotis lucifugus	• Elevated basal ISG expression levels in (primary) skin fibroblasts except OAS3 [174] [178] • No basal expression of OAS2/3 in embryonic fibroblasts [178]
Myotis velifer	• No basal expression of OAS2/3 in embryonic fibroblasts [178]
Rhinolophus sinicus	• IFN α, β, ω, and γ highly expressed in spleen and white adipose tissue [179]
Rhinolophus ferrumequinum	• Elevated basal expression of RIG-I, MDA5 and TLR3 in kidney cells [176]
Eidolon helvum	• Undetectable IFN-α protein levels in blood plasma but constitutive expression of IFN-α mRNA in whole blood [171]
Tadarida brasiliensis	• No basal IFN-α expression in lung cells [153]
Desmodus rotundus	• no basal expression of IFN-α1 or IFN-β in fetal lung cells [180]
Miniopterus fuliginosus	• Elevated basal expression of RIG-I, MDA5 and TLR3 in kidney cells [176]
Eptesicus fuscus	• No basal IFN-β but elevated basal ISG expression in kidney cells [181] • Basal expression of OAS2/3 in skin fibroblasts [178]
Eptesicus nilssonii	• No basal IFN-β but elevated basal ISG expression in kidney cells [181]

Only few studies have been conducted to characterize IFN-II or IFN-III genes in bats. While *P. vampyrus* expresses three IFN-λ subtypes, only two have been identified in the *P. alecto* genome [155]. *P. alecto* IFN-λ have similar antiviral properties than other mammalian type I and III IFNs and induce ISGs [155]. The bat IFNλR complex has a broad tissue distribution in *Pteropus alecto* bats and both epithelial and immune cells respond to IFN-λ treatment [182]. In contrast to other mammals, *IFNG2* was identified in addition to *IFNG1* in *Rousettus aegyptiacus* genome [162].

4.2.2 IFN induction via ligand stimulation

To evaluate the functionality and characterize the basic nature of innate immune responses in bat cell lines, stimulation studies have been performed with the dsRNA ligand, Poly I:C, or universal IFN-α. In general, bat cell lines responded in a similar way than other mammalian cells to these stimuli, with upregulation of IFN-β and ISG expression (Table 6). Some interesting differences could however be observed. Poly I:C challenge of human primary lung fibroblasts resulted in the upregulation of IFN-β, RIG-I, TLR3, TNFα and IL-6, whereas only MDA5 and IFN-β were stimulated in *Rhinolophus sinicus* primary lung fibroblasts [179]. Furthermore, an intricate early and late response pattern could be observed upon Poly I:C stimulation in *Desmodus rotundus* fetal lung cells. Early up-regulation (6-24h) of IFNβ, TLR3, RIG-I, MDA5 and LGP2, followed by a second induction round (24-72h) of IFNα1, TLR7, 8 and 9 was recorded [180].

Table 6: Bat cell response to extrinsic stimulation with Poly I:C or universal IFN-α.

Cell line	Stimulation	Response	Ref
P. alecto primary lung, liver, heart, kidney, small intestine, brain, fetus, salivary gland and muscle cells	Poly I:C	Upregulated IFN-β but unchanged high IFN-α levels	[164]
P. alecto kidney cells	Poly I:C	Induced expression of IFN-β and all three RLRs [73]	[73]
R. aegyptiacus primary kidney cells	Poly I:C	Abundance of IFN-β mRNA, but not IFN-α mRNA	[153]
T. brasiliensis lung cells	Poly I:C	No change in IFN-α nor IFN-β expression	[153]
Desmodus rotundus fetal lung cells	Poly I:C	Upregulation of IFNβ, TLR3, RIG-I, MDA5 and LGP2 (early) and IFNα1, TLR7, 8 and 9 (late)	[180]
Eptesicus fuscus kidney cells	Poly I:C or univ IFN- α	Upregulation of IFN-β and classic ISGs	[181]
Eptesicus nilssonii kidney cells	Poly I:C or univ IFN- α	Upregulation of IFN-β and classic ISGs	[181]
Rhinolophus sinicus splenocytes	Poly I:C	Upregulation of IFN-β to extreme high levels	[183]
Rhinolophus sinicus primary lung fibroblasts	Poly I:C	Upregulation of MDA5 and IFN-β	[179]
Rhinolophus affinis embryonic fibroblasts	Poly I:C	Upregulation of IFN-β to extreme high levels	[183]

4.3 Immune sensing and signaling

4.3.1 PRR expression and sensing

RLRs are expressed in bats from the *Pteropus* and *Myotis* families [73,162,184]. In *P. alecto*, they display similar primary structures and tissue expression patterns than in other mammals. The genomic loci of *RIGI* and *LGP2*, however, are noticeable smaller than human ones [73]. Interestingly, the amino acid sequence of *P. alecto MDA5* is evolutionary closely related to horses [185]. *Rhinolophus affinis* and *R. sinicus RIGI* and *STAT1* showed great sequence similarity to human, mouse, pig and rhesus monkey, and the expression pattern of these genes was similar to their orthologues in mice [183]. *Tadarida brasiliensis MDA5* is evolutionary related to human, pig and horse *MDA5,* but has low sequence similarity to other bat species, suggesting a poor conservation among bats. Moreover, infections of *Tadarida brasiliensis* lung cells with VSV, New Castle Disease virus (NDV) and IAV emphasize an important role of MDA5 in restricting RNA virus infections [186]. Only two NLRs, *NLRC5* and *NLRP3*, both involved in antiviral immunity, could be identified in *P. alecto* genome [160].

Expression of TLRs, especially those involved in viral NA recognition in human cells, have been described in many bat species such as *Pteropus spp., Myotis spp., Rhinolophus spp., Rousettus leschenaultii*, *Desmodus rotundus* and *Eptesicus fuscus* [161,187–190]. Similarly to humans, sheep, cows and pigs, *P. alecto* express ten functional TLR genes (TLR1-10) and one TLR13-like pseudogene [187], whereas *Rousettus aegyptiacus* only express TLR1 to TLR9. [162] *P. alecto* TLRs 7, 8 and 9 have similar tissue expression patterns than humans and seem to be mainly expressed from professional immune cells, as in other mammals [158]. While predominantly expressed by DCs in mice and humans, high levels of *P. alecto* TLR3 have been identified in liver [158]. In *E. fuscus* kidney cells, synthetic dsRNA seems to be primarily recognized through TLR3 with a potential additional role of RIG-I [191].

Comparing the sequence of NA-sensing TLRs 3, 7, 8 and 9 of *Desmodus rotundus* with eight other bats species belonging to three families (*Pteropodidae*, *Vespertilionidae* and *Phyllostomidae*) revealed that chiropteran TLRs harbor unique mutations within their ligand-binding sites, suggesting a positive selection [188]. Diversification appeared to be lineage-specific and occurring at different taxonomic levels, indicating long-term adaptation of bat species to different environment and pathogens [188]. The highest level of positive selection was identified in *TLR9*, followed by *TLR8* and *TLR7*. All selected sites

were located in the leucine-rich repeat (LRR) domain, suggesting a role in pathogen recognition [189]. Similarly, analysis of 21 bat genomes showed that the ligand-binding ectodomain of TLR8 evolved under positive selection. *TLR8* displays extensive sequence variation within bats and exhibits unique features that separates bat TLR8s from humans and other mammals [190].

In general, high basal expression levels of TLR3, RIG-I and MDA5 have been detected in several bat species, including *R. leschenaultia*, *Rhinolophus affinis* and *Rhinolophus sinicus* tissues as well as *Desmodus rotundus* fetal lung cells [179,180,183,187]. Particularly high levels of RIG-I and STAT-1 could be detected by reverse transcription (RT)-qPCR approaches in 3 *Rhinolophus affinis* spleens [183]. TLR3 and 8 were also highly expressed in *Rhinolophus sinicus* lung cells and together with TLR7 and TLR9 in intestine, spleen and white adipose tissue [179]. Functional studies using knockdown approaches via antisense RNA oligonucleotides (ASOs) in *Rhinolophus ferrumequinum* kidney cells have revealed that TLR3, RIG-I and MDA5 contribute to antiviral response against EMCV and JEV [176].

4.3.2 IRF signaling

Unlike human IFR7*, P. alecto* IRF7 has an atypically broad tissue distribution across both immune and non-immune cells [173][192]. It also displays unique nucleotide substitutions in the MyD88 binding domain, which neither influence its binding ability nor its capacity to activate the IFN response [192]. Moreover, it is strongly induced by Poly I:C stimulation in *P. alecto* lung cells [192]. In *P. alecto* kidney cells only IRF1 is induced by Poly I:C but IRF1/7 are induced by IFN-a stimulation [173].

IRF1 and IRF3 basal levels are also elevated in most *P. alecto* tissues, except the heart [173,192]. Similarly, high levels of IRF7 were observed in spleen, white adipose tissue and lung of *Rhinolophus sinicus* [179]. In contrast, most non-immune cells in other mammals express minimal IRF7 and rely on IRF3 for antiviral signaling [173].

Knocking-out the expression of *IRF1* and *IRF7* via CRISPR-Cas9 approaches in *P. alecto* cells revealed that each IRF alters the kinetics of ISG expression and directly regulates a distinct subset of ISGs [173]. Numerous ISGs known to have antiviral activities in human cells were upregulated by IRF1 and 7, including *IFIT2, IFIT1, UBA7, PARP10, OAS3, OAS2, RTP4*, *BST2*, *MX1/2, IFIH1,* and *IFNL1* [173]. Genes such as *PARP15, TRANK1, ZBP1* and *APOBEC3BL* were regulated by IRF7 in an IFN-independent manner [173]. In

response to HSV-1 infection, *P. alecto* kidney cells require IRF1, but not IRF3 or 7, to restrict viral replication [173]. All three IRFs are required for ISG induction during MERS-CoV infection and reduction of viral load during IAV infection. After Pteropine orthoreovirus (PRV3M) infection, *P. alecto* kidney cells with intact IRF3 and IFNAR2 still required IRF7 to mount a full response, indicating additional antiviral functions of the widely distributed IRF7 [173]. These findings are in line with a previous study reporting that IFNAR2 is mandatory for IFN-α signaling in *P. alecto* kidney cells. A basal antiviral state, however, is maintained independently of IFNAR2 expression, suggesting that ISG expression does not exclusively rely on canonical IFN signaling [193].

Furthermore, a serine residue in IRF3 (S185) is positively selected for in multiple bat species, including *Pteropus spp., Myotis spp, Rhinolophus sinicus* and *Eptesicus fuscus* [194]. Replacing the serine residue in batIRF3 with the human leucine residue decreased antiviral protection in *E. fuscus* and *P. alecto* kidney cells, whereas the addition of this serine residue in humanIRF3 significantly enhanced antiviral protection in human cells [194]. Decreased baseline ISG expression in IRF3-L185 expressing *E. fuscus* cells suggests that S185 may contribute to the constitutive expression of IFNs and associated antiviral protection. A similar response in unstimulated *P. alecto* cells, however, could not be observed, highlighting again the species diversity of bats [194]. *E. fuscus* IRF3 seems to have evolved from a common ancestor for bats and felines and this bat/feline IRF3 sequence possibly from a common ancestor shared with camels. Persistent coronavirus infections have been identified in bats and cats, questioning the role played by IRF3 in viral persistence [170].

4.4 IFN response to experimental viral infections in bat cells

Several infection studies with diverse virus families have been conducted in multiple bat cell lines to better understand the chiropteran antiviral mechanisms. Classic responses like IFN-I and ISG upregulation upon infection have been observed for instance in *Rhinolophus spp.* fibroblasts and spleenocytes or *T. brasiliensis* lung cells infected with VSV [179,183,186]. Interesting results were obtained when infecting *Pteropus alecto* or *P. vampyrus* kidney, lung and fetal cells NiV and HeV. They failed to mount an IFN response upon infection [164,175,195]. Knowing that *Pteropus* bats are reservoir of these viruses, these results suggest an IFN-independent control mechanism [195]. The upregulation of TNF-related apoptosis inducing ligand (TRAIL)-mediated apoptosis via NFκB signaling

was identified as alternative antiviral mechanism in HeV infected *P. alecto* kidney cells [196]. Similarly, infection of *P. alecto* splenocytes with other bat-specific viruses, such as the paramyxovirus Tioman virus, resulted only in the upregulation of IFN-III, not IFN-I [155]. In *Rousettus leschenaultii* and *R. ferrumequinum* kidney cells infected with PRV50G resulted in minimal induction of IFN-I response, too [185]. Contrasting observations could be made in other bat cells infected with bat-borne corona- or filoviruses. For instance, *Eptesicus fuscus* kidney cells mount a strong IFN-I response upon MERS-CoV infection, while it was blocked in human cells [170]. *Rousettus aegyptiacus* fetus body and kidney cells also mount a strong IFN response to EBOV and especially MARV, in contrast to a highly variable response in different human cells. Interestingly, transfection of human cells with *Rousettus* IFN-α and IFN-β did not inhibit viral replication, although it resulted in upregulation of ISG expression, emphasizing species-specific antiviral effects of bat IFNs [177].

Flavivirus infections of bat cells from ten different species, including some known to be implicated in the their transmission cycle [197], showed overall limited permissivity to JEV [176] and ambiguous results for DENV with permissive [198] and resistant cell lines [199]. Intriguingly, DENV2 infections of *Pteropus alecto* kidney cells did not result in induction of IFN or ISGs and even inhibited the transcription of *BST2, OAS2, CXCL10, RSAD2* and *IFIT3.* Possible co-evolution of the DENV2 with old-world fruit bats as an transient host could have facilitated this dampening of the IFN response [198].

Finally, antiviral potencies were discovered for less-well characterized IFNs, such as IFN-ω, κ or γ. IFN-γ displayed antiviral activity in *P. alecto* kidney and *T. brasiliensis* lung cells infected with SFV, as well as in *P. alecto* kidney cells infected with HeV [154]. IFN-ω4 was induced after VSV infection in *R. aegyptiacus* kidney cells and displayed antiviral activity even though less potently than IFN-β [167]. IFN-ω4 may induces a unique ISG pattern with virus-specific antiviral activities [167]. Strong activation of IFN signaling by *Eptesicus serotinus* IFN-ω, and slightly weaker by IFN-κ, could be observed *E. serotinus* brain cells and both IFNs inhibited lyssavirus replication [169].

4.5 Bat ISGs and unique antiviral mechanisms

4.5.1 Global ISG expression patterns in bat cells

P. alecto MX1, OAS1 and *PKR* are highly conserved in their functional and promotor domains compared with other mammals. Expression of *MX1* and *OAS1,* but not *PKR,* were upregulated in *P. alecto* kidney cells upon IFN-α treatment or infection with Sendai virus (SeV) and PRV1NB [200]. *P. alecto OAS1* has one additional ISRE motif in its promotor compared to humans, which might explain why *OAS1* was the most inducible ISG following IFN stimulation or viral infection [200]. *Rousettus aegyptiacus* genome contained two OAS-like (*OASL1/2*) and three IFN-α inducible *OAS* genes (*OAS1-3*) [178]. Overall, ISGs in IFN-α stimulated *P. alecto* kidney cells followed two temporal clusters with similar early kinetics but different declining patterns indicating a tighter regulatory mechanism compared to human ISGs, which remained upregulated for prolonged period [172]. Additionally, *P. alecto* kidney cells seem to share with other mammals some mechanisms to negatively regulate the IFN response, since suppressor of cytokine signaling 1 (SOCS1) and ubiquitin specific peptidase 18 (USP18) were highly induced upon IFN-α3 stimulation [193].

By comparing available genomic data, duplications of MX1 and tetherin/BST2 could be identified in the *Vespertilionidae* bat family. *Myotis lucifugus* encode three copies of MX1 and four copies of tetherin, which is more than any other mammal. Moreover, *Myotis brandtii* and *M. davidii,* as well as *Eptesicus fuscus,* harbor several copies of the *BST2* gene, whereas *Miniopterus natalensis* of the family *Miniopteridae* seems to have only one copy. Three tetherin paralogs could also be identified in the *M. daubentonii* kidney cells [166]. *Epomops buettikoferi* and *Hypsignathus monstrosus* tetherins only display 46% sequence homology to their human counterpart [201].

Few transcriptomic studies have been conducted in bat cells to decipher the IFN response and ISG patterns in stimulated bat cells. Comparing the response of IFN-α stimulated primary skin fibroblasts from *Myotis lucifugus* and *Pteropus vampyrus* bats with seven other mammalian species, revealed a relatively conserved overall pattern. Ninety core ISGs were identified amongst all mammals and 15 common ISGs were upregulated in the two bat species. Around 290 ISGs were specific to *P. vampyrus* and 145 to M. *lucifugus* [174]. When comparing the ISG expression profiles of Poly I:C stimulated *Eptesicus fuscus* and *Eptesicus nilssonii* kidney cells with human epithelial cells, 127 ISGs were specific to *Eptesicus* cells and mainly involved in IFN-γ and NFκB signaling. Additionally, 66 ISGs

were unique to *E. fuscus* and 309 to *E. nilssonii* [181]. In IFN-α3 stimulated *P. alecto* kidney cells 578 ISGs could be identified and 160 of these genes seem to be *P. alecto*-specific, including *SLC13A3, RAB19, APAF1* and *RNASEL*. Atypical amongst mammals, 60% of these specific ISGs were enriched in cancer pathways [193]. Transcriptomic studies of IFN-α stimulated *Pteropus alecto* kidney cells revealed around 100 ISGs at 4, 8 h, 12 and 24 h post-treatment, including previously undescribed ISGs (*EMC2, FILIP1, IL17RC, OTOGL, SLC10A2* and *SLC24A1)* [172]. Moreover, while not an ISG in human cells, the ribonuclease L gene (*RNASEL)* was identified as highly IFN-inducible in *P. alecto* cells [172]. IFN-α treatment triggered the upregulation of 196 and 106 ISGs, at 6h and 24h respectively, in *Myotis daubentonii* kidney cells, including poorly characterized ISGs, such as *CSF2, NEURL3, BCL2L14, RNF213, ESIP1* and *PLA1A* [166].

4.5.2 Antiviral function of some conserved ISGs in bat cells

Several functional studies investigating well-studied mammalian ISGs have been conducted in bat cells. While human, mouse or primate tetherins were efficiently antagonized by EBOV glycoproteins in a virus-like particle (VLP) release assay in human HEK293T cells, *Hypsignathus monstrosus* and *Epomops buettikoferi* tetherins were not, and are therefore more potent antiviral effectors against EBOV infection [201]. Additionally, endogenous tetherin in *E. buettikoferi* kidney cells is essential for efficient IFN-mediated inhibition of NiV and VSV infections as siRNA knockdown studies revealed [201].

While not an ISG in human cells, *RNASEL* was identified as highly IFN inducible in *P. alecto* cells [172,193], *Myotis daubentonii* kidney cells [166], and in skin fibroblasts of six other mammals [174]. By contrast, RNASEL was not upregulated in *R. aegyptiacus* kidney cells stimulated with IFN-α treatment but continuously expressed, as in human cells [178]. Its antiviral activity against Sindbis virus (SINV) and Vaccinia virus (VACV) was MAVS-independent and primarily relied on OAS3 signaling in *R. aegyptiacus* kidney cells. Since OAS3 was basally expressed in unstimulated cells, the antiviral OAS-RNASEL pathway might thus be an immediate response pathway upon dsRNA sensing, rather than reliant on previous IFN signaling, in *R. aegyptiacus* kidney cells [178].

Bat MX1 proteins cloned from six bat cell lines (*Carollia perspicillata* lung, *Myotis daubentoniid* kidney, *Pipistrellus pipistrellus* kidney, *Eidolon helvum* kidney, *Hypsignathus monstrosus* kidney and *Rousettus aegyptiacus* kidney) belonging to three bat

families (*Pteropodidae*, *Phyllostomidae* and *Vespertilionidae*) exhibited around 80% sequence identity between the lineages. These six bat MX1s significantly inhibited viral polymerase activity of EBOV, VSV, RVFV and Influenza-A-like viruses using wild-type or reporter viruses when overexpressed in HEK293T cells [202]. This qualifies bat MX1s as broad antiviral effectors. Polymerase activity of tick-transmitted Thogoto virus (THOV), however, which is not known to infect bats, was not blocked by bat MX1 [202]. In contrast, it was extremely sensitive to human and murine MX1 indicating a lack of evolutionary relationship between bats and THOV. Positive selection patterns in all bat *MX1* genes could be observed and indicate species-specific antiviral activities of these proteins [202].

A positive selection analysis of *PKR* genes from 33 bat species revealed a strong diversifying selection and gene duplication events. *Eptesicus fuscus*-borne Eptesipox virus (EPTV), VACV and variola virus (VARV) K3 proteins were counteracted by PKR in a species-specific manner. EPTV K3, in contrast to other orthopoxviruses, displayed a C-terminal insertion which might represent an evolutionary adaptation to maintain PKR antagonism. The adaptive changes in *PKR* of some bat species allowed for enhanced antiviral function, supporting the hypothesis of efficient viral control in bats [163].

In an overexpression screen of conducted with a *P. alecto* cDNA library enriched for antiviral ISGs, RTP4 was identified as the most potent antiviral effector against several *flaviviridae* including HCV, ZIKV, DENV and the bat-borne Entebbe bat virus (ENTV) [203]. Comparing diverse mammalian orthologs of *RTP4* for their ability to inhibit flaviviruses revealed a complex species- and virus-specific pattern. *Rousettus aegyptiacus* bat, *Tadarida brasiliensis* bat, dog and cow *RTP4s* displayed a slightly less but still potent activity against all tested flaviviruses. In contrast, human *RTP4* barely inhibited flavivirus infection, except for ENTV. *P. alecto* and human *RTP4* only share 58% sequence homology [203]. Specific viral antagonism mechanisms could also be observed. *E. helvum* and *R. aegyptiacus* kidney cells showed particularly efficient induction of *MX1* mRNA, the production of the encoded protein, however, was antagonized by the mosquito-borne alphavirus, O'nyong nyong virus (ONNV), in those bat cells to a larger extent than in cells from rodents or primates [204].

NDV infection of *Pteropus vampyrus* kidney cells resulted in 306 upregulated genes including six genes not previously identified as ISGs (*CHAC1, MORC3, PPP1R15A, RND1, SERTAD1* and *NEURL1B*). Further characterization of *RND1* revealed that is was IFN-α inducible in *P. vampyrus* cells but not in *Eidolon helvum* kidney cells, *Epomops*

buettikoferi kidney cells, *Rousettus aegyptiacus* kidney cells, *Myotis velifer incautus* interscapular cells, nor human cells and thus a *P. vampyrus*-specific ISG [175].

4.6 Dampened inflammatory mechanisms in bats

Differenced in the innate immune system of bats compared to other mammals lay not only within the antiviral IFN system but also in the inflammation response. Bats seem to be able to regulate inflammatory pathways better than any other mammal, suggesting that they have a higher tolerance to infection or disease [147].

First, a complete genomic loss of the cytoplasmic dsDNA sensor *AIM2,* which mediates signaling via caspase-1 triggering IL-1β cleavage and finally pyroptotic cell death, has been observed in *Pteropus alecto* and *Myotis davidii* genomes [205]. A larger genomic study including 10 bat genomes covering the entire chiropteran order showed that, apart from *Pteronotus parnellii* which encode a truncated version of *AIM2*, bats seem to have lost the *PYHIN* gene family [206]. These genes encode DNA sensors activating the inflammasome. Divergence of the *PYHIN* genomic loci between different bat families suggests various evolutionary events, all resulting in the loss of *PYHIN* genes [206]. Furthermore, dampened inflammatory responses after infection with IAV, PRV3M and MERS-CoV in primary *P. alecto* immune cells could be observed. The inflammasome sensor NLR family pyrin domain containing 3 (NLRP3) is significantly less activated in *Pteropus alecto* primary immune cells than in human or mouse cells [78]. Genomes of *P. alecto* and *M. davidii* encode an unique splice variant and modified leucine-rich repeat domains of NLRP3 [78], which could explain its reduced activation. The S358 residue of mammalian STING is not maintained in the genomic sequence of 30 bat species. Since S358 phosphorylation is essential for IFN activation and only mammalian STING was able to efficiently block HSV-1 replication, bat STING might be less potent to induce IFN signaling [207]. The evolutionary explanation for displaying altered DNA sensing pathways could be linked to the energetic requirements during powered flight, which cause DNA damage, lead to the release of self-DNA in the cytoplasm and subsequently initiate inflammation.

Bats have also evolved downstream mechanisms to regulate inflammatory pathways and consequently reduce probable immune mediated tissue damage. For instance, an overall complementary mechanism with high caspase-1 activity balanced by reduced IL-1β cleavability, and *vice versa*, result in controlled inflammatory signaling across *P. alecto*,

M. davidii and *E. spelaea* cells [205]. At least three species of bats (*E. fuscus*, *M. davidii* and *M. natalensis)* express c-Rel, a suppressor of gene expression and c-Rel binding sites in the promotor region of the *TNFA* gene, reducing its stimulation [191]. In contrast to stimulated mouse macrophages, induction of nitric oxide (NO), potentially causative of oxidative tissue damage, is absent *Myotis myotis* macrophages [208]. A persistent stimulation of anti-inflammatory IL-10 could also be observed [208]. Finally, genes involved in regulation of inflammation pathways, like *DAZAP2, SUMO2, CTSL, PSMA6* and *HMOX1*, show elevated expression in *Rhinolophus sinicu*s lung tissues [179].

All main innate immune features of bats described in this chapter are summarized and visualized in Figure 11.

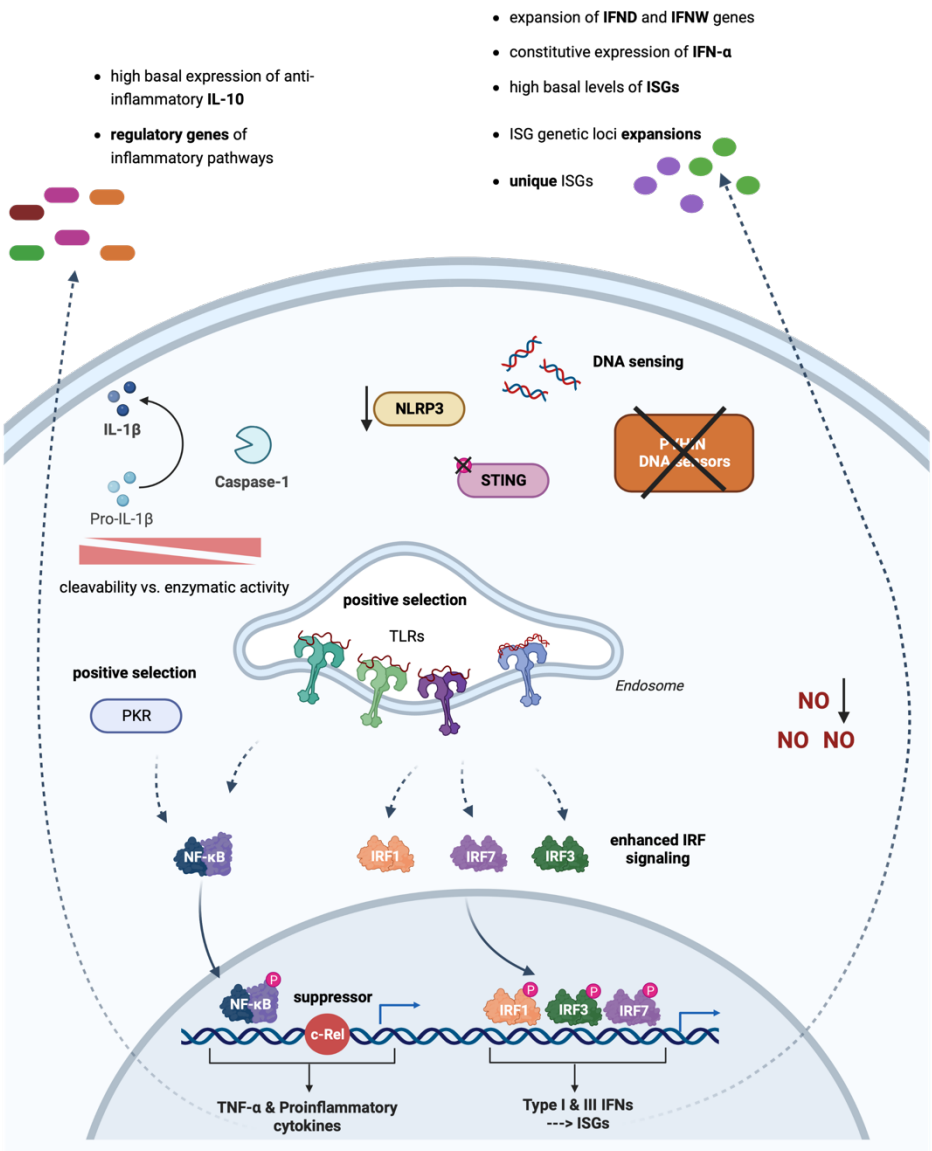

Fig. 11. Characteristics of bat innate immune response displaying enhanced antiviral and dampened inflammatory response. Potent antiviral mechanisms are in place within the innate immune system of bats. Positive selection of NA sensors such as *TLR* and *PKR* genes might lead to optimized recognition of viruses and optimized induction of antiviral signaling pathways. Enhanced and diversified IRF signaling can be observed in bats leading to a stronger induction of IFN responses. Several bat species display an expansion of the genomic loci for IFN-ω and IFN-δ. Constitutive expression of IFN-α and certain ISGs can also be observed. Some ISGs with known antiviral function underwent duplication and genetic expansion events in the *Chiroptera* order. Bats also harbor a set of unique ISGs not previously described in other species. Enhanced tolerance to viral infection might be facilitated by several mechanism which dampen the inflammatory response in bats. Cytosolic DNA sensing is severely downregulated in bats through the evolutionary loss of the PYHIN gene family of DNA sensors, a mutation at a crucial phosphorylation site of STING and less active NLRP3. The *TNFA* gene of several bat species harbors a c-Rel suppressor binding site inhibiting the protein expression. Severely reduced levels of NO could be observed in bat cells. High caspase-1 activity is balanced by reduced cleavability of IL-1β and vice versa, hampering with the induction of pyroptotic cell death induction. Finally, several regulatory genes of inflammatory pathways and the anti-inflammatory IL-10 are constitutively expressed in many bats. Features displayed in this graphic, however, are not all generic to all bats but rather species- or lineage-specific, detailed explanation are given in above section. Figure created with biorender.com.

5. Coronaviruses

5.1 Human coronaviruses

Coronaviruses belong to the order *Nidovirales*, the suborder *Cornidovirineae* and the family *Coronaviridae*. Members of this virus family are further classified into four different genus (alpha-, beta-, gamma- and deltacoronaviruses), based on their phylogenetic relationships, host-range and genomic organization [209]. Alpha- and betacoronaviruses infect only mammals and often cause respiratory illness and gastroenteritis, whereas gamma- and deltacoronaviruses infect primarily birds [209]. Coronaviruses are prone to cross species-barriers because of two specific characteristics: during RNA replication, their polymerase utilize a unique template switching mechanism that can lead to recombination events, which can give rise to novel viral species, and their genome is the largest of all RNA viruses, which allow plasticity for new mutations [14].

Up until the outbreak of SARS-CoV in China in 2002, coronaviruses were not considered to be highly pathogenic to humans. SARS-CoV and MERS-CoV, however, cause severe respiratory syndrome with a high case fatality rate [209]. Four additional coronaviruses circulate in humans: HCoV-NL63, HCoV-229E, HCoV-OC43 and HKU1. They cause only mild upper respiratory diseases. All six human coronaviruses are zoonotic: SARS-CoV, MERS-CoV, HCoV-NL63 and HCoV-229E derived from bat-borne viruses, while HCoV-OC43 and HKU1 likely originate from rodent viruses [209]. While HCoV-NL63 and HCoV-229E are alphacoronaviruses, HCoV-OC43, HKU1, MERS-CoV and SARS-CoV are betacoronaviruses. SARS-CoV and MERS-CoV are further categorized into the subgenera *Sarbecovirus* and *Merbecovirus* respectively (Table 7) [210]. Livestock can be also severely affected by coronavirus infection, as illustrated by diseases caused by porcine enteric diarrhea virus (PEDV), swine acute diarrhea syndrome coronavirus (SADS-CoV) and avian-borne porcine deltacoronavirus (PDCoV) [211].

SARS-CoV emerged in November 2002 in Foshan, China, and caused the first reported human coronavirus pandemic with 8,096 cases, including 774 deaths, in 27 countries [22]. The outbreak terminated in July 2003. The first indication for the animal source of SARS-CoV was the detection of viral RNA in masked palm civets and raccoon dogs [212]. Samples collected from Chinese ferret badgers from live-animal market in Shenzhen, China, were subsequently found positive for viral RNA and were thus suspected as possible intermediate hosts [212]. Later, the sequences of several CoVs closely related to SARS-CoV were found in pooled nasopharyngeal and anal swabs of *Rhinolophus* bats, identifying

the probable host reservoir [213,214]. In 2012, MERS-CoV was discovered for the first time in humans in Jeddah, Saudi Arabia. Since then, the virus causes sporadic outbreaks in Asia and established itself as enzootic pathogen in the Saudi Arabic peninsula. Until November 2019, MERS-CoV has caused 2,494 cases in 27 countries resulting in 858 fatalities. Dromedary camels have been identified as the intermediate hosts and bats of the *Vespertilionidae* family as reservoir species [22,212].

Table 7: Human coronaviruses (adapted from [210])

Virus genus	Subgenus	Species	Year of emergence	Cell surface receptor	Reservoir host	Intermediate host
Alphacoronavirus	Duvinacovirus	HCoV-229E	1966	CD13/APN	*Hipposideros spp*. bats	Dromedary camels, alpacas
	Setracovirus	HCoV-NL63	2004	ACE2	*Triaenops spp.* bats	-
Betacoronavirus	Embecovirus	HCoV-OC43	1967	9-O-Acetylated Sialic Acid	Rodents [148]	Cattle
		HCoV-HKU1	2005	9-O-Acetylated Sialic Acid	Rodents [148,154]	Mice
	Merbecovirus	MERS-CoV	2012	DPP4	*Vespertilionidae* family bats	Dromedary Camels
	Sarbecovirus	SARS-CoV	2003	ACE2	*Rhinolophus* spp. bats	Palm civets, racoon dogs (?)
		SARS-CoV-2	2019	ACE2	*Rhinolophus* spp. bats	?

5.2 Novel pandemic coronavirus SARS-CoV-2

5.2.1 Emergence

Patient clusters with severe pneumonia of possible viral origin alerted regional health facilities in Wuhan, in the Hubei province in China, in December 2019. Patients showed symptoms ranging from fever, cough and chest discomfort to severe dyspnea and bilateral lung infiltration [215]. The infectious agent causing the pneumonia was isolated from bronchoalveolar lavage fluids, identified as novel betacoronavirus which was later named SARS-CoV-2 causing COVID-19. By the end of December 2019, the World Health Organozation (WHO) was notified due to sustained and rapid spread of the viral infection. A public health emergency of international concern (PHEIC) was declared in January 2020

and further defined as global pandemic in March 2020 (Figure 12) [216]. Although the first cases of SARS-CoV-2 in human population were detected in early December 2019, COVID-19 is thought to have been present as early as November 2019 in the Hubei province [217]. Sixty-six percent of the first 41 hospitalized patients could be epidemiologically linked to the Huanan Seafood Wholesale Market, a wet market trading seafood, poultry and exotic animals, located in downtown Wuhan [23]. Since the hypothetical source of SARS-CoV-2 was wildlife sold at the Huanan market, the market was sanitized and closed on January 1st, 2020. Even though the exact settings and upstream events remain to be clarified, epidemiological data supported by biological and environmental samples taken from animals and vendor stalls as well as layout and inventory of the market suggests that the epicenter of the pandemic is the Huanan wet market [217]. Thus, SARS-CoV-2 supposably emerged from wildlife trade in Wuhan [217].

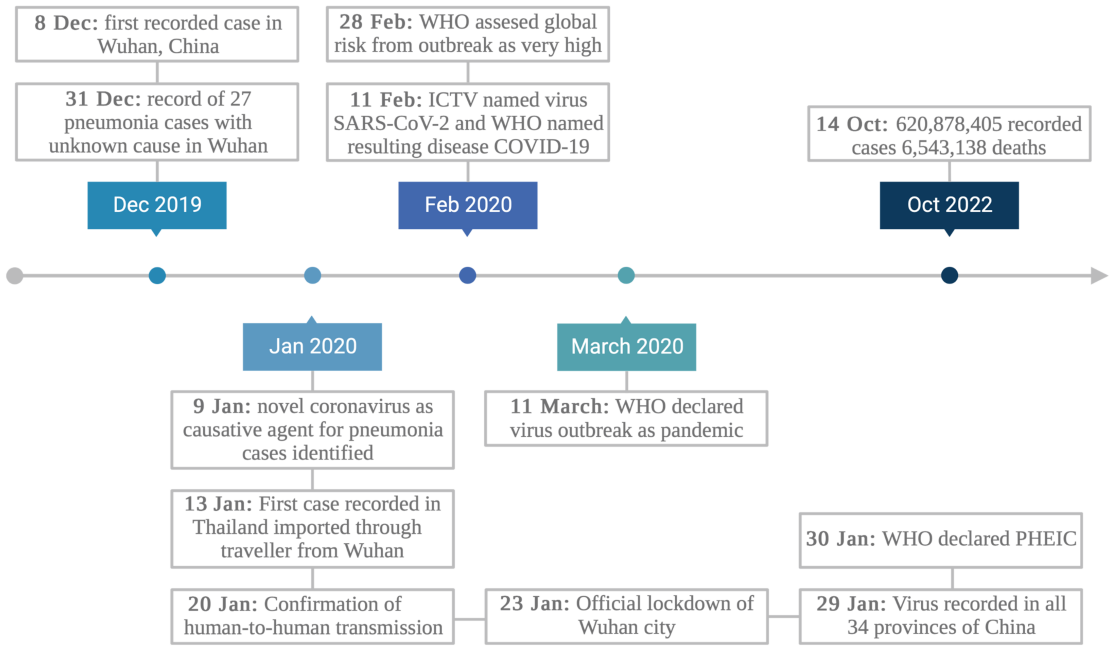

Fig. 12. Timeline of SARS-CoV-2 outbreak. First recorded cases were reported in December 2019 in Wuhan, China. Over the time course of 3 months, the outbreak was declared as worldwide pandemic. Until now, more than 600 million cases and 6,5 million deaths were recorded. ICTV stands for International Committee on Taxonomy of Viruses. Recent numbers are from the WHO SARS-CoV-2 update. Figure adapted from [216] and created with biorender.com.

5.2.2 Animal origin and spillover

CoVs are widespread amongst the animal kingdom, but bats have been identified as the richest source of genetically diverse CoVs with over 200 novel bat CoVs identified till now [218]. In total, around 35% of all bat viruses are CoVs [218]. High recombination frequencies of CoVs could render bats important sources for CoV evolution, similar to birds and pigs for IAVs [218]. One such recombination event most likely occurred between HCoV-229E-like viruses found in *Hipposideros* bats and HCoV-NL63-like viruses found in *Triaenops afer* bats, since the spike protein sequence of the second virus is more closely related to HCoV-229E [219].

Mechanisms for virus spillover events into human population or livestock, however, are largely unknown [218]. Intermediate animal hosts have often been implicated in the zoonotic transmission event of CoVs to humans. For instance, dromedary camels harbor several MERS-CoV lineages and share a common ancestor with HCoV-229E. Several closely related SARS-CoV-1-related-CoV (SC1r-CoVs) have been found in *Rhinolophus sinicus* bats with up to 95% sequence similarity [213,220]. Racoon dogs and civet cats also carry human SC1r-CoVs with high genetic similarity (99,6%), which make them the likely intermediate hosts [68].

In the case of SARS-CoV-2, two sub-lineages with 86-92% similarity to the human strain have been identified in Malayan pangolins [221]. Whereas zoonotic infections of humans with civet-associated SARS-CoV-1 strains seemed plausible due to the close genetic relatedness of these two CoVs, bat-, human- and pangolin-associated SARS-CoV-2 strains are evolutionary further apart. The direct ancestor strain of SARS-CoV-2 infecting humans remains to be determined [68]. Before February 2020, only two lineages (A and B) of SARS-CoV-2 circulated in Wuhan, each likely emerged from a separate spillover event into humans. Zoonotic jumps from a so far unidentified intermediate host at the Huanan market are the most probable explanation for SARS-CoV-2 emergence in human population. Successful transmission of both viral lineages after independent zoonotic events indicate that evolutionary adaptation within humans was not needed for the spread of SARS-CoV-2 [222]. Virus-positive environmental samples from the Huanan market including cages, carts and freezers, inventory lists and special-epidemiological analyses of the first cases suggest that red foxes, hog badgers and racoon dogs, which were all sold live at the Huanan market, could host SARS-CoV-2 progenitor viruses [23].

RNAs from SARS-CoV-2-related-CoV (SC2r-CoVs) have been recently detected in different species of *Rhinolophus* living in Northern Laos [223]. One of these viruses, named

BANAL-20-52, was found in *R. malayanus* and is to date the closest relative to SARS-CoV-2 with an overall sequence identity of 96.8% [223]. Other viruses belonging to this lineage have been identified in *Rhinolophus* bats sampled in China [224,225], Thailand [226], Cambodia [227] and Japan [228] (Figure 13 and Table 8). SC2r-CoVs are thus probably widely circulating in bats of South-East Asia. In addition, numerous other bat species worldwide are infected with betacoronaviruses, including species of the *Myotis*, *Nyctalus*, *Tadarida* and *Eptesicus* genera [229–235].

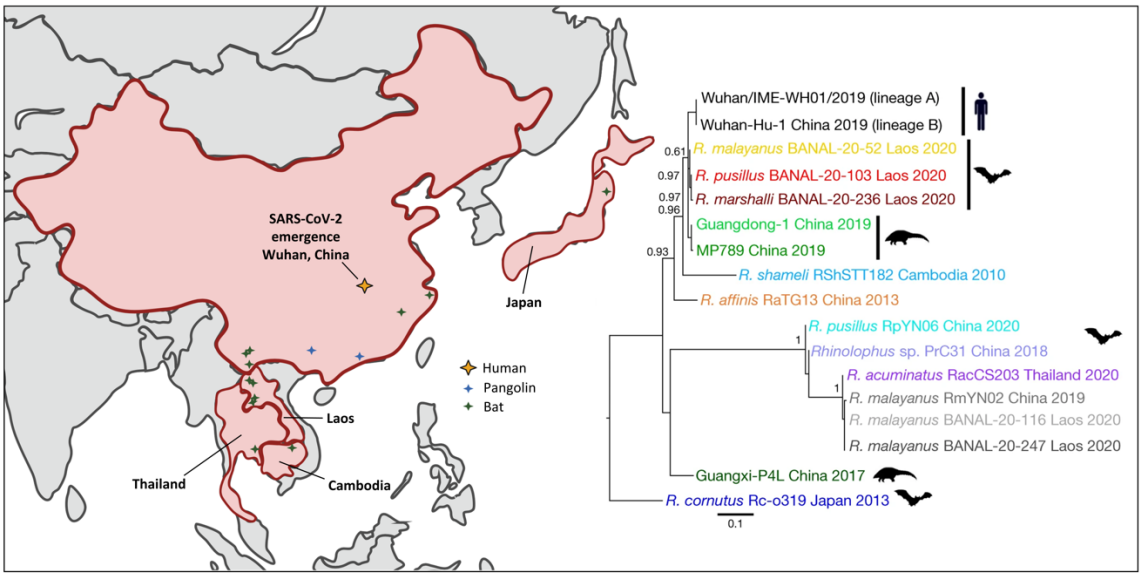

Fig. 13. Map of SC2r-CoV sampling sites. Very closely related bat and pangolin SC2r-CoVs have been sampled in China, Cambodia, Japan, Thailand and Laos. The phylogenetic tree of the protein sequence of the RBD from each sampled virus is indicated on right. Host species for each virus is indicated by pictograms and horseshoe bat species (Rhinolophus) is indicated before the virus name. Sampling site and year is listed after. Figure adapted from [217,236] and created with biorender.com.

Tabel 8: SC2r-CoVs sampled from Rhinolophus bats (adapted from [236,237])

SC2r-CoV	**Location**	**Year**	***Rhinilophus* species**	**Overall NT identity to SARS-CoV-2**
BANAL-20-103	Laos	2020	*R. pusillus*	97,4%
BANAL-20-52	Laos	2020	*R. malayanus*	97,1%
BANAL-20-116	Laos	2020	*R. malayanus*	97,0%
BANAL-20-247	Laos	2020	*R. malayanus*	97,0%
BANAL-20-236	Laos	2020	*R. marshalli*	96,8%
RaTG13	China/Yunnan	2013	*R. affinis*	96,1%
RpYN06	China/Yunnan	2019/20	*R. pusillus*	94,5%
RmYN02	China/Yunnan	2019	*R. malayanus*	93,2%
PrC31	China/Yunnan	2018	*R. blythi*	92,9%
RShSTT182	Cambodia	2010	*R. shameli*	92,6%
RShSTT200	Cambodia	2010	*R. shameli*	92,6%
RacCS203	Thailand	2020	*R. acuminatus*	91,2%
RacCS271	Thailand	2020	*R. acuminatus*	91,2%
SL_CoVZC45	China/Dinghai	2017	*R. pusillus*	87,6%
SL_CoVZXC21	China/Dinghai	2015	*R. pusillus*	87,3%
Rc-o319	Japan	2013	*R. cornutus*	79,1%
RsYN04	China/Yunnan	2019/20	*R. stheno*	76,5%
RmYN05	China/Yunnan	2019/20	*R. malayanus*	76,5%
RmYN08	China/Yunnan	2019/20	*R. malayanus*	76,5%

5.2.3 Transmission

SARS-CoV-2 is mainly transmitted from human-to human via respiratory droplets [238]. Droplet transmission occurs through close contact (< 1m) with an infected person that is speaking, coughing or sneezing. Aerosols, direct contact with contaminated surfaces and fecal–oral transmission routes are alternative routes of transmission [239]. The virus is stable for days on inorganic surfaces and viral RNA was detected for prolonged times in fecal samples [216]. Indirect transmission through contaminated surfaces appears in the immediate environment of an infected person while airborne transmission allows the virus to remain in enclosed environments for prolonged periods of time and infect individuals beyond the close-range limit of droplet transmission. Transmission of the virus can occur before onset of symptoms and the R0 value of the ancestral virus strain is 2.2 [239,240].
The risk of spillback transmission of SARS-CoV-2 from humans to domestic animals or wildlife remains a major concern, as this reverse zoonotic transmission has been already

documented in pet animals, as well as zoo and wild animals [241,242]. Carnivores seem to be particularly susceptible to SARS-CoV-2 in contrast to poultry and other livestock such as cattle or pigs [68]. Positive pet dogs and cats as well as wild cats and other wildlife in zoos and safari parks that have been in close contact with infected humans have been reported. In experimental infections, ferrets, cats, hamsters and rhesus macaques were shown to be susceptible to SARS-CoV-2 [243]. In addition, ferrets and cats efficiently transmit the virus by droplets and airborne routes in experimental settings [243,244]. Furthermore, around 57 mink farms in the Netherlands, 25 in Denmark, 6 in the USA and one in Spain reported outbreaks of the virus within their animals after exposure via infected caretakers [68,243,244]. Infection and animal-to-animal transmission of SARS-CoV-2 has also been reported in white-tailed deer in North America [245]. Animal-to-human reverse transmission events have been reported from pet hamsters in Hong Kong and minks on Dutch farms [246–248]. The role of animals as reservoirs after spillback event, however, remains uncertain and requires further studies [243,244]. Given the likely *Rhinolophus spp.* origin of SARS-CoV-2, bats could be putatively at risk of spillback transmission [249]. The establishment of novel bat reservoirs would have a severe impact on wildlife conservation and public health measures. Sustained viral transmission in nature after spillback events from human to novel animal hosts, has already been reported for white-tailed deer populations in the USA and Canada [250,251].

5.2.4 COVID-19 disease

The pathogenesis of SARS-CoV-2 infection in humans ranges from mild cold-like symptoms to severe respiratory failure. Increased age and comorbidities of the patient worsens the symptoms. The virus travel through the upper respiratory tract and enters ciliated epithelial cells, where it starts replicating [216]. Once virions are released from ciliated epithelial cells, they migrate down to the airways and enter alveolar epithelial cells in the lungs. Massive viral replication in lung cells induces excessive immune and inflammatory responses that lead to a ‘cytokine storm’ [216]. This results in acute respiratory distress syndrome and respiratory failure which is the main cause of death in COVID-19 patients [216]. About 80% of infected patients do not require hospitalization and have a mild course of infection limited to the upper airways. Those patients display symptoms like fever, cough, fatigue, shortness of breath, headache, sputum production and sore throat, similar to other viral infections including the seasonal flu or the common cold

[240]. Anosmia (loss of smell) and dysgeusia (loss of taste) are frequent consequence of COVID-19. Completely asymptomatic individuals have also been reported [252].

5.2.5 Variants of concern

The mutation-prone nature of SARS-CoV-2 replication resulted in the generation of numerous variants, some of which outcompeted and replaced the wild type (WT) or previous variants in the population. Variants with increased transmissibility or virulence, new clinical presentation and decreased effectiveness of vaccines, have been classified as so-called 'variants of concern' (VOCs) by the WHO. VOCs have been named alphabetically after time of emergence: B.1.1.7 (Alpha) in September 2020, B.1.351 (Beta) in December 2020 and P.1 (Gamma) as well as B1.617.2 (Delta) at the beginning of 2021 [253]. The most recently emerged VOC, in November 2021, is B.1.1.529/BA.1 (Omicron) and displays the largest number of mutations, especially in the spike protein, as compared to the initial Wuhan strain [254]. It may have emerged in a chronically infected immunocompromised patient [255]. Further sub-lineages of Omicron were later identified, splitting the variant family into BA.1, BA.1.1, BA.2, BA.2.12.1, BA.3, BA.4 and BA.5. The newest Omicron subvariants, while spreading faster than the previous ones, appear to be causing less fatalities and hospitalizations. Protection against infection, however, is limited through the existing SARS-CoV-2 vaccines or infections with previous variants. Thus, Omicron/VOC-specific vaccines are needed and recently brought on the market [256].

5.3 SARS-CoV-2 genomic characteristics

5.3.1 Genome structure

SARS-CoV-2 is a positive-sense ssRNA virus with a roughly 30000 nt long genome. It comprises open reading frame 1a (Orf1a) and Orf1b at its 5′-terminus that encode two polyproteins, pp1a and pp1ab (Figure 14A). Proteolytic processing by viral proteases subsequently results in 16 non-structural proteins (nsps). The 3′-terminus of the viral genome encodes four structural proteins, including the spike (S) glycoprotein, the envelope (E), the membrane (M) and the nucleocapsid (N) proteins. Nine accessory proteins are also encoded, namely Orf3a, Orf3b, Orf6, Orf7a, Orf7b, Orf8, Orf9b, Orf9 and Orf10 (Figure 14A) [257].

A characteristic of coronaviruses is their discontinuous viral transcription process producing a set of nested 3′ and 5′ co-terminal subgenomic (sg) RNAs. The polymerase complex stops the transcription of the full-length negative-strand genome copy when encountering a transcription-regulating sequence (TRS) element located 3’ upstream of the Orf. Transcription is consecutively re-initiated at the TRS site adjacent to a leader sequence near the 5′ end of the genome, adding a negative-strand copy of the leader sequence to the nascent negative-stranded sgRNA and completing its synthesis. The set of negative-strand sgRNAs is then used as template to synthesize a nested set of positive-sense sgRNA that is subsequently translated into structural and accessory proteins (Figure 14B) [258].

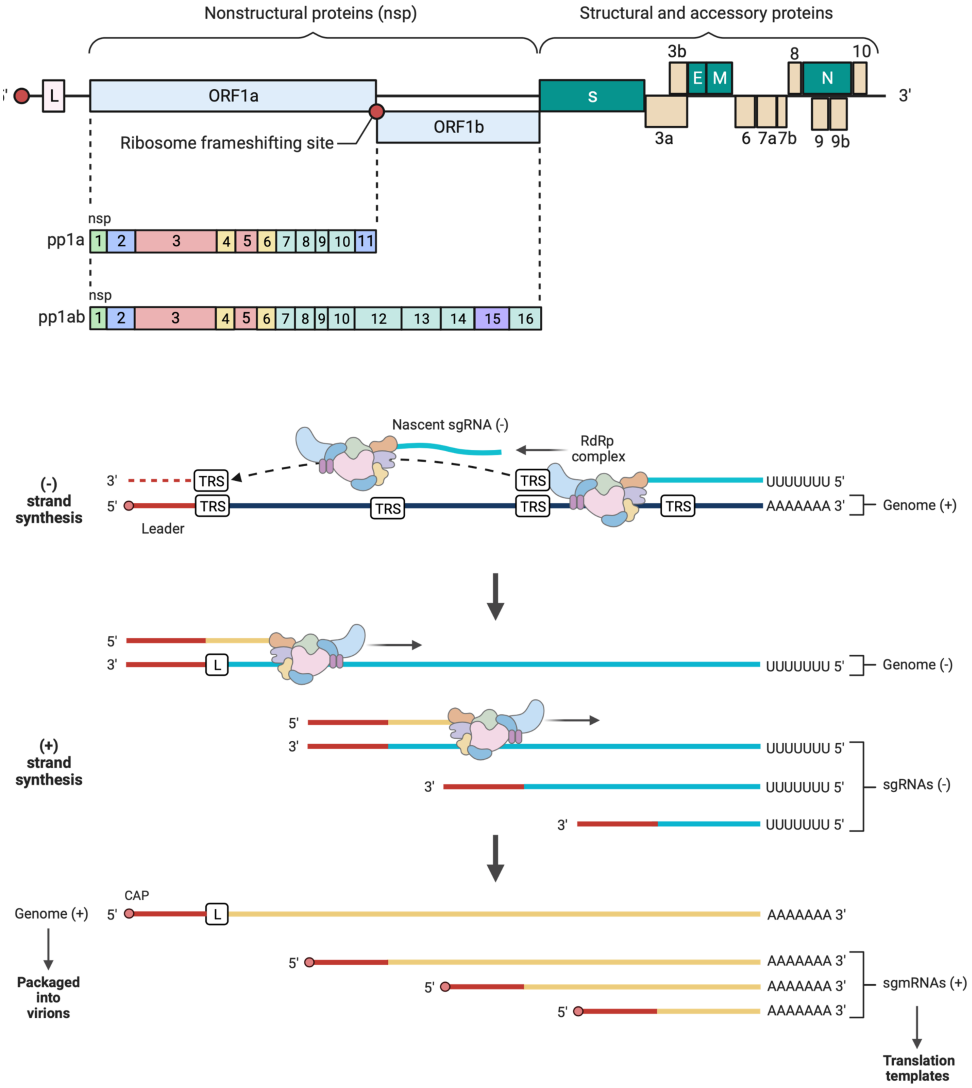

Fig. 14. SARS-CoV-2 genome structure and schematic of coronavirus discontinuous transcription. **A,** SARS-CoV-2 genome harbors accessory proteins (beige), structural proteins (green) and nsps (light blue). Nsps are encoded in ORF1a and ORF1b. Pp1a is subsequently cleaved by viral proteases in nsp1–11 and pp1b produces nsp12–16. The production of either pp depends on whether the stop codon at ORF1a is recognized by the ribosome or bypassed through a change in the reading frame by the ribosome frameshifting site. The structural and accessory proteins are synthesized by translation of their respective subgenomic mRNAs. **B,** The RNA-dependent RNA polymerase (RdRp) complex initiates transcription of the (+) RNA genome into (-) gRNA. In addition to full length copies, RdRp jumps upon encounter of a TRS to the complimentary TRS in the 5' leader sequence (red). Thus, the leader sequence is added to the nascent (-)RNA strand resulting in a set of 5' co-terminal (-) sgRNAs, which themselves serve as templates for (+) sgmRNAs needed for translation. Figure adapted from [259] and created with biorender.com.

5.3.2 Replication Cycle

Coronavirus particles consist of a genome encapsidated in a core made by N proteins and enclosed within a lipid-bilayer envelope derived from the endoplasmic reticulum (ER) decorated with the S, M and E proteins. The M protein facilitates incorporation of viral components into new virion and interacts with the N protein for genome packaging. The ion channel formed by E proteins aids viral assembly while the S protein binds the host receptor and initiates fusion with the host cell membrane [259]. Upon receptor binding, proteolytic processing of S at the plasma membrane (PM) or in endosomes facilitates the fusion of viral and cellular membranes (see paragraph below for more details on viral entry). Following fusion, the core is released into cytoplasm, where the N core is degraded. The viral genome is then freed in into the host cytoplasm (Figure 15). The positive-sense RNA then serves directly as an mRNA for translation of ORF1a and ORF1b by the host translational machinery. Polyproteins pp1a and pp1b are then processed into individual nsps that compose the viral replication and transcription complexes (Figure 14) [258–260]. Viral genomic replication starts with the synthesis of full-length negative-sense genomic copies ((-)gRNAs) from the positive-strand viral genome. (-)gRNAs are then used as templates for (-)sgRNA synthesis which themselves serve as templates for (+)sgmRNA production. Finally, (+)sgmRNA are then used for translation (Figure 14B). Newly generated structural proteins accumulate in the ER membranes and transit through the ER-golgi intermediate compartment (ERGIC), where they interact with N-encapsidated viral genomes. Novel virions are formed via budding into the lumen of secretory vesicular compartments and traffic through the excretory pathway towards the PM, where they are released (Figure 15) [258–260].

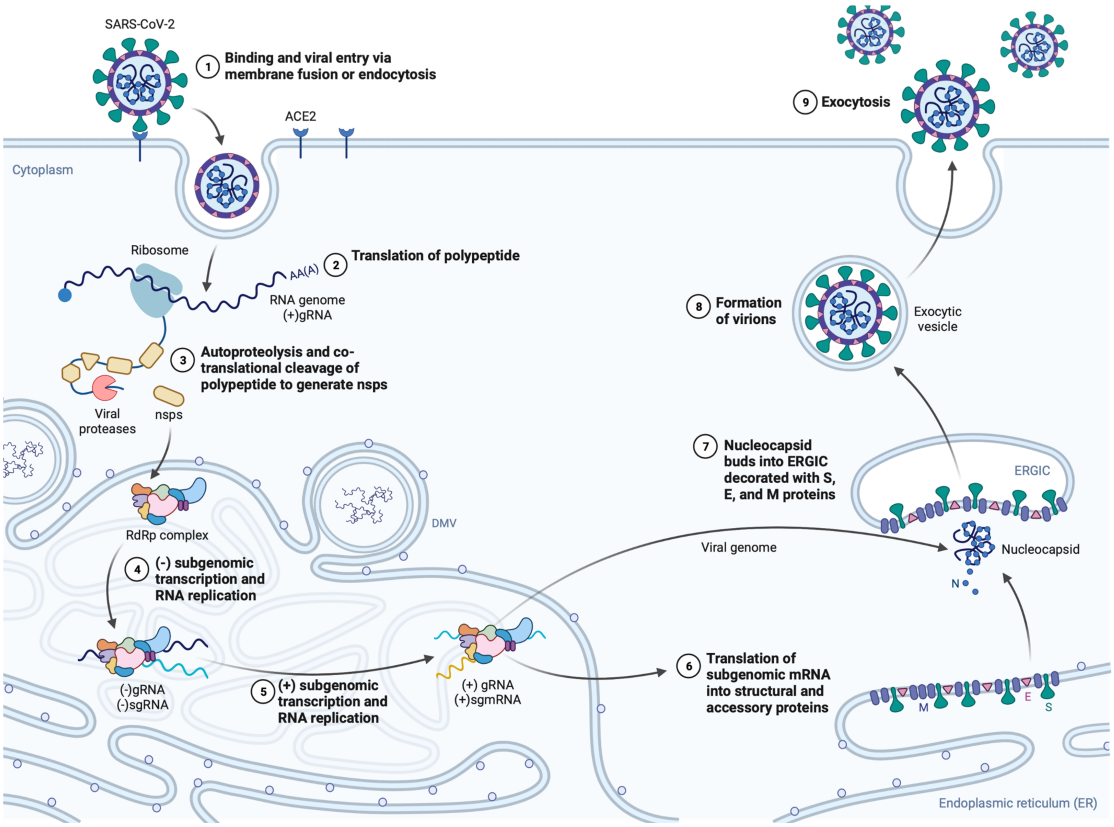

Fig. 15. SARS-CoV-2 replication mechanism. Upon entry (1) and genome release into the host cytoplasm, Orf1a and Orf1b of the (+) RNA genome are immediately translated into the polyproteins (2). These are subsequently processed into nsps (3). Viral replication starts with synthesis of full-length (-) gRNA. Simultaneously, (-) sgRNAs are produced (4). (-) sgRNAs then serve as template for (+) sgmRNA synthesis (5). Structural and accessory proteins are translated from (+) sgmRNAs and accumulate at ER membranes (6). N-encapsidated viral genomes associate with ER-bound viral proteins and bud into ER lumen (7). Newly formed virions use exocytosis pathway to reach PM (8) and exit cell via exocytosis (9). Figure adapted from [259] and modified with biorender.com.

Perinuclear viral replication organelles deriving from the ER are established during replication [261]. These including double-membrane vesicles (DMVs), convoluted membranes (CMs) and small open double-membrane spherules (DMSs). They concentrate viral and cellular components needed for replication and may protect newly synthetized genomes from host immune sensors (Figure 16).

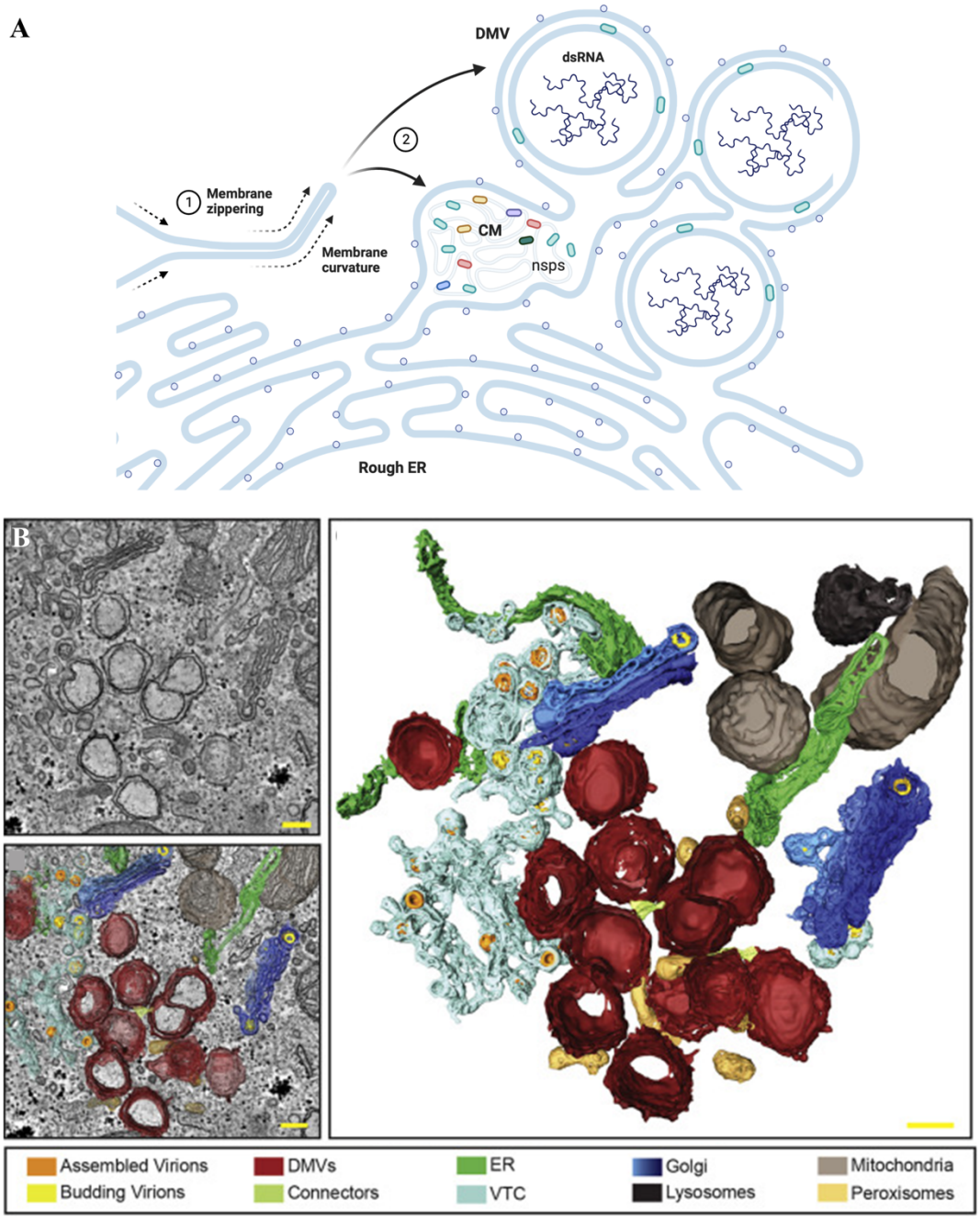

Fig. 16. Formation of DMVs during SARS-CoV-2 replication. **A,** Schematic of DMV or CM development during viral replication. Membrane zippering (1) is initiated by viral nsp causing membrane curvature. Subsequently, viral replication occurs in DMVs or CMs hiding the viral products from sensors in cell cytoplasm and concentrating components needed for replication. Panel A adapted from [259] and modified with biorender.com. **B,** Electron tomography and 3D reconstruction of viral replication sites in SARS-CoV-2-infected Calu-3 cells (MOI = 0.5) harvested 24 hours post infection (hpi). Panel B from [261]

5.5 Entry mechanisms of SARS-CoV-2

5.5.1 Entry into human cells

SARS-CoV and SARS-CoV-2 use the surface receptor Angiotensin I converting enzyme 2 (ACE2) to enter human cells [220,223,225,262,263]. Viral binding to ACE2 is followed by the proteolytic cleavage of the viral S proteins by either the plasma-membrane resident transmembrane serine protease 2 (TMPRSS2) or the endosomal cathepsin L (CTSL) [264]. Two S cleavage events are necessary for infection. First, TMPRSS2 and CTSL cleave S at the junction between its two subunits S1 and S2, revealing a second cleavage site within the S2 domain, the S2' site. Upon S2' cleavage by cathepsins or serine proteases, the S protein initiates membrane fusion [265]. The cleavage is mandatory for the fusion between the viral and cellular membranes. Thus, localization and expression of TMPRSS2 and CTSL dictate whether the virus enters cells by fusing at the cell surface or in endosomes (Figure 17) [264,266].

Moreover, a polybasic furin cleavage site lies at the S1/S2 junction of the S protein and sets SARS-CoV-2 apart from SARS-CoV and SC1r-bat-CoVs. The host protease furin, circulating between Golgi and ER in the excretory pathway, can prime newly formed SARS-CoV-2 virions exiting the cells. This cleavage event, however, is not mandatory for S-mediated entry [267,268]. On the other hand, pre-cleaved virions enter more efficiently into TMPRSS2-expressing cells than non-cleaved ones, facilitating cell surface fusion and avoiding the antiviral functions of endosomal resident IFITM proteins [269,270]. Moreover, a SARS-CoV-2 mutant lacking the furin cleavage site was not able to efficiently replicate in ferrets and could not be transmitted to sentinel animals [270]. The presence of the furin cleavage site might thus affect virus tropism.

Finally, other host factors participate in viral entry. Interaction between S and heparan sulfate enhances S-ACE2 binding [271]. Furin-cleaved S1 fragment binds to cell surface Neuropilin-1 [272,273]. Blocking this interaction with either small-molecule inhibitors, monoclonal antibodies or RNA interference reduced SARS-CoV-2 entry and viral infection in Caco2 and HEK293 cells [272,273].

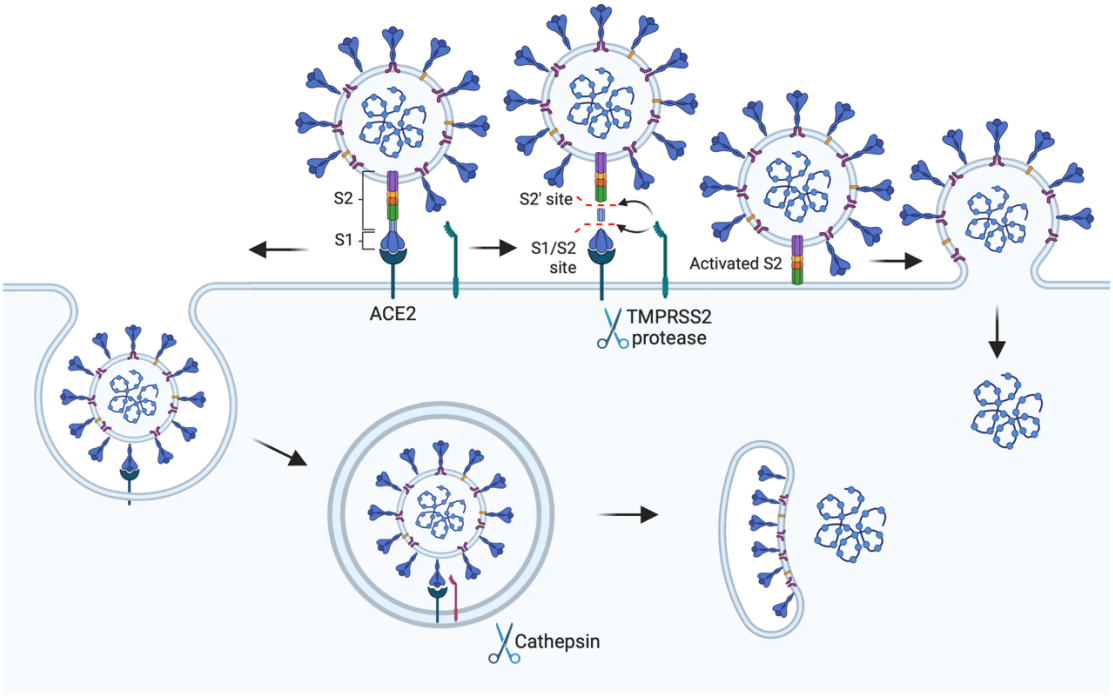

Fig. 17. SARS-CoV-2 cell entry pathways. Two main entry pathways exist for SARS-CoV-2 infection, both mediated by the major receptor ACE2. Either membrane fusion takes place on PM facilitated by surface-expressed membrane protease TMPRSS2 or virion is endocytosed upon binding and fusion occurs in endosomes via cathepsins. Figure created with biorender.com.

5.5.2 Entry into bat cells

The S sequence determines host range since it dictates the binding affinity and accessibility of the receptor binding domain (RBD) to the cellular ACE2 receptors [274]. Most SC2r-CoVs have a limited sequence homology with SARS-CoV-2 in the RBD region, even though their overall identity is over 80% [236,237]. The closest RBDs with over 90% homology were found in BANAL-20-52 sampled from *R. malayanus* in Laos and in RaTG13 sampled from *R. affinis* in China (Figure 18) [223]. Only BANAL-20-236 has been successfully isolated [223]. The virus enters hACE expressing cells [236].

Several approaches have been used to predict the ability of ACE2 from phylogenetically diverse bat species to promote SARS-CoV-2 entry [275–277]. First, comparison of ACE2 protein sequences from 37 bat species, including species of the genus *Rhinolophus*, predicted a low or very low ability to interact with viral S proteins [277]. Second, ectopic expression of ACE2 from several bat species in non-permissive mammalian cells followed by infection with genuine viruses or pseudo-viruses carrying SARS-CoV-2 S proteins revealed that ACE2 from several bat species including *Rhinolophus, Myotis* and *Eptesicus* species allowed viral entry, albeit often less efficiently than human ACE2

[275,276,278,279]. However, these approaches using *in silico* analysis or ectopic expression of bat ACE2 in human or hamster cells do not allow to predict the ability of S proteins to interact with bat ACE2 express in bat cells. Intriguingly, a recent report highlights the ability of bat-borne HCoV-229E to replicate in *Rhinolophus lepidus* kidney cells in a spike-independent manner [280]. After six passages in *R. lepidus* cells, large deletions in the spike region of the CoV could be observed, which resulted in a loss of infectivity in human cells but not in bat cells. An alternative entry mechanism for CoVs might exist in bats that does not rely on the compatibility of S and cellular receptors [280]. Another significant difference between all SC2r-CoVs found in bat or pangolin species is the absence of the furin cleavage site. This site has been identified in other human coronaviruses such as HCoV-HKU1, HCoV-OC43 as well as MERS-CoV and associated with increased transmissibility, virulence and broader host range as described above for SARS-CoV-2 infection in ferrets [68,270]. The furin cleavage site of SARS-CoV-2 could have originated from recombination events between SC2r-CoVs co-circulating in bats or emerged while passaging through an intermediate host or during asymptomatic circulation in human population at the start of the pandemic [236].

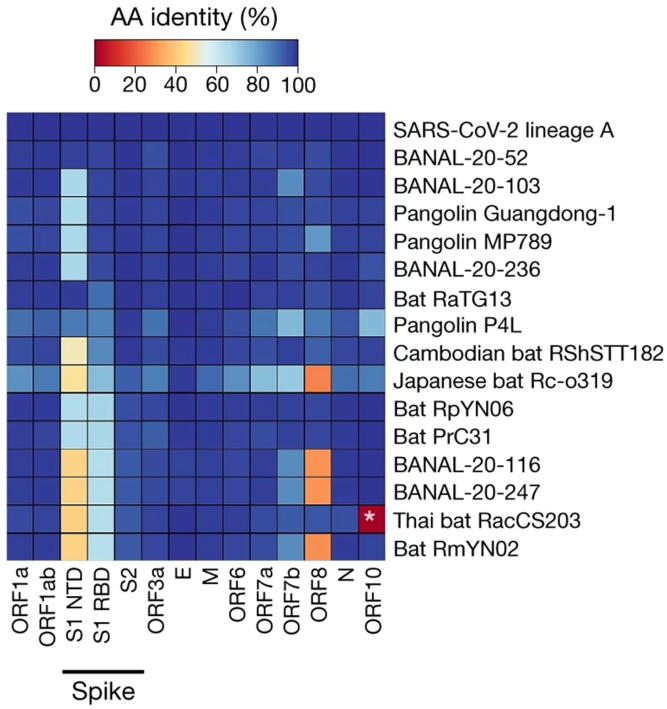

Fig. 18. Spike protein comparison amongst SC2r-CoVs. Amino acid sequence identities of representative bat and pangolin sarbecoviruses compared to human SARS-CoV-2 lineage B. Spike protein has been divided into functional domains, and the sequences are ordered according to percentage of identity of the RBD domain. The asterisk marks the absence of a functional ORF10 in Thai bat RacCS203. Figure adapted from [236].

5.6 Human innate immunity towards SARS-CoV-2

5.6.1 Antiviral innate immune response

To identify the main PRR responsible for sensing SARS-CoV-2 NA in the cytoplasm, knockdown experiments of the three RLRs were performed in several human cell lines including lung cells (Calu-3 and A549-ACE2), Caco2 intestine cells, iPSC-derived airway epithelial cells and primary human air-liquid airway epithelia cultures [281–283]. These studies revealed that IFN-I and IFN-III expression upon SARS-CoV-2 infection was mainly initiated by MDA5 with the support of LGP2 [281–283]. The role of TLR3 was also investigated and it did not seem to contribute to the IFN response in infected cells [283].

However, despite recognition of viral RNA by MDA5, induction of IFN responses after SARS-CoV-2 infection are low, or inexistant, in human lung cells (A549-ACE2, Calu-3 and MRC5) lung tissue [284] or ferrets [285]. Calu-3 cells, intestinal organoids and a primary air-liquid interface lung epithelia system are also poor IFN-I and IFN-III inducers upon infection [282,283,286,287]. Moreover, IFN-I levels in sera of COVID-19 patients are very low [288]. These poor induction of IFN response was previously reported during MERS-CoV or SARS-CoV infection [289]. This is probably due to their multiple strategies to escape and counteract host IFN responses [289] – see paragraph below.

Nevertheless, when human cells are pre-treated with IFN, several ISGs have been shown to exhibit an antiviral effect against SARS-CoV-2. For instance, a ISG-specific gain-of-function screen in human kidney HEK293-ACE2-TMPRSS2 revealed 65 ISGs potentially restricting SARS-CoV-2 replication [290]. These ISGs, which are mainly located in ER and Golgi, are involved in protein degradation, lipid membrane composition and vesicle transport [290]. The antiviral function of tetherin was further validated in Huh7-ACE2-TMPRSS2, HeLa-ACE2 and Calu-3 cells [290]. Additionally, the dsRNA sensor OAS1 has been identified to specifically bind to certain sequence motifs in the 5'UTR of SARS-CoV-2 and block viral replication by activating RNASEL in human lung A549-ACE2-TMPRSS2 cells [291]. This antiviral activity is depended on the prenylation of OAS1 and ablated if OAS1 does not contain a prenylation motif [291]. LY6E blocks SARS-CoV-2 replication in human hepatoma Huh7.5-ACE2-LY6E cells by inhibiting S-mediated membrane fusion [135]. IFITM1-3 interfered with SARS-CoV-2 endosomal fusion [292] and cholesterol 25-hydroxylase (CH25H) blocked endosomal VSV-SARS-CoV-2-spike pseudovirus entry in HEK293-ACE2 cells [293].

In contrast to the weak IFN induction, the expression of proinflammatory cytokines is strongly upregulated upon SARS-CoV-2 infection [294]. Inflammatory processes are majorly dysregulated in patients with severe COVID-19 and a conserved profile of elevated levels of cytokine like IL-6, IL-8, IL-10 and TNF, as well as chemokines like CCL2, CCL3 and CXCL8 could be observed in serum samples. The induction of a similar profile of cytokines was detected in a wide variety of susceptible cell types and organoids [294].

5.6.2 Viral evasion mechanisms

Multiple SARS-CoV-2 proteins inhibit the host innate immune response at multiple levels in human cells (Figure 19) [294,295]. For example, Orf9b antagonized IFN-I production in Calu-3 as well as human airway epithelial cells BEAS-2B [296]. This viral protein inhibits the ubiquitination of NEMO, which blocks the nuclear translocation of NF-κB in HEK293 cells [296]. Nsp1 partially blocks IFN-I by interfering with IRF3 phosphorylation and dampens ISG stimulation by depletion of Tyk2 and STAT2 in HEK293 and Huh7 cells [297]. Nsp5 proteolytically cleaves RIG-I and additionally induces the ubiquitin- and proteosome-mediated degradation of MAVS via its E3 ligase activity in HEK293 and Caco-2 cells [298]. At least two SARS-CoV-2 proteins antagonize the cGAS-STING pathway in A549 and Huh7 cells. Orf3a blocked the nuclear accumulation of p65 and consecutive NF-κB by binding STING. 3CL inhibited K63-ubiquitin modification of STING to hinder the assembly of STING functional complexes and downstream signaling [299]. Orf6 inhibits the induction of IFN-I and IFN-III, as well as the expression of ISGs in HEK293T cells, likely by blocking the nuclear translocation of IRF3 [300]. Truncated SARS-CoV-2 Orf3b suppressed IFN-I production in A549 lung cells, in contrast to SARS-CoV Orf3b. Phylogenetic analysis further showed that the premature stop codon is also found in SC2r-CoVs Orf3b from bats and pangolins demonstrating a similar anti-interferon effect [301].

Moreover, several SARS-CoV-2 proteins counteract the antiviral function of potent antiviral ISGs. For instance, the accessory protein Orf7a blocks the activity of tetherin, which retains SARS-CoV-2 virions at the PM [290]. SARS-CoV-2 phosphodiesterase (PDE) can degrade OAS1, thus evading the above-described antiviral activity. Interestingly, the members of the *Rhinolophoidea* bat superfamily express a non-prenylated OAS1 that is unable to restrict viral replication [291]. This might explain, at least in part, why these bats serve as a reservoirs for sarbecoviruses [291].

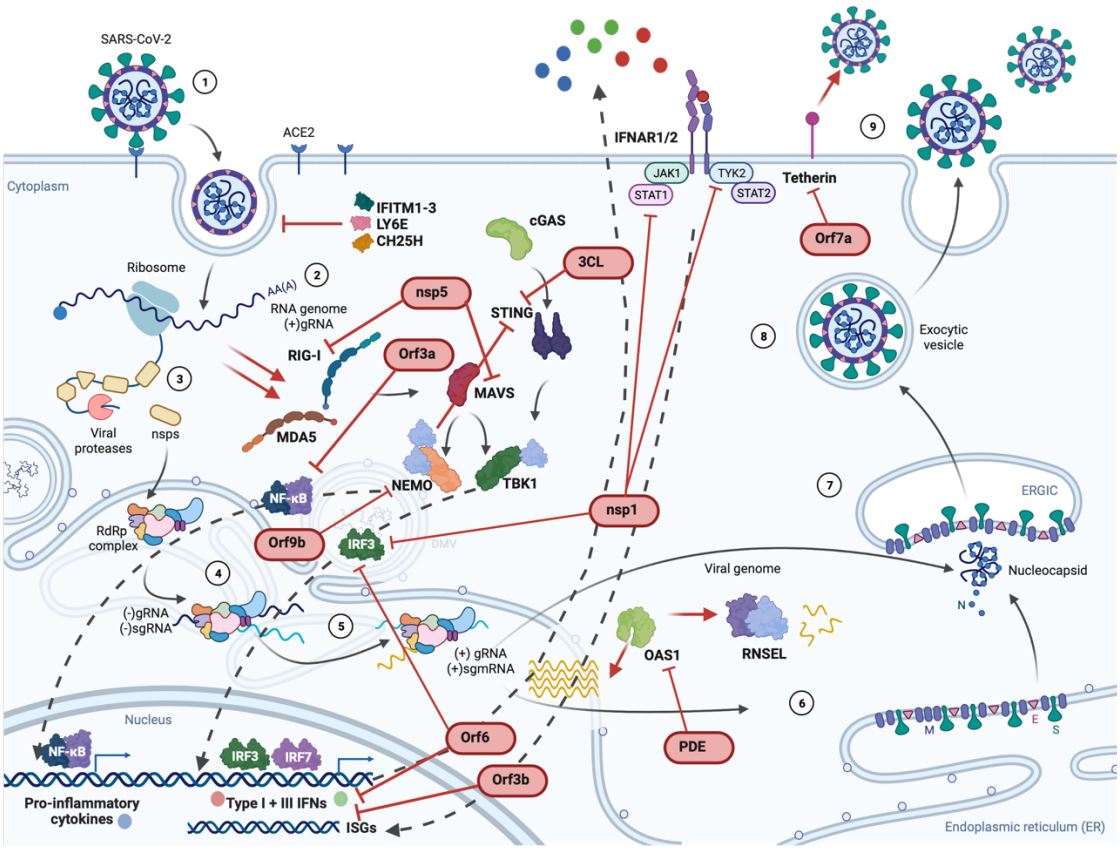

Fig. 19. SARS-CoV-2 evasion mechanisms of the innate immune response. Human innate immune response antagonizes SARS-CoV-2 infection on many levels. Some examples are depicted in this graphic. IFITM1-3, LY6E as well as CH25H interfere with viral membrane fusion at the entry step. RIG-I as well as MDA5 sense the viral genome leading to the induction of IFN-I/III and proinflammatory cytokines. OAS1 senses replicative forms of the RNA genomes and activated the RNASEL pathway for degradation. Tetherin hinders the release or new virions. SARS-CoV-2, on the other hand, has evolved multiple proteins that interfere with several aspects of the innate immune signaling pathways in human cells. Some viral protein examples are shown in red. Orf9b antagonizes IFN-I production by inhibiting NEMO phosphorylation. Nsp1 interferes with IRF3 phosphorylation and depletes TYP2 as well as STAT1. Orf6 also inhibits nuclear translocation of IRF3 and together with Orf3b blocks IFN-I expression. Nsp5 cleaves RIG-I and degrades MAVS. Orf3a blocks nuclear accumulation of p65 and binds STING. 3CL interferes with STING ubiquitination and blocks formation of functional STING complexes. Orf7a blocks tetherin and PDE degrades OAS1. Figure created with biorender.com.

6. Aims and Objectives

The overall goal of my PhD thesis is to investigate susceptibility and innate immune responses of *in vitro* models of reservoir species to emerging viruses. I started my doctoral studies with a focus on avian hosts and flaviviruses. With the start of the COVID-19 pandemic in spring 2020, I decided to refocus my investigations on interaction between bat cells and SARS-CoV-2.

Bats are natural reservoirs for numerous coronaviruses, including SC1r- and SC2r-CoV. BANAL-20-52 virus, which has a nucleotide sequence similarity of 96.8% to SARS-CoV-2, was sampled from anal swabs of *Rhinolophus malayanus* bats in the Feuang district of the Vientiane province in Laos in 2020 [223]. Several other bat species worldwide are infected with betacoronaviruses, including *Myotis* spp., *Eptesicus* spp. and *Nyctalus* spp [229,230,232–234,231,235]. Knowledge concerning the interaction of coronaviruses and bat cells, however, is sparse. There is thus a need to develop bat cellular models to understand cellular tropism, viral replication, and virus-induced cell responses.

I first was interested in studying SARS-CoV-2 replication in bat cellular models and aimed to facilitate a better understanding of the molecular interaction between virus and host reservoir responses. After demonstrating resistance to infection in a panel of primary and continuous bat cells belonging to five different bat species, I generated susceptible chiropteran cell models for SARS-CoV-2 infection via transduction of a lentivirus construct expressing hACE2. Infection studies in these new models led to the identification of key differences in susceptibility and antiviral responses between different bat species. My results revealed species-specific restrictions to viral replication in bat cells on multiple steps of the replication cycle. This study has been published in Journal of Virology in July 2022 [302].

I then focused on innate immune responses in various bat cell lines. I conducted RNA-sequencing (RNASeq) analysis on a panel of bat cell lines stimulated with a synthetic dsRNA ligand to induce IFN responses. I chose cells belonging to eight different species covering a wide range of the phylogenetic chiropteran tree, including two different *Rhinolophus* species, which are relevant for sarbecovirus biology. My aim was to identify a common set of bat genes that are induced in response to the stimulus. As control cells, I included human lung cells in the analysis. Our comparative transcriptomics analysis revealed unique features of chiropteran cells, such as novel innate immune genes but also a set of conserved mammalian orthologues with potential immune functions. Follow-up

studies will be necessary to uncover the mechanisms of some of the identified bat innate immune genes in the context of infection with bat-borne viruses.

In sum, I have generated and characterized novel bat cellular models, identified different defense strategies against SARS-CoV-2 infection in diverse bat cells and discovered new bat immune genes. My studies have provided novel insight on the interaction between SARS-CoV-2 and bats cells as well as knowledge on the innate immune responses of these important viral reservoirs. My work may lead to the identification and characterization of previously uncharacterized antiviral genes expressed in bat cells.

Chapter II – Species-specific molecular barriers to SARS-CoV-2 replication in bat cells

1. Preamble

As mentioned above, bats are natural reservoirs of numerous coronaviruses, including the potential ancestor of SARS-CoV-2 [217]. Knowledge and progress in investigating the interaction between coronaviruses and bat cells, however, remains sparse. This is in part explainable by the limited number of bat cellular models [303]. In face of the ongoing SARS-CoV-2 pandemic and the likely bat origin of the virus, it is crucial to establish infection models in the host species.

Several studies were performed to predict the compatibility of diverse bat(b)ACE2 and the RBD of SARS-CoV-2 in silico [276,304–306]. Prediction results were validated by overexpressing bACE2 in human or hamster cells lacking hACE2 and subsequent infection with SARS-CoV-2 or pseudotyped viruses [276,304–306]. The results obtained from these studies showed inefficient entry of the virus via most bACE2. Other factors unique to bat cells may potentially modulate viral entry and replication. Experiments performed with cells derived from lung tissue of *Rhinolophus landeri* and *Myotis daubentonii* showed that they were not susceptible to infection with vesicular stomatitis viruses (VSV) bearing SARS-CoV-2 S proteins despite positive interaction prediction of their respective ACE2 and the RBD [263]. Similarly, cells originating from lung and kidney tissue of *Rhinolophus sinicus* and *Eptesicus fuscus* were neither permissive to SARS-CoV-2 [307,308]. These studies underline the limitation of predicting the ability of S proteins to interact with ACE2 orthologs based on computational models or ectopic expression.

Only a handful of models are available to study the replication of betacoronaviruses in bat cells. Viral replication was detected in *Rhinolophus sinicus* lung and brain cells, as well as in *Pipistrellus abramus* kidney cells [309], but viral titers were very low. By contrast, SARS-CoV-2 replicated efficiently in *R. sinicus* intestinal organoids [310], confirming further the ability of *Rhinolophus* cells to support viral replication. Intranasal inoculation of SARS-CoV-2 in *Rousettus aegyptiacus* bats resulted in transient infection of their respiratory tract and oral shedding of the virus [311], indicating that bats unrelated to the *Rhinolophus* genus can be productively infected with the virus. Since the manipulation of bat organoid and animal models remain challenging, there is a need to develop cell lines from various organs and species to gain deeper insights into bat-virus co-evolution [303].

Here, we developed novel cellular models derived from understudied bat species widely circulating in Europe and Asia. We investigated the ability of primary cells from *Rhinolophus* and *Myotis* species, as well as of established and novel cell lines from *Myotis myotis*, *Eptesicus serotinus*, *Tadarida brasiliensis* and *Nyctalus noctula*, to support SARS-CoV-2 replication. The varying susceptibilities and permissivities of the cells to SARS-CoV-2 infection offered the opportunity to uncover unique molecular restrictions to viral replication. Our data highlight the existence of species- and cell-specific molecular barriers to viral replication in bat cells. These novel chiropteran cellular models are valuable tools to investigate the molecular interplays between bat cells and viruses.

2. Material & Methods

2.1 Bat primary cells

M. myotis samples were collected in July 2020 from two bat colonies in Inca and Llucmajor on Mallorca (Balearic Islands, Spain) (agreement CEP 31/2020 delivered by the Ministry of the Environment and Territory, government of the Balearic Islands). *R. ferrumequinum* biopsies were collected in France in 2020. Authorization for bat capture was delivered by the French Ministry of Ecology, Environment and Sustainable development (approval C692660703 from the Departmental Direction of Population Protection (DDPP), Rhone, France). All methods were approved by the 'Société Française pour l'Étude et la Protection des Mammifères (SFEPM)'. Patagium biopsies were shipped in freezing medium Cryo-SFM (PromoCell), on dry ice or at 4°C with ice packs. Primary cells were obtained as previously described [312,313]. Briefly, skin biopsies were washed twice with sterile phosphate buffered saline (PBS), excised in small pieces and enzymatically digested, either with 500 µL of collagenase D (1 mg/mL) (Roche) and overnight incubation at 37°C without agitation, or with 100-200 µL of TrypLE Express Enzyme (Gibco) and incubation 10 min at 37°C under gentle agitation. Dissociated cells and remaining pieces of tissue were placed in a single well of a 6-well plate containing 2 mL of Dulbecco's Modified Eagle Medium (DMEM, Gibco) containing 20% heat-inactivated fetal bovine serum (FBS) (Eurobio), 1% penicillin/streptomycin (P/S) (Gibco), and 50 µg/mL gentamycin (Gibco), and incubated at 37°C under 5% CO_2. Cell cultures were regularly checked to determine the need for media refreshment or splitting. After 5-10 passages, cells were grown in DMEM supplemented with 10% FBS.

2.2 Cell lines

FLG-ID, FLG-R, FLN-ID, FLN-R and Tb1Lu cell lines (Table 1) were maintained in equal volumes of Ham's F12 and Iscove's modified Dulbecco's medium (IMDM, Gibco), supplemented with 10% FBS and 1% P/S (Gibco) in non-vented flasks. Mm cells, which were obtained from a single mouse-eared bat (*Myotis myotis*), were previously described [314]. Nn kidney-, liver- and lung-derived cell cultures were obtained from a common noctule bat (*Nyctalus noctula*) euthanized because of poor chance of survival associated with traumatic injuries sustained while a dead tree sheltering bat hibernaculum was cut. The decision to euthanize the specimen was made by a veterinarian following inspection of a group of noctule bats presented for examination and therapy in the rescue center at the

University of Veterinary and Pharmaceutical Sciences Brno, Czech Republic, in November 2015 [315]. The bat was anesthetized with isofluranum (Piramal Enterprises Ltd.) and euthanized by quick decapitation. The cadaver was immersed into 96% ethanol for a few seconds and then subjected to necropsy under aseptic conditions to collect organs which were loosened mechanically with scalpel blades, minced into small pieces, suspended in DMEM (Biosera) containing 1 mg/ml collagenase (Thermo Fisher Scientific) and 1 mg/ml trypsin (Sigma-Aldrich), and incubated at 37 °C on a shaking thermoblock for 45 min. The cells were then separated through a 100 μm nylon filter and washed twice in a medium supplemented with 10% FBS to stop enzymatic digestion. The cells yielded in this way were cultured in DMEM supplemented with 10% FBS and 1% P/S (Sigma). Primary cells were immortalized by transfection of pRSVAg1 plasmid expressing Simian Virus 40 large T antigen (SV40T) with lipofectamine 2000 (Invitrogen) according to the manufacturer's protocol, expanded and cryopreserved. Mm and Nn cell lines (Table 1), as well as African green monkey Vero E6 cells (ATCC CRL-1586), human lung epithelial A549 cells (kind gift from Frédéric Tangy, Institut Pasteur, Paris) and human colorectal adenocarcinoma Caco TC7 cells (ATCC HTB-37), were maintained in DMEM (Gibco), supplemented with 10% FBS and 1% P/S in vented flasks. All cells were maintained at 37°C in a humidified atmosphere with 5% CO_2. Bat and A549 cells were modified to stably express hACE2 using the pLenti6-hACE2 lentiviral transduction as described previously [316]. Briefly, $2x10^5$ cells were resuspended in 150 μl of culture medium containing 15 μl of ultracentrifuged lentiviral vectors supplemented with 2mM HEPES buffer (Gibco) and 4 μg/ml polybrene (Sigma). Cells were agitated for 30 sec every 5 min for 2.5 h at 37°C in a Thermomixer and then plated. 48 h after transduction, blasticidin (concentrations ranging from 7-15 μg/ml depending on cell lines) was added in the culture media.

Table 1. Overview of the primary and immortalized bat cells used in the study.

Name	Bat species	Common name	Family	Organ	Transformation method	Reference
16104	*Rhinolophus ferrumequinum*	Greater horseshoe bat	Rhinolophidea	Skin (patagium)	None – primary cells	This study
29B	*Myotis myotis*	Greater mouse-eared bat	Vespertilionidae	Skin (patagium)	None – primary cells	This study
19PL15	*Myotis nattereri*	Natterer's bat	Vespertilionidae	Skin (patagium)	None – primary cells	This study
MBra10	*Myotis brandtii*	Brandt's bat	Vespertilionidae	Skin (patagium)	None – primary cells	This study
FLG-ID	*Eptesicus serotinus*	Common serotine bat	Vespertilionidae	Brain	Immortalized FLG-R cells with SV40 large T antigen	CCLV-RIE 1152
FLG-R	*Eptesicus serotinus*	Common serotine bat	Vespertilionidae	Brain	Natural	CCLV-RIE 1093
FLN-ID	*Eptesicus serotinus*	Common serotine bat	Vespertilionidae	Kidney	Immortalized FLN-R cells with SV40 large T antigen	CCLV-RIE 1134
FLN-R	*Eptesicus serotinus*	Common serotine bat	Vespertilionidae	Kidney	Natural	CCLV-RIE 1091
MmBr	*Myotis myotis*	Greater mouse-eared bat	Vespertilionidae	Brain	SV40 large T antigen	[314]
MmNep	*Myotis myotis*	Greater mouse-eared bat	Vespertilionidae	Nasal epithelium	SV40 large T antigen	[314]
MmNol	*Myotis myotis*	Greater mouse-eared bat	Vespertilionidae	Nerve	SV40 large T antigen	[314]
MmPca	*Myotis myotis*	Greater mouse-eared bat	Vespertilionidae	Macrophage	SV40 large T antigen	[314]
MmTo	*Myotis myotis*	Greater mouse-eared bat	Vespertilionidae	Tonsil	SV40 large T antigen	[314]
NnKi	*Nyctalus noctula*	Common noctule	Vespertilionidae	Kidney	SV40 large T antigen	this study
NnLi	*Nyctalus noctula*	Common noctule	Vespertilionidae	Liver	SV40 large T antigen	this study
NnLu	*Nyctalus noctula*	Common noctule	Vespertilionidae	Lung	SV40 large T antigen	this study
Tb1Lu	*Tadarida brasiliensis*	Mexican/Brazilian free-tailed bat	Molossidae	Lung	Natural?	CCLV-RIE 0072

2.3 Viruses and infections

The SARS-CoV-2 strain BetaCoV/France/IDF0372/2020 (historical) and hCoV-19/France/PDL-IPP01065/2021 (20H/501Y.V2 or SA) were supplied by the French National Reference Centre for Respiratory Viruses hosted by Institut Pasteur (Paris, France) and headed by Pr. S. van der Werf. The human samples from which the historical and South African strains were isolated were provided by Dr. X. Lescure and Pr. Y. Yazdanpanah from the Bichat Hospital, Paris, France and Dr. Vincent Foissaud, HIA

Percy, Clamart, France, respectively. These strains were supplied through the European Virus Archive goes Global (EVAg) platform, a project that has received funding from the European Union's Horizon 2020 research and innovation program under grant agreement #653316. The hCoV-19/Japan/TY7-501/2021 strain (20J/501Y.V3 or Brazil) was kindly provided by Jessica Vanhomwegen (Environment and Infectious Risks Research and Expertise Unit; Institut Pasteur). Viral stocks were produced by amplification on Vero E6 cells, for 72 h in DMEM supplemented with 2% FBS and 1% P/S. The cleared supernatant was stored at -80°C and titrated on Vero E6 cells by using standard plaque assays to measure plaque-forming units per mL (PFU/mL). Cells were infected at the indicated multiplicities of infection (MOI) in DMEM without FBS. Virus inoculum was either removed after 6 h and replaced or topped up with FBS containing culture medium to a final concentration of 2% FBS and 1% P/S. For infections with proteolytically activated SARS-CoV-2, cell monolayers were washed twice with PBS before adding virus inoculum in DMEM supplemented with 2 or 4 µg/ml of trypsin TPCK (Sigma) and no FBS. After 4h, DEMEM containing FBS was added to a final concentration of 2%.

2.4 $TCID_{50}$ assays

Supernatants of infected cells were first cleared of cell debris by centrifugation at 3500 rpm for 10 min at 4°C. They were 10-fold serially diluted in DMEM supplemented with 2% FBS and 1% P/S. For "ultracentrifugation" condition in MmBr-ACE2 TCID50 assay, cleared supernatants were ultracentrifuged for 1 h at 45k rpm at 4°C. to remove cytokines and other proteins. Virus-containing pellets were resuspended in DMEM with 2% FBS and 1% P/S after 4 h incubation at 4°C. For "lysate" condition, infected MmBr-ACE2 or A459-ACE2 cells were lysed and scraped in ddH_2O. After one freeze-thaw cycle, whole cell lysates were cleared by centrifugation, supplemented with 10x PBS to a physiological condition and used for serial dilutions. Around $9x10^3$ Vero E6 cells and 50 µl of serially diluted virus suspensions were deposited in 96-well plate in quintuplicate wells. Cells were fixed with 4% paraformaldehyde (PFA) for 30 min at RT and revealed with crystal violet 5 days later. Cytopathic effects (CPE) were assessed by calculating the 50% tissue culture infective dose ($TCID_{50}$) using the Spearman-Karber method [317].

2.5 Flow cytometry

Cells were detached with trypsin or versene for hACE2 staining. Cells were then fixed in 4% PFA for 30 min at 4°C and staining was performed in PBS, 2% BSA, 2mM EDTA and 0.1% Saponin (FACS buffer). Cells were incubated with goat pAB anti-hACE2-647 (1:100, FAB933R R&D Systems) and/or with antibodies recognizing the spike protein of SARS-CoV (anti-S, 1:1000, GTX632604 Genetex) or anti-S mAb10 (1 µg/ml, a kind gift from Dr. Hugo Mouquet, Institut Pasteur, Paris, France) and subsequently with secondary antibodies anti-human AlexaFluor-647 (1:1000, A21455 Thermo), anti-mouse AlexaFluor-488 (1:1000, A28175 Thermo) or Dylight488 (1:100, SA5-10166 Thermo) for 30 min at 4°C. Cells were acquired on an Attune NxT Flow Cytometer (Thermo Fisher) and data analyzed with FlowJo software v10 (TriStar).

2.6 RNA extraction and RT-qPCR assays

Total RNA was extracted from cells with the NucleoSpin RNA II kit (Macherey-Nagel) according to the manufacturer's instructions. First-strand complementary DNA (cDNA) synthesis was performed with the RevertAid H Minus M-MuLV Reverse Transcriptase (Thermo Fisher Scientific) using random primers. For batACE2 determination, total RNA was treated with DNAse I (DNAse-free kit, Thermo Fisher Scientific) for 30 min at 37°C before cDNA synthesis with SuperScript IV reverse transcriptase. Quantitative real-time PCR was performed on a real-time PCR system (QuantStudio 6 Flex, Applied Biosystems) with Power SYBR Green RNA-to-CT 1-Step Kit (Thermo Fisher Scientific). Data were analyzed using the 2-ΔΔCT method, with all samples normalized to GAPDH. Genome equivalent concentrations were determined by extrapolation from a standard curve generated from serial dilutions of the pcDNA3.1-hACE2 plasmid (addgene, 145033) or plasmids encoding a fragment of the RNA-dependent RNA polymerase (RdRp)-IP4 of SARS-CoV-2 or a fragment of the ACE2 genome of each bat species. Primers used for RT-qPCR analysis are given in Table 2.

Table 2. Primers used for RT-qPCR analysis.

Target gene	Forward primer	Reverse primer
ACE2 human	GGACCCAGGAAATGTTCAGA	GGCTGCAGAAAGTGACATGA
ACE2 FLG	TGGGACTCTACCGTTCACTTA	GCTTCATCTCCCACCACTTT
ACE2 Mm	TGCTTATGTCAGGGCAAAGT	CCCACATATCACCAAGCAAATG
ACE2 Nn	CAGTCCTGGGATGCAGATAAG	TGGCTCAGTTAGCATGGATTTA
GAPDH human	GGTCGGAGTCAACGGATTTG	TGGCTCAGTTAGCATGGATTTA
GAPDH FLG	TCATCAACGGAAAGTCCATCTC	ACATACTCAGCACCAGCATC
GAPDH Mm	GTAGTGAAGCAGGCATCAGAG	GGAGTGGGTGTCACTGTTAAA
GAPDH Nn	CCTGTTCGTCAGACAGCCTT	TTGATGGCGACAACTTGCAC
IFIH1 human	ACACGTTCTTTGCGATTTCC	ACCAAATACAGGAGCCATGC
IFIH1 Mm/FLG	GGAGTCAAAGCCCACCATCT	TCCAGACCTTCTTCTGCCAC
IFIH1 Nn	TTTGCCAAGTGAGCCCAATG	AAGCGGTCTTTGCGATTTCC
OAS human	GAGCTCCTGACGGTCTATGC	TTCGTGAGCTGCCTTCTCAG
OAS pan-bat	GGAAGGAGGGCGAGTTCTC	GGTACCAGTGCTTGACCAGG
SARS-CoV-2 nsp12 polymerase	GGTAACTGGTATGATTTC	CTGGTCAAGGTTAATATAGG

2.7 Cloning of qPCR amplicon

To quantify the amounts of bat ACE2 in each cell line, plasmids containing the qPCR amplicon obtained with the primers described in table 2 were generated via TOPO cloning. Briefly, total RNA was extracted from a cadaver of *Myotis myotis* stored at the University of Veterinary and Pharmaceutical Sciences in Brno. For the remaining two bat species, total RNA extracted from NnKi and FLG-R cells were used. RNA was treated for 30 min at 37°C with DNAse I and cDNA synthesized with SuperScript IV reverse transcriptase. These cDNAs were then used as template for PCR amplification of the qPCR bACE2 amplicon using the primers in table 2 and Phusion High-fidelity DNA Polymerase (Thermo). PCR products were gel-purified (NucleoSpin gel and PCR clean-up kit, Macherey-Nagel) and cloned into pCR-Blunt II-TOPO vectors using the Zero Blunt TOPO PCR Cloning Kit (Thermo). Inserts were verified via Sanger sequencing. Plasmids were then used as quantitative qPCR standards.

2.8 Western blot analysis

Proteins extracted from cell lysates were resolved by SDS-polyacrylamide gel electrophoresis on 4-12% NuPAGE Bis-Tris Gel (Life Technologies) with MOPS running buffer and semi-dry transferred to a nitrocellulose membrane with Trans-Blot Turbo system (Bio-Rad). After blocking with 0.05% Tween20 in PBS (PBST) containing 5% dry milk powder for 1 h at room temperature (RT), the membrane was incubated with goat pAB anti-hACE2-700 (1:200, FAB933N R&D Systems) and mouse mAB anti-b-actin (1:5000, A5316 Sigma) diluted in blocking buffer overnight at 4°C. The membranes were then

incubated with DyLight800 secondary AB (1:5000, 46421 Thermo) diluted in blocking buffer for 1 h. Finally, the membranes were revealed using an Odyssey CLx infrared imaging system (LI-COR Bioscience).

2.9 Immunofluorescence microscopy and live cell imaging

Cells grown on glass coverslips were fixed in 4% PFA for 30 min at RT and permeabilized with 0.2% Triton X-100 (Sigma/Merck) in PBS for 10 min at RT. Following blocking with 3% bovine serum albumin (BSA, Sigma) in PBS for 1 h at RT, cells were incubated with goat pAB anti-hACE2 (1:50, AF933 R&D Systems) and mAB anti-SARS-CoV-2-spike (1:1000, GTX632604 Genetex) in 1% BSA in PBS (AB buffer) for 1h at RT or overnight at 4°C. Subsequently, cells were incubated with anti-goat Alexa488 (A-11055, Thermo Fisher Scientific) and anti-mouse Alexa555 (A21427, Thermo Fisher Scientific) secondary antibodies diluted 1:500 in AB buffer for 30 min at RT. Finally, cells were stained with NucBlue Fixed Cell ReadyProbes reagent (Thermo) in PBS for 5 min at RT. Coverslips were washed with ultrapure water (Gibco) and mounted in ProLong Gold antifade (Life Technologies). Sample were visualized with a Leica TCS SP8 confocal microscope (Leica Microsystems) and a white light excitation laser and a 405nm diode laser were used for excitation. Confocal images were taken with automatically optimized pixel format, a 4× frame averaging and a scan speed of 400 Hz through an HC PL APO CS2 63x NA 1.4 oil immersion objective. Overlay pictures of single channel images were digitally processed in Leica LAS X lite software. For live imaging, $5.4x10^4$ to 10^5 cells were plated per quadrant in a µ-Dish 35 mm Quad dish (80416, Ibidi). Cells were infected the next day with SARS-CoV-2 at a MOI of 1 in culture media supplemented with 2.5% FBS and 1% P/S containing propidium iodide. Transmission and fluorescence images were taken at 37°C every 15 min, up to 48 h, using a Nikon BioStation IMQ, with three fields for each condition.

2.10 Attachment and entry assays

Cells plated in monolayers were pre-chilled on ice for 10 min and washed once with cold PBS. Cells were then incubated with SARS-CoV-2 at a MOI of 1 for 1 h on ice. Following three washes with cold PBS, half of the cells was lysed in RA1 lysis buffer (Macherey-Nagel) (“on ice”). The second half of the cells was trypsinized for 15 min on ice and 15min at 37°C after washing of the virus inoculum, then washed with PBS and lysed (“on ice +

trypsin"). The remaining cells were directly transferred to 37°C after washing of the virus inoculum and incubated for 2 or 6 h in warm culture media supplemented with 2% FBS and 1% P/S. After this incubation period, those cells were trypsinized for 30 min at 37°C, washed with PBS and lysed in RA1 buffer ("2h", "6h"). Finally, total RNA was extracted from all cell lysates using the NucleoSpin RNA II kit (Macherey-Nagel).

2.11 VSV-based entry assays

VSV encoding green fluorescent protein (GFP) has been previously described as VSV* [318]. The chimeric virus VSV*ΔG-SARS-CoV-2-$S_{\Delta 21}$ (VSV*ΔG-S), which lacks the homotypic glycoprotein G but rather encodes the spike protein of SARS-CoV-2 (Wuhan-Hu-1 strain) along with GFP has recently been described [319]. Cells were seeded at $1x10^5$ cells per well in 24-well plates in DMEM with 1% FBS. The next day, cells were infected with VSV* (at the indicated MOI) or VSV*ΔG-S (MOI 7) in DMEM without FBS. The virus suspension was removed after 2h and replaced with DMEM with 1% FBS. 16 hpi, cells were washed once with PBS, trypsinized and subsequently fixed in 4% PFA. Fixed cells were washed once with PBS and analyzed by flow cytometry. The percentage of infected cells was identified based on GFP expression.

2.12 Transmission Electron Microscopy

Infected and mock-infected MmBr-ACE2 cells were fixed at 16 hpi by incubation for 24 h in 1% glutaraldehyde/ 4% paraformaldehyde (Sigma, St-Louis, MO) in 0.1 M phosphate buffer (pH 7.2). Samples were then washed in PBS and post-fixed by incubation for 1 h with 2% osmium tetroxide (Agar Scientific, Stansted, UK). Cells were then fully dehydrated in a graded series of ethanol solutions and propylene oxide. They were impregnated with a mixture of (1:1) propylene oxide/Epon resin (Sigma) and left overnight in pure resin. Samples were then embedded in Epon resin (Sigma), which was allowed to polymerize for 48 hours at 60°C. Ultra-thin sections (90 nm) of these blocks were obtained with a Leica EM UC7 ultramicrotome (Wetzlar, Germany). Sections were stained with 2% uranyl acetate (Agar Scientific), 5% lead citrate (Sigma), and observations were made with a transmission electron microscope (JEOL 1011, Tokyo, Japan).

2.13 Poly I:C stimulation

Cells were plated in monolayers in 24-well culture plates. The next day, they were transfected with 250 ng low molecular weight Poly I:C (InvivoGen) or PBS, respectively, using INTERFERin (Polyplus transfection) transfection reagent. Cells were lysed 16 h after transfection and total RNA was extracted using the NucleoSpin RNA II kit (Macherey-Nagel).

2.14 Statistical analysis

Graphical representation and statistical analyses were performed using GraphPad Prism Version 9.0.2 software (GraphPad). Unless otherwise stated, results are shown as means ± SD from 3 independent experiments. Significance was calculated using either Dunnett's multiple comparison test on a two-way ANOVA analysis or Tukey's multiple comparisons test on a two-way ANOVA analysis as indicated. Statistically significant differences are indicated as follows: $^{*}p < 0.05$; $^{**}p < 0.01$; $^{***}p < 0.001$; $^{****}p < 0.0001$; and ns, not significant.

3. Results

3.1 Resistance to SARS-CoV-2 infection in selected bat cell lines

Species belonging to the *Rhinolophus* genus are known natural hosts for numerous SARS-CoV-related betacoronaviruses [320]. Alphacoronaviruses [232,321,322], and possibly betacoronaviruses [230,320], circulate in species belonging to the *Myotis* genera. Primary cells generated from wing biopsies of *R. ferrumequinum*, *M. myotis*, *M. nattereri* and *M. brandtii* (Table 1) were subjected to infection by SARS-CoV-2 at a MOI of 1. Flow cytometry analyses were performed using anti-S antibodies at 24 hpi to assess viral antigen expression. Vero E6 cells, which are African green monkey kidney cells known to be permissive to SARS-CoV-2 [323], were used as positive controls. Around 40% of Vero E6 cells were positive for the viral S protein (Fig. 1A-B). Neither *R. ferrumequinum.* nor *Myotis* spp. primary cells were permissive for productive infection (Fig. 1A-B).

We then tested the permissivity of previously described, immortalized cell lines generated from *Eptesicus serotinus* [324], *Myotis myotis* [314] and *Tadarida brasiliensis* (Table 1) to SARS-CoV-2. *E. serotinus* cells were isolated from brain (FLG) and kidney (FLN) [324] (Table 1). *M. myotis* cells were established from brain (MmBr), tonsil (MmTo), peritoneal cavity (MmPca), nasal epithelium (MmNep) and nervus olfactorius (MmNol) [314] (Table 1). Tb1Lu cells are *T. brasiliensis* lung cells. We also generated immortalized *Nyctalus noctula* cell lines from lung (NnLu), liver (NnLi) and kidney (NnKi) (Table 1). Betacoronaviruses have been sampled in species belonging to all 4 bat genera [230–235]. Human intestinal Caco-TC7 cells and human lung A549 cells, which are both representative of tissues targeted by the virus in infected patients [325], were used as controls. All cells were infected with SARS-CoV-2 at a MOI of 1. Around 23% of Caco-TC7 cells were positive for the viral S protein at 24 hpi (Fig. 1C-D). None of the other selected cells were permissive for productive infection (Fig. 1C-D).

The lack of production of viral protein in the primary and immortalized bat cells, as well as in A549 cells, might be explained by the absence of one or several key pro-viral factor(s) and/or the presence of potent antiviral factor(s).

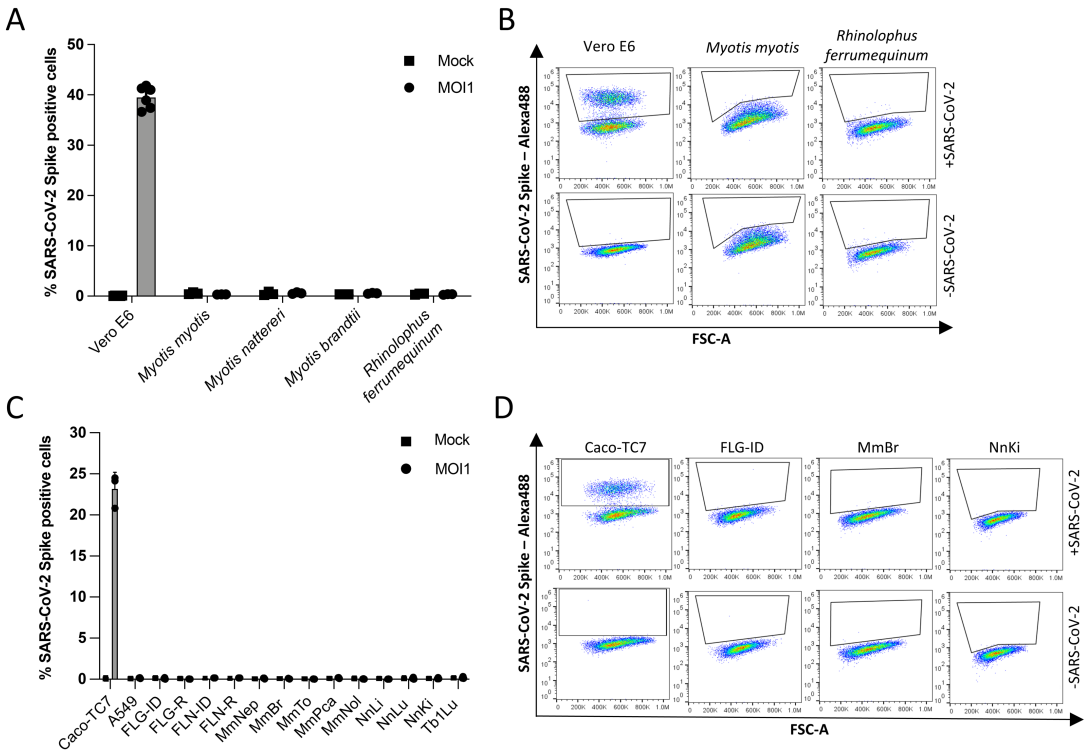

Fig 1. **Resistance to SARS-CoV-2 infection in selected bat cell lines. A**, Primary bat cells derived from wing tissues from four different species, as well as Vero E6 cells, were left uninfected (Mock) or were infected with SARS-CoV-2 at a MOI of 1 for 24 hours and analyzed via flow cytometry for viral spike (S) protein expression. **B**, Representative dot plots of selected primary bat cells and Vero E6 cells. Data points represent three technical replicates. **C,** Immortalized bat cell lines from four different species, as well as Caco TC7 human intestine and A549 human lung epithelial cells, were left uninfected (Mock) or were infected with SARS-CoV-2 at a MOI of 1 for 24 hours and analyzed via flow cytometry for S expression. **D,** Representative dot plots of selected immortalized cells. Data points represent three independent experiments with the exception of A549, FLN-ID and FLN-R cells, where data points represent three technical replicates.

3.2 Expression of endogenous ACE2 and ectopically expressed hACE2 in bat cell lines

To determine whether the absence or low expression of ACE2 was the main limiting factor for SARS-CoV-2 replication in the selected bat cell lines, we evaluated the level of ACE2 expression by RT-qPCR analysis. Levels of ACE2 were above the detection limit in FLG-R, MmTo, MmPca, MmNol cells and in the three Nn cells (Fig. 2A). These cells did not, however, support viral replication (Fig. 1C-D). Thus, the SARS-CoV-2 S protein may have a low affinity for ACE2 expressed in these cells. An alternative explanation might be that the cells analyzed were deficient in expression of both TMPRSS2 and CTSL. To test this hypothesis, viral input was treated with the serine-protease trypsin to activate the S protein and allow viral fusion in a TMPRSS2- and CTSL-independent manner [264]. The assay was performed with NnKi cells since they express the highest level of ACE2 of all bat cells (Fig. 2A). A549-ACE2 cells, which stably overexpressed ACE2, served as positive control cells as they express low levels of TMPRSS2 and moderate levels of CTSL [264]. Pre-

activation of viruses with trypsin increased the percentage of A549-ACE2 cells that were expressing the viral protein S, in a concentration-dependent manner (Fig. 2B). NnKi cells were resistant to productive infection with virions treated or not with trypsin (Fig. 2B), suggesting that cleavage of the S protein is not the factor limiting viral infection in NnKi cells.

To bypass entry-mediated restriction(s) and subsequently investigate the ability of SARS-CoV-2 to replicate in bat cells, we used lentiviral transduction to stably express hACE2 in bat cells. A549-ACE2 served as positive control cells. Six of the 13 bat cell lines, representing three species (*Myotis myotis, Nyctalus noctula* and *Eptesicus serotinus)* tolerated the lentiviral transduction and antibiotic selection. We used RT-qPCR and Western blot analyses to evaluate hACE2 expression in these cell lines (Fig. 2C-D). RT-qPCR analysis revealed that hACE2 mRNA abundances in all transduced cells were higher than in Caco-TC7 cells (Fig. 2C), which support SARS-CoV-2 replication (Fig. 1C-D). This suggests that the transduced cells expressed hACE2 at levels that should permit viral entry. In line with the RT-qPCR analysis (Fig. 2C), Western blot analysis showed that MmBr-ACE2 cells expressed the highest level of hACE2 among all transduced cell lines (Fig. 2D). ACE2 was barely detectable in Caco-TC7 cells (Fig. 2D). A faint band was also detected in non-transduced NnKi cells, likely representing endogenous bACE2. This suggests that *N. noctula* ACE2 is recognized by the antibody raised against hACE2 in this assay and that Nnki cells expressed higher levels of ACE2 than lung and liver cells from the same bat. These data are in line with the RT-qPCR analysis of endogenous ACE2 expression (Fig. 2A). These assays revealed that the level of hACE2 expression varied considerably among transduced bat cell lines. Expression of hACE2 and antibiotic resistance are under the control of 2 different promoters in the bicistronic lentiviral vector used. Variable strength of the two promoters in the different cell lines could generate cells that survived the antibiotic treatment but did not express hACE2 (or very little of it). Nevertheless, despite expressing differential levels of hACE2, the transduced cells offered the opportunity to investigate the interaction between viruses belonging to the SARS-CoV-2 lineage and bat cells.

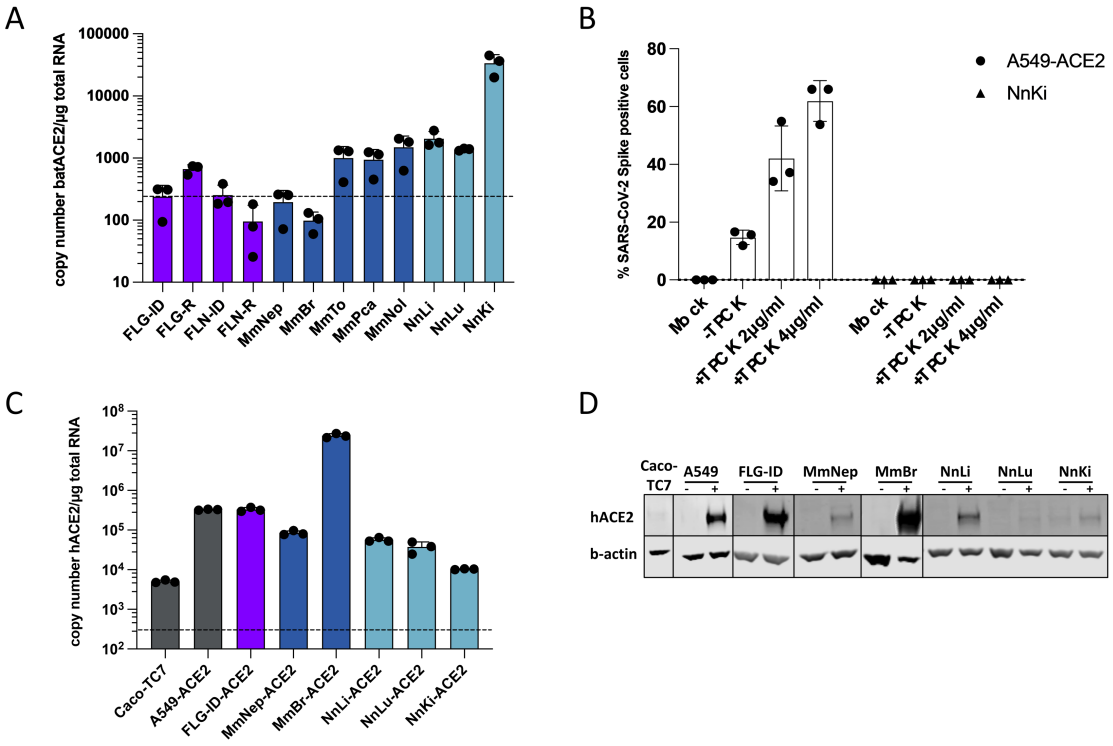

Fig. 2. Expression of endogenous ACE2 or ectopically-expressed hACE2 in bat cell lines. a, Quantification of copy numbers per µg of total cellular RNA of endogenously expressed ACE2 in indicated bat cell lines via qPCR analysis. **B.** A549-ACE2 and NnKi cells were left uninfected (Mock) or were infected with SARS-CoV-2 at a MOI of 1 in the absence of FBS and TPCK (-TPCK), or in the absence of FBS and presence of trypsin TPCK at 2µg/ml or 4 µg/ml. The percentages of S-positive cells were determined by flow cytometric analysis. Data points represent three biological replicates. **C, D,** Indicated bat and human cell lines were stably transduced with a lentivirus vector expressing the hACE2 gene and selected with blasticidin treatment. Human Caco-TC7 intestine cell line served as non-transduced control. **B,** Amount of ectopically-expressed hACE2 gene in each cell line was measured by qPCR analysis and indicated as gene copy number per µg of total cellular RNA. **C,** Whole-cell lysates were analyzed by Western blotting with antibodies against the indicated proteins. Western blots are representative of two independent experiments. (A, B) dotted line indicated limit of detection in qPCR assays.

3.3 Expression of hACE2 allows efficient replication of SARS-CoV-2 in *Eptesicus serotinus* and *Myotis myotis* brain cells

The six transduced bat cell lines and A549-ACE2 cells were infected with SARS-CoV-2 for 24 hours at a MOI of 1. CPEs were observed in MmBr-ACE2 cells. To illustrate this, we performed time-lapse microscopy of MmBr-ACE2 cells, infected or not, in the presence of propidium iodide (PI) for 48 hours. Cells were rapidly forming syncytia (around 12 hours). Cell death was observed as early as 34 hours, as assessed by the PI uptake due to the loss of membrane integrity (Fig. 3A and movies 1 and 2). Syncytia represent cell-to-cell fusing events mediated by the interaction between cell-surface expressed S protein and

ACE2 [316]. Neither CPE nor syncytia formation were observed in the other cells, as illustrated by the video of infected FLG-ID-ACE2 cells (Fig. 3B and movies 3 and 4).

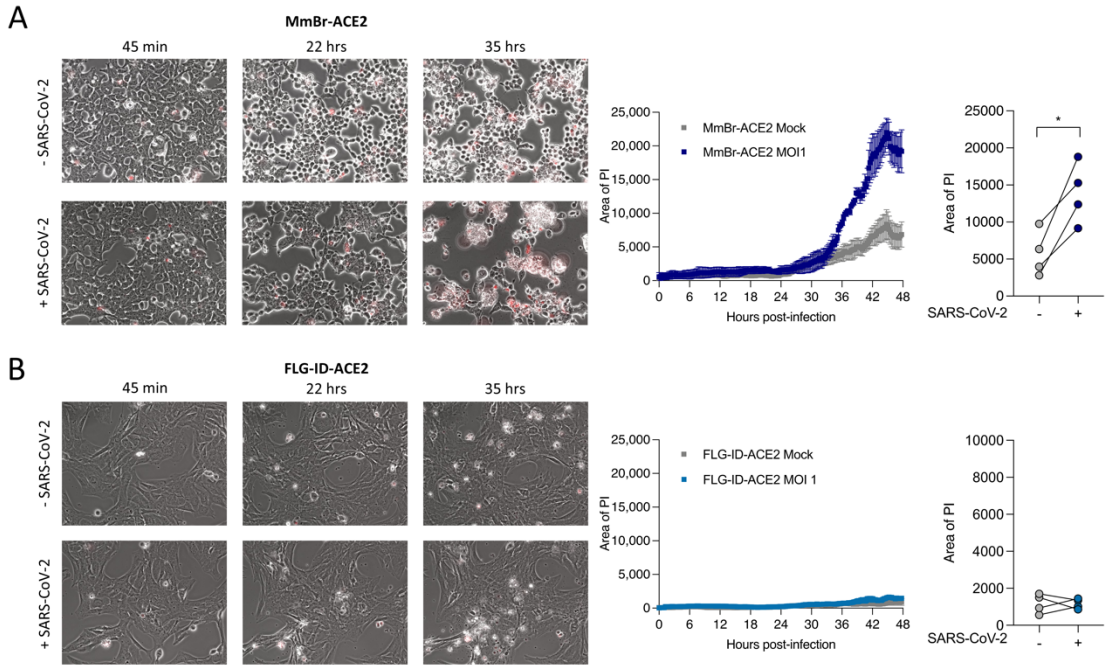

Fig. 3. Time-lapse microscopy of *Myotis myotis* and *Eptesicus serotinus* brain cells during SARS-CoV-2 infection. MmBr-ACE2 (**A**) and FLG-ID-ACE2 (**B**) cells were left uninfected (Mock) or were infected with SARS-CoV-2 at a MOI of 1 in media containing propidium iodide (PI) as cell death marker. Images were taken every 10 minutes. Quantification of cell death (area of PI) displayed on the right of corresponding video cutouts. Results are mean ± SD from three fields per condition.

To avoid cell death, MmBr-ACE2 cells were infected with 25 times lower virus doses (MOI of 0.04) than the other cells (Fig. 4). Assessment of viral replication by RT-qPCR revealed that viral RNA yields increased between 6 and 24 hpi in A549-ACE2 cells, and subsequently reached a plateau (Fig. 4A). Viral RNA yields also increased between 6 and 24 hpi in FLG-ID-ACE2 cells but then dropped back to their 6h-levels at 48 hpi (Fig. 4A), suggesting that these cells efficiently controlled viral replication. Viral RNA abundance slightly increased between 6 and 24 hpi in MmNep-ACE2 cells (Fig. 4A), suggesting a low level of viral RNA production, before decreasing at 48 hpi. The profile of viral RNA yield was similar in MmBr-ACE2 cells than in A549-ACE2 cells (Fig. 4A), indicating a robust viral replication, especially when considering that the cells were infected with 25 times less viruses than the others. No increase in viral RNA yield was observed in the 3 Nn cell lines between 6 hpi and later time points (Fig. 4A), suggesting an absence of viral replication.

A549-ACE2, FLG-ID-ACE2, MmNep-ACE2 and MmBr-ACE2 cells, which are competent for viral RNA production (Fig. 4A), were analyzed for the expression of viral

proteins through immunofluorescence imaging using antibodies specific for S and hACE2 at 24 hpi. NnKi-ACE2 cells were included in the analysis for comparison. Cells positive for S protein were observed in all cell lines (Fig 4B). However, the proportion of positive cells seemed to vary considerably among cell lines (Fig 4B), which agrees with the disparities in the ability of the cells to sustain a productive infection (Fig. 4A). As expected (Fig. 4A), almost none of the NnKi-ACE2 cells were expressing the S protein (Fig. 4B). An hACE2 signal was only detected in MmBr-ACE2 cells (Fig. 4B). These cells expressed the highest levels of hACE2 among the transduced cell lines (Fig. 2C-D). Thus, the selected anti-hACE2 antibodies appeared to allow detection by immunofluorescence analysis only when the protein was expressed at high levels. The confocal images also confirmed the presence of syncytia in MmBr-ACE2 infected cells (Fig. 4B).

Flow cytometry analyses were used to further evaluate hACE2 expression in transduced bat cells. They revealed that around 80% of MmBr-ACE2 cells were positive for hACE2 (Fig. 4C), which is in line with the RT-qPCR and Western blot and analyses (Fig. 2C-D). About 10% of FLG-ID-ACE2 brain cells were positive for hACE2 (Fig. 4C). On average, 1-4% of A549-ACE2 and MmNep-ACE2 cells were positive for hACE2 and even lower percentages of Nn cells were expressing hACE2 (Fig. 4C). These low percentages were surprising in light of the RT-qPCR and Western blot data (Fig. 2C and 2D). Cells counted as negative for hACE2 signal may, however, express levels that are under the detection limit of the assay. Alternatively, anti-ACE2 antibodies may recognize only a subpopulation of the protein by cytometry, such as, for instance, glycosylated and/or truncated forms [326,327]. To reduce the disparities between cell lines and to obtain cell populations that were enriched for hACE2 expression ($ACE2^+$), live MmNep-ACE2 and Nn-ACE2 cells were sorted based on hACE2 cell surface expression. Our attempts to produce NnKi-$ACE2^+$ and NnLu-$ACE2^+$ cells remained unsuccessful. By contrast, flow cytometric analysis revealed a significant enrichment of cells expressing hACE2 in MmNep-$ACE2^+$ and NnLi cells-$ACE2^+$ cells (Fig. 4C). On average, 20% of MmNep-$ACE2^+$ cells and 40% of NnLi-$ACE2^+$ cells were positive for hACE2 (Fig. 4C).

Flow cytometry analyses were performed to estimate the number of transduced cells positive for S. On average 25% of A549-ACE2 cells were positive for S proteins when infected for 24 hours at a MOI of 1 (Fig. 4D). This was surprising since only 3% of them appeared hACE2-positive (Fig. 4C). Knowing that these cells are not permissive to viral replication in the absence of hACE2 over-expression (Fig. 1C), these results further suggest that the anti-hACE2 antibodies recognized only a subpopulation of hACE2. Around 25%

of MmBr-ACE2 cells and 5% of FLG-ID-ACE2 were positive for S protein when infected for 24 hours at a MOI of 0.04 or 1, respectively (Fig. 4D). Very little MmNep-ACE2 cells (around 1%) were expressing the S protein upon infection. Despite being significantly more enriched in ACE2-positive cells (Fig. 4C), only 3% of MmNep-ACE2^{+} cells were infected (Fig. 4D). Similarly, NnLi-ACE2^{+}, which expressed significantly more ACE2 than the initial NnLi-ACE2 population (Fig. 4C), were poorly infected (Fig. 4D). This suggests that expression of hACE2 was not sufficient to allow robust viral replication in NnLi-ACE2 and MmNep-ACE2 cells. Less than 0.2% of the NnLu-ACE2 and NnKi-ACE2 cells were positive for the S protein (Fig. 4D). These flow cytometry data were consistent with viral RNA yield (Fig. 4A). Trypsin activation did not enhanced infection of MmNep-ACE2+ or NnLi-ACE2+ cells (Fig. 4E), suggesting that cleavage of the S protein was not the factor limiting viral infection in these cells.

To assess whether infectious virions were released from transduced bat cells, all cells were all infected at a MOI of 1 and supernatants were collected at 6, 16, 24 and 48 hpi. Viral titers were evaluated on Vero E6 cells (Fig. 4F). Approximately 200 PFU/ml were collected from the supernatant of all cell lines at 6 hpi (Fig. 4F). These infectious viruses represent input viruses that were carried over from the inoculum. A549-ACE2 cells released around $8x10^3$ PFU/ml and $2x10^4$ PFU/ml at 16 and 24 hpi, respectively (Fig. 4F). Production of infectious viruses reached $2x10^5$ PFU/ml at 48 hpi in these cells (Fig. 4F). Despite producing around 1 log less viral RNA than A549-ACE2 cells at 24 hpi (Fig 4A), FLG-ID-ACE2 cells released similar amounts of infectious particles at 24 hpi (Fig. 4F). This suggests that A549-ACE2 cells produce more non-infectious defective genomes than FLG-ID-ACE2 cells. Significantly less infectious particles were produced by FLG-ID-ACE2 cells at 48 hpi than at 24 hpi (Fig. 4F), which is in accordance with a decrease of viral RNA production between 24 hpi and 48 hpi (Fig. 4A) and further suggests a control of viral infection. Approximately 200 PFU/ml were collected from the supernatant of Mm and Nn transduced cell lines at all time point, including the two cell lines enriched in ACE2, which suggests that none of these cells release infectious particles. Based on viral RNA and viral protein quantification (Fig. 4A and 4D), transduced Nn cells were not expected to produce infectious particles. By contrast, it was surprising that MmBr-ACE2 cells did not release infectious virions since they produced viral RNA and proteins (Fig. 4A and D).

Together, these data revealed that expression of hACE2 allowed the virus to complete its replication cycle in *E. serotinus* FLG-ID brain cells, suggesting that once the ACE2-mediated refractory state to SARS-CoV replication is overcome, these cells are permissive

for productive infection. Overcoming the ACE2-mediated restriction in *M. myotis* brain cells stably expressing hACE2 (MmBr-ACE2) renders the cells competent for production of viral RNA and proteins. Infectious particles, however, were not released from these cells, suggesting the existence of another cellular restriction at a late stage of the viral replication cycle. In MmNep-ACE2+ and NnLi-ACE2+ cells, high expression of hACE2 was not sufficient to allow robust viral replication, suggesting a deficiency in key proviral factor(s) and/or expression of potent antiviral factor(s) that act at an early stage or viral replication.

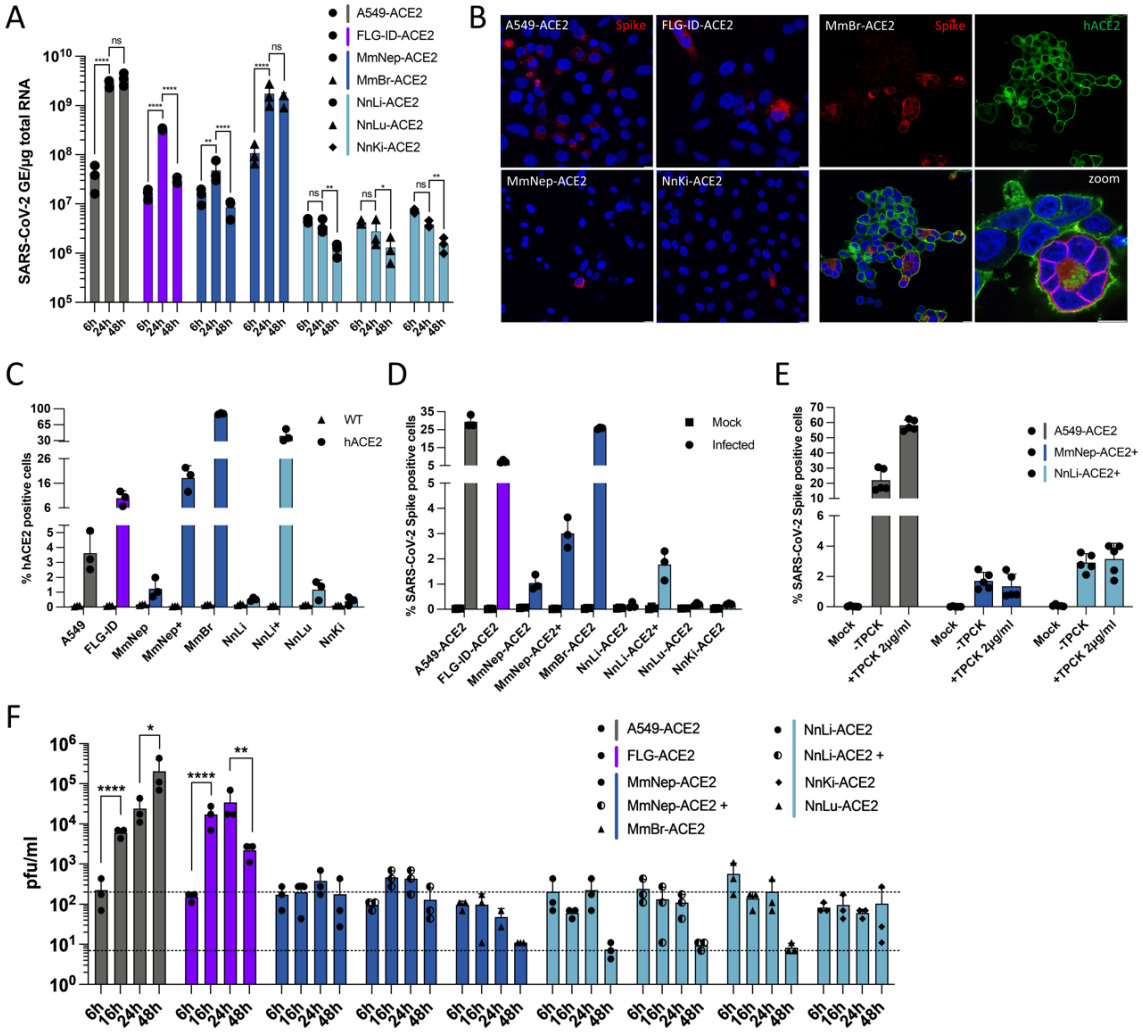

Fig. 4. Expression of hACE2 allows efficient replication of SARS-CoV-2 in *Myotis myotis* and *Eptesicus serotinus* cells. Transduced bat cell lines were left uninfected (Mock) or were infected with SARS-CoV-2 at a MOI of 1, with the exception of MmBr cells that were infected at a MOI of 0.04 (A, B and E). **A,** The relative amounts of cell-associated viral RNA were determined by qPCR analysis and are expressed as genome equivalents (GE) per µg of total cellular RNA at different time post-infection. All results are expressed as fold-increases relative to uninfected cells. **B,** Infected cells were stained at 24 hpi with anti-SARS-CoV-2 S protein (red) and/or anti-hACE2 antibodies (green). Nuclei were stained with Nucblue (blue). Scale bar, 10 µm. **C, D**, The percentages of the indicated cells that expressed hACE2 (C) or SARS-CoV-2 S proteins (D) were determined by flow cytometric analysis at 24 hpi. **E,** A549-ACE2, MmNep-ACE2+ and NnLi-ACE2+ cells were left uninfected (Mock) or were infected with SARS-CoV-2 at a MOI of 1 in the absence of FBS and TPCK (-TPCK), or in the absence of FBS and presence of trypsin TPCK at 2µg/ml. The percentages of S-positive cells were determined by flow cytometric analysis. Data points represent three biological replicates. **F,** The presence of extracellular infectious viruses in the culture medium of the indicated cells was determined by $TCID_{50}$ assays with Vero E6 cells at 6, 16, 24 and 48 hpi. The lower dashed line indicates the limit of detection and the upper dashed line indicates the viral input (based on the average titration values at 6h). (A, D, E, F) Data points represent three independent experiments. Statistical test: (a) Dunnett's multiple comparison test on a two-way ANOVA analysis (n.s: not significant; * p-value < 0.05, ** p-value < 0.01, *** p-value < 0.001, **** p-value < 0.0001); (e, f) Tukey's multiple comparisons test on a two-way ANOVA analysis (n.s: not significant, * p-value < 0.05, ** p-value < 0.01, *** p-value < 0.001, **** p-value < 0.0001).

3.4 An abortive entry route exists in bat cells

To investigate further ACE2-mediated restriction, we performed viral binding and entry assays on a selection of bat cells, transduced or not with hACE2 (Fig. 5A). Infected cells were kept on ice for 1 hour, washed three times and then either lysed ('on ice') or incubated at 37 degrees for 2 or 6 hours. To remove potential residual bound particles, the warmed cells were treated with trypsin for 30 minutes prior to lysis (Fig. 5A). We performed the assays with A549, FLG-ID and NnKi cells since they tolerated the three washes on ice without detaching from the plates. For each cell line, we compared viral RNA abundance in wild-type *versus* hACE2-expressing cells. Viral RNA detected in cells that were kept on ice represent input viruses bound to cellular membranes. In all six cell lines, we indeed detected viral RNA bound to cell membranes (Fig. 5B), suggesting that hACE2 expression is not required for viral attachment to the cell surface. Such ACE2-independent binding of the S protein could be mediated by heparan sulfate, as described in several human cell lines [271,328], or by endogenous bat ACE2 when it is expressed at detectable levels (Fig. 2A). hACE2 expression may however enhance viral binding to A549 and FLG cell membranes since around 500 more viral genome copies per µg of total RNA were detected in cold transduced cells than in unmodified ones (Fig. 5B). The abundance of viral RNAs increased between 2 and 6 hours both in A549-ACE2 and FLG-ACE2 cells but not in wild-type cells (Fig. 5B). These results confirm that viral replication occurred in hACE-2 expressing A549 and FLG cells (Fig. 4). No increase in viral RNA yield was observed between 2 and 6 hours

in NnKi-ACE2 cells (Fig. 5B), confirming the inability of the virus to replicate in these cells (Fig. 4). Viral RNA detected at 2 or 6 hpi in non-transduced cells (Fig. 5B) may represent viruses that remained attached to the cell surface despite the trypsin treatment, or viruses that penetrated the cells via an hACE2-independent route.

To address whether SARS-CoV-2 enters and fuses with endosomal membranes of bat cells, we took advantage of a chimeric VSV*ΔG-SARS-CoV-2-$S_{\Delta 21}$ (VSV*ΔG-S), which lacks its homotypic glycoprotein G but encodes for the spike protein of SARS-CoV-2 (Wuhan-Hu-1 strain) along with GFP instead [319]. Human A549 and hamster BHK-21 cells, which are not susceptible to SARS-CoV-2 [263,306], were used as negative controls, while human A549-ACE2 and Caco-TC7 cells served as positive controls. We first tested the ability of a GFP-recombinant VSV harboring its glycoprotein G (VSV*) to replicate in FLG-ID, MmNep, MmBr, NnLi and NnKi cells. VSV* replicated in all transduced and non-transduced bat and human cell lines, as well as in BHK-21 cells (Fig. 5C and 5D), albeit at different levels. For instance, around 90% of MmBr cells were expressing GFP when infected with a MOI of 0.001 while only 10% of FLG cells were GFP positive when infected with a MOI of 5 (Fig. 5D).

As expected, Caco-TC7 cells were susceptible to VSV*ΔG-S, whereas BKH-21 cells were not (Fig. 5E). No GFP-positive A549 cells were identified following VSV*ΔG-S infection (Fig. 5E). However, detection of viral RNA in A549 cells at early times post-infection (Fig. 5B) and at 24 hpi [329] suggest that the virus can be internalized by these cells. The fusion step may thus be the step limiting viral replication in A549 cells. Non-transduced FLG-ID, MmNep, NnLi and NnKi cells were not susceptible to S-mediated entry of the chimeric virus (Fig. 5E). By contrast, around 2% of non-transduced MmBr cells were GFP positive (Fig. 5E), indicating that at least a fraction of MmBr cells are competent for viral entry and fusion.

Around 15% of A549-ACE2 cells and 1% of FLG-ID-ACE2 cells were expressing GFP upon VSV*ΔG-S infection (Fig. 5F). This was surprising since both cell lines express similar level of hACE2 (Fig. 2C). This difference could be due to a poor replication of VSV in FLG-ID cells (Fig. 5C). The percentage of MmNep-ACE2, MmNep-ACE2+, MmBR-ACE2, NnLi-ACE2, NnLi-ACE2+ and NnKi-ACE2 that were expressing GFP varied considerably from one cell line to another (Fig. 5F). These percentages correlated with the level of hACE2 expression (Fig. 4C). For instance, around 30% of MmNep-ACE2+ cells and 10% of NnLi-ACE2+ cells were expressing GFP upon VSV*ΔG-S infection while only

around 1% of MmNep-ACE2 cells and NnLi-ACE2 were GFP-positive (Fig. 5E). Thus, the level of hACE2 expression in transduced bat cells largely contribute to their susceptibility.

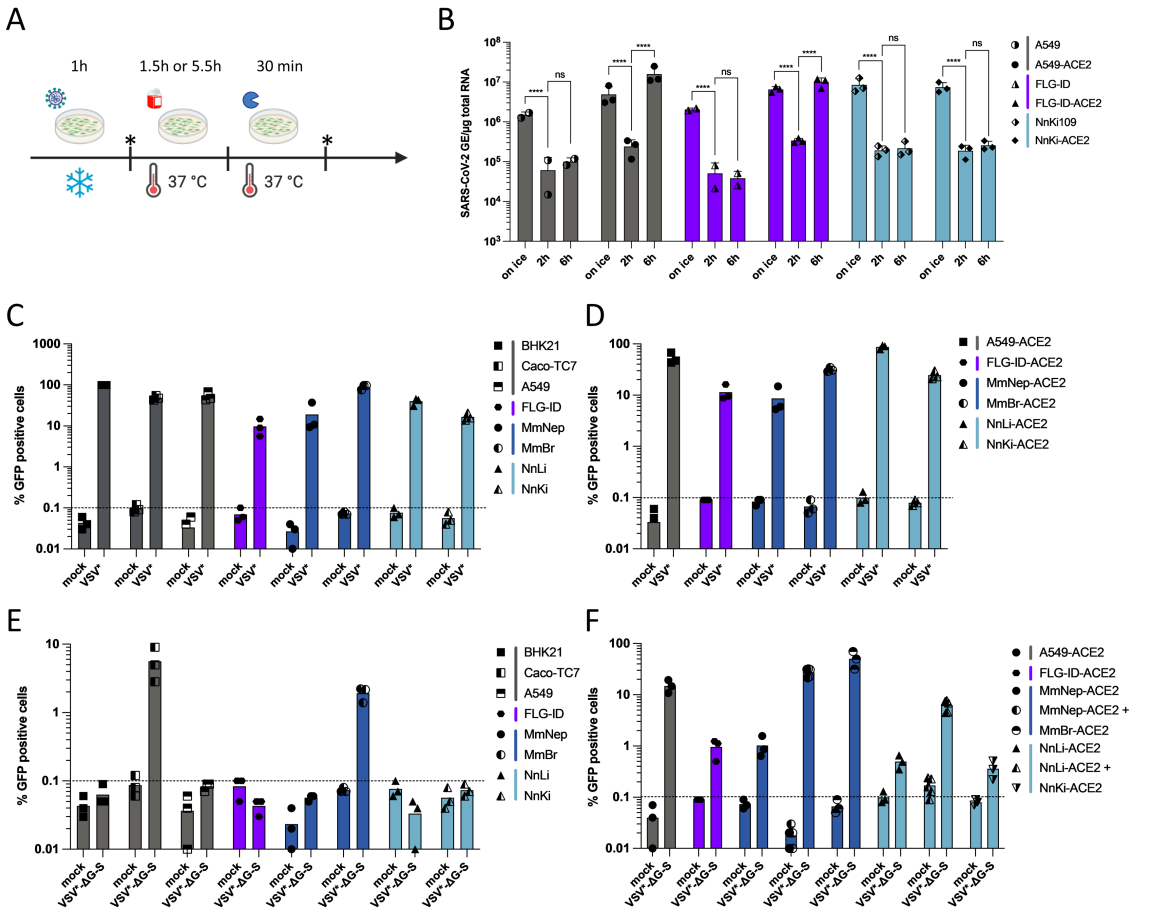

Fig. 5. An abortive entry route exists in bat and human cells. A, scheme summarizing the experimental workflow Cells were incubated with SARS-CoV-2 at a MOI of 1 for 1 hour on ice to allow viral attachment. After extensive washing, a portion of the cells was lysed ("on ice") and the remaining cells were incubated for 2 or 6 hours at 37°C to permit viral internalization. After the incubation period, these cells were lysed after 30 min trypsinization to remove bound viruses from the cell surface ("2h", "6h"). **B**, The relative amounts of cell-associated viral RNA were determined by qPCR analysis and are expressed as genome equivalents (GE) per µg of total cellular RNA at the indicated time post-infection. All results are expressed as fold-increases relative to uninfected cells. Data points represent three independent experiments. Statistical test: Dunnett's multiple comparison test on a two-way ANOVA analysis (n.s: not significant, * p-value < 0.05, ** p-value < 0.01, *** p-value < 0.001, **** p-value < 0.0001). **C-F.** Indicated cell lines were infected with VSV* (MOI ranging from 0.001 to 5) or with VSV*ΔG-S at a MOI of 7. Percentage of infected cells was determined at 16-18hpi through GFP expression and flow cytometry analysis. Data points represent independent experiments. Dotted lines represent the limit of sensibility of the assay. **C.** BHK21, Caco-TC7, A549 and MmNep cells were infected with a MOI of 0.001, MmBr cells with a MOI of 0.05, FLG-ID cells with a MOI of 5, NnLi cells with a MOI of 0.5 and NnKi cells with a MOI of 0.1. **D**. A549-ACE2 and MmBr-ACE2 cells were infected with a MOI of 0.001, MmNep-ACE2 with a MOI of 0.005, FLG-ID-ACE2 cells with a MOI of 5, NnLi cells with a MOI of 0.1 and NnKi cells with a MOI of 0.05.

3.5 Infectious particles are produced by MmBr-ACE2 cells but are not released

Since MmBr-ACE2 cells sustained the production of viral RNA and proteins (Fig. 4A and D), we were intrigued by the absence of infectious particle release (Fig. 4F). Despite infecting these cells with a MOI of 0.04 (Fig. 4A, B and D) to reduce the CPEs observed at a MOI of 1 (Fig. 3), we wondered whether cytokines released by infected cells and/or dying cells may stimulate damage-associated molecular patterns (DAMPs) and thus trigger an antiviral response inhibiting viral replication in Vero E6 cells. Other possibilities include a defect in viral assembly and/or in viral transport through the secretory pathway in MmBr-ACE2 cells. Alternatively, these cells may only produce immature non-infectious viral particles. To investigate these hypotheses, supernatants collected from MmBr-ACE2 cells, and as controls, from A549-ACE2 cells, were titrated on Vero E6 cells. Prior to titration, supernatants were first clarified to remove cell debris and then subjected to ultracentrifugation to pellet the virus and remove potential cytokines. Flow cytometry analyses using anti-S antibodies were done on the same samples to verify that the cells were infected (Fig. 6A). Supernatants from A549-ACE2 cells contained around 10^4 PFU/ml infectious particles (Fig. 6B). In line with previous analysis (Fig. 4F), only infectious particles representing input viruses were recovered in supernatants, ultracentrifuged or not, of infected MmBr-ACE2 cells (Fig. 6B). These data suggest that immune-stimulatory components, such as dying cells or cytokines, that may be present in infected MmBr-ACE2 cell culture supernatants, did not affect the results of the titration assays. To assess the presence of intracellular infectious particles in MmBr-ACE2 cells, the titration assays were performed on crude cell lysates collected at 24 hpi. Around one log more infectious particles were retrieved from lysed A549-ACE2 cells than from their supernatant (Fig. 6B). About 10^4 PFU/ml were retrieved from lysed MmBr-ACE2 cells, which is around 3 log more than in the culture supernatant (Fig. 6B), suggesting that viral assembly and maturation takes place in these cells. The absence of viral release may thus be due to a defect in viral transport through the secretory pathway.

To investigate the fate of infectious virions in MmBr-ACE2 cells, we performed a transmission electron microscopy analysis of cells infected at a MOI of 0,04 for 24 h (Fig. 6C-D). Non-infected cells served as negative control cells (Fig. 6E). As previously described in SARS-CoV-2 infected cells [330,331], viral replication factories, which consisted of double-membrane vesicles (DMVs), were observed in infected MmBr-ACE2 cells (Fig. 6C-D). The virions were around 80-100 nm in diameter, which is the expected size for SARS-CoV2 virus [331]. The images showed that virions remained bound to the

surface of infected MmBr-ACE2 cells (Fig. 6C-D). Such retention could be due to an endogenous expression of tetherin, an interferon (IFN)-induced gene known to retain SARS-CoV-2 at the cell surface of human cells [332] or to a high expression of hACE2.

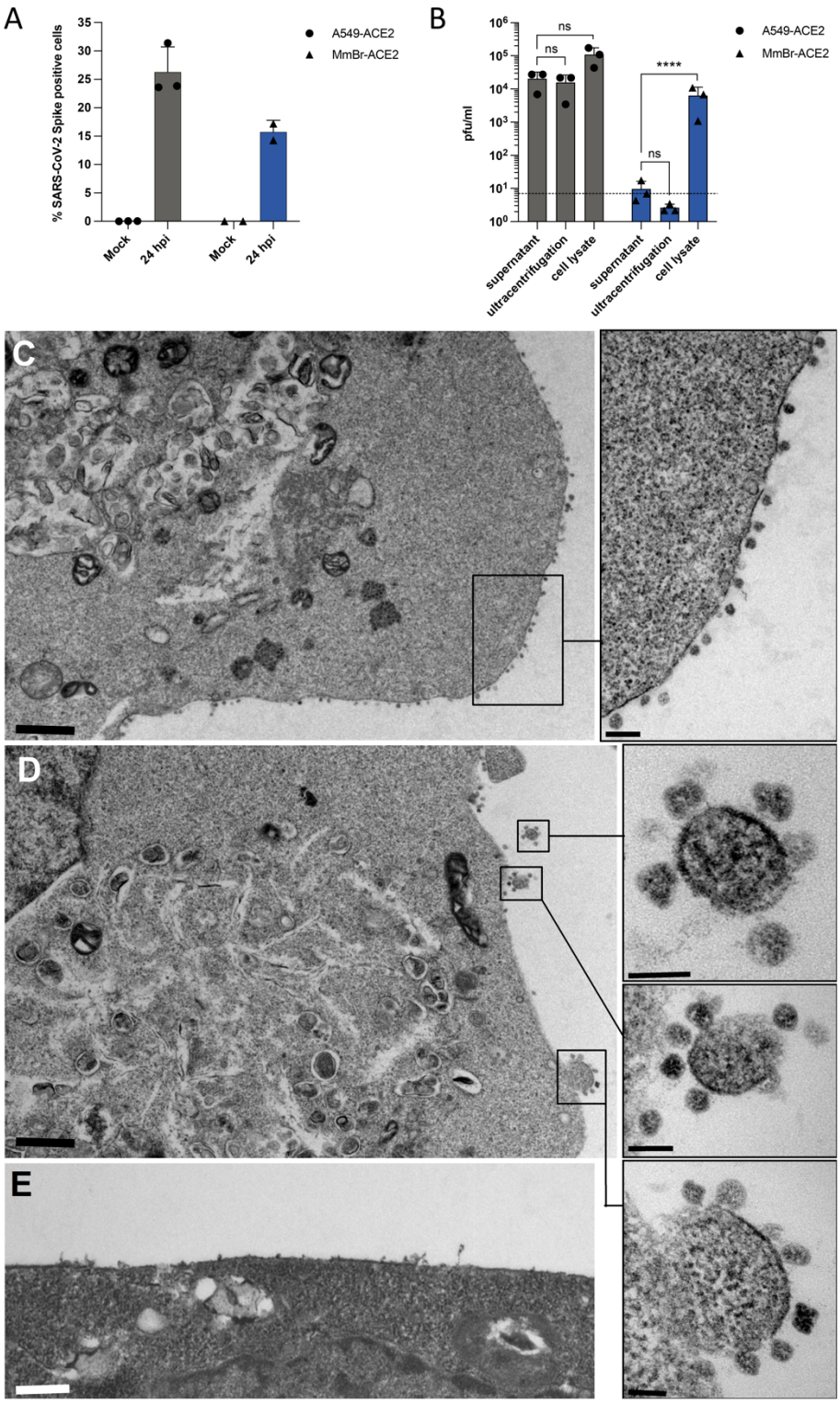

Fig. 6. Infectious particles are retained at the surface of MmBr-ACE2 cells. A549-ACE2 and MmBr-ACE2 cells were left uninfected (Mock) or were infected for 24 hours at a MOI of 1 or 0.04, respectively. **A,** The percentages of cells that contained SARS-CoV-2 S proteins were determined by flow cytometric analysis. **B,** The presence of extracellular infectious viruses in the culture medium of the cells was determined by $TCID_{50}$ assays performed on Vero E6 cells. Supernatants were either clarified or clarified and purified by ultracentrifugation. Alternatively, cell-associated infectious virions were titrated on Vero E6 cells from whole cell lysates. Data points represent three independent experiments. Statistical test: Dunnett's multiple comparison test on a two-way ANOVA analysis (n.s: not significant, * p-value < 0.05, ** p-value < 0.01, *** p-value < 0.001, **** p-value < 0.0001). **C-E**, At 16 h post-infection, numerous viral particles were observed on the cell surface of MmBr-ACE2 cells, attached to the plasma membrane (C, D). Boxed areas in the low magnification photographs in C and D are shown at higher magnification in the right panels. Uninfected cells showed no viral particles on their surface (E). Bars are 1mm in C and D; 0,5mm in E; 200 nm and 100 nm in the high magnification panels extracted from the photographs C and D, respectively.

3.6 Viral IFN counteraction mechanisms are species-specific

Quantification of intracellular viral RNA and titration assays revealed that FLG-ACE2 cells, and, to a lesser extent, MmNep-ACE2 cells, controlled viral replication over time (Fig. 4A). By contrast, viral RNA yield remained high between 24 and 48 hpi in A549-ACE2 and MmBr-ACE2 cells (Fig. 4A). To assess whether the IFN response could contribute to viral containment in FLG-ACE2 and MmNep-ACE2 cells, we compared mRNA abundance of two ISGs upon stimulation or infection in these four cell lines. We selected OAS1 and IFIH1, two ISGs that are conserved across vertebrate species [174]. Moreover, OAS1 expression is associated with reduced COVID-19 death [333] and IFIH1 codes for Mda5, the protein responsible for sensing SARS-CoV-2 replication intermediates, and thus initiating the IFN response, in human cells [282,283]. We first evaluated the expression of the two selected ISGs upon transfection with Poly I:C, a synthetic dsRNA analog. All four cell lines contained transcripts for these two ISGs and responded well to the stimulation (Fig. 7A-B), demonstrating that they possess intact IFN-induction and -signaling pathways.

We then evaluated the mRNA abundance of these two ISGs in cells infected for 6, 24 and 48 hours (Fig. 7C-D). No increase of OAS1 and IFIH1 expression was observed in A549-ACE2 cells (Fig. 7C-D). This agrees with a previous report showing that infection of A549-ACE2 by SARS-CoV-2 is characterized by an absence of IFN response [334]. By contrast, the abundance of OAS1 and IFIH1 transcripts increased between 6 and 24 hpi in FLG-ACE2 and MmNep-ACE2 cells (Fig. 7C-D) and remained elevated at 48 hpi in both cell lines (Fig. 7C-D). In MmBr-ACE2 cells, the infection triggered the induction of OAS1 expression but not of IFIH1 (Fig. 7C-D), suggesting that the virus is able to dampen the expression of at least one ISG in this cell type.

Together, our data confirmed that SARS-CoV-2 efficiently counteracts ISG induction in A549-ACE2 cells [334] and revealed that it is not the case in FLG-ACE2 and MmNep-ACE2 cells. The control of viral replication observed in these two cell lines (Fig. 5) could thus be due to the expression of a set of ISGs with potent antiviral functions. Interestingly, IFN-mediated barriers could also differ in bat cells derived from different organs since the virus seems to dampen IFIH1 expression in MmBr-ACE2 cells but not in MmNep-ACE2 cells.

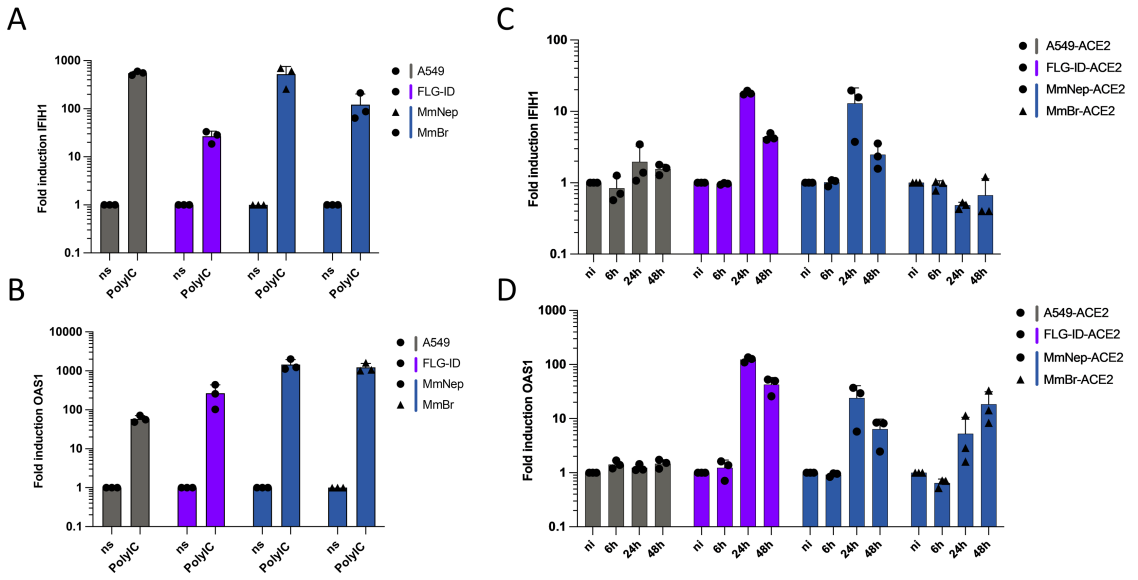

Fig. 7. Viral IFN counteraction mechanisms are species-specific. A, B, Non-transduced cell lines were transfected with 250 ng low-molecular weight Poly I:C or were treated with PBS for 16 hours. The relative amounts of *IFIH1* mRNA (a) and *OAS1* mRNA (b) were determined by qPCR analysis. Results are expressed as fold-increases relative to unstimulated PBS-treated cells. **C, D**, Whole cell lysates of infected cells (same lysates used for viral quantification in panel 4a) were analyzed via RT-qPCR assays for the relative amounts of *IFIH1* mRNA (c) and *OAS1* mRNA (d). Results are expressed as fold-increases relative to uninfected cells. (**A-D**) Glyceraldehyde 3-phosphate dehydrogenase (GAPDH) of corresponding species was used as house-keeping gene. Data points represent three independent experiments.

4. Discussion

The development of novel bat cellular models is essential to understand the molecular mechanisms underlying the ability of bats to serve as reservoirs for numerous viruses, including alpha- and beta-coronaviruses. We first produced *R. ferrumequinum*, *M. myotis*, *M. nattereri* and *M. brandtii* primary cells to evaluate their permissivity to infection with SARS-CoV-2. None of them supported viral replication, not even *R. ferrumequinum* cells, which have been isolated from bats belonging to the same genus as the bat host of BANAL-52, a potential ancestor of SARS-CoV-2 [335]. These primary cells, which were generated from patagium biopsies of living bats, exhibited a dermal-fibroblast phenotype. A single-cell transcriptomic analysis showed that *R. sinicus* skin cells express moderate levels of ACE2 and very little TMPRSS2 [336]. The virus may thus be able to enter the skin primary cells but the fusion between viral and membrane may not take place as the S protein is not cleaved. Further experiments will be required to identify at which step of the replication cycle the virus is stopped in these primary cells.

We established the first three immortalized *Nyctalus noctula* cell lines using liver, kidney and lung tissues from a single bat. These organs may be physiologically relevant for bat infection since bat coronaviruses, such as MERS-CoV, infect lung and liver of fruit bats [320]. In addition to coronaviruses, *N. noctula* carry other viruses with zoonotic potential such as paramyxoviruses and hantaviruses [337,338]. The Nn cells that we have developed represent thus novel opportunities to study bat-borne viruses. We found that Nn kidney cells expressed higher levels of ACE2 than Nn cells derived from lung or liver. Likewise, ACE2 is expressed at high levels in *R. sinicus* kidney, as revealed by comparative single-cell transcriptomic [336] and *in silico* analysis of ACE2 expression pattern in various tissues. ACE2 is also highly expressed in human kidney [339]. Thus, kidney cells appear relevant to study betacoronavirus replication.

Myotis myotis, *Tadarida brasiliensis, Eptesicus serotinus*, and *Nyctalus noctula* cells were resistant to infection. ACE2 from *M. myotis* and *T. brasiliensis*, as well as from a species of the *Eptesicus* genus, permitted S-mediated entry of pseudotyped VSV when ectopically expressed in human cells refractory to SARS-CoV-2 infection [340]. This means that when expressed at high levels, ACE2 from these three species interacts with the viral S protein. As in human A549 cells, ACE2 may be expressed at a level which is too low to allow viral entry in our bat cell lines. Potential ability of *N. noctula* ACE2 to bind S protein has not been reported and the genome of this bat genus is yet to be sequenced. Hence, low affinity

between S protein and ACE2 and/or low level of ACE2 expression may hamper viral replication in these cells. Our results highlight the importance of performing experiments in the context of genuine infection of bat cells to predict their ability to support viral replication.

SARS-CoV-2 RNA was detected in non-transduced A549, FLG-ID and NnKi cells at early time post-infection. As the virus could not be removed by trypsin treatment of the cells, it likely represents input virus that entered the cells via an ACE2-independent manner, as described previously for Vero E6 cells [264] and human H522 lung adenocarcinoma cells [341]. The VSV-based entry assay clearly showed that A549, FLG-ID and NnKi cells are not susceptible to S-mediated infection. On the contrary, the same assay demonstrated that a subset of MmBr cells is susceptible to S-mediated infection, suggesting that these cells express all the factors necessary for binding, entry and viral fusion. However, since they were not permissive to SARS-CoV-2, they probably lack factors that are essential for viral replication. Alternatively, they may express potent viral restriction factors that remain to be identified.

To bypass entry-mediated restriction(s), we have generated eight bat cell lines stably expressing hACE2. Four cell lines (MmNep-ACE2, NnLi-ACE2, NnLu-ACE2 and NnKi-ACE2) expressed too little hACE2 to draw conclusion about a potential rescue of infection. Four cell lines (FLG-ID-ACE2, MmBr-ACE2, MmNep-ACE2+ and NnLi-ACE2+ cells) expressed more hACE2 than A549-ACE2, which were competent for viral replication. The virus completed its replication cycle in FLG-ID-ACE2 cells. MmBr-ACE2 cells were competent for production of viral RNA and proteins but not for infectious particles release. The virus replicated poorly in MmNep-ACE2+ and NnLi-ACE2+ cells, even when pre-treated with trypsin. A protease-independent restriction may thus exist in these cells. The varying permissivities of these four cell lines to SARS-CoV-2 infection offer opportunities to decipher species-specific and tissue-specific antiviral mechanisms that have evolved in bats. Efficient viral RNA and protein production in A549-ACE2, FLG-ID-ACE2 and MmBr-ACE2 cells suggest that they express proteases that cleave S proteins. It also shows that ACE2 alone was responsible for the lack of viral replication in non-transduced A549, FLG-ID and MmBr cells. This ACE2-mediated entry block might be rather due to a low or absent ACE2 expression than to an incompatibility between ACE2 and S protein since ectopic expression of *Myotis* spp. and *Eptesicus* spp. ACE2 facilitated S-mediated entry of pseudo-viruses [306,340]. Infectious particles were produced in MmBr cells but were retained at the cell surface. This block may be mediated by the restriction factor tetherin,

which retains numerous enveloped viruses, including SARS-CoV-2, at the surface of human cells [332]. An analysis of the tetherin gene of 27 species of bats indicates that bats have undergone tetherin gene expansion and diversification relative to other mammals [342]. Bats belonging to the genus *Myotis* possess five unique tetherin variants that may potently restrict SARS-CoV-2 release [342]. Alternatively, infectious virion retention in MmBr cells could be due to an overexpression of hACE2 and may thus not be bat-specific. Since infection induced S-mediated syncytia formation in MmBr cells, viruses might spread from cell-to-cell via syncytia, as do other syncytia-forming viruses such as respiratory syncytial virus, parainfluenza viruses and measles virus [343]. Syncytia-mediated intercellular spreading allows viruses to escape virus-neutralizing antibodies. Such mode of transport has been previously proposed in human cells infected with the MERS-CoV [344], another betacoronavirus. Analysis of *post-mortem* samples of patients that succumb of COVID-19 revealed the presence of syncytial pneumocytes positives for viral RNAs [345]. However, the significance of syncytia formation for virus pathogenicity remains to be investigated.

SARS-CoV-2 has evolved numerous synergetic mechanisms to evade the IFN response in human cells [346], resulting in an absence of IFN and ISG expression in some cells, including A549 cells [334,347]. The virus was unable to counteract *OAS1* and *IFIH1* induction in *Eptesicus serotinus* kidney cells and in *Myotis myotis* nasal epithelial cells. This is especially intriguing in *E. serotinus* cells since the virus replicates to high levels in these cells and thus produce viral proteins with described IFN antagonist activities. Similarly, MERS-CoV suppresses the antiviral IFN response in human cells but not in *E. fuscus* cells [348]. One can envisage that escape of IFN-mediated restriction by betacoronaviruses is species-specific. For instance, SARS-CoV-2 Nsp14 targets human IFNAR1 for lysosomal degradation [346], but may be unable to degrade bat IFNAR1. This inability to evade the expression of two ISGs in *E. serotinus* kidney cells and in *Myotis myotis* nasal epithelial cells may contribute to the cellular control of infection in these cells, as in experimentally infected *E. fuscus* [349]. Alternatively, the basal level of IFN may be high in these two cell lines, as reported in several other bat species [351,352]. Expression of a mutated form of IRF3, which is a key transcription factor involved in the induction of the IFN signaling cascade, contributes to enhanced IFN responses in bat species, including *E. fuscus,* as compared to humans [194]. Investigation of IRF7, another transcription factor that mediates IFN expression, in *Pteropus alecto* cells revealed a more widespread tissue distribution in bats than in humans [72,353]. Bats may thus launch IFN-dependent

measures against viruses in a faster and broader manner than humans [147]. Expression of atypical ISGs has been reported for different bat species, including RNASEL in *P. alecto* cells and RNA-binding Microrchidia 3 (MORC3) in *Pteropus vampyrus* and *Eidolon helvum* cells [350,354]. Pursuing the characterization of bat innate immunity in relevant *in vitro* models is essential to understand the mechanisms by which they control the replication of numerous unrelated viruses.

An obvious need to develop additional bat cell lines still remains [303]. Particularly valuable cells would be cells derived from bat intestine, a tissue that expresses high level of proteins known to mediate or facilitate cellular entry of bat-borne betacoronaviruses, such as ACE2 and TMPRSS2, at least in *R. sinicus* [336]. This tissue is relevant for coronavirus infection, as demonstrated by the detection of viral genomes in duodenum tissue of *Rousettus aegyptiacus* experimentally infected with SARS-CoV-2 [311] and in anal swabs of *Rhinolophus* bats infected with SC2r-CoVs [223].

5. Limitations and Perspectives

Species-specific biological features of bats, such as longevity (Chapter 1, subsection 3), innate immune responses (Chapter 1, subsection 4) and expression of proviral factors, including receptors, determine the fate of infection. It is thus not surprising that most bat-borne viruses have a narrow host tropism. The existence of such species-specific restrictions was (re)-demonstrated by experimentally infecting, via the nasopharyngeal route, three bat species with SARS-CoV-2. *Tadarida brasiliensis* [355] and *Rousettus aegyptiacus* [311] supported viral replication but only *Tadarida brasiliensis* transmitted the virus to other animals. By contrast, *Eptesicus fuscus* bats were resistant to SARS-CoV-2 infection [349]. Our study, performed with a panel of bat cell lines derived from insectivorous species known to harbor coronaviruses [302], confirm such species-specific restrictions to SARS-CoV-2 replication. Similar studies conducted in the context of SARS-CoV showed that the virus efficiently replicates in *Rhinolophus sinicus* kidney cells, the species likely to be the reservoir of its ancestor, but not in other bat cell lines [356]. *Rhinolophus* bats are also the likely reservoir of the ancestor of SARS-CoV-2 [223]. *Rhinolophus* cells are unfortunately lacking in our comparative study since we did not have access to them at the time. We now have two lung cell lines generated from *Rhinolophus alcyone* (RhiLu) and *Rhinolophus ferrumequinum* (RhiFLu) in the lab [357] and we started performing infection experiments. Preliminary quantification of viral RNA yields and viral protein production, performed by RT-qPCR and flow cytometry analysis at different time post-infection revealed that SARS-CoV-2 did not replicate in these 2 cell lines (data not shown). This is consistent with studies showing that SARS-CoV-2 replicated poorly in *Rhinolophus sinicus* lung and brain cells [358] and in a spontaneously immortalized kidney cell line (Rhileki) from *Rhinolophus lepidus* [359]. The virus replicated, albeit not very efficiently, however, in RhiLu and RhiFLu cells when hACE2 was stably overexpressed (data not shown). These results suggest that *Rhinolophus* ACE2 (rhiACE2) maybe be expressed at a low level in RhiLu and RhiFLu cells or that it is not interacting with the S protein. It would be relevant to conduct infection experiments in *Rhinolophus* cells with BANAL-20-236, a likely ancestor of SARS-CoV-2, which has been isolated by some colleagues of the Institut Pasteur in anal swabs of *Rhinolophus spp*. form Laos [223]. Preliminary RT-qPCR and flow cytometry showed that BANAL-20-236 is unfortunately not replicating in RhiLu and RhiFLu cells, even when they are stably expressing hACE2 (not shown). Recent findings suggests that the overexpression of ACE2 from *Rhinolophus*

cornutus (RcACE2) might enhance bat-coronavirus infection in cellular models as demonstrated in increased infectivity of Vero-RcACE2 cells [360]. We are cloning ACE2 sequences from RhiLu and RhiFLu cells and we plan to establish rhiACE2 overexpressing RhiLu and RhiFLu cells. We will test their susceptibility and permissivity to BANAL-20-236 and SARS-CoV-2. One can envisage, however, that SC2r-CoVs, including BANAL-20-236 and SARS-CoV-2, use ACE2-independent mechanisms to enter bat cells. Indeed, bat-derived sarbecoviruses infect human cells independently of ACE2 [361]. Moreover, when the bat-derived human coronavirus 229E was serially passaged in *Rhinolophus lepidus* cells, large deletions arise in the sequence coding for the S protein. Infectivity in human cells was subsequently lost but maintained in *Rhinolophus* cells. This suggests that 229E may use a S-independent entry way in *Rhinolophus* cells [280]. Other bat-specific mechanism may also contribute to SC2r-CoVs entry into cells. One of the major difference between SARS-CoV-2 and closely related bat SC2r-CoVs, including BANAL-20-52 and 236, is the lack of the furin cleavage site in S [223]. In human and other vertebrate species, this site is require for increased transmission and syncytia formation [362], as well as broader host tropism [270]. When serially passaging SARS-CoV-2 in *Eptesicus fuscus* cells, specific mutations arise that render the furin cleavage site deficient for cleavage with human furin (Dr. A. Banerjee, personal communication and manuscript in preparation). This suggests that other proteases able to cleave S might be expressed in *Eptesicus fuscus* cells. Alternatively, the furin-mediated cleavage could be irrelevant for infectivity in *E. fuscus cells.* Our study also revealed that the ability of SARS-CoV-2 to replicate in bat cells is not only dependent on the species but also on the tissues from which the cells derived. For instance, the virus replicated efficiently in *Myotis myotis* brain cells but not in nasal epithelial cells generated from the same animal. Coronavirus infections are mostly gastrointestinal in bats and not respiratory, like in humans [218]. Thus, the virus faces a completely different cellular environment in bats and conclusion drawn from bat cellular models of lung, kidney or brain cells might not depict the host response in natural infection environments. To date, there are no intestinal cell lines from any bat species available. An intestinal organoid system, however, was established from *R. sinicus* bats and supports SARS-CoV-2 replication [363]. Consequently, it would be of interest to generate bat intestinal cell lines. Novel cellular models, ideally, a collection a *Rhinolophus* intestinal cell lines, are needed to pursue investigating the relationship between SC2r-CoVs and their natural hosts. Once these models are established, large-scale strategies, such as CRISPR-

mediated knock-out or knock-in screens, could be implemented to identify pro- and anti-viral host factors.

Chapter III – Comparative study of the chiropteran immune gene landscape

1. Preamble

Most emerging viruses spillover to human population from an animal host. Amongst all mammalian reservoirs, bats harbor most viruses per species [13]. In the past two decades, bat-borne viruses have caused large outbreaks, epidemics or even pandemics associated with severe human diseases, like SARS-CoVs, Lassa virus or Ebola viruses [364]. To successfully establish infection in a novel host, any given virus has to circumvent the innate immune system [86]. Although being broadly conserved amongst vertebrate species [174], more and more evidence indicate that reservoir species possess special innate immune features (Chapter I, subsection 4) [14,62]. Mapping the effectors of the innate immune response in bats may thus provide a better understanding of their ability to sustain viral infection.

With over 1300 species, only rodents are more numerous than bats amongst mammals [33]. This vast species diversity is, however, often underestimated and findings in one bat species are too often generalized. The literature tends to refer to "bat-specific" features but as described in the Chapter I on the example of innate immunity, even within one bat family large discrepancies can be found. Some events, such as the loss of the PYHN gene family seem so be true for the whole chiropteran order [365], while others, like the high basal expression of IFN-α, is rather *Pteropus* genus-specific [351]. Not only immune mechanisms but also virus-bat relationships seem to be, to some extend, species-specific. For instance, henipaviruses have only been identified in pteropid bats [366] and SCr-CoVs only in *Rhinolophus* bats [218].

Even though increased interest to study a wider selection of bat species could be observed in the recent years, the availability of molecular tools and cell lines still hampers research efforts. Mainly reports on *Pteropodid* bat models have been published and conclusions are biased towards this family. Recently more cellular models have been generated, such the *Nyctalus noctula* cell lines described in Chapter 2. Other bat-specific molecular tools, like KO cell lines for immune genes, novel bat-specific immortalization techniques using bat polyomavirus large T antigen, single-cell transcriptomic atlas of *Rhinolophus* bats and recombinant bat IFNs, have also been established and shared [169,303,336,351].

With the increasing availability of reagents, we wanted to perform a more global study of innate immune responses in several bat species. We hypothesized that some uncharacterized bat innate immune genes, species- and lineage-specific, might possess antiviral activities and thus contribute to the ability of bats to control viruses. Here, we used a comparative transcriptomic approach to map innate immune genes of seven different bat cell lines belonging to three different superfamilies *(Rhinolophidae, Pteropodidae* and *Vespertilionidae***)**, including Yinpterochiroptera as well as Yangochiroptera. Only a handful of innate immune system studies using a transcriptomic approach in bat cells were previously published [166,173,181,193,350,354]. These studies focus mainly only one [166,193,350,354] or two closely related species [181]. To our knowledge, our work represents the first comparative study of innate immune transcriptomes from unrelated bat species.

2. Material & Methods

2.1 Cell culture

Previously described MmTo, MmPca, NnKi, EfK3b cell lines (Table 1) [302,314,367], as well as human lung epithelial A549 cells (kindly gifted from Frédéric Tangy, Institut Pasteur, Paris) were maintained in high glucose DMEM (Gibco), supplemented with 10% FBS and 1% P/S in vented flasks. FLN-ID and FLG-ID cell lines (Table 1) were maintained in a mixture of equal volumes of Ham's F12 (Gibco) and Iscove's modified Dulbecco's medium (IMDM, Gibco), supplemented with 10% FBS and 1% P/S (Gibco) in non-vented flasks. EidNi/41.3, EidLu/20.2, RhiLu/1 and RhiFLu/II.1 cells (Table 1) were maintained in high glucose DMEM, supplemented with 10% FBS, 1% P/S, 1% L-Glutamine 200 mM (Gibco), 1% Sodium Pyruvate 100mM (Gibco) and 1% MEM nonessential amino acids 100x concentrate (Gibco) in vented flasks. All cells were regularly tested for mycoplasma, passaged maximally 20 times and cultured at 37°C and 5% CO_2.

Table 1. Overview of bat cell lines used in this chapter (* unpublished, Dr. M. Müller, Charité, Berlin)

Name	Bat species	Common name	Family	Organ	Transformation method	Ref
EidNi/41.3	*Eidolon helvum*	Straw-coloured fruit bat	Pteropodidae	Kidney	SV40 large T antigen	[204]
EidLu/20.2	*Eidolon helvum*	Straw-coloured fruit bat	Pteropodidae	Lung	SV40 large T antigen	[368]
EfK3b	*Eptesicus fuscus*	Big brown bat	Vespertilionidae	Kidney	Myotis polyomavirus T antigen	[367]
FLG-ID	*Eptesicus serotinus*	Common serotine bat	Vespertilionidae	Brain	Immortalized FLG-R cells with SV40 large T antigen	CCLV-RIE 1152
FLN-ID	*Eptesicus serotinus*	Common serotine bat	Vespertilionidae	Kidney	Immortalized FLN-R cells with SV40 large T antigen	CCLV-RIE 1134
MmPca	*Myotis myotis*	Greater mouse-eared bat	Vespertilionidae	Macrophage	SV40 large T antigen	[314]
MmTo	*Myotis myotis*	Greater mouse-eared bat	Vespertilionidae	Tonsil	SV40 large T antigen	[314]
NnKi	*Nyctalus noctula*	Common noctule	Vespertilionidae	Kidney	SV40 large T antigen	[302]
RhiFLu/II.1	*Rhinolophus ferrumequinum*	Greater horseshoe bat	Rhinolophidae	Lung	SV40 large T antigen	*
RhiLu/1	*Rhinolophus alcyone*	Halcyon horseshoe bat	Rhinolophidae	Lung	SV40 large T antigen	[357]

2.2 Universal IFN-α and Poly I:C stimulation

Cells were plated in monolayers in 12-well culture plates. The following day, cells were either transfected with 100 ng/ml (A549, EfK3b and NnKi cells) or 300 ng/ml low molecular weight Poly I:C (InvivoGen) or PBS, respectively, using INTERFERin (Polyplus transfection) transfection reagent. Alternatively, culture media containing universal IFN-α (pbl Assay Science) to a final concentration of 1000 U/ml or only culture media was added to the cells. Cells were lysed 16 h after transfection or IFN-α addition in the RA1 lysis buffer of the NucleoSpin RNA II kit (Macherey-Nagel) and total RNA was subsequently extracted using the same kit.

2.3 RNA extraction and RT-qPCR assays

Total RNA from the cells was obtained via the NucleoSpin RNA II kit (Macherey-Nagel) and following manufacturer's instructions. First-strand cDNA was synthesized using RevertAid H Minus M-MuLV Reverse Transcriptase (Thermo Fisher Scientific) with random primers. Power SYBR Green RNA-to-CT 1-Step Kit (Thermo Fisher Scientific) and the real-time PCR system QuantStudio 6 Flex (Applied Biosystems) were used to perform RT-qPCR analysis. Data were analyzed using the 2-ΔΔCT method, with all samples normalized to GAPDH of each species. Primers details for RT-qPCR assays are listed in Table 2.

Table 2. RT-qPCR primers used for indicated species

Target gene	Forward primer	Reverse primer
GAPDH human	GGTCGGAGTCAACGGATTTG	TGGCTCAGTTAGCATGGATTTA
GAPDH Eptesicus	TCATCAACGGAAAGTCCATCTC	ACATACTCAGCACCAGCATC
GAPDH Myotis	GTAGTGAAGCAGGCATCAGAG	GGAGTGGGTGTCACTGTTAAA
GAPDH Nyctalus	CCTGTTCGTCAGACAGCCTT	TTGATGGCGACAACTTGCAC
GAPDH Rhinolophus	GACAACTTCGGCATCGTGGA	TGCCAGTGAGCTTTCCATTGAG
GAPDH Eidolon	TCAATGGAAAGCCCATCACCA	CCAGCCTTCTCCAAGGTAGTG
OAS1 human	GAGCTCCTGACGGTCTATGC	TTCGTGAGCTGCCTTCTCAG
OAS1 Myotis/ Eptesicus/Nyctalus	GGAAGGAGGGCGAGTTCTC	GGTACCAGTGCTTGACCAGG
OAS1 Rhinolophus	CAAAGTCGTGAAGGGTGGCTC	AACTTCTGAGGTGGCTGAGG
OAS1 Eidolon	TTCCTGAAGCAGAGACCAGC	TTCCACGTTCCCAAGCGTAG
MX1 human	GGCCAGGAGCTAGGTTTCG	CGGCGTTCTTCACTCCAGAT
MX1 Myotis/Eptesicus/ Nyctalus	GGCTACATGATCGTCAAGTGC	GATGGTCCTCGAAGAAGGCC
MX1 Rhinolophus	CTCGGGGTAGGAGAGTTTCG	TGTTCTTCTACGCCTCCCGT
MX1 Eidolon	TCCCAGACCTGACCCTCATC	GTGGCGATGTCCACGTTACT
RSAD2 human	TGGGTGCTTACACCTGCTG	GAAGTGATAGTTGACGCTGGTT
RSAD2 Myotis/Eptesicus	CGTGAGCATCGTCAGCAAC	CAGGAGATGGCGAGGATGTC
RSAD2 Nyctalus	TCATCAACCGCTTCAACGTG	TCAATGAGGAGGCACTGGAAC
RSAD2 Rhinolophus	CCCTGAGAGAAGCAGAACGA	AGTTCAGGAAGCGCATGTAT
RSAD2 Eidolon	CTATCACTTCACCCGCCAGT	TCTCCGCCCGAAAAGTTGAT

2.4 Library preparation & Sequencing

Libraries were prepared using the Illumina Stranded mRNA kit. Briefly, 200ng of total RNA were Poly(A) enriched, followed by enzymatic fragmentation, cDNA synthesis, anchors ligation and PCR amplification as recommended by Illumina. Quality control of the libraries were made using the Agilent Fragment Analyzer High Sensitivity NGS kit. For transcriptomics analysis, all samples were pooled and sequenced using the Illumina's Nextseq 2000 sequencer, P3 sequencing format, generating single reads with 68 base-pairs long. For the *de novo* analysis, 12 samples were pooled and sequenced using the Illumina's Nextseq 2000 sequencer, P3 format, generating paired-end reads with 109 base-pairs long.

2.5 RNASeq analysis

The RNA-seq analysis was performed with Sequana v0.12.7 [369]. More specifically, we used the RNA-seq pipeline (v0.15.1, https://github.com/sequana/sequana_rnaseq) built on top of Snakemake 6.15.5 [370]. To check the efficiency of the depletion in ribosomal RNAs, reads were mapped using Bowtie1 [371] on the rRNA annotated features of the corresponding genome. Low quality reads were removed and adapters trimmed using fastp 0.20.1 [372]. High quality reads were then mapped to the corresponding genome assembly downloaded from NCBI using STAR 2.7.8a [373]. FeatureCounts 2.0.1 [374] was used to produce the count matrix, assigning reads to features using annotation provided by NCBI and with strand-specificity information. Quality control statistics were summarized using MultiQC 1.8 [375]. Statistical analysis on the count matrix was performed to identify differentially expressed genes, comparing Poly I:C transfected and PBS mock-transfected control cells within species. Clustering of transcriptomic profiles were assessed using a Principal Component Analysis (PCA) based on the 500 genes with the most expression variance. Differential expression testing was conducted using DESeq2 library 1.30.0 [376] indicating the significance (Benjamini-Hochberg adjusted p-values, false discovery rate FDR < 0.05) and the effect size (fold-change) for each comparison.

2.6 Assignment of human orthologues to undefined bat genes

For around 14% of bat genes identified by RNA-Seq, no human orthologue was annotated. To facilitate comparison between the species and allow pathway enrichment analysis, the genomes of *Eptesicus fuscus*, *Myotis myotis*, *Pipistrellus kuhlii*, *Pteropus alecto* and *Rhinolophus ferrumequinum* were re-annotated using the OrthoFinder software [377]. Proteomes of the bat species of interest, humans, as well as several related species of *Larasiatheria* and *Eurchontoglires* (see table 3) were retrieved from NCBI genome, filtered for the longest isoform of each gene and used as an input for OrthoFinder, using its default settings. OrthoFinder groups orthologous genes in so called phylogenetic hierarchical orthogroups (HOGs). Each bat gene was assigned the human gene from its HOG as an orthologue. Due to gene duplications a HOG might contain multiple genes from one species. In that case, the human and bat genes were ranked according to their baseMean (the average of the normalized count values over all samples) and the bat genes were assigned a human orthologue according to their rank. In the case of more genes from a specific bat species the lowest ranking bat genes were assigned the highest ranking human

gene and annotated with "_2;_3;_4…". If there was no human gene available in a given HOG, a gene from another species with a valid gene symbol was chosen as an orthologue. Gene symbols that also occur in the human genome were preferred. For the pathway enrichment analysis genes that were assigned an ambiguous symbol (_2;_3;_4…) were filtered out.

Table 3: Proteomes used for Orthofinder

Group	**Common name**	**Latin name**	**RefSeq**
Laurasiatheria	Hedgehog	*Erinaceus europaeus*	GCF_000296755.1
Laurasiatheria	Horse	*Equus caballus*	GCF_002863925.1
Laurasiatheria	Large flying fox	*Pteropus vampyrus*	GCF_000151845.1
Laurasiatheria	little brown bat	*Myotis lucifugus*	GCF_000147115.1
Laurasiatheria	pale spear-nosed bat	*Phyllostomus discolor*	GCF_004126475.2
Laurasiatheria	Egyptian rousette	*Rousettus aegyptiacus*	GCF_014176215.1
Laurasiatheria	Molossus molossus	*Pallas's mastiff bat*	GCF_014108415.1
Euarchontoglires	Mouse	*Mus musculus*	GCF_000001635.27
Euarchontoglires	Rabbit	*Oryctolagus cuniculus*	GCF_000003625.3
Euarchontoglires	Ring-tailed lemur	*Lemur catta*	GCF_020740605.2
Euarchontoglires	Chimpanzee	*Pan paniscus*	GCF_013052645.1

2.7 Pathway enrichment analysis

Using the transcriptomic results, differentially expressed genes (DEGs) pathway enrichment analysis was performed using ClueGO [378] and CluePedia [379] plugin from Cytoscape software [380]. The Gene Ontology (GO) Biological Process terms were detected using GO-Term fusion and a Tree interval 1-5. Represented GO Terms have a P value ≤ 0.05 and at least 12 significative DEGs for *Rhinolophus* cell lines (Fig. 5) or 4 significative DEGs for analysis of 84 common to all bat cells (Fig. 3) or 5% of the total associated genes for such pathway.

3. Results

3.1 Innate immune responses in bat cell lines can be triggered by Poly I:C

We first examined whether IFN responses could be triggered by universal IFN-α or Poly I:C (low molecular weight, LMW) treatment in a panel of bat cell lines: *Eptesicus fuscus* kidney cells (EfK3b), *Eptesicus serotinus* kidney cells (FLN-ID), *E. serotinus* brain cells (FLG-ID), *Nyctalus noctula* kidney cells (NnKi), *Eidolon helvum* kidney cells (EidNi), *E. helvum* kidney cells (EidLu), *Myotis myotis* macrophages (MmPca), *M. myotis* tonsil cells (MmTo), *Rhinolophus ferrumequinum* lung cells (RhiFLu) and *Rhinolophus alcyone* cells (RhiLu). As comparison, human A549 lung carcinoma cells were included in the analysis. mRNA abundance of three ISGs (*MX1, RSAD2* and *OAS1*) were quantified by RT-qPCR analysis. These ISGs were selected since they are part of a conserved mammalian ISG set [174]. Upon 16 h of universal IFN-α treatment, *MX1, RSAD2* and *OAS1* mRNA abundances increased in all cell lines except in NnKi cells (Fig. 1A-C). This suggests that the IFNAR receptors are able to recognize the universal IFN-α and the IFN signaling pathway is functional in all bat cells tested, with the exception of NnKi cells. These cells may express an IFNAR receptor that is not compatible with the IFN-α that we used. Some differences, however, were notable between the stimulated cells. For instance, *MX1* mRNAs increased by ten thousand-fold in EidNi cells, only by 100- fold in A549 as well as EidLu cells and by about 10-fold in the remaining bat cells. The expression of the same three ISGs were upregulated after 16 h of Poly I:C treatment in all bat cells (Fig. 1D-F), including NnKi cells, indicating that they all possess intact IFN induction and signaling pathways. This is agreement with previous studies performed in NnKi [302], FLG-ID [302], EfK3b [381] and EidNi cells [204]. The induction pattern of each ISG was comparable with the one observed upon IFN-α treatment (Fig. 1A-F).

Based on these data, we selected for further studies one bat cell line that responded well to Poly I:C stimulation per species.

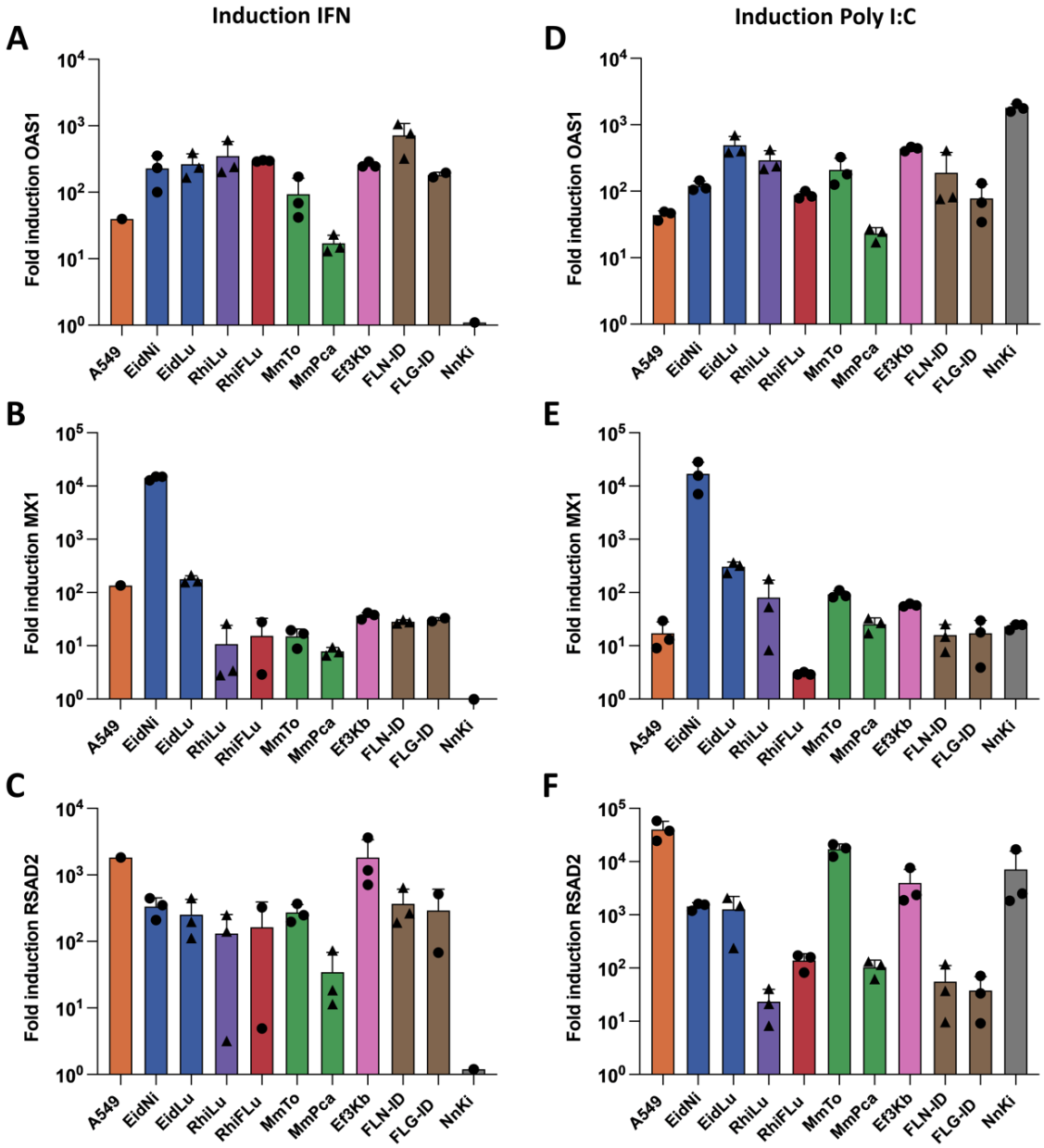

Fig. 1. Innate immune responses in bat cell lines upon IFN-α and Poly I:C stimulation. A-C, Indicated bat cell lines were treated with 1000U/ml universal IFN-α for 16 hours. The relative amounts of *OAS1* mRNA (A), *MX1* mRNA (B) and *RSAD2* mRNA (C) were determined by RT-qPCR analysis. Results are expressed as fold-increases relative to unstimulated cells. **D-F,** Indicated bat cell lines were transfected with 100 or 300 ng low-molecular weight Poly I:C or with mock-transfected with PBS for 16 hours. The relative amounts of *OAS1* mRNA (D), *MX1* mRNA (E) and *RSAD2* mRNA (F) were determined by RT-qPCR analysis. Results are expressed as fold-increases relative to unstimulated PBS-treated cells. (**A-F**) Glyceraldehyde 3-phosphate dehydrogenase (GAPDH) of corresponding species was used as an house-keeping gene. Data points represent independent experiments.

3.2 Experimental outline and workflow to compare transcriptomes of stimulated bat cells

To obtain a comprehensive insight into immune responses in different bat cell lines, we performed RNASeq analysis of stimulated A549, EidNi, Ef3Kb, FLN-ID, MmTo, NnKi, RhiFLu and RhiLu cells. Based on the data shown in Figure 1, we harvested whole cell lysates of Poly I:C or PBS treated cells after 16h and extracted total RNA of each cell line in three independent biological repeats (Fig. 2A).

From total RNA of all 48 samples, poly(A) enriched cDNA libraries were generated. Libraries were subsequently sequenced with an average depth of 20 million strand-specific, single reads per sample, except for the NnKi samples, which were sequenced with an average depth of 60 million strand-specific, paired-end reads per sample. We chose a more in-depth sequencing format for the NnKi cell line since the *Nyctualus noctula* genome has yet to be fully sequenced. We are hoping to eventually perform the *de novo* assembly of this transcriptome (Fig. 2B).

First, the alignment against rRNA genomic features of the sequencing data revealed an absence of ribosomal contamination. High quality reads were generated since mean quality scores per bases were above Q30 for all runs. Trimming using fastp was only superficial since above 99% reads passed the quality filter (Fig. 2C). Since not all bat genomes from the species of the selected cell lines have been sequenced to a sufficient quality to serve as reference genome, datasets were mapped on genomes of the closest available bat species if the identical one was unavailable (Fig. 2D).

The STAR alignment software is commonly used for eukaryote RNASeq data mapping, mainly for its capacity to handle splicing events (Fig. 2E) [373,382]. Despite partial genome mismatches, all datasets were over 70% aligned with the corresponding reference genome (Table 4). The percentage values were averaged over the six samples (three PBS control and three Poly I:C samples) for each cell line. The “aligned” column describes the percentage of reads aligned with the corresponding reference genome. The “assigned” column describes the percentage of aligned reads, which were assigned to a known gene through genome annotation (unassigned reads meaning reads mapped to unannotated parts of the genome).

Table 4: Mapping percentages for bat cell lines

Cell line	Aligned	Assigned
EidNi	75%	86,9%
EfK3b	89,25%	80,7%
FLN-ID	85,8%	79,6%
RhiFLu	91,8%	75,4%
RhiLu	84,3%	74%
MmTo	91,7%	78,2%
NnKi	83,6%	74,8%

About 14% of annotated genes were unidentified in the different bat cell datasets and were therefore annotated with a "LOC" identifier. To better annotate these genes based on known human orthologues, we performed subsequent re-annotation using the Orthofinder software as described above.

Finally, reads were quantified using feature_counts (Fig. 2F) and differential expression analysis was performed with DeSeq2 (Fig. 2G). Results were represented in various graphs and tables (Fig. 2H). All statistics were summarized in multiqc files.

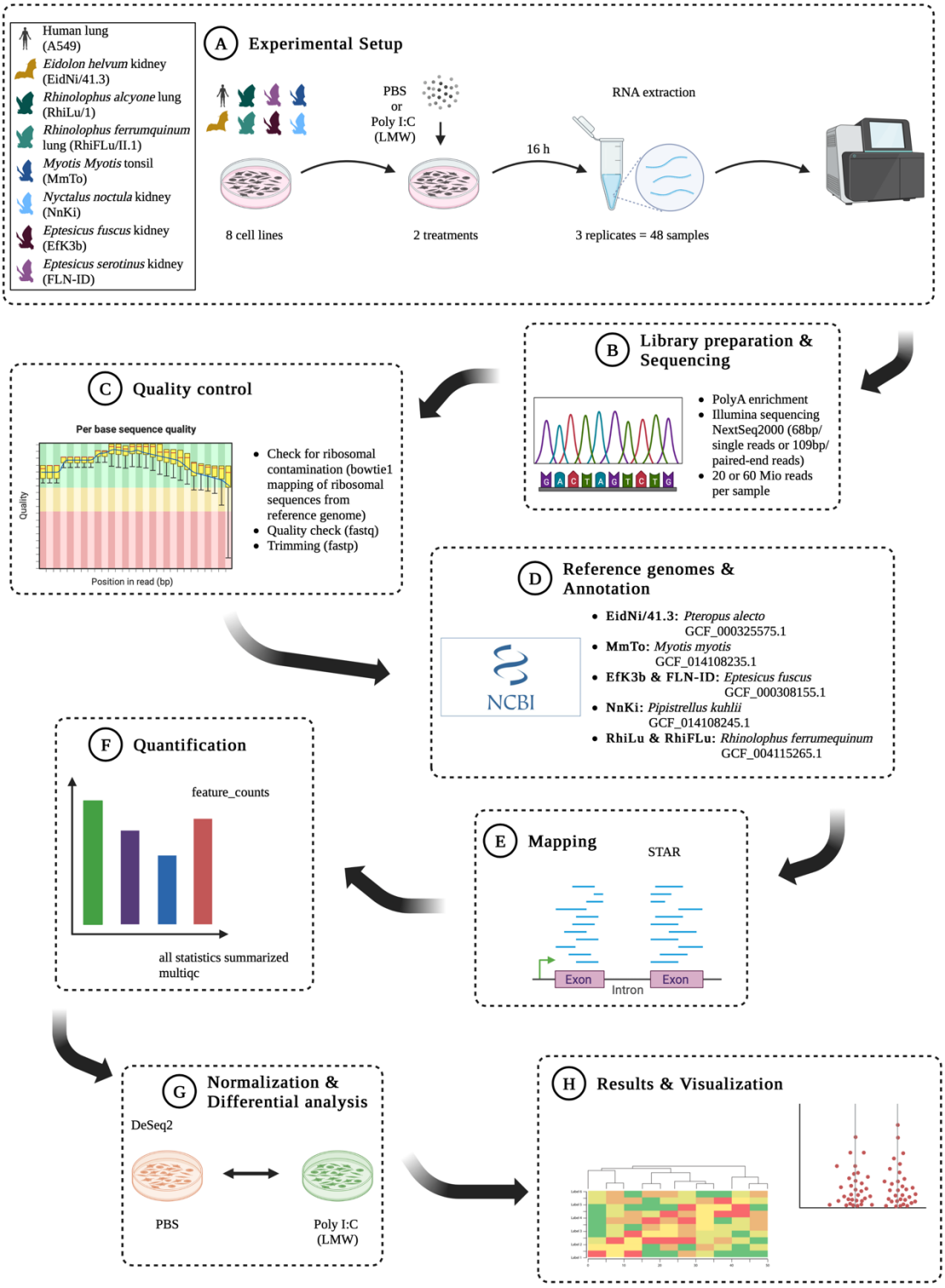

Fig. 2. Workflow for comparative transcriptomics of poly:IC stimulation in bat cells. Experimental, sequencing and analysis setup for processing bat cell RNA-seq data sets. Different bat and human cell lines were stimulated with Poly I:C LMW and subsequently RNA-Seq analysis were performed using Illumina NextSeq2000 sequencer. Quality of data was reviewed using fastq and fastp. Reads were mapped to indicated reference genomes using STAR. Feature_counts was used for quantifying raw read counts and DeSeq2 was next used for DEGs analysis to identify up- and down-regulated genes. Results are displayed using Prism 9 and Python 3.9 with extra libraries such as pandas, matplotlib, seaborn, and upsetplot.

3.3 Common gene expression profiles in bat cells upon Poly I:C treatment

To visualize the overall transcriptomic pattern in the selected cell lines and to estimate the similarity between the datasets, we performed a PCA (Fig. 3A). Individual biological replicates of each cell line cluster together in treatment as well as control conditions (Fig. 3A). The first dimension of the PCA (PC1) accounted for 66% variability in gene expression between cell lines. Subsequently, the strongest separation in the data (PC1 with 66%) is found between FLN-ID and human A549 cells. The second dimension of the PCA (PC2) depicted a total of 8% variability. The strongest separation in data (PC2 8%) here is observed between NnKi and MmTo cells. The PCA also revealed that the transcriptomes of the two *Rhinolophus* cell lines (RhiLu and RhiFlu) are highly similar. EidNi and EfK3b cells also clustered together indicating high levels of similarity in gene expression profiles, which was surprising for these 2 unrelated species. The second *Eptesicus* cell line, FLN-ID, was found in proximity to the *Rhinolophus* cells and therefore highly variant from EfK3b cells, which was also unexpected. Expression pattern in human cells is most similar to EfK3b cells.

Genes with a FDR of $< 0{,}005$ and log2FC cutoff were considered differentially expressed genes (DEGs), as previously done in a transcriptomic comparison of IFN-stimulated genes amongst different vertebrates [174]. The absolute number of DEGs in each species varies between 2000 and 3000 upregulated genes and around 2000 downregulated ones. This is at the exception of FLN-ID cells, in which remarkably less DEGs could be found (Table 5) (Fig. 3B). The pattern of DEGs in response to Poly I:C is widely similar between all cell lines (Fig. 3B) with most DEGs having a log2 Fold Change (log2FC) between -1 and 1. In absolute numbers, the DEG pattern in human cells is most similar to EidNi cells but the DEG distribution follows the one of EfK3b cells (Fig. 3B), supporting the clustering in the PCA (Fig. 3A).

Table 5: Number of differentially expressed genes in response to Poly I:C treatment

Cell line	Down	Up
Human	1731 (377)	2638 (1350)
EidNi	1895 (335)	2673 (730)
Ef3Kb	3033 (531)	3284 (1314)
FLN-ID	7 (0)	138 (84)
NnKi	2013 (29)	2332 (234)
MmTo	2566 (247)	2955 (649)
RhiLu	2064 (116)	2525 (645)
RhiFlu	1868 (81)	1782 (476)

() numbers of DRGs with log2FC>1

To further characterize Poly I:C stimulated genes in bat cells, we compared the DEGs within the seven chiropteran cell lines. We identified 84 common DEGs, among which 83 were upregulated and one (*PANK3)* was downregulated (Fig. 3C). These 84 common genes were enriched for the following GO pathways: innate immune response, regulation of type 1 IFN response, regulation of response to cytokine stimulus, cellular and defense response to virus as well as viral life cycle (Fig. 3D). A key central GO term is found in 'positive regulation of responses to cytokine stimulus' as it contains DEGs from divergent GO terms such as 'regulation of response to biotic stimulus', 'negative regulation of viral process' and 'regulation of type I interferon production'. Analysis of the interactions between nodes showed that the 'interferon 1 beta production' is closely related to the 'pattern recognition receptor pathway' term. Similarly, a close relation between 'response to interferon gamma' and 'viral gene expression' is found. Overall, the enriched pathways from DEGs commonly found between all the tested cell lines shows a conserved innate immune response against viral infections.

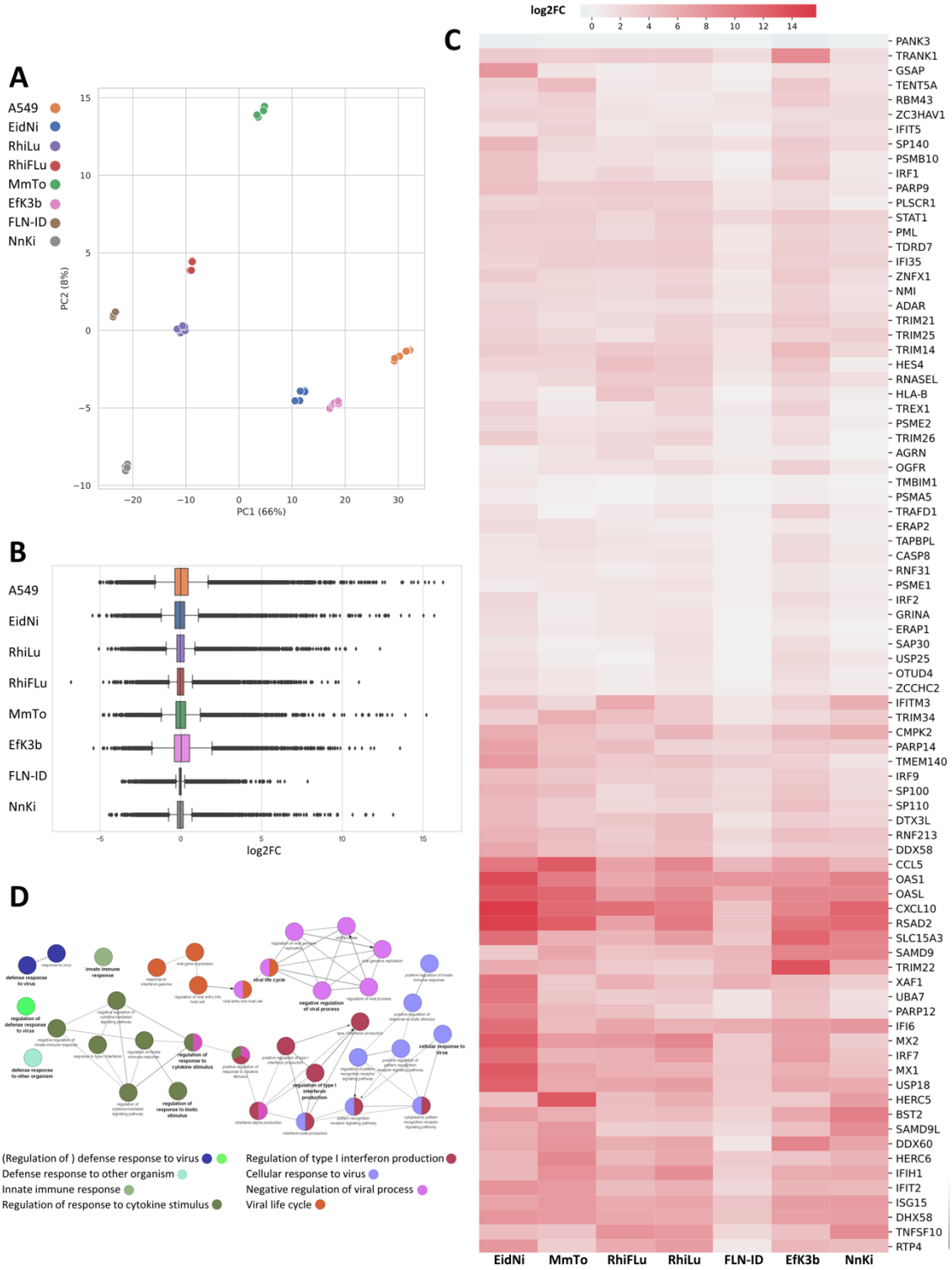
A
A549
EidNi
RhiLu
RhiFLu
MmTo
EfK3b
FLN-ID
NnKi
PC2 (8%)
PC1 (66%)
B
log2FC
C
log2FC
0 2 4 6 8 10 12 14
PANK3
TRANK1
GSAP
TENT5A
RBM43
ZC3HAV1
IFIT5
SP140
PSMB10
IRF1
PARP9
PLSCR1
STAT1
PML
TDRD7
IFI35
ZNFX1
NMI
ADAR
TRIM21
TRIM25
TRIM14
HES4
RNASEL
HLA-B
TREX1
PSME2
TRIM26
AGRN
OGFR
TMBIM1
PSMA5
TRAFD1
ERAP2
TAPBPL
CASP8
RNF31
PSME1
IRF2
GRINA
ERAP1
SAP30
USP25
OTUD4
ZCCHC2
IFITM3
TRIM34
CMPK2
PARP14
TMEM140
IRF9
SP100
SP110
DTX3L
RNF213
DDX58
CCL5
OAS1
OASL
CXCL10
RSAD2
SLC15A3
SAMD9
TRIM22
XAF1
UBA7
PARP12
IFI6
MX2
IRF7
MX1
USP18
HERC5
BST2
SAMD9L
DDX60
HERC6
IFIH1
IFIT2
ISG15
DHX58
TNFSF10
RTP4
EidNi
MmTo
RhiFLu
RhiLu
FLN-ID
EfK3b
NnKi
D
(Regulation of) defense response to virus
Defense response to other organism
Innate immune response
Regulation of response to cytokine stimulus
Regulation of type I interferon production
Cellular response to virus
Negative regulation of viral process
Viral life cycle

Fig. 3. Differential gene expression patterns in bat and A549 cell lines upon Poly I:C stimulation. A, PCA of the 500 most variant genes in all cell lines. Each point represents one cell line and is composed of the 3 biological replicates for Poly I:C treatment as well as PBS control. The distribution of the samples represents the similarity in expression pattern. **B,** Distribution patterns of up or down regulated DEGs within each cell lines. Boxplot depicts the scattering (25st percentile, 75th percentile and median) of the up and down regulation of DEGs for different bat and human cell lines. DEG mean and standard deviation are represented, dots are single outlier datapoints. **C,** Heatmap of relative expression of 84 genes identified as common DEGs in all 7 bat cell lines (Table 3). Log2FC of each common DEG is displayed for every bat cell line. **D,** Node plot of GO pathway enrichment of common DEGs. Major GO Terms are represented in bold. These GO Terms correspond to 'defense response to virus (GO:0051607), 'innate immune response' (GO:0045087), 'regulation of defense response to virus (GO:0050688), 'defense response to other organism' (GO:0098542), 'regulation of response to biotic stimulus' (GO:0002831), 'regulation of response to cytokine stimulus' (GO:0060759), 'regulation of type I interferon production' GO:0032479, 'negative regulation of innate immune process' (GO:0045824), 'cellular response to virus' (GO:0098586) and viral life cycle (GO:0019058). Each of these GO Terms and its related nodes are color-coded using the same color.

3.4 Identification of DEGs in bat cells

After identifying the DEGs common to the seven bat cell lines, we had a closer look at the single bat species and pair-wise comparisons. A surprisingly high amount of DEGs unique to each cell line could be identified (Fig. 4A). Stimulated EfK3b cells expressed the highest number of unique DEGs (Fig. 4A). Around 20% of downregulated genes were unique in stimulated MmTo and EfK3b cells (Fig. 4A). FLN-ID cells did not display any unique DEGs and were therefore excluded from the plot (Fig. 4A).

An upset plot was used to describe the overlap of DEGs between samples, in pair- and group-wise comparisons (Fig. 4B). The rows of the plot correspond to the dataset of each bat cell line and the columns to the intersection between them. The total number of overlapping DEGs are depicted in the bar chart (Fig. 4B). The highest number of unique DEGs were found in single bat cell lines, like EfK3b cells, which expressed close to 1400 DEGs (sum of up and downregulated unique DEGs from Fig. 4A). The highest amount of intersecting DEGs can be found in MmTo and EfK3b cells, with approximately 450 common DEGs (Fig. 4B). 340 DEGs were common to 6 bat cell lines disregarding FLN-ID (Fig. 4B). The two *Rhinolophus* cell lines share approximately 300 DEGs (Fig. 4B).

To identify bat DEGs that are not differentially expressed in stimulated human cells, the lists of DEGs common to seven, six or five bat cell lines were compared with the lists of genes identified as human ISGs from two different transcriptomic studies including approximately 450 ISGs [383] and 2100 ISGs [384]. The genes were also compared to human ISGs either stimulated with IFN-I or IFN-III in an interferome database that lists over 7000 ISGs [125]. Genes were considered ISGs when they were upregulated with log2FC > 1 in all entries. If genes displayed ambiguous experimental data indicating both up and downregulation in different settings, they were disregarded.

Table 6 displays bat-specific DEGs found in all seven cell lines and all DEGs with a log2FC >1 for at least 2 bat cells in the lists of DEGs common to six or five bat cells. *SAP30* and *TMBIM1* were the two genes found upregulated in all bat cells and not known as ISGs in human cells. Interestingly, another *TMBIM* family members (TMBIM6) was slightly upregulated in six bat cells. *PANK3* was included in the table since it was downregulated in all seven cell lines and not present in human cells. *ICAM4* was the highest upregulated DEG common to 6 bat cells. *FOXS1* has also highly upregulated in 5 bat cells.

Table 6: Selection of DEGs in bat cells, log2FC displayed for each cell line

Gene	EidNi	MmTo	RhiFlu	RhiLu	FLN-ID	Ef3Kb	NnKi	
SAP30	1.38	0.40	0.71	1.77	0.25	1.87	0.41	7
TMBIM1	1.10	0.48	0.19	0.58	0.25	0.56	0.27	7
TMBIM6	0.43	0.47	0.46	0.83	0.13	0.34		6
PANK3[1]	-0.54	-0.27	-0.27	-0.25	-0.21	-0.79	-0.40	7
ATAD1	1.78	1.41	0.39	0.73		0.20	0.10	6
ERRFI1	2.11	0.71	0.84	0.54		2.10	0.68	6
FLT3LG	2.07	1.14	1.52	1.26		1.33	0.66	6
HMGA1	0.74	1.01	0.32	0.20		1.37	0.30	6
HMGA2[2]	0.92	1.37	1.77	0.86		0.91	0.52	6
ICAM4	6.24	3.45	2.96	2.53		2.08	1.36	6
PALM2	2.18	0.54	0.47	1.16		0.84	0.21	6
RANBP2	1.15	0.40	0.45	1.35		1.08	0.96	6
RGCC	4.01	1.24	0.44	1.06		2.69	0.45	6
SLC3A2[2]	0.39	1.81	0.33	0.34		3.42	1.13	6
SLC7A5[2]	0.77	1.05	0.16	0.20		1.67	0.46	6
SMAGP	1.58	1.31	0.59	0.59		1.59	1.09	6
SMPD5	4.21	0.54	2.39	2.47		1.61	0.25	6
TTC31	1.57	0.74	0.65	0.73		2.05	1.08	6
VWA5A	1.42	0.59	0.50	0.64		1.69	1.54	6
AKNA		1.90	0.39	0.48		1.39	0.86	5
BHLHE41	1.29	1.49		0.88		4.84	1.15	5
CASP2		0.36	0.28	0.29		1.13	0.29	5
CASP4		0.87	1.84	3.21	0.72	2.39		5
DIO2		0.83	0.49	3.39		3.93	1.93	5
DNASE2	2.07	2.13		0.46		2.42	1.60	5
E2F2[2]	1.99	0.79	0.43			2.40	1.53	5
FAM76A		1.05		0.54	0.31	1.08	0.49	5
FOXSI[2]	6.16	5.61	4.33	5.24		2.47		5
KLHL21	1.23	2.02		0.27		1.41	0.44	5
PCNX1	1.51	0.71		0.44		1.24	0.13	5
PLSCR3	0.80	0.73	0.45	1.23		2.27		5
SESN2		2.48	0.92	0.86		2.18	0.66	5
SGMS2	2.00		1.17	1.19		0.80	0.50	5
SIDT2	0.95		0.97	1.98	0.25	2.95		5
TAF4B	2.10	1.11	0.45	0.91			0.46	5
TUT7	1.54	1.18		0.30		1.78	0.86	5

[1]only gene downregulated in all 7 bat cells; [2]downregulated in A549 set; numbers on the right indicate in how many bat cell lines respective gene was upregulated.

Panels C-F of figure 4 show the RNASeq data of four DEGs of interest (*FOXS1*, *ICAM4, TMBIM1* and *SAP30)*, in expression box plots for all bat cell lines. Normalized read counts indicate the basal *versus* upregulated levels of transcripts for each of the four genes. Interestingly, *SAP30, ICAM4* and *FOXS1* were not, or barely, upregulated upon stimulation in FLN-ID and NnKi cells, but were expressed at high basal levels as compared to the other bat cells (Fig. 4C, E, F). *ICAM4* was also highly expressed in EfK3b cells (Fig. 4E). *TMBIM1* expression was generally high in the seven bat cell lines as compared with A549 cells, with a modest but conserved upregulation upon stimulation (Fig. 4D).

Some DEGs, such as *FOXS1,* were upregulated in at least five bat cell lines but downregulated in A459 cell dataset (Table 7 and Fig. 4F). Similarly, the interferome database identified *KLHL21, PDXK* and *SESN2* as downregulated upon IFN stimulation in human cells, while these genes were upregulated in at least five bat cell lines upon stimulation. *ENDOV*, however, was identified as DEG that is downregulated or barely induced by Poly I:C in all but *Rhinolophus* cells and might indicate some specificity in these cells.

Table 7: DEGs in bat cells that are downregulated in human cells, log2FC displayed for each cell line

Gene	EidNi	MmTo	RhiFlu	RhiLu	FLN-ID	Ef3Kb	NnKi	A549
AKAP1	0.69	0.19	0.40	0.24		0.63	0.30	-0.43
E2F2	1.99	0.79	0.43			2.40	1.53	-0.90
ENDOV*		-1.42	1.84	3.53		0.80	-0.38	-0.51
FOXS1	6.16	5.61	4.33	5.24		2.47		-2.85
HMGA2	0.92	1.37	1.77	0.86		0.84	0.21	-1.08
IRF2BP2	0.26	0.33	0.59			0.33	0.26	-0.38
PDXK		0.19	0.26	0.14		0.64	0.23	-0.39
SLC3A2	0.39	1.81	0.33	0.34		1.08	0.96	-0.23
SLC7A5	0.77	1.05	0.16	0.20		2.69	0.45	-0.49
TGFBR2		0.38	0.36	0.49		0.49	0.26	-0.58
ZNF469		1.96	0.38	0.56		0.67	0.38	-0.91

*only highly upregulated *Rhinolophus* cells and slightly in Ef3Kb, downregulated in all other cell lines

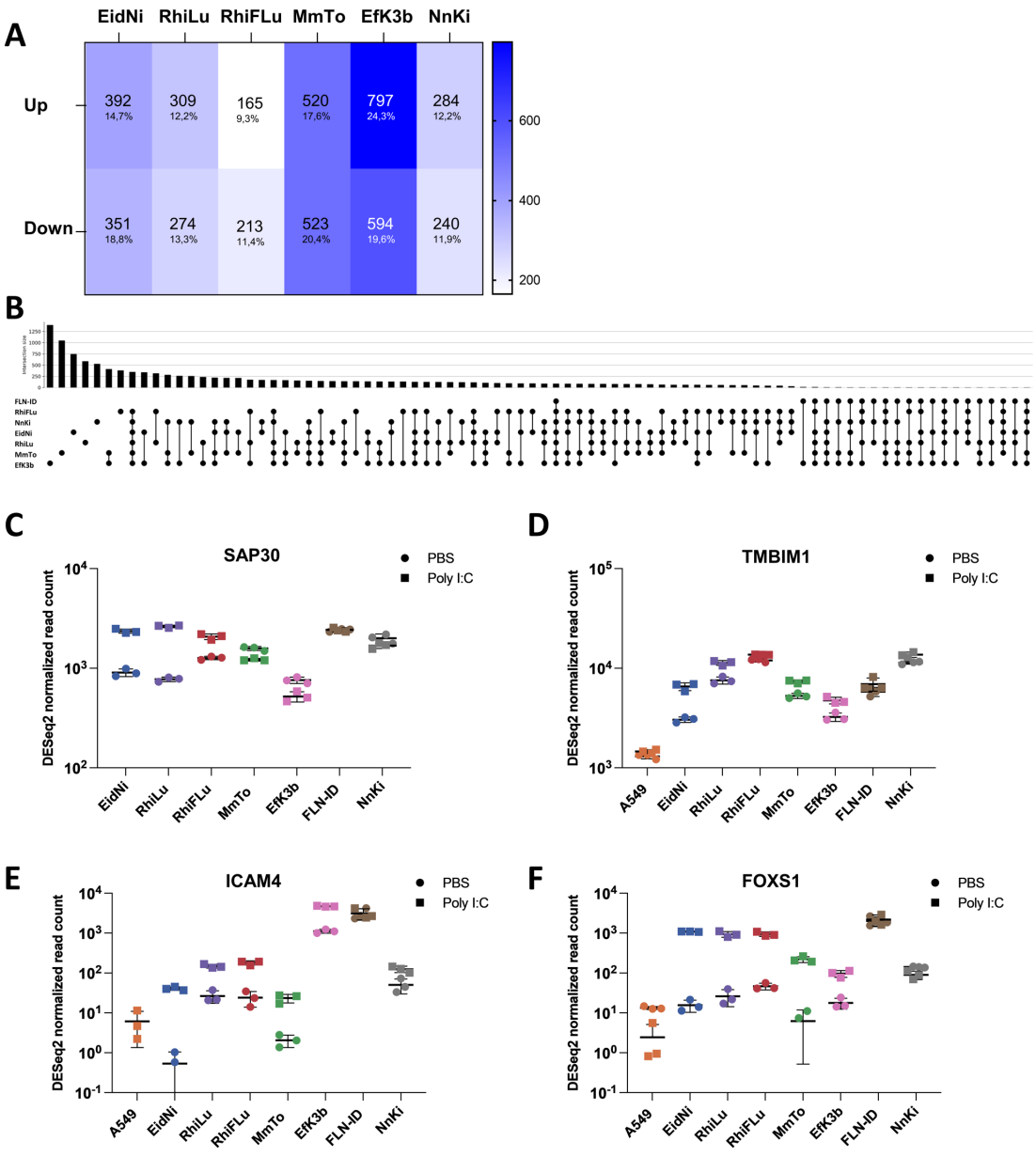

Fig. 4. Identification of DEGs in bat cells. A, Heatmap of genes specifically up or down regulated in the indicated bat cell line. Exact number of genes in each category for each cell line is indicated and the percentage of unique DEGs among all DEGs identified in a given cell line. No unique genes were identified for FLN-IC cells. **B,** Upset plot to visualize the intersection of different bat cell DEG data sets. Rows correspond to the different bat cell lines and columns to the intersections of different DEG sets compared with each other. The size of the intersection is depicted in the bar graph as number of genes represented in the respective comparison. For instance, EfK3b cells express roughly 1400 unique DEGs (first bar of upset plot or sum of second column of heatmap in **4A**). EfK3b and MmTo share roughly 450 DEGs (sixth bar of upset plot). **C-F,** Expression plots of selected bat-specific genes that were either commonly upregulated in all 7 bat cell lines (**C and D**) or the genes with the highest average log2FC to the genes common to 6 (**E**) and 5 (**F**) cell lines (Table 4). DESeq2-normalized expression values are displayed for the 3 biological replicates of each cell line as data point. Scatter plots additionally show mean values and standard deviations.

3.5 Innate immune responses in *Rhinolophus* cells

The close relationship between *Rhinolophus* bats and recently emerged coronaviruses renders this genus particularly interesting to decipher unique innate immune features. To our knowledge, this is the first transcriptomic study comparing the innate immune response of two different *Rhinolophus* cell lines with human or other chiropteran cells. After noticing *ENDOV,* a gene that codes for an endonuclease cleaving single-stranded RNA at the 3' position [385], as upregulated gene in RhiLu and RhiFLu cells and not in other cell lines, we searched for other DEGs uniquely present in these two *Rhinolophus* datasets. To limit the hit list, we focused on DEGs upregulated in both cell lines with a log2FC > 1 in at least one of them. We found 56 unique *Rhinolophus* DEGs that fulfil these criteria. These genes have not previously been reported as innate immune genes in human cells. They were not upregulated in stimulated A549 cells and six of them were downregulated in the human cell line (Table 8).

Intriguingly, these 56 unique *Rhinolophus* DEGs are among the most upregulated genes in both RhiLu and RhiFLu datasets, with expression levels higher than core vertebrate ISGs like *OAS1* or *RSAD2.* Among these 56 unique *Rhinolophus* DEGs, 13 could not be annotated with a known mammalian orthologue ID even after re-annotation of the sequencing data using the Orthofinder software. These "LOC" genes are either assigned to orthogroups that only contain other unannotated "LOC" genes that were previously found in different mammals. These genes may be too different from other mammalian orthologues and therefore can't be assigned to any orthogroup and could thus represent potentially uncharacterized *Rhinolophus* genes.

Table 8: DEGs in *Rhinolophus* cells with log2FC > 1 in at least one of the 2 cell lines

Gene	RhiFlu	RhiLu	Gene	RhiFlu	RhiLu
LOC117030247	9.59	5.84	***CEP112***	1.53	0.46
HLA-DQA2	8.17	5.90	***PRXL2B***[2]	1.52	1.05
TMEM156	7.46	5.31	***CLDN5***	1.49	2.84
FMO2	7.07	5.20	***CEBPZOS***[2]	1.46	1.96
LOC117031175	6.84	6.82	***SPOCD1***	1.46	1.89
LOC117016745	6.71	4.06	***A630001G21RIK***	1.45	1.98
LOC117015994	5.30	5.08	***PCIF1***	1.45	1.35
TRIM10	5.15	3.90	***CANT1***	1.39	3.09
LOC117026872	3.66	3.56	***C2H21orf91***	1.30	1.72
CYP3A7-CYP3A51P	3.61	4.06	***LOC117031500***	1.26	2.02
SNAP91	3.56	5.87	***LOC117017037***	1.24	2.70
LOC117019483	3.48	2.55	***MHCX1_4***	1.18	2.15
SUN3	3.37	5.82	***ATP8B1***[2]	1.04	1.20
MHCX1_3	3.35	2.16	***ST8SIA6***	1.02	2.52
MHCX1_6	3.03	2.39	***DAPK2***	0.93	1.16
ACP3	2.95	2.56	***ZNF597***	0.90	1.65
AOX1	2.86	1.32	***LRRN4CL***	0.73	1.55
LOC117020280	2.79	3.94	***LOC117012895***	0.73	1.24
MFAP5	2.64	6.53	***ZBTB5***	0.71	1.80
CYP3A5[2]	2.59	4.93	***LOC117025698***	0.52	1.06
HLA-DRB1	2.55	1.77	***NR3C2***	0.45	1.49
C7	2.51	2.36	***CYB5R4***	0.45	1.02
SFRP4[2]	2.24	0.96	***DERA***	0.38	1.02
LOC117031210	2.06	2.30	***KCNF1***[2]	0.38	3.07
LOC117016891	2.05	2.82	***KCTD12***	0.36	1.63
C4B_2	1.62	0.54	***OLFML2B***	0.34	1.02
			POSTN	0.28	2.37

[2]downregulated in A549 set

A Gene Onthology (GO) analysis of the 56 selected RhiLu and RhiFLu DEGs was performed to determine the cellular canonical pathways significantly enriched in each data set (Fig. 5A). GO analysis revealed that most genes belong to antiviral innate immune response, similar to what was observed for the common DEGs (Fig. 3D) and expected since cells were stimulated with a dsRNA ligand. GO pathways enriched in the RhiFLu dataset were: regulation of immune system process, negative regulation of viral process and antigen presentation, interspecies interaction and myeloid cell homeostasis (Fig. 5A). The latter was a pathway found uniquely in this dataset. Some of these pathways were shared in the RhiLu dataset and additional ones, like regulation of locomotion, response to chemical, cell-cell signaling, growth or biomineralization, were identified. Of note, this

'biomineralization' pathway was not identified in any other bat datasets. Many genes are present in more than one pathway, indicating a high degree of overlap between different immune pathways.

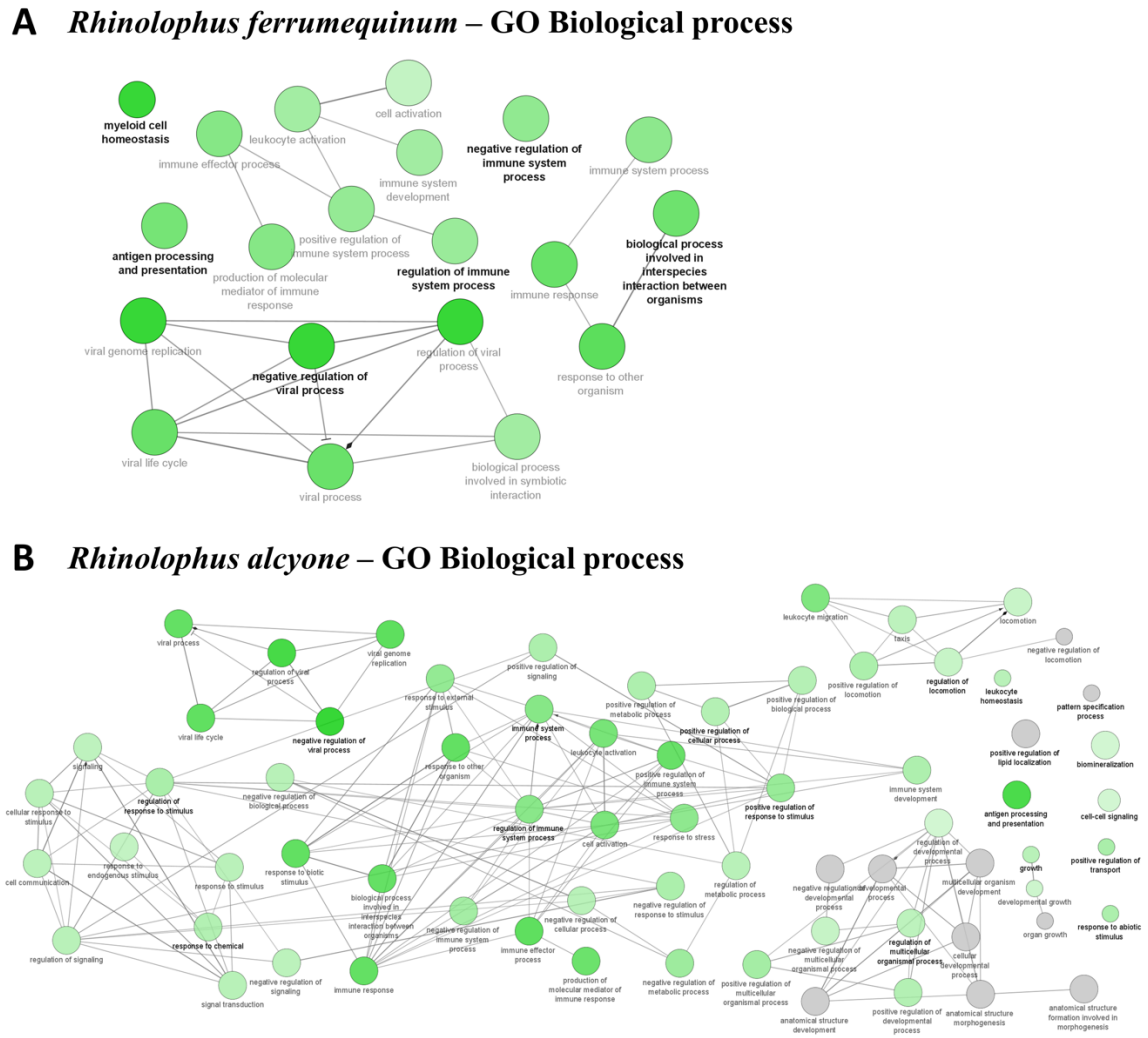

Fig. 5. Pathway enrichment analysis of *Rhinolophus* DEGs. Pathway enrichment analysis of **(A)** *Rhinolophus ferrumequinum* and **(B)** *Rhinolophus alcyone* lung cells stimulated with poli IC after x hours. Nodes corresponds to GO biological process terms. GO tree interval was set at 1 - 2 for identification of GO Terms. Displayed GO Terms have a p-value ≤ 0,05 and a minimum number of genes per group was of12 or 5% of the total associated genes. Green color depicts upregulated GO Terms while red nodes indicate downregulated GO Terms).

3.6 Comparison with other bat cell transcriptomic datasets

Only few transcriptomic studies have been performed in bat cells. Available transcriptomic datasets include an analysis of primary skin fibroblasts from nine vertebrate species treated with universal IFN-α, including *Pteropus vampyrus* and *Myotis lucifugus* bats [174]. Another analysis identified DEGs in *Myotis daubentonii* kidney cell line, either treated with

universal IFN-α or infected with an attenuated IFN-inducing RVFV clone for 6 or 24h [166]. Lists of DEGs identified in *Eptesicus fuscus* and *Eptesicus nilssonii* cells exposed to Poly I:C for 12 and 24h are also available [181], as well as list of DEGs identified in *Pteropus vampyrus* kidney cells infected during 24h with the paramyxovirus NDV [175]. Finally, transcriptomic data obtained by stimulating *Pteropus alecto* kidney cells for 4, 8, 12 or 24h with universal IFN-α [386] or for 6h with *P. alecto* IFN-α3 [193] are available. It is, however, difficult to directly compare our lists of DEGs with these, as only the *Eptesicus* cells were treated with Poly I:C.

Some interesting information can, however, be obtained from crossing these gene lists to the 84 genes that we identified as common bat DEGs or to the common *Rhinolophus* DEGs (56 genes minus the uncharacterized 13 LOC genes). For instance, *TAF4B*, which was upregulated in five out of seven of our bat cell lines (Table 6), was identified as an ISG in all bat transcriptomic studies mentioned above [166,174,175,181,386]. *FOXS1,* which was also upregulated in five out of seven of our bat cell lines (Table 6), was classified as ISG in *Pteropus spp.* [174,175,350] and *Myotis lucifugus* cells [174]. Four of the common bat DEGs, *RANBP2, CASP2, PALM2* and *TUT7,* have not been observed as DEGs in other bat cells, before. Amongst the 56 selected *Rhinolophus* DEGs, only nine of the were previously reported as ISGs, including *FMO2* in infected *Myotis daubentonii* cells [166] and *TRIM10* in two *Pteropus vampyrus* cells [174]. Thus 47 of our *Rhinolophus* DEGs have never been identified as ISGs previously, such as *SUN3, MHCX1, ACP3* or *AOX1*. This is reinforcing the possibility that they could be immune genes specific to *Rhinolophus* cells. *ENDOV,* however, was only upregulated in rat and chicken [174] but no other bat cells upon IFN stimulation.

4. Discussion

The aim of our study was to obtain a broader understanding of the innate immune response in bat cells. We used seven bat species, *Eptesicus fuscus, Eptesicus serotinus, Eidolon helvum, Myotis myotis, Nyctalus noctula, Rhinolophus alcyone* and *Rhinolophus ferrumequinum*, which belong to three superfamilies (*Rhinolophidae, Pteropodidae* and *Vespertilionidae*) and include Yinptero- as well as Yangochiroptera. This selection of cells thus covers a large spectrum of species of the chiropteran order. Transcriptional analysis of Poly I:C stimulated cells revealed hundreds of DEGs in each cell line, including family- and species-specific DEGs as well as a core set of 83 common DEGs. Several of the DEGs described in this study were not previously reported as innate immune genes in humans or other vertebrate species and may thus be bat-specific immune genes.

We first examined whether the selected bat cell lines responded to stimulation with universal IFNα, which is a hybrid IFN generated from two ligand-binding subunits common to all members of the IFN-I family (Human IFN-Alpha A/D [BglII], pbl assay science) and widely used to successfully stimulate mammalian cell lines including bat cells [166,174,386,387]. The same selection of cells was stimulated by Poly I:C, a dsRNA ligand. Even though we identified *IFNAR1*and *IFNAR2* transcripts in NnKi cells, which suggests that the 2 receptors are expressed, the universal IFN-α failed to trigger the expression of three ISGs in this cell line. Nn IFNAR1/2 may not be structurally compatible with universal IFNα. Alternatively, binding may occur between universal IFNα and Nn IFNAR1/2, but the receptors may not undergo the conformational changes required to initiate JAK/STAT signaling. Similarly, incompatibility between *P. vampyrus* IFNs and monkey IFNAR1/2 was previously suggested [175]. Supernatant from NDV-infected *P. vampyrus* kidney cells restricted NDV infection in the same cells but not in African Green Monkey Vero cells. Thus, antiviral cytokines, and presumably IFNs, secreted by infected *P. vampyrus* cells seem to exhibit a species-specific protective activity [175]. Induction of ISG expression upon Poly I:C stimulation suggests that both IFN induction and signaling pathways are functional in NnKi cells, unless ISG expression would be directly stimulated by Poly I:C without the contribution of the JAK/STAT pathway. Such direct induction of a subset of ISGs has been already shown amongst others in IRF3-deficient human fibroblast cells [388] and in IFNAR KO *P. alecto* kidney cells [173].

Transfecting Poly I:C into cells leads to activation of TLR3 and cytoplasmic RLRs [389]. The profile of the identified DEGs in this study might therefore be different than what

would be observed upon viral infections when viral RNA is preferentially sensed by a unique PRR (as described in Chapter I, subsection 5.3). In *P. alecto* kidney cells, clear differences in responsiveness to Poly I:C compared to *P. alecto* IFN-α3 or viral infection have previously been observed [173]. Genes induced by each of the three stimuli overlap partially but display unique profiles [173]. Similarly, genes that are upregulated upon either IFN treatment or attenuated RVFV infection differ in *M. daubentonii* cells [166].

We then performed a comparative RNA-Seq experiment on Poly I:C stimulated bat cells. High quality reference genomes are required for analyzing transcriptomic approach. One caveat of our study is the lack of available reference genomes for four of the seven selected species. Despite recent efforts to sequence bat genomes, mainly made by the Bat1K project [33], only 21 bat genomes have been fully sequenced and assembled. Not all of these genomes are yet extensively annotated. For instance, the *Eidolon helvum* genome is only at the "scaffold stage". This means that sequencing reads can be mapped on different scaffolds but these scaffolds are not linked yet to information on the chromosomal level or actual gene IDs. Additionally, there is a discrepancy between the two main databases for reference genomes, Ensembl and NCBI, in quality and availably of certain bat genomes. Despite the accessibility of high-quality genomes on Ensembl, not all genomes of relevant bat species were available in this database. We thus chose to use genomes deposited in the NCBI database for coherence and comparative studies. Despite lacking the genomes of *Nyctalus noctula, Eidolon helvum*, *Eptesicus serotinus* as well as *Rhinolophus alcyone* and mapping the corresponding sequencing reads to the genome of closely related species, we achieved a mapping percentage superior to 75% for all combinations. As a comparison, the human mapping percentage was 89,4%. Our analysis is therefore representative of the selected bat cell lines despite partially mismatching reference genomes.

The NnKi samples were sequenced with a higher depth than the samples from the other cell lines. We are planning to perform a *de novo* assembly of the NnKi transcriptome in the future. In the meantime, we used the *Pipistrellus kuhlii* genome to analyze the transcriptomic data. In brief, a *de novo* assembly of transcriptomic data assembles complete transcripts from short sequencing reads, similar to what is done in genomic assemblies. These transcript sequences are then blasted to identify their corresponding gene. Using this method, novel transcripts and splicing variants can be discovered which is not possible when mapping to an existing reference genome. Furthermore, a (re-) annotation based on the proximity of the actual sequences to published transcript sequences (not necessarily

from bat species but from any vertebrate) is possible. Using this method, we should thus be able to retrieve novel information from the transcriptome of *Nyctalus noctula* cells.

After analyzing the transcriptomes of the seven cell lines, we observed expected clustering patterns in the PCA, such as cells belonging to same species cluster together, independently of the Poly I:C treatment. Most of the depicted variance corresponds to variance between species, more than between treatment. The PCA also revealed unexpected clustering. *Eidolon helvum* (EidNi) is phylogenetically closer to *Rhinolophus* spp. (RhiLu and RhiFLU) bats than to *Eptesicus spp.* bats. This relationship is not depicted in the PCA, indicating that relatedness on the genomic level does not necessarily correlate with transcriptomic similarity of the expression of the 500 most differentially expressed genes. Additionally, transcriptomes are highly dependent on variables like sampling time, treatment period or tissue identity, while genomes at the nucleotide level stay identical. Interestingly, the human dataset is not very different in gene expression pattern to the ones of EidNi and EfK3b. This is probably due to the fact that the genes induced with a dsRNA ligand that mimics viral infection are widely conserved amongst mammals and even vertebrates [174]. A set of core ISGs common to phylogenetically distinct vertebrates, ranging from human, bat, over chicken to pig, has previously been identified and the overall gene expression pattern upon IFN stimulation of cell lines from these species was also similar [174]. To our surprise, FLN-ID and Ef3Kb cells, both derived from *Eptesicus* bats and both kidney cell lines, cluster far apart in the PCA. These *Eptesicus* cell lines have been generated by different approaches which might contribute to their distinct gene expression patterns. Whereas FLN-ID cells were immortalized with SV40 large T antigen [302], EfK3b cells were immortalized using *Myotis* polyomavirus T antigen [367]. Using either a simian or a bat antigen could create different phenotypes in the two cell lines. Generally, this observation could also be a consequence of using immortalized cell lines which do not necessarily represent primary cells. Studying primary bat cells is however challenging since bats are under protection in most parts of the world and no common laboratory models exist. In a previous study [174], primary skin fibroblasts from different animal species were used. Even though this circumvents having to sacrifice the animal and could be a good alternative approach to cell lines, this cell type only has limited biological relevance in most viral infection or innate immune processes. We indeed planned to include primary *Rhinolophus* cells in the RNASeq analysis, cells derived from wing tissue biopsies of *R. ferrumequinum,* but the RNA yield was unfortunately too low to be used.

Of note, since the cells were stimulated with Poly I:C rather than with IFN, the differentially expressed genes are not genuine ISGs and we thus choose to refer to them as DEGs. In all analysis, FLN-ID cells showed very different characteristics than the other cell lines. Overall, very few DEGs and no unique ones could be identified in these cells. The basal expression levels of the common DEGs of interest were higher in this cell line compared to the rest. FLN-ID cells might have a high overall basal level of the genes identified as DEGs in the other bat cell lines and therefore be "less responsive" to stimulation. The high basal expression of ISGs has previously been described in several bat cell lines as described in detail in Chapter I, subsection 3.2.

Our study identified interesting DEG candidates, common to multiple bat cells (Table 6 and 7) or common to *Rhinolophus* cells (Table 9). Amongst the common bat DEGs, Transmembrane BAX Inhibitor Motif Containing 1 (*TMBIM1*) has been identified as an inhibitor for liver adipogenesis in mice and primates by lysosomal degradation of TLR4 [390]. Intriguingly, stable knockdown of TMBIM1 in hepatocellular carcinoma cells increased intracellular ROS [391]. This suggests a regulatory role of TMBIM1 in oxidative stress pathways and links it to the observations described in Chapter 1, subsection 2. Another candidate that draws our attention is SIN3A Associated Protein 30 (SAP30), a transcription factor with several reported functions. It is a component of the SIN3A complex, which is a multifunctional transcription regulator complex involved in the maintenance of pluripotency in embryonic stem cells [392]. SIN3A seems to also act as a corepressor in memory and synaptic plasticity, as its deletion resulted in enhanced hippocampal long-term potentiation and long-term contextual fear memory [393]. SAP30 is moreover potentially involved in muscle hypertrophy in chicken [394]. The transcription factor Forkhead Box S1 (*FOXS1*) has been described as colorectal tumor enhancer by raising the expression levels of CXCL8 [395]. High expression of FOXS1 in various cancer types has been positively related to immune cell infiltration and positively influences the expression of various immune-suppression genes [396]. Finally, Intercellular Adhesion Molecule 4 (*ICAM4*) participated in the leukocyte–endothelium interaction. The adhesion mechanism of leucocytes is facilitated by integrins on leukocytes and ICAMS on endothelium cells [397].

The TATA-Box Binding Protein Associated Factor 4b (*TAF4B*) has been identified in all but the two *Eptesicus* cell lines and additionally in all bat cell transcriptomic datasets we compared our results to. TAF4B is a gonadal-enriched subunit of the multi-protein general transcription factor complex TFIID complex. TFIID is composed of the TATA-box binding

protein (TBP) with 14 TBP-associated factors (TAFs) and critical for female fertility. The TAF4B transcription network is involved in the early oocyte differentiation in mice and human [398]. The same transcription factor is also required for spermatogenesis in mice [399].

The general high prevalence of uncharacterized genes (13 out of 56 species-specific DEGs) in the list highly regulated *Rhinolophus* DEGs (Table 8) indicates that these bat species might indeed harbor novel innate immune mechanisms. Interesting hits with known mammalian orthologues are Transmembrane Protein 156 (*TMEM156*), Flavin Containing Dimethylaniline Monoxygenase 2 (*FMO2*) and *ENDOV*. Almost no functional studies exist for TMEM156. It has recently been identified as biomarker for predicting the prognosis of breast cancer and head and neck squamous cell carcinoma [400] as well as a biomarker in cow milk to evaluate the presence of enzootic bovine leukosis [401]. It was, however, not further studied in the context of tumorigenesis. The five human (or nine in mice) FMO genes, in contrast, are well studied for their role in drug metabolism. FMO2 is mainly expressed in lung tissues but also found in kidney. A multitude of different drug substrates is metabolized by FMO proteins, some of the exclusively. Interestingly, most humans do not express functional FMO2, the main player is FMO3 [402]. *ENDOV* belongs to a highly conserved gene family and orthologues are widespread amongst the animal kingdoms. The protein localized to human nucleoli and the cytoplasm [403]. Its deaminated adenosine (inosine)-specific cleavage of ssRNA in humans differs drastically from its mechanism in *E.coli* bacteria where it was discovered. In *E.coli*, ENDOV is an DNA repair proteins that removes inosine from the genome [385].

Bats, birds and rodents are amongst the major reservoir groups for viruses [29]. As second order of flying vertebrates, birds have similarly reduced genome dimensions and non-redundant, rational genomic structures than bats [33]. They furthermore display high species diversity and similar migration and roosting behavior [14]. Rodents host less zoonotic viruses per species compared to bats but the highest total number of zoonotic viruses due to their impressing species diversity [404]. When crossing our common bat DEGs with the vertebrate dataset [174], only *ENDOV* could be identified as DEG in bats, chicken and rats [161]. It is to some extend surprising that there is not more overlap in unique innate immune genes in these important reservoir species. This could be due to the fact that we compare different cell types and stimulation techniques.

Additionally, we found several DEGS involved in the Major Histocompatibility Complex (MHC) in *Rhinolophus* cells (*HLA-DRB1, HLA-DQA2 and MHCX1).* The MHC class I

genes in humans are called human leukocyte antigen (HLA) class I genes. These molecules function as the ligands for receptors on NK cells, which can be majorly divided into killer-cell immunoglobulin-like receptors (KIRs) and killer cell lectin-like receptor (KLRs) [405]. In line with our findings, previous reports show modifications in NK receptor signaling in bats. Surprisingly, several of the two known MHC class I NK cell receptor types of NK cells were absent in *P. alecto*, *P. vampyrus* or *M. davidii* genomes which might indicate atypical NK cell responses in bats [49,160]. Additionally, the coverage of NK cell-related genes was generally sparse in the *Artibeus jamaicensis* and *R. aegyptiacus* transcriptomes [161,162]. KLRC (NKG2) and KLRD (CD94) receptor gene families were expanded in *R. aegyptiacus* relative to other mammalian species and differ in features and expression patterns. NKG2/CD94 receptors, which are rather linked to an inhibitory response in other species, might serve as the primary NK cell receptors in *R. aegyptiacus* bats [167]. Unique organization of the NK cell receptors in multiple bat species strengthens the theory that bats might contain a different NK cell receptor repertoire than other species.

Even though our study did not focus on identifying novel bat ISGs but rather genes whose expression was stimulated by a synthetic dsRNA mimicking viral RNA in bat cells, we identified several interesting candidates which could have functional relevance in bat antiviral responses. As next steps, we are planning to validate these hits by treating the selected bat cell lines with different stimuli, including Poly I:C and IFN, and assess the corresponding mRNA levels by RT-qPCR analysis. We will evaluate the potential antiviral function of our candidate genes in the context of infection with relevant viruses, such as the bat-borne flaviviruses (for instance Rio Bravo virus), or coronaviruses, such as SARS-CoV-2 and BANAL-20-236 [223]. We will select a set of interesting bat DEGs, such as *TMBIM1, SAP30, FOXS1, ICAM4, TAF4B, ENDOV, TMEM156* and *FMO2,* to conduct siRNA-mediated loss-of-function studies and evaluate whether these candidates modulate viral replication and/or affect innate immune response in chiropteran cells. We have already established several bat cellular models to study SARS-CoV-2 replication through hACE2 overexpression and have since acquired relevant hACE2-*Rhinolphus* cell lines through a collaboration with Marcel Müller (Charité University). For genes significantly changing the infection outcome, it would be of interest to perform in-dept mechanistical studies to characterize their antiviral functions.

Identifying genes involved in controlling viral infection in bat cells can uncover promising approaches to develop novel antivirals. For instance, a genome-wide RNA interference (RNAi) and CRISPR screens recovered genes involved in the antiviral response against

IVA and Mumps virus (MuV) in *P. alecto* kidney cells [406], including MTHFD1, which acted as a broad-spectrum pro-viral host factor. MTHFD1 is involved in the C1 metabolism, responsible for the production of building blocks for NA synthesis [406]. Its inhibitor, carolacton, potently blocked replication of several RNA viruses, including ZIKV, MuV and SARS-CoV-2 in human and bat cells. Knockdown of MTHFD1 additionally inhibited the replication of HSV-1 [406].

Nevertheless, whether bats have truly unique immune mechanisms remains to be further investigate. It is necessary to expand comparisons amongst diverse non model species, as done in [174] and here, to generate a picture of innate immune pathways that is less biased towards inbred laboratory mouse models and immortalized human cell lines.

Chapter IV – General discussion and Perspectives

Identification of bat reservoir hosts on the species-level through enhanced field sampling is indispensable to predict spillover events. Powerful tools to detect viruses in these samples would also help generate databases useful for predicting future outbreaks. The development of accurate mathematical models based on experimental studies that characterize the replication of these novel viruses and on the eco-epidemiological factors of the host are also required to better understand zoonotic spillover. Collecting these information will allow to build risk indexes within regions and countries and inform the planning of largescale projects involving major changes in land-use, such as mining constructions, dam-building or road development [12]. Furthermore, these data will guide intervention strategies to minimize contact between reservoir species and humans in these environments and help establish surveillance programs [12,63].

The USAID PREDITC program was put in place to facilitate a global understanding of the bat virome and point to potential spillover events. Via a combination of PCR screening and deep sequencing techniques, thousands of novel viral sequences in samples collected from healthy bats around the world were collected. Characterizing the diversity of naturally occurring bat-borne viruses lead for example to the discovery of a novel non-pathogenic henipavirus, Cedar virus, that represents a valuable tool to study henipaviral infections outside of costly BSL4 environments [63]. Similar one-health programs aiming to understand better the human-animal-environment interface and involving collaborative efforts among multiple relevant disciplines and sectors [68], should be established.

The field of bat virology and immunology made some advancements in the recent years through the establishment of novel tools like, for instance, the single cell transcriptomic atlas of *Rhinolophus sinicus* bats [179], recombinant *P. alecto* IFN-α3 [164] or *E. serotinus* IFN-κ and IFN-ω [169] and a bat-specific IFN-β promoter activation reporter assay in *Eidolon helvum* cells. The latter system expresses luciferase genes under the *IFNB* promoter of *Rousettus aegyptiacus* and seems to be universally applicable to any transfectable bat cell [368]. Additionally, new methods and protocols to immortalize bat cells with a *Myotis*-specific polyomavirus large T antigen [367] have been established, as well as primary skin fibroblast cell lines in a non-invasive way [161]. Bat intestinal organoids [363] and *Pteropus alecto* bone marrow-derived DCs and macrophages, which

are professional immune cells, have been generated. All these novel tools will allow future studies of the chiropteran immune system [407].

The question, why bats are such special viral reservoirs, is still open. While it is now widely accepted that these animals display a unique balance of enhanced antiviral defense responses and immune tolerance facilitated through dampened inflammation [147], the underlying molecular mechanism remain to be clarified. Original assumptions like the "always on hypothesis" or the "flight as fever hypothesis" have been questioned based on experimental data. Elevated temperatures did not increase filoviral replication in a panel of six different bat cell lines [408] and the beneficial impact of "fever" during infection is rather depended on increased IFN, proinflammatory cytokine and prostaglandin expression than on temperature itself [409]. High, constitutive expression of IFNs seems to be restricted to pteropid bats [164] since the basal level of IFN is not elevated in several other bat species [153,166,180]. Even within the family of *Pteropodidae* differences between "always on"-IFN pathway in *P. alecto* cells and "only on upon stimulation"-IFN pathway in *R. aegyptiacus* cells could be identified [410].

Moreover, immune response kinetics may play a major role in responding to viral infections in bats. Strongly time-dependent transcriptional immune profiles have been observed in *M. daubentonii* cells [166] as well as *P. alecto* cells [386]. Two clusters of early and late induced immune genes exist in *M. daubentonii* cells [166], while similar early induction patterns but differential late phase decline separated two gene subclusters in *P. alecto* cells [386]. Human cells, in contrast, depicted less tightly-regulated induction kinetics and ISGs stayed induced for a prolonged period of time [386].

Further differences in immunity between bats and other mammals lay within the adaptive responses [411]. Delayed and limited responses to antigens were observed in B and T cells of *Pteropus giganteus* [412] and less somatic hypermutation was found in *Myotis lucifugus* [413]. Substantial differences in abundances and phenotypes of major immune cell types, like T and B cells, monocytes, macrophages, granulocytes and DCs, in blood and organs of *Rousettus aegyptiacus* in relation to their age were also observed [414]. Subsequently, disease tolerance may establish with increased age, modulate pathogen dynamics in individual animals and determine time of pathogen spread [414]. Analyzing the spleens of wild-caught *Pteropus alecto* bats, a predominance of CD8+ T cells was observed, suggesting persisting infection or a resting immune state primed for antiviral responses [89]. Also, in *Rhinolophus sinicus*, CD8+ T cells were predominant over CD4+ T cell [179]. Circulating, lymph node and bone marrow resident T cells in *P. alecto* were mainly

CD4+ cells, however, with a strikingly high ratio of 2:1 compared to CD8+ cells in bone marrow, whereas in human or mouse the ration is 1:235. Thus, bat bone marrow could function like human thymus with regards to T cell development or persistent infections and inflammatory stimuli could be the reason for CD4+ T cell expansion [89].

In summary, bats display a plethora of species-specific mechanisms which renders them unique viral reservoir species. There is yet a lot of space to further characterize or discover novel immune pathways and antiviral mechanisms in over 1300 bat species. A deeper understanding of bat immunity may provide insights to aid prevention, predict and control zoonotic spillover from bats to humans. It can also provide new approaches and ideas to study and thus ultimately combat ageing- and inflammation- related diseases, as well as cancer, in humans [147].

References

1. Bedhomme S, Hillung J, Elena SF. Emerging viruses: why they are not jacks of all trades? Current Opinion in Virology. 2015;10: 1–6. doi:10.1016/j.coviro.2014.10.006

2. Subudhi S, Rapin N, Misra V. Immune System Modulation and Viral Persistence in Bats: Understanding Viral Spillover. Viruses. 2019;11: 192. doi:10.3390/v11020192

3. Han BA, Kramer AM, Drake JM. Global Patterns of Zoonotic Disease in Mammals. Trends in Parasitology. 2016;32: 565–577. doi:10.1016/j.pt.2016.04.007

4. Plowright RK, Parrish CR, McCallum H, Hudson PJ, Ko AI, Graham AL, et al. Pathways to zoonotic spillover. Nat Rev Microbiol. 2017;15: 502–510. doi:10.1038/nrmicro.2017.45

5. Kilpatrick AM. Globalization, Land Use, and the Invasion of West Nile Virus. Science. 2011;334: 323–327. doi:10.1126/science.1201010

6. Altizer S, Bartel R, Han BA. Animal Migration and Infectious Disease Risk. Science. 2011;331: 296–302. doi:10.1126/science.1194694

7. Schountz T. Immunology of Bats and Their Viruses: Challenges and Opportunities. Viruses. 2014;6: 4880–4901. doi:10.3390/v6124880

8. Downs CJ, Schoenle LA, Han BA, Harrison JF, Martin LB. Scaling of Host Competence. Trends in Parasitology. 2019;35: 182–192. doi:10.1016/j.pt.2018.12.002

9. Plowright RK, Eby P, Hudson PJ, Smith IL, Westcott D, Bryden WL, et al. Ecological dynamics of emerging bat virus spillover. Proc R Soc B. 2015;282: 20142124. doi:10.1098/rspb.2014.2124

10. Tian J, Sun J, Li D, Wang N, Wang L, Zhang C, et al. Emerging viruses: Cross-species transmission of coronaviruses, filoviruses, henipaviruses, and rotaviruses from bats. Cell Reports. 2022;39: 110969. doi:10.1016/j.celrep.2022.110969

11. Lawrence P, Escudero-Pérez B. Henipavirus Immune Evasion and Pathogenesis Mechanisms: Lessons Learnt from Natural Infection and Animal Models. Viruses. 2022;14: 936. doi:10.3390/v14050936

12. Allen T, Murray KA, Zambrana-Torrelio C, Morse SS, Rondinini C, Di Marco M, et al. Global hotspots and correlates of emerging zoonotic diseases. Nat Commun. 2017;8: 1124. doi:10.1038/s41467-017-00923-8

13. Olival KJ, Hosseini PR, Zambrana-Torrelio C, Ross N, Bogich TL, Daszak P. Host and viral traits predict zoonotic spillover from mammals. Nature. 2017;546: 646–650. doi:10.1038/nature22975

14. Chan JF-W, To KK-W, Tse H, Jin D-Y, Yuen K-Y. Interspecies transmission and emergence of novel viruses: lessons from bats and birds. Trends in Microbiology. 2013;21: 544–555. doi:10.1016/j.tim.2013.05.005

15. Carlson CJ, Albery GF, Merow C, Trisos CH, Zipfel CM, Eskew EA, et al. Climate change increases cross-species viral transmission risk. Nature. 2022;607: 555–562. doi:10.1038/s41586-022-04788-w

16. Trovato M, Sartorius R, D'Apice L, Manco R, De Berardinis P. Viral Emerging Diseases: Challenges in Developing Vaccination Strategies. Front Immunol. 2020;11: 2130. doi:10.3389/fimmu.2020.02130

17. Ilori EA, Furuse Y, Ipadeola OB, Dan-Nwafor CC, Abubakar A, Womi-Eteng OE, et al. Epidemiologic and Clinical Features of Lassa Fever Outbreak in Nigeria, January 1–May 6, 2018. Emerg Infect Dis. 2019;25: 1066–1074. doi:10.3201/eid2506.181035

18. Brauburger K, Hume AJ, Mühlberger E, Olejnik J. Forty-Five Years of Marburg Virus Research. Viruses. 2012;4: 1878–1927. doi:10.3390/v4101878

19. Coltart CEM, Lindsey B, Ghinai I, Johnson AM, Heymann DL. The Ebola outbreak, 2013–2016: old lessons for new epidemics. Phil Trans R Soc B. 2017;372: 20160297. doi:10.1098/rstb.2016.0297

20. Taubenberger JK, Morens DM. 1918 Influenza: the Mother of All Pandemics. Emerg Infect Dis. 2006;12: 15–22. doi:10.3201/eid1209.05-0979

21. Garten RJ, Davis CT, Russell CA, Shu B, Lindstrom S, Balish A, et al. Antigenic and Genetic Characteristics of Swine-Origin 2009 A(H1N1) Influenza Viruses Circulating in Humans. Science. 2009;325: 197–201. doi:10.1126/science.1176225

22. de Wit E, van Doremalen N, Falzarano D, Munster VJ. SARS and MERS: recent insights into emerging coronaviruses. Nat Rev Microbiol. 2016;14: 523–534. doi:10.1038/nrmicro.2016.81

23. Worobey M, Levy JI, Malpica Serrano L, Crits-Christoph A, Pekar JE, Goldstein SA, et al. The Huanan Seafood Wholesale Market in Wuhan was the early epicenter of the COVID-19 pandemic. Science. 2022;377: 951–959. doi:10.1126/science.abp8715

24. Stenseth NChr, Dharmarajan G, Li R, Shi Z-L, Yang R, Gao GF. Lessons Learnt From the COVID-19 Pandemic. Front Public Health. 2021;9: 694705. doi:10.3389/fpubh.2021.694705

25. Kmiec D, Kirchhoff F. Monkeypox: A New Threat? IJMS. 2022;23: 7866. doi:10.3390/ijms23147866

26. Trovato M, Sartorius R, D'Apice L, Manco R, De Berardinis P. Viral Emerging Diseases: Challenges in Developing Vaccination Strategies. Front Immunol. 2020;11: 2130. doi:10.3389/fimmu.2020.02130

27. Keusch GT, Amuasi JH, Anderson DE, Daszak P, Eckerle I, Field H, et al. Pandemic origins and a One Health approach to preparedness and prevention: Solutions based on SARS-CoV-2 and other RNA viruses. Proceedings of the National Academy of Sciences. 2022;119: e2202871119. doi:10.1073/pnas.2202871119

28. Weinberg M, Yovel Y. Revising the paradigm: Are bats really pathogen reservoirs or do they possess an efficient immune system? iScience. 2022;25: 104782. doi:10.1016/j.isci.2022.104782

29. Mollentze N, Streicker DG. Viral zoonotic risk is homogenous among taxonomic orders of mammalian and avian reservoir hosts. Proc Natl Acad Sci USA. 2020;117: 9423–9430. doi:10.1073/pnas.1919176117

30. Rothenburg S, Brennan G. Species-Specific Host-Virus Interactions: Implications for Viral Host Range and Virulence. Trends Microbiol. 2019/10/11 ed. 2020;28: 46–56. doi:10.1016/j.tim.2019.08.007

31. Tsetsarkin KA, Vanlandingham DL, McGee CE, Higgs S. A Single Mutation in Chikungunya Virus Affects Vector Specificity and Epidemic Potential. Holmes EC, editor. PLoS Pathog. 2007;3: e201. doi:10.1371/journal.ppat.0030201

32. Carlson CJ, Zipfel CM, Garnier R, Bansal S. Global estimates of mammalian viral diversity accounting for host sharing. Nat Ecol Evol. 2019;3: 1070–1075. doi:10.1038/s41559-019-0910-6

33. Teeling EC, Vernes SC, Dávalos LM, Ray DA, Gilbert MTP, Myers E, et al. Bat Biology, Genomes, and the Bat1K Project: To Generate Chromosome-Level Genomes for All Living Bat Species. Annu Rev Anim Biosci. 2018;6: 23–46. doi:10.1146/annurev-animal-022516-022811

34. Geiser F, Stawski C. Hibernation and Torpor in Tropical and Subtropical Bats in Relation to Energetics, Extinctions, and the Evolution of Endothermy. Integrative and Comparative Biology. 2011;51: 337–348. doi:10.1093/icb/icr042

35. Teeling EC, Springer MS, Madsen O, Bates P, O'Brien SJ, Murphy WJ. A Molecular Phylogeny for Bats Illuminates Biogeography and the Fossil Record. Science, New Series. 2005;307: 580–584.

36. Podlutsky AJ, Khritankov AM, Ovodov ND, Austad SN. A New Field Record for Bat Longevity. The Journals of Gerontology Series A: Biological Sciences and Medical Sciences. 2005;60: 1366–1368. doi:10.1093/gerona/60.11.1366

37. Wilkinson GS, Adams DM. Recurrent evolution of extreme longevity in bats. Biol Lett. 2019;15: 20180860. doi:10.1098/rsbl.2018.0860

38. Pan Y-H, Zhang Y, Cui J, Liu Y, McAllan BM, Liao C-C, et al. Adaptation of Phenylalanine and Tyrosine Catabolic Pathway to Hibernation in Bats. Seebacher F, editor. PLoS ONE. 2013;8: e62039. doi:10.1371/journal.pone.0062039

39. Foley NM, Petit EJ, Brazier T, Finarelli JA, Hughes GM, Touzalin F, et al. Drivers of longitudinal telomere dynamics in a long-lived bat species, *Myotis myotis*. Mol Ecol. 2020;29: 2963–2977. doi:10.1111/mec.15395

40. Foley NM, Hughes GM, Huang Z, Clarke M, Jebb D, Whelan CV, et al. Growing old, yet staying young: The role of telomeres in bats' exceptional longevity. Sci Adv. 2018;4: eaao0926. doi:10.1126/sciadv.aao0926

41. Harper JM, Salmon AB, Leiser SF, Galecki AT, Miller RA. Skin-derived fibroblasts from long-lived species are resistant to some, but not all, lethal stresses and to the mitochondrial inhibitor rotenone. Aging Cell. 2007;6: 1–13. doi:10.1111/j.1474-9726.2006.00255.x

42. Pickering AM, Lehr M, Kohler WJ, Han ML, Miller RA. Fibroblasts From Longer-Lived Species of Primates, Rodents, Bats, Carnivores, and Birds Resist Protein Damage. The Journals of Gerontology: Series A. 2015;70: 791–799. doi:10.1093/gerona/glu115

43. Pride H, Yu Z, Sunchu B, Mochnick J, Coles A, Zhang Y, et al. Long-lived species have improved proteostasis compared to phylogenetically-related shorter-lived species. Biochem Biophys Res Commun. 2015;457: 669–675. doi:10.1016/j.bbrc.2015.01.046

44. Chionh YT, Cui J, Koh J, Mendenhall IH, Ng JHJ, Low D, et al. High basal heat-shock protein expression in bats confers resistance to cellular heat/oxidative stress. Cell Stress and Chaperones. 2019;24: 835–849. doi:10.1007/s12192-019-01013-y

45. Kacprzyk J, Locatelli AG, Hughes GM, Huang Z, Clarke M, Gorbunova V, et al. Evolution of mammalian longevity: age-related increase in autophagy in bats compared to other mammals. Aging. 2021;13: 7998–8025. doi:10.18632/aging.202852

46. Seluanov A, Gladyshev VN, Vijg J, Gorbunova V. Mechanisms of cancer resistance in long-lived mammals. Nat Rev Cancer. 2018;18: 433–441. doi:10.1038/s41568-018-0004-9

47. Brunet-Rossinni AK. Reduced free-radical production and extreme longevity in the little brown bat (Myotis lucifugus) versus two non-flying mammals. Mechanisms of Ageing and Development. 2004;125: 11–20. doi:10.1016/j.mad.2003.09.003

48. Salmon AB, Leonard S, Masamsetti V, Pierce A, Podlutsky AJ, Podlutskaya N, et al. The long lifespan of two bat species is correlated with resistance to protein oxidation and enhanced protein homeostasis. FASEB j. 2009;23: 2317–2326. doi:10.1096/fj.08-122523

49. Zhang G, Cowled C, Shi Z, Huang Z, Bishop-Lilly KA, Fang X, et al. Comparative Analysis of Bat Genomes Provides Insight into the Evolution of Flight and Immunity. Science. 2013;339: 456–460. doi:10.1126/science.1230835

50. Huang Z, Jebb D, Teeling EC. Blood miRNomes and transcriptomes reveal novel longevity mechanisms in the long-lived bat, Myotis myotis. BMC Genomics. 2016;17: 906. doi:10.1186/s12864-016-3227-8

51. Ball HC, levari-Shariati S, Cooper LN, Aliani M. Comparative metabolomics of aging in a long-lived bat: Insights into the physiology of extreme longevity. Ho PL, editor. PLoS ONE. 2018;13: e0196154. doi:10.1371/journal.pone.0196154

52. O'Shea TJ, Cryan PM, Cunningham AA, Fooks AR, Hayman DTS, Luis AD, et al. Bat Flight and Zoonotic Viruses. Emerg Infect Dis. 2014;20: 741–745. doi:10.3201/eid2005.130539

53. Shen Y-Y, Liang L, Zhu Z-H, Zhou W-P, Irwin DM, Zhang Y-P. Adaptive evolution of energy metabolism genes and the origin of flight in bats. Proc Natl Acad Sci USA. 2010;107: 8666–8671. doi:10.1073/pnas.0912613107

54. Cabrera-Campos I, Carballo-Morales JD, Saldaña-Vázquez RA, Villalobos F, Ayala-Berdon J. Body mass explains digestive traits in small vespertilionid bats. J Comp Physiol B. 2021;191: 427–438. doi:10.1007/s00360-021-01348-y

55. Caviedes-Vidal E, Karasov WH, Chediack JG, Fasulo V, Cruz-Neto AP, Otani L. Paracellular Absorption: A Bat Breaks the Mammal Paradigm. Humphries S, editor. PLoS ONE. 2008;3: e1425. doi:10.1371/journal.pone.0001425

56. Kelm DH, Simon R, Kuhlow D, Voigt CC, Ristow M. High activity enables life on a high-sugar diet: blood glucose regulation in nectar-feeding bats. Proc R Soc B. 2011;278: 3490–3496. doi:10.1098/rspb.2011.0465

57. Peng X, He X, Liu Q, Sun Y, Liu H, Zhang Q, et al. Flight is the key to postprandial blood glucose balance in the fruit bats *Eonycteris spelaea* and *Cynopterus sphinx*. Ecol Evol. 2017;7: 8804–8811. doi:10.1002/ece3.3416

58. Ingala MR, Simmons NB, Perkins SL. Bats Are an Untapped System for Understanding Microbiome Evolution in Mammals. McMahon K, editor. mSphere. 2018;3: e00397-18. doi:10.1128/mSphere.00397-18

59. Hughes GM, Leech J, Puechmaille SJ, Lopez JV, Teeling EC. Is there a link between aging and microbiome diversity in exceptional mammalian longevity? PeerJ. 2018;6: e4174. doi:10.7717/peerj.4174

60. Simões BF, Foley NM, Hughes GM, Zhao H, Zhang S, Rossiter SJ, et al. As Blind as a Bat? Opsin Phylogenetics Illuminates the Evolution of Color Vision in Bats. Russo C, editor. Molecular Biology and Evolution. 2019;36: 54–68. doi:10.1093/molbev/msy192

61. Jones G, Teeling EC, Rossiter SJ. From the ultrasonic to the infrared: molecular evolution and the sensory biology of bats. Front Physiol. 2013;4. doi:10.3389/fphys.2013.00117

62. Brook CE, Dobson AP. Bats as 'special' reservoirs for emerging zoonotic pathogens. Trends in Microbiology. 2015;23: 172–180. doi:10.1016/j.tim.2014.12.004

63. Letko M, Seifert SN, Olival KJ, Plowright RK, Munster VJ. Bat-borne virus diversity, spillover and emergence. Nat Rev Microbiol. 2020;18: 461–471. doi:10.1038/s41579-020-0394-z

64. Serra-Cobo J, López-Roig M. Bats and Emerging Infections: An Ecological and Virological Puzzle. In: Rezza G, Ippolito G, editors. Emerging and Re-emerging Viral Infections. Cham: Springer International Publishing; 2016. pp. 35–48. doi:10.1007/5584_2016_131

65. Streicker DG, Gilbert AT. Contextualizing bats as viral reservoirs. Science. 2020;370: 172–173. doi:10.1126/science.abd4559

66. Luis AD, Hayman DTS, O'Shea TJ, Cryan PM, Gilbert AT, Pulliam JRC, et al. A comparison of bats and rodents as reservoirs of zoonotic viruses: are bats special? Proc R Soc B. 2013;280: 20122753. doi:10.1098/rspb.2012.2753

67. Amman BR, Nyakarahuka L, McElroy AK, Dodd KA, Sealy TK, Schuh AJ, et al. Marburgvirus Resurgence in Kitaka Mine Bat Population after Extermination Attempts, Uganda. Emerg Infect Dis. 2014;20: 1761–1764. doi:10.3201/eid2010.140696

68. Jo WK, Oliveira-Filho EF, Rasche A, Greenwood AD, Osterrieder K, Drexler JF. Potential zoonotic sources of SARS-CoV-2 infections. Transbound Emerg Dis. 2021;68: 1824–1834. doi:10.1111/tbed.13872

69. Daszak P, Zambrana-Torrelio C, Bogich TL, Fernandez M, Epstein JH, Murray KA, et al. Interdisciplinary approaches to understanding disease emergence: The past, present, and future drivers of Nipah virus emergence. Proc Natl Acad Sci USA. 2013;110: 3681–3688. doi:10.1073/pnas.1201243109

70. Wang L-F, Anderson DE. Viruses in bats and potential spillover to animals and humans. Current Opinion in Virology. 2019;34: 79–89. doi:10.1016/j.coviro.2018.12.007

71. Jebb D, Huang Z, Pippel M, Hughes GM, Lavrichenko K, Devanna P, et al. Six reference-quality genomes reveal evolution of bat adaptations. Nature. 2020;583: 578–584. doi:10.1038/s41586-020-2486-3

72. Brook CE, Boots M, Chandran K, Dobson AP, Drosten C, Graham AL, et al. Accelerated viral dynamics in bat cell lines, with implications for zoonotic emergence. eLife. 2020;9: e48401. doi:10.7554/eLife.48401

73. Cowled C, Baker ML, Zhou P, Tachedjian M, Wang L-F. Molecular characterisation of RIG-I-like helicases in the black flying fox, Pteropus alecto. Developmental & Comparative Immunology. 2012;36: 657–664. doi:10.1016/j.dci.2011.11.008

74. Irving AT, Ahn M, Goh G, Anderson DE, Wang L-F. Lessons from the host defences of bats, a unique viral reservoir. Nature. 2021;589: 363–370. doi:10.1038/s41586-020-03128-0

75. Paweska JT, Jansen van Vuren P, Masumu J, Leman PA, Grobbelaar AA, Birkhead M, et al. Virological and Serological Findings in Rousettus aegyptiacus Experimentally Inoculated with Vero Cells-Adapted Hogan Strain of Marburg Virus. Markotter W, editor. PLoS ONE. 2012;7: e45479. doi:10.1371/journal.pone.0045479

76. Williamson MM, Hooper PT, Selleck PW, Westbury HA, Slocombe RF. Experimental Hendra Virus Infectionin Pregnant Guinea-pigs and Fruit Bats(Pteropus poliocephalus). Journal of Comparative Pathology. 2000;122: 201–207. doi:10.1053/jcpa.1999.0364

77. Middleton DJ, Morrissy CJ, van der Heide BM, Russell GM, Braun MA, Westbury HA, et al. Experimental Nipah Virus Infection in Pteropid Bats (Pteropus poliocephalus). Journal of Comparative Pathology. 2007;136: 266–272. doi:10.1016/j.jcpa.2007.03.002

78. Ahn M, Anderson DE, Zhang Q, Tan CW, Lim BL, Luko K, et al. Dampened NLRP3-mediated inflammation in bats and implications for a special viral reservoir host. Nat Microbiol. 2019;4: 789–799. doi:10.1038/s41564-019-0371-3

79. Turmelle AS, Jackson FR, Green D, McCracken GF, Rupprecht CE. Host immunity to repeated rabies virus infection in big brown bats. Journal of General Virology. 2010;91: 2360–2366. doi:10.1099/vir.0.020073-0

80. Calisher CH, Ellison JA. The other rabies viruses: The emergence and importance of lyssaviruses from bats and other vertebrates. Travel Medicine and Infectious Disease. 2012;10: 69–79. doi:10.1016/j.tmaid.2012.01.003

81. Cogswell-Hawkinson A, Bowen R, James S, Gardiner D, Calisher CH, Adams R, et al. Tacaribe Virus Causes Fatal Infection of An Ostensible Reservoir Host, the Jamaican Fruit Bat. J Virol. 2012;86: 5791–5799. doi:10.1128/JVI.00201-12

82. Negredo A, Palacios G, Vázquez-Morón S, González F, Dopazo H, Molero F, et al. Discovery of an Ebolavirus-Like Filovirus in Europe. Basler CF, editor. PLoS Pathog. 2011;7: e1002304. doi:10.1371/journal.ppat.1002304

83. Hayman DTS. Bats as Viral Reservoirs. Annu Rev Virol. 2016;3: 77–99. doi:10.1146/annurev-virology-110615-042203

84. Fumagalli MR, Zapperi S, La Porta CAM. Role of body temperature variations in bat immune response to viral infections. J R Soc Interface. 2021;18: 20210211. doi:10.1098/rsif.2021.0211

85. Mandl JN, Schneider C, Schneider DS, Baker ML. Going to Bat(s) for Studies of Disease Tolerance. Front Immunol. 2018;9: 2112. doi:10.3389/fimmu.2018.02112

86. Parkin J, Cohen B. An overview of the immune system. The Lancet. 2001;357: 1777–1789. doi:10.1016/S0140-6736(00)04904-7

87. Borghesi L, Milcarek C. Innate versus Adaptive Immunity: A Paradigm Past Its Prime? Cancer Research. 2007;67: 3989–3993. doi:10.1158/0008-5472.CAN-07-0182

88. Lazear HM, Schoggins JW, Diamond MS. Shared and Distinct Functions of Type I and Type III Interferons. Immunity. 2019;50: 907–923. doi:10.1016/j.immuni.2019.03.025

89. Martínez Gómez JM, Periasamy P, Dutertre C-A, Irving AT, Ng JHJ, Crameri G, et al. Phenotypic and functional characterization of the major lymphocyte populations in the fruit-eating bat Pteropus alecto. Sci Rep. 2016;6: 37796. doi:10.1038/srep37796

90. Chow KT, Gale M, Loo Y-M. RIG-I and Other RNA Sensors in Antiviral Immunity. Annu Rev Immunol. 2018;36: 667–694. doi:10.1146/annurev-immunol-042617-053309

91. Takeuchi O, Akira S. Pattern Recognition Receptors and Inflammation. Cell. 2010;140: 805–820. doi:10.1016/j.cell.2010.01.022

92. Streicher F, Jouvenet N. Stimulation of Innate Immunity by Host and Viral RNAs. Trends in Immunology. 2019;40: 1134–1148. doi:10.1016/j.it.2019.10.009

93. Rehwinkel J, Gack MU. RIG-I-like receptors: their regulation and roles in RNA sensing. Nat Rev Immunol. 2020;20: 537–551. doi:10.1038/s41577-020-0288-3

94. Baldaccini M, Pfeffer S. Untangling the roles of RNA helicases in antiviral innate immunity. Hobman TC, editor. PLoS Pathog. 2021;17: e1010072. doi:10.1371/journal.ppat.1010072

95. Dias Junior AG, Sampaio NG, Rehwinkel J. A Balancing Act: MDA5 in Antiviral Immunity and Autoinflammation. Trends in Microbiology. 2019;27: 75–85. doi:10.1016/j.tim.2018.08.007

96. Loo Y-M, Fornek J, Crochet N, Bajwa G, Perwitasari O, Martinez-Sobrido L, et al. Distinct RIG-I and MDA5 signaling by RNA viruses in innate immunity. J Virol. 2008;82: 335–345. doi:10.1128/JVI.01080-07

97. Kawai T, Akira S. Innate immune recognition of viral infection. Nat Immunol. 2006;7: 131–137. doi:10.1038/ni1303

98. Negishi H, Taniguchi T, Yanai H. The Interferon (IFN) Class of Cytokines and the IFN Regulatory Factor (IRF) Transcription Factor Family. Cold Spring Harb Perspect Biol. 2018;10: a028423. doi:10.1101/cshperspect.a028423

99. Randall RE, Goodbourn S. Interferons and viruses: an interplay between induction, signalling, antiviral responses and virus countermeasures. J Gen Virol. 2007/12/20 ed. 2008;89: 1–47. doi:10.1099/vir.0.83391-0

100. Roach JC, Glusman G, Rowen L, Kaur A, Purcell MK, Smith KD, et al. The evolution of vertebrate Toll-like receptors. Proc Natl Acad Sci USA. 2005;102: 9577–9582. doi:10.1073/pnas.0502272102

101. Lind NA, Rael VE, Pestal K, Liu B, Barton GM. Regulation of the nucleic acid-sensing Toll-like receptors. Nat Rev Immunol. 2022;22: 224–235. doi:10.1038/s41577-021-00577-0

102. Webb LG, Fernandez-Sesma A. RNA viruses and the cGAS-STING pathway: reframing our understanding of innate immune sensing. Current Opinion in Virology. 2022;53: 101206. doi:10.1016/j.coviro.2022.101206

103. Ma Z, Ni G, Damania B. Innate Sensing of DNA Virus Genomes. Annu Rev Virol. 2018;5: 341–362. doi:10.1146/annurev-virology-092917-043244

104. Aguirre S, Luthra P, Sanchez-Aparicio MT, Maestre AM, Patel J, Lamothe F, et al. Dengue virus NS2B protein targets cGAS for degradation and prevents mitochondrial DNA sensing during infection. Nat Microbiol. 2017;2: 17037. doi:10.1038/nmicrobiol.2017.37

105. Unterholzner L, Keating SE, Baran M, Horan KA, Jensen SB, Sharma S, et al. IFI16 is an innate immune sensor for intracellular DNA. Nat Immunol. 2010;11: 997–1004. doi:10.1038/ni.1932

106. Jiang Z, Wei F, Zhang Y, Wang T, Gao W, Yu S, et al. IFI16 directly senses viral RNA and enhances RIG-I transcription and activation to restrict influenza virus infection. Nat Microbiol. 2021;6: 932–945. doi:10.1038/s41564-021-00907-x

107. Wichit S, Hamel R, Yainoy S, Gumpangseth N, Panich S, Phuadraksa T, et al. Interferon-inducible protein (IFI) 16 regulates Chikungunya and Zika virus infection in human skin fibroblasts. EXCLI Journal; 18:Doc467; ISSN 1611-2156. 2019 [cited 19 Sep 2022]. doi:10.17179/EXCLI2019-1271

108. Kim B, Arcos S, Rothamel K, Jian J, Rose KL, McDonald WH, et al. Discovery of Widespread Host Protein Interactions with the Pre-replicated Genome of CHIKV Using VIR-CLASP. Molecular Cell. 2020;78: 624-640.e7. doi:10.1016/j.molcel.2020.04.013

109. García MA, Meurs EF, Esteban M. The dsRNA protein kinase PKR: Virus and cell control. Biochimie. 2007;89: 799–811. doi:10.1016/j.biochi.2007.03.001

110. Cesaro T, Michiels T. Inhibition of PKR by Viruses. Front Microbiol. 2021;12: 757238. doi:10.3389/fmicb.2021.757238

111. Hornung V, Hartmann R, Ablasser A, Hopfner K-P. OAS proteins and cGAS: unifying concepts in sensing and responding to cytosolic nucleic acids. Nat Rev Immunol. 2014;14: 521–528. doi:10.1038/nri3719

112. Pennemann FL, Mussabekova A, Urban C, Stukalov A, Andersen LL, Grass V, et al. Cross-species analysis of viral nucleic acid interacting proteins identifies TAOKs as innate immune regulators. Nat Commun. 2021;12: 7009. doi:10.1038/s41467-021-27192-w

113. Takaoka A, Wang Z, Choi MK, Yanai H, Negishi H, Ban T, et al. DAI (DLM-1/ZBP1) is a cytosolic DNA sensor and an activator of innate immune response. Nature. 2007;448: 501–505. doi:10.1038/nature06013

114. Hornung V, Ablasser A, Charrel-Dennis M, Bauernfeind F, Horvath G, Caffrey DanielR, et al. AIM2 recognizes cytosolic dsDNA and forms a caspase-1-activating inflammasome with ASC. Nature. 2009;458: 514–518. doi:10.1038/nature07725

115. Zhang X, Brann TW, Zhou M, Yang J, Oguariri RM, Lidie KB, et al. Cutting Edge: Ku70 Is a Novel Cytosolic DNA Sensor That Induces Type III Rather Than Type I IFN. JI. 2011;186: 4541–4545. doi:10.4049/jimmunol.1003389

116. Tisoncik JR, Korth MJ, Simmons CP, Farrar J, Martin TR, Katze MG. Into the Eye of the Cytokine Storm. Microbiol Mol Biol Rev. 2012;76: 16–32. doi:10.1128/MMBR.05015-11

117. Griffith JW, Sokol CL, Luster AD. Chemokines and Chemokine Receptors: Positioning Cells for Host Defense and Immunity. Annu Rev Immunol. 2014;32: 659–702. doi:10.1146/annurev-immunol-032713-120145

118. Aggarwal BB, Gupta SC, Kim JH. Historical perspectives on tumor necrosis factor and its superfamily: 25 years later, a golden journey. Blood. 2012;119: 651–665. doi:10.1182/blood-2011-04-325225

119. Krause CD, Pestka S. Cut, copy, move, delete: The study of human interferon genes reveal multiple mechanisms underlying their evolution in amniotes. Cytokine. 2015;76: 480–495. doi:10.1016/j.cyto.2015.07.019

120. García-Sastre A. Ten Strategies of Interferon Evasion by Viruses. Cell Host & Microbe. 2017;22: 176–184. doi:10.1016/j.chom.2017.07.012

121. Philips RL, Wang Y, Cheon H, Kanno Y, Gadina M, Sartorelli V, et al. The JAK-STAT pathway at 30: Much learned, much more to do. Cell. 2022;185: 3857–3876. doi:10.1016/j.cell.2022.09.023

122. Schoggins JW. Interferon-Stimulated Genes: What Do They All Do? Annu Rev Virol. 2019;6: 567–584. doi:10.1146/annurev-virology-092818-015756

123. Marie I. Differential viral induction of distinct interferon-alpha genes by positive feedback through interferon regulatory factor-7. The EMBO Journal. 1998;17: 6660–6669. doi:10.1093/emboj/17.22.6660

124. Fujita T, Reis LF, Watanabe N, Kimura Y, Taniguchi T, Vilcek J. Induction of the transcription factor IRF-1 and interferon-beta mRNAs by cytokines and activators of second-messenger pathways. Proc Natl Acad Sci USA. 1989;86: 9936–9940. doi:10.1073/pnas.86.24.9936

125. Rusinova I, Forster S, Yu S, Kannan A, Masse M, Cumming H, et al. INTERFEROME v2.0: an updated database of annotated interferon-regulated genes. Nucleic Acids Research. 2012;41: D1040–D1046. doi:10.1093/nar/gks1215

126. Smith S, Weston S, Kellam P, Marsh M. IFITM proteins—cellular inhibitors of viral entry. Current Opinion in Virology. 2014;4: 71–77. doi:10.1016/j.coviro.2013.11.004

127. Rivera-Serrano EE, Gizzi AS, Arnold JJ, Grove TL, Almo SC, Cameron CE. Viperin Reveals Its True Function. Annu Rev Virol. 2020;7: 421–446. doi:10.1146/annurev-virology-011720-095930

128. Sharma A, Lal SK. Is tetherin a true antiviral: The influenza a virus controversy. Rev Med Virol. 2019;29: e2036. doi:10.1002/rmv.2036

129. Shaw AE, Hughes J, Gu Q, Behdenna A, Singer JB, Dennis T, et al. Fundamental properties of the mammalian innate immune system revealed by multispecies comparison of type I interferon responses. PLoS Biol. 2017;15: e2004086–e2004086. doi:10.1371/journal.pbio.2004086

130. McDougal MB, Boys IN, De La Cruz-Rivera P, Schoggins JW. Evolution of the interferon response: lessons from ISGs of diverse mammals. Current Opinion in Virology. 2022;53: 101202. doi:10.1016/j.coviro.2022.101202

131. Busnadiego I, Fernbach S, Pohl MO, Karakus U, Huber M, Trkola A, et al. Antiviral Activity of Type I, II, and III Interferons Counterbalances ACE2 Inducibility and Restricts SARS-CoV-2. Palese P, editor. mBio. 2020;11: e01928-20. doi:10.1128/mBio.01928-20

132. Goujon C, Moncorgé O, Bauby H, Doyle T, Ward CC, Schaller T, et al. Human MX2 is an interferon-induced post-entry inhibitor of HIV-1 infection. Nature. 2013;502: 559–562. doi:10.1038/nature12542

133. Rinkenberger N, Schoggins JW. Mucolipin-2 Cation Channel Increases Trafficking Efficiency of Endocytosed Viruses. Reich NC, editor. mBio. 2018;9: e02314-17. doi:10.1128/mBio.02314-17

134. Mar KB, Rinkenberger NR, Boys IN, Eitson JL, McDougal MB, Richardson RB, et al. LY6E mediates an evolutionarily conserved enhancement of virus infection by targeting a late entry step. Nat Commun. 2018;9: 3603. doi:10.1038/s41467-018-06000-y

135. Pfaender S, Mar KB, Michailidis E, Kratzel A, Boys IN, V'kovski P, et al. LY6E impairs coronavirus fusion and confers immune control of viral disease. Nat Microbiol. 2020;5: 1330–1339. doi:10.1038/s41564-020-0769-y

136. Persi E, Wolf YI, Koonin EV. Positive and strongly relaxed purifying selection drive the evolution of repeats in proteins. Nat Commun. 2016;7: 13570. doi:10.1038/ncomms13570

137. Fros JJ, Liu WJ, Prow NA, Geertsema C, Ligtenberg M, Vanlandingham DL, et al. Chikungunya Virus Nonstructural Protein 2 Inhibits Type I/II Interferon-Stimulated JAK-STAT Signaling. J Virol. 2010;84: 10877–10887. doi:10.1128/JVI.00949-10

138. Xue W, Ding C, Qian K, Liao Y. The Interplay Between Coronavirus and Type I IFN Response. Front Microbiol. 2022;12: 805472. doi:10.3389/fmicb.2021.805472

139. Miorin L, Maestre AM, Fernandez-Sesma A, García-Sastre A. Antagonism of type I interferon by flaviviruses. Biochemical and Biophysical Research Communications. 2017;492: 587–596. doi:10.1016/j.bbrc.2017.05.146

140. Sridharan H, Zhao C, Krug RM. Species Specificity of the NS1 Protein of Influenza B Virus: NS1 BINDS ONLY HUMAN AND NON-HUMAN PRIMATE UBIQUITIN-LIKE ISG15 PROTEINS *. Journal of Biological Chemistry. 2010;285: 7852–7856. doi:10.1074/jbc.C109.095703

141. Ding Q, Gaska JM, Douam F, Wei L, Kim D, Balev M, et al. Species-specific disruption of STING-dependent antiviral cellular defenses by the Zika virus NS2B3 protease. Proc Natl Acad Sci U S A. 2018/06/20 ed. 2018;115: E6310-e6318. doi:10.1073/pnas.1803406115

142. Rathinam VAK, Fitzgerald KA. Inflammasome Complexes: Emerging Mechanisms and Effector Functions. Cell. 2016;165: 792–800. doi:10.1016/j.cell.2016.03.046

143. Newton K, Dixit VM. Signaling in Innate Immunity and Inflammation. Cold Spring Harbor Perspectives in Biology. 2012;4: a006049–a006049. doi:10.1101/cshperspect.a006049

144. Sokol CL, Luster AD. The Chemokine System in Innate Immunity. Cold Spring Harb Perspect Biol. 2015;7: a016303. doi:10.1101/cshperspect.a016303

145. Fajgenbaum DC, June CH. Cytokine Storm. Longo DL, editor. N Engl J Med. 2020;383: 2255–2273. doi:10.1056/NEJMra2026131

146. Crow YJ, Stetson DB. The type I interferonopathies: 10 years on. Nat Rev Immunol. 2022;22: 471–483. doi:10.1038/s41577-021-00633-9

147. Irving AT, Ahn M, Goh G, Anderson DE, Wang L-F. Lessons from the host defences of bats, a unique viral reservoir. Nature. 2021;589: 363–370. doi:10.1038/s41586-020-03128-0

148. Banerjee A, Baker ML, Kulcsar K, Misra V, Plowright R, Mossman K. Novel Insights Into Immune Systems of Bats. Front Immunol. 2020;11: 26. doi:10.3389/fimmu.2020.00026

149. Banerjee A, Baker ML, Kulcsar K, Misra V, Plowright R, Mossman K. Novel Insights Into Immune Systems of Bats. Front Immunol. 2020;11: 26. doi:10.3389/fimmu.2020.00026

150. Baker ML, Tachedjian M, Wang L-F. Immunoglobulin heavy chain diversity in Pteropid bats: evidence for a diverse and highly specific antigen binding repertoire. Immunogenetics. 2010;62: 173–184. doi:10.1007/s00251-010-0425-4

151. Omatsu T, Nishimura Y, Bak EJ, Ishii Y, Tohya Y, Kyuwa S, et al. Molecular cloning and sequencing of the cDNA encoding the bat CD4. Veterinary Immunology and Immunopathology. 2006;111: 309–313. doi:10.1016/j.vetimm.2005.12.002

152. Kepler TB, Sample C, Hudak K, Roach J, Haines A, Walsh A, et al. Chiropteran types I and II interferon genes inferred from genome sequencing traces by a statistical gene-family assembler. BMC Genomics. 2010;11: 444. doi:10.1186/1471-2164-11-444

153. Omatsu T, Bak E-J, Ishii Y, Kyuwa S, Tohya Y, Akashi H, et al. Induction and sequencing of Rousette bat interferon α and β genes. Veterinary Immunology and Immunopathology. 2008;124: 169–176. doi:10.1016/j.vetimm.2008.03.004

154. Janardhana V, Tachedjian M, Crameri G, Cowled C, Wang L-F, Baker ML. Cloning, expression and antiviral activity of IFNγ from the Australian fruit bat, Pteropus alecto. Developmental & Comparative Immunology. 2012;36: 610–618. doi:10.1016/j.dci.2011.11.001

155. Zhou P, Cowled C, Todd S, Crameri G, Virtue ER, Marsh GA, et al. Type III IFNs in Pteropid Bats: Differential Expression Patterns Provide Evidence for Distinct Roles in Antiviral Immunity. JI. 2011;186: 3138–3147. doi:10.4049/jimmunol.1003115

156. Fujii H, Watanabe S, Yamane D, Ueda N, Iha K, Taniguchi S, et al. Functional analysis of Rousettus aegyptiacus "signal transducer and activator of transcription 1" (STAT1). Developmental & Comparative Immunology. 2010;34: 598–602. doi:10.1016/j.dci.2010.01.004

157. Iha K, Omatsu T, Watanabe S, Ueda N, Taniguchi S, Fujii H, et al. Molecular Cloning and Sequencing of the cDNAs Encoding the Bat Interleukin (IL)-2, IL-4, IL-6, IL-10, IL-12p40, and Tumor Necrosis Factor-Alpha. J Vet Med Sci. 2009;71: 1691–1695. doi:10.1292/jvms.001691

158. Cowled C, Baker M, Tachedjian M, Zhou P, Bulach D, Wang L-F. Molecular characterisation of Toll-like receptors in the black flying fox Pteropus alecto. Developmental & Comparative Immunology. 2011;35: 7–18. doi:10.1016/j.dci.2010.07.006

159. Kelley J, de Bono B, Trowsdale J. IRIS: A database surveying known human immune system genes. Genomics. 2005;85: 503–511. doi:10.1016/j.ygeno.2005.01.009

160. Papenfuss AT, Baker ML, Feng Z-P, Tachedjian M, Crameri G, Cowled C, et al. The immune gene repertoire of an important viral reservoir, the Australian black flying fox. BMC Genomics. 2012;13: 261. doi:10.1186/1471-2164-13-261

161. Shaw TI, Srivastava A, Chou W-C, Liu L, Hawkinson A, Glenn TC, et al. Transcriptome Sequencing and Annotation for the Jamaican Fruit Bat (Artibeus jamaicensis). Baker ML, editor. PLoS ONE. 2012;7: e48472. doi:10.1371/journal.pone.0048472

162. Lee AK, Kulcsar KA, Elliott O, Khiabanian H, Nagle ER, Jones MEB, et al. De novo transcriptome reconstruction and annotation of the Egyptian rousette bat. BMC Genomics. 2015;16: 1033. doi:10.1186/s12864-015-2124-x

163. Jacquet S, Culbertson M, Zang C, El Filali A, De La Myre Mory C, Pons J-B, et al. Adaptive duplication and functional diversification of Protein kinase R contribute to the uniqueness of bat-virus interactions. Evolutionary Biology; 2022 Jun. doi:10.1101/2022.06.28.497829

164. Zhou P, Tachedjian M, Wynne JW, Boyd V, Cui J, Smith I, et al. Contraction of the type I IFN locus and unusual constitutive expression of IFN-α in bats. PNAS. 2016;113: 2696–2701. doi:10.1073/pnas.1518240113

165. He G, He B, Racey PA, Cui J. Positive Selection of the Bat Interferon Alpha Gene Family. Biochem Genet. 2010;48: 840–846. doi:10.1007/s10528-010-9365-9

166. Hölzer M, Schoen A, Wulle J, Müller MA, Drosten C, Marz M, et al. Virus- and Interferon Alpha-Induced Transcriptomes of Cells from the Microbat Myotis daubentonii. iScience. 2019;19: 647–661. doi:10.1016/j.isci.2019.08.016

167. Pavlovich SS, Lovett SP, Koroleva G, Guito JC, Arnold CE, Nagle ER, et al. The Egyptian Rousette Genome Reveals Unexpected Features of Bat Antiviral Immunity. Cell. 2018;173: 1098-1110.e18. doi:10.1016/j.cell.2018.03.070

168. Walker AM, Roberts RM. Characterization of the bovine type I IFN locus: rearrangements, expansions, and novel subfamilies. BMC Genomics. 2009;10: 187. doi:10.1186/1471-2164-10-187

169. He X, Korytář T, Schatz J, Freuling CM, Müller T, Köllner B. Anti-Lyssaviral Activity of Interferons κ and ω from the Serotine Bat, Eptesicus serotinus. Lyles DS, editor. J Virol. 2014;88: 5444–5454. doi:10.1128/JVI.03403-13

170. Banerjee A, Falzarano D, Rapin N, Lew J, Misra V. Interferon Regulatory Factor 3-Mediated Signaling Limits Middle-East Respiratory Syndrome (MERS) Coronavirus Propagation in Cells from an Insectivorous Bat. Viruses. 2019;11. doi:10.3390/v11020152

171. Bondet V, Le Baut M, Le Poder S, Lécu A, Petit T, Wedlarski R, et al. Constitutive IFNα Protein Production in Bats. Front Immunol. 2021;12: 735866. doi:10.3389/fimmu.2021.735866

172. De La Cruz-Rivera PC, Kanchwala M, Liang H, Kumar A, Wang L-F, Xing C, et al. The IFN Response in Bats Displays Distinctive IFN-Stimulated Gene Expression Kinetics with Atypical RNASEL Induction. JI. 2018;200: 209–217. doi:10.4049/jimmunol.1701214

173. Irving AT, Zhang Q, Kong P-S, Luko K, Rozario P, Wen M, et al. Interferon Regulatory Factors IRF1 and IRF7 Directly Regulate Gene Expression in Bats in Response to Viral Infection. Cell Reports. 2020;33: 108345. doi:10.1016/j.celrep.2020.108345

174. Shaw AE, Hughes J, Gu Q, Behdenna A, Singer JB, Dennis T, et al. Fundamental properties of the mammalian innate immune system revealed by multispecies comparison of type I interferon responses. Malik H, editor. PLoS Biol. 2017;15: e2004086. doi:10.1371/journal.pbio.2004086

175. Glennon NB, Jabado O, Lo MK, Shaw ML. Transcriptome Profiling of the Virus-Induced Innate Immune Response in Pteropus vampyrus and Its Attenuation by Nipah Virus Interferon Antagonist Functions. Journal of Virology. 2015;89: 17.

176. Tarigan R, Shimoda H, Doysabas KCC, Ken M, Iida A, Hondo E. Role of pattern recognition receptors and interferon-beta in protecting bat cell lines from encephalomyocarditis virus and Japanese encephalitis virus infection. Biochemical and Biophysical Research Communications. 2020;527: 1–7. doi:10.1016/j.bbrc.2020.04.060

177. Kuzmin IV, Schwarz TM, Ilinykh PA, Jordan I, Ksiazek TG, Sachidanandam R, et al. Innate Immune Responses of Bat and Human Cells to Filoviruses: Commonalities and Distinctions. Lyles DS, editor. J Virol. 2017;91: e02471-16. doi:10.1128/JVI.02471-16

178. Li Y, Dong B, Wei Z, Silverman RH, Weiss SR. Activation of RNase L in Egyptian Rousette Bat-Derived RoNi/7 Cells Is Dependent Primarily on OAS3 and Independent of MAVS Signaling. mBio. 2019;10. doi:10.1128/mBio.02414-19

179. Ren L, Wu C, Guo L, Yao J, Wang C, Xiao Y, et al. Single-cell transcriptional atlas of the Chinese horseshoe bat (*Rhinolophus sinicus*) provides insight into the cellular mechanisms which enable bats to be viral reservoirs. Cell Biology; 2020 Jun. doi:10.1101/2020.06.30.175778

180. Sarkis S, Lise M-C, Darcissac E, Dabo S, Falk M, Chaulet L, et al. Development of molecular and cellular tools to decipher the type I IFN pathway of the common vampire bat. Developmental & Comparative Immunology. 2018;81: 1–7. doi:10.1016/j.dci.2017.10.023

181. Lin H, Horie M, Tomonaga K. A comprehensive profiling of innate immune responses in *Eptesicus* bat cells. Microbiology and Immunology. 2022;66: 97–112. doi:10.1111/1348-0421.12952

182. Zhou P, Cowled C, Marsh GA, Shi Z, Wang L-F, Baker ML. Type III IFN Receptor Expression and Functional Characterisation in the Pteropid Bat, Pteropus alecto. Fugmann SD, editor. PLoS ONE. 2011;6: e25385. doi:10.1371/journal.pone.0025385

183. Li J, Zhang G, Cheng D, Ren H, Qian M, Du B. Molecular characterization of RIG-I, STAT-1 and IFN-beta in the horseshoe bat. Gene. 2015;561: 115–123. doi:10.1016/j.gene.2015.02.013

184. He X, Korytář T, Zhu Y, Pikula J, Bandouchova H, Zukal J, et al. Establishment of Myotis myotis Cell Lines - Model for Investigation of Host-Pathogen Interaction in a Natural Host for Emerging Viruses. Schnell MJ, editor. PLoS ONE. 2014;9: e109795. doi:10.1371/journal.pone.0109795

185. Tarigan R, Katta T, Takemae H, Shimoda H, Maeda K, Iida A, et al. Distinct interferon response in bat and other mammalian cell lines infected with Pteropine orthoreovirus. Virus Genes. 2021;57: 510–520. doi:10.1007/s11262-021-01865-6

186. Wang J, Lin Z, Liu Q, Fu F, Wang Z, Ma J, et al. Bat Employs a Conserved MDA5 Gene to Trigger Antiviral Innate Immune Responses. Front Immunol. 2022;13: 904481. doi:10.3389/fimmu.2022.904481

187. Iha K, Omatsu T, Watanabe S, Ueda N, Taniguchi S, Fujii H, et al. Molecular Cloning and Expression Analysis of Bat Toll-Like Receptors 3, 7 and 9. J Vet Med Sci. 2010;72: 217–220. doi:10.1292/jvms.09-0050

188. Escalera-Zamudio M, Zepeda-Mendoza ML, Loza-Rubio E, Rojas-Anaya E, Méndez-Ojeda ML, Arias CF, et al. The evolution of bat nucleic acid-sensing Toll-like receptors. Mol Ecol. 2015;24: 5899–5909. doi:10.1111/mec.13431

189. Jiang H, Li J, Li L, Zhang X, Yuan L, Chen J. Selective evolution of Toll-like receptors 3, 7, 8, and 9 in bats. Immunogenetics. 2017;69: 271–285. doi:10.1007/s00251-016-0966-2

190. Schad J, Voigt CC. Adaptive evolution of virus-sensing toll-like receptor 8 in bats. Immunogenetics. 2016;68: 783–795. doi:10.1007/s00251-016-0940-z

191. Banerjee A, Rapin N, Bollinger T, Misra V. Lack of inflammatory gene expression in bats: a unique role for a transcription repressor. Sci Rep. 2017;7: 2232. doi:10.1038/s41598-017-01513-w

192. Zhou P, Cowled C, Mansell A, Monaghan P, Green D, Wu L, et al. IRF7 in the Australian Black Flying Fox, Pteropus alecto: Evidence for a Unique Expression Pattern and Functional Conservation. Fugmann SD, editor. PLoS ONE. 2014;9: e103875. doi:10.1371/journal.pone.0103875

193. Zhang Q, Zeng L-P, Zhou P, Irving AT, Li S, Shi Z-L, et al. IFNAR2-dependent gene expression profile induced by IFN-α in Pteropus alecto bat cells and impact of IFNAR2 knockout on virus infection. Meurs EF, editor. PLoS ONE. 2017;12: e0182866. doi:10.1371/journal.pone.0182866

194. Banerjee A, Zhang X, Yip A, Schulz KS, Irving AT, Bowdish D, et al. Positive Selection of a Serine Residue in Bat IRF3 Confers Enhanced Antiviral Protection. iScience. 2020;23: 100958. doi:10.1016/j.isci.2020.100958

195. Virtue ER, Marsh GA, Baker ML, Wang L-F. Interferon Production and Signaling Pathways Are Antagonized during Henipavirus Infection of Fruit Bat Cell Lines. Tripp R, editor. PLoS ONE. 2011;6: e22488. doi:10.1371/journal.pone.0022488

196. Wynne JW, Shiell BJ, Marsh GA, Boyd V, Harper JA, Heesom K, et al. Proteomics informed by transcriptomics reveals Hendra virus sensitizes bat cells to TRAIL mediated apoptosis. Genome Biol. 2014;15: 532. doi:10.1186/PREACCEPT-1718798964145132

197. Kading RC, Schountz T. Flavivirus Infections of Bats: Potential Role in Zika Virus Ecology. The American Journal of Tropical Medicine and Hygiene. 2016;95: 993–996. doi:10.4269/ajtmh.16-0625

198. Irving AT, Rozario P, Kong P-S, Luko K, Gorman JJ, Hastie ML, et al. Robust dengue virus infection in bat cells and limited innate immune responses coupled with positive serology from bats in IndoMalaya and Australasia. Cell Mol Life Sci. 2020;77: 1607–1622. doi:10.1007/s00018-019-03242-x

199. Moreira-Soto A, Soto-Garita C, Corrales-Aguilar E. Neotropical primary bat cell lines show restricted dengue virus replication. Comparative Immunology, Microbiology and Infectious Diseases. 2017;50: 101–105. doi:10.1016/j.cimid.2016.12.004

200. Zhou P, Cowled C, Wang L-F, Baker ML. Bat Mx1 and Oas1, but not Pkr are highly induced by bat interferon and viral infection. Developmental & Comparative Immunology. 2013;40: 240–247. doi:10.1016/j.dci.2013.03.006

201. Hoffmann M, Nehlmeier I, Brinkmann C, Krähling V, Behner L, Moldenhauer A-S, et al. Tetherin Inhibits Nipah Virus but Not Ebola Virus Replication in Fruit Bat Cells. Dermody TS, editor. J Virol. 2019;93: e01821-18. doi:10.1128/JVI.01821-18

202. Fuchs J, Hölzer M, Schilling M, Patzina C, Schoen A, Hoenen T, et al. Evolution and Antiviral Specificities of Interferon-Induced Mx Proteins of Bats against Ebola, Influenza, and Other RNA Viruses. Williams BRG, editor. J Virol. 2017;91: e00361-17. doi:10.1128/JVI.00361-17

203. Boys IN, Xu E, Mar KB, De La Cruz-Rivera PC, Eitson JL, Moon B, et al. RTP4 Is a Potent IFN-Inducible Anti-flavivirus Effector Engaged in a Host-Virus Arms Race in Bats and Other Mammals. Cell Host Microbe. 2020/10/29 ed. 2020;28: 712-723.e9.

204. Biesold SE, Ritz D, Gloza-Rausch F, Wollny R, Drexler JF, Corman VM, et al. Type I Interferon Reaction to Viral Infection in Interferon-Competent, Immortalized Cell Lines from the African Fruit Bat Eidolon helvum. Fooks AR, editor. PLoS ONE. 2011;6: e28131. doi:10.1371/journal.pone.0028131

205. Goh G, Ahn M, Zhu F, Lee LB, Luo D, Irving AT, et al. Complementary regulation of caspase-1 and IL-1β reveals additional mechanisms of dampened inflammation in bats. Proc Natl Acad Sci USA. 2020;117: 28939–28949. doi:10.1073/pnas.2003352117

206. Ahn M, Cui J, Irving AT, Wang L-F. Unique Loss of the PYHIN Gene Family in Bats Amongst Mammals: Implications for Inflammasome Sensing. Sci Rep. 2016;6: 21722. doi:10.1038/srep21722

207. Xie J, Li Y, Shen X, Goh G, Zhu Y, Cui J, et al. Dampened STING-Dependent Interferon Activation in Bats. Cell Host & Microbe. 2018;23: 297-301.e4. doi:10.1016/j.chom.2018.01.006

208. Kacprzyk J, Hughes GM, Palsson-McDermott EM, Quinn SR, Puechmaille SJ, O'Neill LAJ, et al. A Potent Anti-Inflammatory Response in Bat Macrophages May Be Linked to Extended Longevity and Viral Tolerance. Acta Chiropterologica. 2017;19: 219–228. doi:10.3161/15081109ACC2017.19.2.001

209. Cui J, Li F, Shi Z-L. Origin and evolution of pathogenic coronaviruses. Nat Rev Microbiol. 2019;17: 181–192. doi:10.1038/s41579-018-0118-9

210. Ravelomanantsoa NAF, Guth S, Andrianiaina A, Andry S, Gentles A, Ranaivoson HC, et al. The zoonotic potential of bat-borne coronaviruses. Low J, editor. Emerging Topics in Life Sciences. 2020;4: 365–381. doi:10.1042/ETLS20200097

211. Wang Q, Vlasova AN, Kenney SP, Saif LJ. Emerging and re-emerging coronaviruses in pigs. Current Opinion in Virology. 2019;34: 39–49. doi:10.1016/j.coviro.2018.12.001

212. Kirtipal N, Bharadwaj S, Kang SG. From SARS to SARS-CoV-2, insights on structure, pathogenicity and immunity aspects of pandemic human coronaviruses. Infection, Genetics and Evolution. 2020;85: 104502. doi:10.1016/j.meegid.2020.104502

213. Lau SKP, Woo PCY, Li KSM, Huang Y, Tsoi H-W, Wong BHL, et al. Severe acute respiratory syndrome coronavirus-like virus in Chinese horseshoe bats. Proc Natl Acad Sci USA. 2005;102: 14040–14045. doi:10.1073/pnas.0506735102

214. Li W. Bats Are Natural Reservoirs of SARS-Like Coronaviruses. Science. 2005;310: 676–679. doi:10.1126/science.1118391

215. Zhu N, Zhang D, Wang W, Li X, Yang B, Song J, et al. A Novel Coronavirus from Patients with Pneumonia in China, 2019. N Engl J Med. 2020;382: 727–733. doi:10.1056/NEJMoa2001017

216. Hu B, Guo H, Zhou P, Shi Z-L. Characteristics of SARS-CoV-2 and COVID-19. Nat Rev Microbiol. 2021;19: 141–154. doi:10.1038/s41579-020-00459-7

217. Lytras S, Xia W, Hughes J, Jiang X, Robertson DL. The animal origin of SARS-CoV-2. Science. 2021;373: 968–970. doi:10.1126/science.abh0117

218. Banerjee A, Kulcsar K, Misra V, Frieman M, Mossman K. Bats and Coronaviruses. Viruses. 2019;11: E41. doi:10.3390/v11010041

219. Tao Y, Shi M, Chommanard C, Queen K, Zhang J, Markotter W, et al. Surveillance of Bat Coronaviruses in Kenya Identifies Relatives of Human Coronaviruses NL63 and 229E and Their Recombination History. Perlman S, editor. J Virol. 2017;91: e01953-16. doi:10.1128/JVI.01953-16

220. Ge X-Y, Li J-L, Yang X-L, Chmura AA, Zhu G, Epstein JH, et al. Isolation and characterization of a bat SARS-like coronavirus that uses the ACE2 receptor. Nature. 2013;503: 535–538. doi:10.1038/nature12711

221. Lam TT-Y, Jia N, Zhang Y-W, Shum MH-H, Jiang J-F, Zhu H-C, et al. Identifying SARS-CoV-2-related coronaviruses in Malayan pangolins. Nature. 2020;583: 282–285. doi:10.1038/s41586-020-2169-0

222. Pekar JE, Magee A, Parker E, Moshiri N, Izhikevich K, Havens JL, et al. The molecular epidemiology of multiple zoonotic origins of SARS-CoV-2. Science. 2022;377: 960–966. doi:10.1126/science.abp8337

223. Temmam S, Vongphayloth K, Salazar EB, Munier S, Bonomi M, Régnault B, et al. Coronaviruses with a SARS-CoV-2-like receptor-binding domain allowing ACE2-mediated entry into human cells isolated from bats of Indochinese peninsula. 2021. doi:10.21203/rs.3.rs-871965/v1

224. Zhou H, Chen X, Hu T, Li J, Song H, Liu Y, et al. A Novel Bat Coronavirus Closely Related to SARS-CoV-2 Contains Natural Insertions at the S1/S2 Cleavage Site of the Spike Protein. Current Biology. 2020;30: 2196-2203.e3. doi:10.1016/j.cub.2020.05.023

225. Zhou P, Yang X-L, Wang X-G, Hu B, Zhang L, Zhang W, et al. A pneumonia outbreak associated with a new coronavirus of probable bat origin. Nature. 2020;579: 270–273. doi:10.1038/s41586-020-2012-7

226. Wacharapluesadee S, Tan CW, Maneeorn P, Duengkae P, Zhu F, Joyjinda Y, et al. Evidence for SARS-CoV-2 related coronaviruses circulating in bats and pangolins in Southeast Asia. Nature Communications. 2021;12: 972. doi:10.1038/s41467-021-21240-1

227. Delaune D, Hul V, Karlsson EA, Hassanin A, Ou TP, Baidaliuk A, et al. A novel SARS-CoV-2 related coronavirus in bats from Cambodia. Nat Commun. 2021;12: 6563. doi:10.1038/s41467-021-26809-4

228. Murakami S, Kitamura T, Suzuki J, Sato R, Aoi T, Fujii M, et al. Detection and Characterization of Bat Sarbecovirus Phylogenetically Related to SARS-CoV-2, Japan. Emerg Infect Dis. 2020;26: 3025–3029. doi:10.3201/eid2612.203386

229. Banerjee A, Kulcsar K, Misra V, Frieman M, Mossman K. Bats and Coronaviruses. Viruses. 2019;11. doi:10.3390/v11010041

230. Frutos R, Serra-Cobo J, Pinault L, Lopez Roig M, Devaux CA. Emergence of Bat-Related Betacoronaviruses: Hazard and Risks. Front Microbiol. 2021;12. doi:10.3389/fmicb.2021.591535

231. Lecis R, Mucedda M, Pidinchedda E, Pittau M, Alberti A. Molecular identification of Betacoronavirus in bats from Sardinia (Italy): first detection and phylogeny. Virus Genes. 2019;55: 60–67. doi:10.1007/s11262-018-1614-8

232. De Benedictis P, Marciano S, Scaravelli D, Priori P, Zecchin B, Capua I, et al. Alpha and lineage C betaCoV infections in Italian bats. Virus Genes. 2014;48: 366–371. doi:10.1007/s11262-013-1008-x

233. Lee S, Jo S-D, Son K, An I, Jeong J, Wang S-J, et al. Genetic Characteristics of Coronaviruses from Korean Bats in 2016. Microb Ecol. 2018;75: 174–182. doi:10.1007/s00248-017-1033-8

234. Falcón A, Vázquez-Morón S, Casas I, Aznar C, Ruiz G, Pozo F, et al. Detection of alpha and betacoronaviruses in multiple Iberian bat species. Arch Virol. 2011;156: 1883. doi:10.1007/s00705-011-1057-1

235. Lelli D, Papetti A, Sabelli C, Rosti E, Moreno A, Boniotti MB. Detection of Coronaviruses in Bats of Various Species in Italy. Viruses. 2013;5: 2679–2689. doi:10.3390/v5112679

236. Temmam S, Vongphayloth K, Baquero E, Munier S, Bonomi M, Regnault B, et al. Bat coronaviruses related to SARS-CoV-2 and infectious for human cells. Nature. 2022;604: 330–336. doi:10.1038/s41586-022-04532-4

237. Zhou H, Ji J, Chen X, Bi Y, Li J, Wang Q, et al. Identification of novel bat coronaviruses sheds light on the evolutionary origins of SARS-CoV-2 and related viruses. Cell. 2021;184: 4380-4391.e14. doi:10.1016/j.cell.2021.06.008

238. Leung NHL. Transmissibility and transmission of respiratory viruses. Nat Rev Microbiol. 2021;19: 528–545. doi:10.1038/s41579-021-00535-6

239. Harrison AG, Lin T, Wang P. Mechanisms of SARS-CoV-2 Transmission and Pathogenesis. Trends in Immunology. 2020;41: 1100–1115. doi:10.1016/j.it.2020.10.004

240. Chams N, Chams S, Badran R, Shams A, Araji A, Raad M, et al. COVID-19: A Multidisciplinary Review. Front Public Health. 2020;8: 383. doi:10.3389/fpubh.2020.00383

241. Patterson EI, Elia G, Grassi A, Giordano A, Desario C, Medardo M, et al. Evidence of exposure to SARS-CoV-2 in cats and dogs from households in Italy. Nature Communications. 2020;11: 6231. doi:10.1038/s41467-020-20097-0

242. Koopmans M. SARS-CoV-2 and the human-animal interface: outbreaks on mink farms. The Lancet Infectious Diseases. 2021;21: 18–19. doi:10.1016/S1473-3099(20)30912-9

243. Hossain MdG, Javed A, Akter S, Saha S. SARS-CoV-2 host diversity: An update of natural infections and experimental evidence. Journal of Microbiology, Immunology and Infection. 2020; S168411822030147X. doi:10.1016/j.jmii.2020.06.006

244. Islam A, Ferdous J, Islam S, Sayeed MdA, Rahman MdK, Saha O, et al. Transmission dynamics and susceptibility patterns of SARS-CoV-2 in domestic, farmed and wild animals: Sustainable One Health surveillance for conservation and public health to prevent future epidemics and pandemics. Transbounding Emerging Dis. 2021; tbed.14356. doi:10.1111/tbed.14356

245. Cool K, Gaudreault NN, Morozov I, Trujillo JD, Meekins DA, McDowell C, et al. Infection and transmission of ancestral SARS-CoV-2 and its alpha variant in pregnant white-tailed deer. Emerg Microbes Infect. 2021; 1–39. doi:10.1080/22221751.2021.2012528

246. Yen H-L, Sit THC, Brackman CJ, Chuk SSY, Gu H, Tam KWS, et al. Transmission of SARS-CoV-2 delta variant (AY.127) from pet hamsters to humans, leading to onward human-to-human transmission: a case study. The Lancet. 2022;399: 1070–1078. doi:10.1016/S0140-6736(22)00326-9

247. Lu L, Sikkema RS, Velkers FC, Nieuwenhuijse DF, Fischer EAJ, Meijer PA, et al. Adaptation, spread and transmission of SARS-CoV-2 in farmed minks and associated humans in the Netherlands. Nat Commun. 2021;12: 6802. doi:10.1038/s41467-021-27096-9

248. Oude Munnink BB, Sikkema RS, Nieuwenhuijse DF, Molenaar RJ, Munger E, Molenkamp R, et al. Transmission of SARS-CoV-2 on mink farms between humans and mink and back to humans. Science. 2021;371: 172–177. doi:10.1126/science.abe5901

249. Olival KJ, Cryan PM, Amman BR, Baric RS, Blehert DS, Brook CE, et al. Possibility for reverse zoonotic transmission of SARS-CoV-2 to free-ranging wildlife: A case study of bats. Lakdawala S, editor. PLoS Pathog. 2020;16: e1008758. doi:10.1371/journal.ppat.1008758

250. Hale VL, Dennis PM, McBride DS, Nolting JM, Madden C, Huey D, et al. SARS-CoV-2 infection in free-ranging white-tailed deer. Nature. 2022;602: 481–486. doi:10.1038/s41586-021-04353-x

251. Martins M, Boggiatto PM, Buckley A, Cassmann ED, Falkenberg S, Caserta LC, et al. From Deer-to-Deer: SARS-CoV-2 is efficiently transmitted and presents broad tissue tropism and replication sites in white-tailed deer. Munster V, editor. PLoS Pathog. 2022;18: e1010197. doi:10.1371/journal.ppat.1010197

252. Salian VS, Wright JA, Vedell PT, Nair S, Li C, Kandimalla M, et al. COVID-19 Transmission, Current Treatment, and Future Therapeutic Strategies. Mol Pharmaceutics. 2021;18: 754–771. doi:10.1021/acs.molpharmaceut.0c00608

253. Zhang Y, Zhang H, Zhang W. SARS-CoV-2 variants, immune escape, and countermeasures. Front Med. 2022;16: 196–207. doi:10.1007/s11684-021-0906-x

254. Zhang L, Li Q, Liang Z, Li T, Liu S, Cui Q, et al. The significant immune escape of pseudotyped SARS-CoV-2 variant Omicron. Emerging Microbes & Infections. 2022;11: 1–5. doi:10.1080/22221751.2021.2017757

255. Tan CW, Chia WN, Zhu F, Young BE, Chantasrisawad N, Hwa S-H, et al. SARS-CoV-2 Omicron variant emerged under immune selection. Nat Microbiol. 2022 [cited 15 Oct 2022]. doi:10.1038/s41564-022-01246-1

256. Dhawan M, Saied AA, Mitra S, Alhumaydhi FA, Emran TB, Wilairatana P. Omicron variant (B.1.1.529) and its sublineages: What do we know so far amid the emergence of recombinant variants of SARS-CoV-2? Biomedicine & Pharmacotherapy. 2022;154: 113522. doi:10.1016/j.biopha.2022.113522

257. Wu A, Peng Y, Huang B, Ding X, Wang X, Niu P, et al. Genome Composition and Divergence of the Novel Coronavirus (2019-nCoV) Originating in China. Cell Host & Microbe. 2020;27: 325–328. doi:10.1016/j.chom.2020.02.001

258. V'kovski P, Kratzel A, Steiner S, Stalder H, Thiel V. Coronavirus biology and replication: implications for SARS-CoV-2. Nat Rev Microbiol. 2021;19: 155–170. doi:10.1038/s41579-020-00468-6

259. Hartenian E, Nandakumar D, Lari A, Ly M, Tucker JM, Glaunsinger BA. The molecular virology of coronaviruses. Journal of Biological Chemistry. 2020;295: 12910–12934. doi:10.1074/jbc.REV120.013930

260. Brant AC, Tian W, Majerciak V, Yang W, Zheng Z-M. SARS-CoV-2: from its discovery to genome structure, transcription, and replication. Cell Biosci. 2021;11: 136. doi:10.1186/s13578-021-00643-z

261. Cortese M, Lee J-Y, Cerikan B, Neufeldt CJ, Oorschot VMJ, Köhrer S, et al. Integrative Imaging Reveals SARS-CoV-2-Induced Reshaping of Subcellular Morphologies. Cell Host & Microbe. 2020;28: 853-866.e5. doi:10.1016/j.chom.2020.11.003

262. Lu R, Zhao X, Li J, Niu P, Yang B, Wu H, et al. Genomic characterisation and epidemiology of 2019 novel coronavirus: implications for virus origins and receptor binding. The Lancet. 2020;395: 565–574. doi:10.1016/S0140-6736(20)30251-8

263. Hoffmann M, Kleine-Weber H, Schroeder S, Krüger N, Herrler T, Erichsen S, et al. SARS-CoV-2 Cell Entry Depends on ACE2 and TMPRSS2 and Is Blocked by a Clinically Proven Protease Inhibitor. Cell. 2020;181: 271-280.e8. doi:10.1016/j.cell.2020.02.052

264. Murgolo N, Therien AG, Howell B, Klein D, Koeplinger K, Lieberman LA, et al. SARS-CoV-2 tropism, entry, replication, and propagation: Considerations for drug discovery and development. PLOS Pathogens. 2021;17: e1009225. doi:10.1371/journal.ppat.1009225

265. Benton DJ, Wrobel AG, Xu P, Roustan C, Martin SR, Rosenthal PB, et al. Receptor binding and priming of the spike protein of SARS-CoV-2 for membrane fusion. Nature. 2020;588: 327–330. doi:10.1038/s41586-020-2772-0

266. Koch J, Uckeley ZM, Doldan P, Stanifer M, Boulant S, Lozach P-Y. TMPRSS2 expression dictates the entry route used by SARS-CoV-2 to infect host cells. The EMBO Journal. 2021;40: e107821. doi:10.15252/embj.2021107821

267. Walls AC, Park Y-J, Tortorici MA, Wall A, McGuire AT, Veesler D. Structure, Function, and Antigenicity of the SARS-CoV-2 Spike Glycoprotein. Cell. 2020;181: 281-292.e6. doi:10.1016/j.cell.2020.02.058

268. Chambers JP, Yu J, Valdes JJ, Arulanandam BP. SARS-CoV-2, Early Entry Events. Franciosa G, editor. Journal of Pathogens. 2020;2020: 1–11. doi:10.1155/2020/9238696

269. Rajah MM, Bernier A, Buchrieser J, Schwartz O. The Mechanism and Consequences of SARS-CoV-2 Spike-Mediated Fusion and Syncytia Formation. Journal of Molecular Biology. 2022;434: 167280. doi:10.1016/j.jmb.2021.167280

270. Peacock TP, Goldhill DH, Zhou J, Baillon L, Frise R, Swann OC, et al. The furin cleavage site in the SARS-CoV-2 spike protein is required for transmission in ferrets. Nat Microbiol. 2021;6: 899–909. doi:10.1038/s41564-021-00908-w

271. Clausen TM, Sandoval DR, Spliid CB, Pihl J, Perrett HR, Painter CD, et al. SARS-CoV-2 Infection Depends on Cellular Heparan Sulfate and ACE2. Cell. 2020;183: 1043-1057.e15. doi:10.1016/j.cell.2020.09.033

272. Cantuti-Castelvetri L, Ojha R, Pedro LD, Djannatian M, Franz J, Kuivanen S, et al. Neuropilin-1 facilitates SARS-CoV-2 cell entry and infectivity. Science. 2020;370: 856–860. doi:10.1126/science.abd2985

273. Daly JL, Simonetti B, Klein K, Chen K-E, Williamson MK, Antón-Plágaro C, et al. Neuropilin-1 is a host factor for SARS-CoV-2 infection. Science. 2020;370: 861–865. doi:10.1126/science.abd3072

274. Letko M, Marzi A, Munster V. Functional assessment of cell entry and receptor usage for SARS-CoV-2 and other lineage B betacoronaviruses. Nat Microbiol. 2020;5: 562–569. doi:10.1038/s41564-020-0688-y

275. Conceicao C, Thakur N, Human S, Kelly JT, Logan L, Bialy D, et al. The SARS-CoV-2 Spike protein has a broad tropism for mammalian ACE2 proteins. Microbiology; 2020 Jun. doi:10.1101/2020.06.17.156471

276. Yan H, Jiao H, Liu Q, Zhang Z, Wang X, Guo M, et al. Many bat species are not potential hosts of SARS-CoV and SARS-CoV-2: Evidence from ACE2 receptor usage. Ecology; 2020 Sep. doi:10.1101/2020.09.08.284737

277. Damas J, Hughes GM, Keough KC, Painter CA, Persky NS, Corbo M, et al. Broad Host Range of SARS-CoV-2 Predicted by Comparative and Structural Analysis of ACE2 in Vertebrates. Genomics; 2020 Apr. doi:10.1101/2020.04.16.045302

278. Zhou P, Yang X-L, Wang X-G, Hu B, Zhang L, Zhang W, et al. A pneumonia outbreak associated with a new coronavirus of probable bat origin. Nature. 2020;579: 270–273. doi:10.1038/s41586-020-2012-7

279. Liu K, Tan S, Niu S, Wang J, Wu L, Sun H, et al. Cross-species recognition of SARS-CoV-2 to bat ACE2. Proc Natl Acad Sci USA. 2021;118: e2020216118. doi:10.1073/pnas.2020216118

280. Mah MG, Linster M, Low DH, Yan Z, Jayakumar J, Samsudin F, et al. Spike-independent infection of human coronavirus 229E in bat cells. Microbiology; 2021 Sep. doi:10.1101/2021.09.18.460924

281. Jouvenet N, Goujon C, Banerjee A. Clash of the titans: interferons and SARS-CoV-2. Trends in Immunology. 2021;42: 1069–1072. doi:10.1016/j.it.2021.10.009

282. Rebendenne A, Valadão ALC, Tauziet M, Maarifi G, Bonaventure B, McKellar J, et al. SARS-CoV-2 Triggers an MDA-5-Dependent Interferon Response Which Is Unable To Control Replication in Lung Epithelial Cells. Journal of Virology. 2021;95. doi:10.1128/JVI.02415-20

283. Yin X, Riva L, Pu Y, Martin-Sancho L, Kanamune J, Yamamoto Y, et al. MDA5 Governs the Innate Immune Response to SARS-CoV-2 in Lung Epithelial Cells. Cell Rep. 2021;34: 108628. doi:10.1016/j.celrep.2020.108628

284. Blanco-Melo D, Nilsson-Payant BE, Liu W-C, Uhl S, Hoagland D, Møller R, et al. Imbalanced Host Response to SARS-CoV-2 Drives Development of COVID-19. Cell. 2020;181: 1036-1045.e9. doi:10.1016/j.cell.2020.04.026

285. Chu H, Chan JF-W, Wang Y, Yuen TT-T, Chai Y, Hou Y, et al. Comparative Replication and Immune Activation Profiles of SARS-CoV-2 and SARS-CoV in Human Lungs: An Ex Vivo Study With Implications for the Pathogenesis of COVID-19. Clinical Infectious Diseases. 2020;71: 1400–1409. doi:10.1093/cid/ciaa410

286. Banerjee A, El-Sayes N, Budylowski P, Jacob RA, Richard D, Maan H, et al. Experimental and natural evidence of SARS-CoV-2-infection-induced activation of type I interferon responses. iScience. 2021;24: 102477. doi:10.1016/j.isci.2021.102477

287. Stanifer ML, Kee C, Cortese M, Zumaran CM, Triana S, Mukenhirn M, et al. Critical Role of Type III Interferon in Controlling SARS-CoV-2 Infection in Human Intestinal Epithelial Cells. Cell Reports. 2020;32: 107863. doi:10.1016/j.celrep.2020.107863

288. Hadjadj J, Yatim N, Barnabei L, Corneau A, Boussier J, Smith N, et al. Impaired type I interferon activity and inflammatory responses in severe COVID-19 patients. Science. 2020;369: 718–724. doi:10.1126/science.abc6027

289. Ribero MS, Jouvenet N, Dreux M, Nisole S. Interplay between SARS-CoV-2 and the type I interferon response. PLOS Pathogens. 2020;16: e1008737. doi:10.1371/journal.ppat.1008737

290. Martin-Sancho L, Lewinski MK, Pache L, Stoneham CA, Yin X, Becker ME, et al. Functional landscape of SARS-CoV-2 cellular restriction. Molecular Cell. 2021;81: 2656-2668.e8. doi:10.1016/j.molcel.2021.04.008

291. Wickenhagen A, Sugrue E, Lytras S, Kuchi S, Noerenberg M, Turnbull Matthew L, et al. A prenylated dsRNA sensor protects against severe COVID-19. Science. 0: eabj3624. doi:10.1126/science.abj3624

292. Shi G, Kenney AD, Kudryashova E, Zani A, Zhang L, Lai KK, et al. Opposing activities of IFITM proteins in SARS-CoV-2 infection. EMBO J. 2021;40. doi:10.15252/embj.2020106501

293. Zang R, Case JB, Yutuc E, Ma X, Shen S, Gomez Castro MF, et al. Cholesterol 25-hydroxylase suppresses SARS-CoV-2 replication by blocking membrane fusion. Proc Natl Acad Sci USA. 2020;117: 32105–32113. doi:10.1073/pnas.2012197117

294. Lowery SA, Sariol A, Perlman S. Innate immune and inflammatory responses to SARS-CoV-2: Implications for COVID-19. Cell Host & Microbe. 2021;29: 1052–1062. doi:10.1016/j.chom.2021.05.004

295. Bouayad A. Innate immune evasion by SARS-CoV -2: Comparison with SARS-CoV. Rev Med Virol. 2020;30: 1–9. doi:10.1002/rmv.2135

296. Wu J, Shi Y, Pan X, Wu S, Hou R, Zhang Y, et al. SARS-CoV-2 ORF9b inhibits RIG-I-MAVS antiviral signaling by interrupting K63-linked ubiquitination of NEMO. Cell Reports. 2021;34: 108761. doi:10.1016/j.celrep.2021.108761

297. Kumar A, Ishida R, Strilets T, Cole J, Lopez-Orozco J, Fayad N, et al. SARS-CoV-2 Nonstructural Protein 1 Inhibits the Interferon Response by Causing Depletion of Key Host Signaling Factors. Gallagher T, editor. J Virol. 2021;95: e00266-21. doi:10.1128/JVI.00266-21

298. Liu Y, Qin C, Rao Y, Ngo C, Feng JJ, Zhao J, et al. SARS-CoV-2 Nsp5 Demonstrates Two Distinct Mechanisms Targeting RIG-I and MAVS To Evade the Innate Immune Response. Zheng C, editor. mBio. 2021;12: e02335-21. doi:10.1128/mBio.02335-21

299. Rui Y, Su J, Shen S, Hu Y, Huang D, Zheng W, et al. Unique and complementary suppression of cGAS-STING and RNA sensing- triggered innate immune responses by SARS-CoV-2 proteins. Sig Transduct Target Ther. 2021;6: 123. doi:10.1038/s41392-021-00515-5

300. Kimura I, Konno Y, Uriu K, Hopfensperger K, Sauter D, Nakagawa S, et al. Sarbecovirus ORF6 proteins hamper induction of interferon signaling. Cell Reports. 2021;34: 108916. doi:10.1016/j.celrep.2021.108916

301. Konno Y, Kimura I, Uriu K, Fukushi M, Irie T, Koyanagi Y, et al. SARS-CoV-2 ORF3b Is a Potent Interferon Antagonist Whose Activity Is Increased by a Naturally Occurring Elongation Variant. Cell Reports. 2020;32: 108185. doi:10.1016/j.celrep.2020.108185

302. Aicher S-M, Streicher F, Chazal M, Planas D, Luo D, Buchrieser J, et al. Species-Specific Molecular Barriers to SARS-CoV-2 Replication in Bat Cells. Heise MT, editor. J Virol. 2022;96: e00608-22. doi:10.1128/jvi.00608-22

303. Banerjee A, Misra V, Schountz T, Baker ML. Tools to study pathogen-host interactions in bats. Virus Research. 2018;248: 5–12. doi:10.1016/j.virusres.2018.02.013

304. Damas J, Hughes GM, Keough KC, Painter CA, Persky NS, Corbo M, et al. Broad Host Range of SARS-CoV-2 Predicted by Comparative and Structural Analysis of ACE2 in Vertebrates. Genomics; 2020 Apr. doi:10.1101/2020.04.16.045302

305. Liu K, Tan S, Niu S, Wang J, Wu L, Sun H, et al. Cross-species recognition of SARS-CoV-2 to bat ACE2. Proc Natl Acad Sci U S A. 2021;118. doi:10.1073/pnas.2020216118

306. Conceicao C, Thakur N, Human S, Kelly JT, Logan L, Bialy D, et al. The SARS-CoV-2 Spike protein has a broad tropism for mammalian ACE2 proteins. PLOS Biology. 2020;18: e3001016. doi:10.1371/journal.pbio.3001016

307. Chu H, Chan JF-W, Yuen TT-T, Shuai H, Yuan S, Wang Y, et al. Comparative tropism, replication kinetics, and cell damage profiling of SARS-CoV-2 and SARS-CoV with implications for clinical manifestations, transmissibility, and laboratory studies of COVID-19: an observational study. The Lancet Microbe. 2020;1: e14–e23. doi:10.1016/S2666-5247(20)30004-5

308. Harcourt J, Tamin A, Lu X, Kamili S, Sakthivel SK, Murray J, et al. Severe Acute Respiratory Syndrome Coronavirus 2 from Patient with Coronavirus Disease, United States. Emerg Infect Dis. 2020;26: 1266–1273. doi:10.3201/eid2606.200516

309. Lau SKP, Wong ACP, Luk HKH, Li KSM, Fung J, He Z, et al. Early Release - Differential Tropism of SARS-CoV and SARS-CoV-2 in Bat Cells - Volume 26, Number 12—December 2020 - Emerging Infectious Diseases journal - CDC. [cited 17 Sep 2020]. doi:10.3201/eid2612.202308

310. Zhou J, Li C, Liu X, Chiu MC, Zhao X, Wang D, et al. Infection of bat and human intestinal organoids by SARS-CoV-2. Nat Med. 2020;26: 1077–1083. doi:10.1038/s41591-020-0912-6

311. Schlottau K, Rissmann M, Graaf A, Schön J, Sehl J, Wylezich C, et al. SARS-CoV-2 in fruit bats, ferrets, pigs, and chickens: an experimental transmission study. The Lancet Microbe. 2020;1: e218–e225. doi:10.1016/S2666-5247(20)30089-6

312. Yohe LR, Devanna P, Davies KTJ, Potter JHT, Rossiter SJ, Teeling EC, et al. Tissue Collection of Bats for -Omics Analyses and Primary Cell Culture. J Vis Exp. 2019. doi:10.3791/59505

313. Aurine N, Baquerre C, Gaudino M, Jean C, Dumont C, Rival-Gervier S, et al. Reprogrammed Pteropus Bat Stem Cells Present Distinct Immune Signature and are Highly Permissive for Henipaviruses. bioRxiv. 2019; 846410. doi:10.1101/846410

314. He X, Korytář T, Zhu Y, Pikula J, Bandouchova H, Zukal J, et al. Establishment of Myotis myotis Cell Lines - Model for Investigation of Host-Pathogen Interaction in a Natural Host for Emerging Viruses. PLOS ONE. 2014;9: e109795. doi:10.1371/journal.pone.0109795

315. Pikula J, Bandouchova H, Kovacova V, Linhart P, Piacek V, Zukal J. Reproduction of Rescued Vespertilionid Bats (Nyctalus noctula) in Captivity: Veterinary and Physiologic Aspects. Vet Clin North Am Exot Anim Pract. 2017;20: 665–677. doi:10.1016/j.cvex.2016.11.013

316. Buchrieser J, Dufloo J, Hubert M, Monel B, Planas D, Rajah MM, et al. Syncytia formation by SARS-CoV-2-infected cells. EMBO J. 2021;40: e107405. doi:10.15252/embj.2020107405

317. Ramakrishnan MA. Determination of 50% endpoint titer using a simple formula. World J Virol. 2016;5: 85–86. doi:10.5501/wjv.v5.i2.85

318. Hoffmann M, Wu Y-J, Gerber M, Berger-Rentsch M, Heimrich B, Schwemmle M, et al. Fusion-active glycoprotein G mediates the cytotoxicity of vesicular stomatitis virus M mutants lacking host shut-off activity. J Gen Virol. 2010;91: 2782–2793. doi:10.1099/vir.0.023978-0

319. Cramer J, Lakkaichi A, Aliu B, Jakob RP, Klein S, Cattaneo I, et al. Sweet Drugs for Bad Bugs: A Glycomimetic Strategy against the DC-SIGN-Mediated Dissemination of SARS-CoV-2. J Am Chem Soc. 2021;143: 17465–17478. doi:10.1021/jacs.1c06778

320. Ruiz-Aravena M, McKee C, Gamble A, Lunn T, Morris A, Snedden CE, et al. Ecology, evolution and spillover of coronaviruses from bats. Nat Rev Microbiol. 2021; 1–16. doi:10.1038/s41579-021-00652-2

321. Dominguez SR, O'Shea TJ, Oko LM, Holmes KV. Detection of Group 1 Coronaviruses in Bats in North America. Emerg Infect Dis. 2007;13: 1295–1300. doi:10.3201/eid1309.070491

322. Mendenhall IH, Kerimbayev AA, Strochkov VM, Sultankulova KT, Kopeyev SK, Su YCF, et al. Discovery and Characterization of Novel Bat Coronavirus Lineages from Kazakhstan. Viruses. 2019;11. doi:10.3390/v11040356

323. Ogando NS, Dalebout TJ, Zevenhoven-Dobbe JC, Limpens RWAL, van der Meer Y, Caly L, et al. SARS-coronavirus-2 replication in Vero E6 cells: replication kinetics, rapid adaptation and cytopathology. J Gen Virol. 2020;101: 925–940. doi:10.1099/jgv.0.001453

324. Richter M, Reimann I, Schirrmeier H, Kirkland PD, Beer M. The viral envelope is not sufficient to transfer the unique broad cell tropism of Bungowannah virus to a related pestivirus. Journal of General Virology,. 2014;95: 2216–2222. doi:10.1099/vir.0.065995-0

325. Puelles VG, Lütgehetmann M, Lindenmeyer MT, Sperhake JP, Wong MN, Allweiss L, et al. Multiorgan and Renal Tropism of SARS-CoV-2. New England Journal of Medicine. 2020;383: 590–592. doi:10.1056/NEJMc2011400

326. Onabajo OO, Banday AR, Stanifer ML, Yan W, Obajemu A, Santer DM, et al. Interferons and viruses induce a novel truncated ACE2 isoform and not the full-length SARS-CoV-2 receptor. Nature Genetics. 2020;52: 1283–1293. doi:10.1038/s41588-020-00731-9

327. Allen JD, Watanabe Y, Chawla H, Newby ML, Crispin M. Subtle Influence of ACE2 Glycan Processing on SARS-CoV-2 Recognition. Journal of Molecular Biology. 2021;433: 166762. doi:10.1016/j.jmb.2020.166762

328. Zhang Q, Chen CZ, Swaroop M, Xu M, Wang L, Lee J, et al. Heparan sulfate assists SARS-CoV-2 in cell entry and can be targeted by approved drugs in vitro. Cell Discovery. 2020;6: 1–14. doi:10.1038/s41421-020-00222-5

329. Cao Y, Xu X, Kitanovski S, Song L, Wang J, Hao P, et al. Comprehensive Comparison of RNA-Seq Data of SARS-CoV-2, SARS-CoV and MERS-CoV Infections: Alternative Entry Routes and Innate Immune Responses. Front Immunol. 2021;12: 656433. doi:10.3389/fimmu.2021.656433

330. Eymieux S, Rouillé Y, Terrier O, Seron K, Blanchard E, Rosa-Calatrava M, et al. Ultrastructural modifications induced by SARS-CoV-2 in Vero cells: a kinetic analysis of viral factory formation, viral particle morphogenesis and virion release. Cell Mol Life Sci. 2021;78: 3565–3576. doi:10.1007/s00018-020-03745-y

331. Cortese M, Lee J-Y, Cerikan B, Neufeldt CJ, Oorschot VMJ, Köhrer S, et al. Integrative Imaging Reveals SARS-CoV-2-Induced Reshaping of Subcellular Morphologies. Cell Host & Microbe. 2020;28: 853-866.e5. doi:10.1016/j.chom.2020.11.003

332. Martin-Sancho L, Lewinski MK, Pache L, Stoneham CA, Yin X, Becker ME, et al. Functional landscape of SARS-CoV-2 cellular restriction. Mol Cell. 2021;81: 2656-2668.e8. doi:10.1016/j.molcel.2021.04.008

333. Zhou S, Butler-Laporte G, Nakanishi T, Morrison DR, Afilalo J, Afilalo M, et al. A Neanderthal OAS1 isoform protects individuals of European ancestry against COVID-19 susceptibility and severity. Nature Medicine. 2021;27: 659–667. doi:10.1038/s41591-021-01281-1

334. Blanco-Melo D, Nilsson-Payant BE, Liu W-C, Uhl S, Hoagland D, Møller R, et al. Imbalanced Host Response to SARS-CoV-2 Drives Development of COVID-19. Cell. 2020;181: 1036-1045.e9. doi:10.1016/j.cell.2020.04.026

335. Temmam S, Vongphayloth K, Baquero E, Munier S, Bonomi M, Regnault B, et al. Bat coronaviruses related to SARS-CoV-2 and infectious for human cells. Nature. 2022;604: 330–336. doi:10.1038/s41586-022-04532-4

336. Ren L, Wu C, Guo L, Yao J, Wang C, Xiao Y, et al. Single-cell transcriptional atlas of the Chinese horseshoe bat (*Rhinolophus sinicus*) provides insight into the cellular mechanisms which enable bats to be viral reservoirs. Cell Biology; 2020 Jun. doi:10.1101/2020.06.30.175778

337. Straková P, Dufkova L, Širmarová J, Salát J, Bartonička T, Klempa B, et al. Novel hantavirus identified in European bat species Nyctalus noctula. Infect Genet Evol. 2017;48: 127–130. doi:10.1016/j.meegid.2016.12.025

338. Kurth A, Kohl C, Brinkmann A, Ebinger A, Harper JA, Wang L-F, et al. Novel Paramyxoviruses in Free-Ranging European Bats. PLoS One. 2012;7. doi:10.1371/journal.pone.0038688

339. Hikmet F, Méar L, Edvinsson Å, Micke P, Uhlén M, Lindskog C. The protein expression profile of ACE2 in human tissues. Molecular Systems Biology. 2020;16: e9610. doi:10.15252/msb.20209610

340. Yan H, Jiao H, Liu Q, Zhang Z, Xiong Q, Wang B-J, et al. ACE2 receptor usage reveals variation in susceptibility to SARS-CoV and SARS-CoV-2 infection among bat species. Nature Ecology & Evolution. 2021; 1–9. doi:10.1038/s41559-021-01407-1

341. Puray-Chavez M, LaPak KM, Schrank TP, Elliott JL, Bhatt DP, Agajanian MJ, et al. Systematic analysis of SARS-CoV-2 infection of an ACE2-negative human airway cell. Cell Reports. 2021;36: 109364. doi:10.1016/j.celrep.2021.109364

342. Hayward JA, Tachedjian M, Johnson A, Irving AT, Gordon TB, Cui J, et al. Unique Evolution of Antiviral Tetherin in Bats. 2020 Nov p. 2020.04.08.031203. doi:10.1101/2020.04.08.031203

343. Cifuentes-Muñoz N, Dutch RE, Cattaneo R. Direct cell-to-cell transmission of respiratory viruses: The fast lanes. PLOS Pathogens. 2018;14: e1007015. doi:10.1371/journal.ppat.1007015

344. Qian Z, Dominguez SR, Holmes KV. Role of the Spike Glycoprotein of Human Middle East Respiratory Syndrome Coronavirus (MERS-CoV) in Virus Entry and Syncytia Formation. PLOS ONE. 2013;8: e76469. doi:10.1371/journal.pone.0076469

345. Bussani R, Schneider E, Zentilin L, Collesi C, Ali H, Braga L, et al. Persistence of viral RNA, pneumocyte syncytia and thrombosis are hallmarks of advanced COVID-19 pathology. EBioMedicine. 2020;61: 103104. doi:10.1016/j.ebiom.2020.103104

346. Hayn M, Hirschenberger M, Koepke L, Nchioua R, Straub JH, Klute S, et al. Systematic Functional Analysis of SARS-CoV-2 Proteins Uncovers Viral Innate Immune Antagonists and Remaining Vulnerabilities. Cell Reports. 2021; 109126. doi:10.1016/j.celrep.2021.109126

347. Stukalov A, Girault V, Grass V, Karayel O, Bergant V, Urban C, et al. Multilevel proteomics reveals host perturbations by SARS-CoV-2 and SARS-CoV. Nature. 2021. doi:10.1038/s41586-021-03493-4

348. Banerjee A, Falzarano D, Rapin N, Lew J, Misra V. Interferon Regulatory Factor 3-Mediated Signaling Limits Middle-East Respiratory Syndrome (MERS) Coronavirus Propagation in Cells from an Insectivorous Bat. Viruses. 2019;11. doi:10.3390/v11020152

349. Hall JS, Knowles S, Nashold SW, Ip HS, Leon AE, Rocke T, et al. Experimental challenge of a North American bat species, big brown bat (Eptesicus fuscus), with SARS-CoV-2. Transboundary and Emerging Diseases. n/a. doi:https://doi.org/10.1111/tbed.13949

350. De La Cruz-Rivera PC, Kanchwala M, Liang H, Kumar A, Wang L-F, Xing C, et al. The IFN Response in Bats Displays Distinctive IFN-Stimulated Gene Expression Kinetics with Atypical RNASEL Induction. JI. 2018;200: 209–217. doi:10.4049/jimmunol.1701214

351. Zhou P, Tachedjian M, Wynne JW, Boyd V, Cui J, Smith I, et al. Contraction of the type I IFN locus and unusual constitutive expression of IFN-α in bats. PNAS. 2016;113: 2696–2701. doi:10.1073/pnas.1518240113

352. Bondet V, Le Baut M, Le Poder S, Lécu A, Petit T, Wedlarski R, et al. Constitutive IFNα Protein Production in Bats. Frontiers in Immunology. 2021;12. Available: https://www.frontiersin.org/article/10.3389/fimmu.2021.735866

353. Zhou P, Cowled C, Mansell A, Monaghan P, Green D, Wu L, et al. IRF7 in the Australian Black Flying Fox, Pteropus alecto: Evidence for a Unique Expression Pattern and Functional Conservation. Fugmann SD, editor. PLoS ONE. 2014;9: e103875. doi:10.1371/journal.pone.0103875

354. Glennon NB, Jabado O, Lo MK, Shaw ML. Transcriptome Profiling of the Virus-Induced Innate Immune Response in Pteropus vampyrus and Its Attenuation by Nipah Virus Interferon Antagonist Functions. Journal of Virology. 2015;89: 17.

355. Hall J, Hofmeister E, Ip H, Nashold S, Leon A, Malavé C, et al. Experimental infection of Mexican free-tailed bats (*Tadarida brasiliensis)* with SARS-CoV-2. Pathology; 2022 Jul. doi:10.1101/2022.07.18.500430

356. Lau SKP, Fan RYY, Luk HKH, Zhu L, Fung J, Li KSM, et al. Replication of MERS and SARS coronaviruses in bat cells offers insights to their ancestral origins. Emerging Microbes & Infections. 2018;7: 1–11. doi:10.1038/s41426-018-0208-9

357. Hoffmann M, Müller MA, Drexler JF, Glende J, Erdt M, Gützkow T, et al. Differential Sensitivity of Bat Cells to Infection by Enveloped RNA Viruses: Coronaviruses, Paramyxoviruses, Filoviruses, and Influenza Viruses. Thiel V, editor. PLoS ONE. 2013;8: e72942. doi:10.1371/journal.pone.0072942

358. Lau SKP, Wong ACP, Luk HKH, Li KSM, Fung J, He Z, et al. Early Release - Differential Tropism of SARS-CoV and SARS-CoV-2 in Bat Cells - Volume 26, Number 12—December 2020 - Emerging Infectious Diseases journal - CDC. [cited 17 Sep 2020]. doi:10.3201/eid2612.202308

359. Auerswald H, Low DHW, Siegers JY, Ou T, Kol S, In S, et al. A Look inside the Replication Dynamics of SARS-CoV-2 in Blyth's Horseshoe Bat (*Rhinolophus lepidus*) Kidney Cells. Rajao DS, editor. Microbiol Spectr. 2022;10: e00449-22. doi:10.1128/spectrum.00449-22

360. Murakami S, Kitamura T, Matsugo H, Kamiki H, Oyabu K, Sekine W, et al. Isolation of bat sarbecoviruses of SARS-CoV-2 clade, Japan. Microbiology; 2022 May. doi:10.1101/2022.05.16.492045

361. Khaledian E, Ulusan S, Erickson J, Fawcett S, Letko MC, Broschat SL. Sequence determinants of human-cell entry identified in ACE2-independent bat sarbecoviruses: A combined laboratory and computational network science approach. eBioMedicine. 2022;79: 103990. doi:10.1016/j.ebiom.2022.103990

362. Frolova EI, Palchevska O, Lukash T, Dominguez F, Britt W, Frolov I. Acquisition of Furin Cleavage Site and Further SARS-CoV-2 Evolution Change the Mechanisms of Viral Entry, Infection Spread, and Cell Signaling. Gallagher T, editor. J Virol. 2022;96: e00753-22. doi:10.1128/jvi.00753-22

363. Zhou J, Li C, Liu X, Chiu MC, Zhao X, Wang D, et al. Infection of bat and human intestinal organoids by SARS-CoV-2. Nat Med. 2020;26: 1077–1083. doi:10.1038/s41591-020-0912-6

364. Keusch GT, Amuasi JH, Anderson DE, Daszak P, Eckerle I, Field H, et al. Pandemic origins and a One Health approach to preparedness and prevention: Solutions based on SARS-CoV-2 and other RNA viruses. Proceedings of the National Academy of Sciences. 2022;119: e2202871119. doi:10.1073/pnas.2202871119

365. Ahn M, Cui J, Irving AT, Wang L-F. Unique Loss of the PYHIN Gene Family in Bats Amongst Mammals: Implications for Inflammasome Sensing. Sci Rep. 2016;6: 21722. doi:10.1038/srep21722

366. Mougari S, Gonzalez C, Reynard O, Horvat B. Fruit bats as natural reservoir of highly pathogenic henipaviruses: balance between antiviral defense and viral tolerance. Current Opinion in Virology. 2022;54: 101228. doi:10.1016/j.coviro.2022.101228

367. Banerjee A, Rapin N, Miller M, Griebel P, Zhou Y, Munster V, et al. Generation and Characterization of Eptesicus fuscus (Big brown bat) kidney cell lines immortalized using the Myotis polyomavirus large T-antigen. Journal of Virological Methods. 2016;237: 166–173. doi:10.1016/j.jviromet.2016.09.008

368. Papies J, Sieberg A, Ritz D, Niemeyer D, Drosten C, Müller MA. Reduced IFN-ß inhibitory activity of Lagos bat virus phosphoproteins in human compared to Eidolon helvum bat cells. Xing Z, editor. PLoS ONE. 2022;17: e0264450. doi:10.1371/journal.pone.0264450

369. Cokelaer T, Desvillechabrol D, Legendre R, Cardon M. "Sequana": a Set of Snakemake NGS pipelines. JOSS. 2017;2: 352. doi:10.21105/joss.00352

370. Koster J, Rahmann S. Snakemake--a scalable bioinformatics workflow engine. Bioinformatics. 2012;28: 2520–2522. doi:10.1093/bioinformatics/bts480

371. Langmead B. Aligning Short Sequencing Reads with Bowtie. Curr Protoc Bioinform. 2010;32. doi:10.1002/0471250953.bi1107s32

372. Chen S, Zhou Y, Chen Y, Gu J. fastp: an ultra-fast all-in-one FASTQ preprocessor. Bioinformatics. 2018;34: i884–i890. doi:10.1093/bioinformatics/bty560

373. Dobin A, Davis CA, Schlesinger F, Drenkow J, Zaleski C, Jha S, et al. STAR: ultrafast universal RNA-seq aligner. Bioinformatics. 2013;29: 15–21. doi:10.1093/bioinformatics/bts635

374. Liao Y, Smyth GK, Shi W. featureCounts: an efficient general purpose program for assigning sequence reads to genomic features. Bioinformatics. 2014;30: 923–930. doi:10.1093/bioinformatics/btt656

375. Ewels P, Magnusson M, Lundin S, Käller M. MultiQC: summarize analysis results for multiple tools and samples in a single report. Bioinformatics. 2016;32: 3047–3048. doi:10.1093/bioinformatics/btw354

376. Love MI, Huber W, Anders S. Moderated estimation of fold change and dispersion for RNA-seq data with DESeq2. Genome Biol. 2014;15: 550. doi:10.1186/s13059-014-0550-8

377. Emms DM, Kelly S. OrthoFinder: phylogenetic orthology inference for comparative genomics. Genome Biol. 2019;20: 238. doi:10.1186/s13059-019-1832-y

378. Bindea G, Mlecnik B, Hackl H, Charoentong P, Tosolini M, Kirilovsky A, et al. ClueGO: a Cytoscape plug-in to decipher functionally grouped gene ontology and pathway annotation networks. Bioinformatics. 2009;25: 1091–1093. doi:10.1093/bioinformatics/btp101

379. Bindea G, Galon J, Mlecnik B. CluePedia Cytoscape plugin: pathway insights using integrated experimental and in silico data. Bioinformatics. 2013;29: 661–663. doi:10.1093/bioinformatics/btt019

380. Shannon P, Markiel A, Ozier O, Baliga NS, Wang JT, Ramage D, et al. Cytoscape: A Software Environment for Integrated Models of Biomolecular Interaction Networks. Genome Res. 2003;13: 2498–2504. doi:10.1101/gr.1239303

381. Banerjee A, Zhang X, Yip A, Schulz KS, Irving AT, Bowdish D, et al. Positive Selection of a Serine Residue in Bat IRF3 Confers Enhanced Antiviral Protection. iScience. 2020;23: 100958. doi:10.1016/j.isci.2020.100958

382. Conesa A, Madrigal P, Tarazona S, Gomez-Cabrero D, Cervera A, McPherson A, et al. A survey of best practices for RNA-seq data analysis. Genome Biol. 2016;17: 13. doi:10.1186/s13059-016-0881-8

383. Schoggins JW, Wilson SJ, Panis M, Murphy MY, Jones CT, Bieniasz P, et al. A diverse range of gene products are effectors of the type I interferon antiviral response. Nature. 2011;472: 481–485. doi:10.1038/nature09907

384. OhAinle M, Helms L, Vermeire J, Roesch F, Humes D, Basom R, et al. A virus-packageable CRISPR screen identifies host factors mediating interferon inhibition of HIV. eLife. 2018;7: e39823. doi:10.7554/eLife.39823

385. Sebastian Vik E, Sameen Nawaz M, Strøm Andersen P, Fladeby C, Bjørås M, Dalhus B, et al. Endonuclease V cleaves at inosines in RNA. Nat Commun. 2013;4: 2271. doi:10.1038/ncomms3271

386. Cruz-Rivera PCDL, Kanchwala M, Liang H, Kumar A, Wang L-F, Xing C, et al. The IFN Response in Bats Displays Distinctive IFN-Stimulated Gene Expression Kinetics with Atypical RNASEL Induction. The Journal of Immunology. 2018;200: 209–217. doi:10.4049/jimmunol.1701214

387. Zhang Q, Zeng L-P, Zhou P, Irving AT, Li S, Shi Z-L, et al. IFNAR2-dependent gene expression profile induced by IFN-α in Pteropus alecto bat cells and impact of IFNAR2 knockout on virus infection. Meurs EF, editor. PLoS ONE. 2017;12: e0182866. doi:10.1371/journal.pone.0182866

388. Ashley C, Abendroth A, McSharry B, Slobedman B. Interferon-Independent Upregulation of Interferon-Stimulated Genes during Human Cytomegalovirus Infection is Dependent on IRF3 Expression. Viruses. 2019;11: 246. doi:10.3390/v11030246

389. Palchetti S, Starace D, De Cesaris P, Filippini A, Ziparo E, Riccioli A. Transfected Poly(I:C) Activates Different dsRNA Receptors, Leading to Apoptosis or Immunoadjuvant Response in Androgen-independent Prostate Cancer Cells. Journal of Biological Chemistry. 2015;290: 5470–5483. doi:10.1074/jbc.M114.601625

390. Zhao G-N, Zhang P, Gong J, Zhang X-J, Wang P-X, Yin M, et al. Tmbim1 is a multivesicular body regulator that protects against non-alcoholic fatty liver disease in mice and monkeys by targeting the lysosomal degradation of Tlr4. Nat Med. 2017;23: 742–752. doi:10.1038/nm.4334

391. Zhang VX, Sze KM-F, Chan L-K, Ho DW-H, Tsui Y-M, Chiu Y-T, et al. Antioxidant supplements promote tumor formation and growth and confer drug resistance in hepatocellular carcinoma by reducing intracellular ROS and induction of TMBIM1. Cell Biosci. 2021;11: 217. doi:10.1186/s13578-021-00731-0

392. Feng J, Zhu F, Ye D, Zhang Q, Guo X, Du C, et al. Sin3a drives mesenchymal-to-epithelial transition through cooperating with Tet1 in somatic cell reprogramming. Stem Cell Res Ther. 2022;13: 29. doi:10.1186/s13287-022-02707-4

393. Bridi M, Schoch H, Florian C, Poplawski SG, Banerjee A, Hawk JD, et al. Transcriptional corepressor SIN3A regulates hippocampal synaptic plasticity via Homer1/mGluR5 signaling. JCI Insight. 2020;5: e92385. doi:10.1172/jci.insight.92385

394. Petry B, Moreira GCM, Copola AGL, Souza MM de, da Veiga FC, Jorge EC, et al. SAP30 Gene Is a Probable Regulator of Muscle Hypertrophy in Chickens. Front Genet. 2021;12: 709937. doi:10.3389/fgene.2021.709937

395. Qiu J, Li M, Su C, Liang Y, Ou R, Chen X, et al. FOXS1 Promotes Tumor Progression by Upregulating CXCL8 in Colorectal Cancer. Front Oncol. 2022;12: 894043. doi:10.3389/fonc.2022.894043

396. Liu Y, Tu M, Wang L. Pan-Cancer Analysis Predicts FOXS1 as a Key Target in Prognosis and Tumor Immunotherapy. IJGM. 2022;Volume 15: 2171–2185. doi:10.2147/IJGM.S354195

397. Wautier J-L, Wautier M-P. Cellular and Molecular Aspects of Blood Cell–Endothelium Interactions in Vascular Disorders. IJMS. 2020;21: 5315. doi:10.3390/ijms21155315

398. Grive KJ, Gustafson EA, Seymour KA, Baddoo M, Schorl C, Golnoski K, et al. TAF4b Regulates Oocyte-Specific Genes Essential for Meiosis. Barsh GS, editor. PLoS Genet. 2016;12: e1006128. doi:10.1371/journal.pgen.1006128

399. Lovasco LA, Gustafson EA, Seymour KA, Rooij DG, Freiman RN. TAF4b is Required for Mouse Spermatogonial Stem Cell Development. Stem Cells. 2015;33: 1267–1276. doi:10.1002/stem.1914

400. Koteluk O, Bielicka A, Lemańska Ż, Jóźwiak K, Klawiter W, Mackiewicz A, et al. The Landscape of Transmembrane Protein Family Members in Head and Neck Cancers: Their Biological Role and Diagnostic Utility. Cancers. 2021;13: 4737. doi:10.3390/cancers13194737

401. Hiraoka M, Takashima S, Wakihara Y, Kamatari YO, Shimizu K, Okada A, et al. Identification of Potential mRNA Biomarkers in Milk Small Extracellular Vesicles of Enzootic Bovine Leukosis Cattle. Viruses. 2022;14: 1022. doi:10.3390/v14051022

402. Phillips IR, Shephard EA. Drug metabolism by flavin-containing monooxygenases of human and mouse. Expert Opinion on Drug Metabolism & Toxicology. 2017;13: 167–181. doi:10.1080/17425255.2017.1239718

403. Fladeby C, Vik ES, Laerdahl JK, Gran Neurauter C, Heggelund JE, Thorgaard E, et al. The Human Homolog of Escherichia coli Endonuclease V Is a Nucleolar Protein with Affinity for Branched DNA Structures. Zhou Z, editor. PLoS ONE. 2012;7: e47466. doi:10.1371/journal.pone.0047466

404. Luis AD, Hayman DTS, O'Shea TJ, Cryan PM, Gilbert AT, Pulliam JRC, et al. A comparison of bats and rodents as reservoirs of zoonotic viruses: are bats special? Proc R Soc B. 2013;280: 20122753. doi:10.1098/rspb.2012.2753

405. Guethlein LA, Norman PJ, Hilton HG, Parham P. Co-evolution of MHC class I and variable NK cell receptors in placental mammals. Immunol Rev. 2015;267: 259–282. doi:10.1111/imr.12326

406. Anderson DE, Cui J, Ye Q, Huang B, Tan Y, Jiang C, et al. Orthogonal genome-wide screens of bat cells identify MTHFD1 as a target of broad antiviral therapy. Proc Natl Acad Sci USA. 2021;118: e2104759118. doi:10.1073/pnas.2104759118

407. Zhou P, Chionh YT, Irac SE, Ahn M, Jia Ng JH, Fossum E, et al. Unlocking bat immunology: establishment of Pteropus alecto bone marrow-derived dendritic cells and macrophages. Sci Rep. 2016;6: 38597. doi:10.1038/srep38597

408. Miller MR, McMinn RJ, Misra V, Schountz T, Müller MA, Kurth A, et al. Broad and Temperature Independent Replication Potential of Filoviruses on Cells Derived From Old and New World Bat Species. J Infect Dis. 2016;214: S297–S302. doi:10.1093/infdis/jiw199

409. Schountz T, Baker ML, Butler J, Munster V. Immunological Control of Viral Infections in Bats and the Emergence of Viruses Highly Pathogenic to Humans. Front Immunol. 2017;8: 1098. doi:10.3389/fimmu.2017.01098

410. Brook CE, Boots M, Chandran K, Dobson AP, Drosten C, Graham AL, et al. Accelerated viral dynamics in bat cell lines, with implications for zoonotic emergence. eLife. 2020;9: e48401. doi:10.7554/eLife.48401

411. Fehervari Z. Bat adaptive immunity. Nat Immunol. 2019;20: 1414–1414. doi:10.1038/s41590-019-0533-8

412. Chakraborty AK, Chakravarty AK. Antibody-mediated immune response in the bat, Pteropusgiganteus. Developmental & Comparative Immunology. 1984;8: 415–423. doi:10.1016/0145-305X(84)90048-X

413. Bratsch S, Wertz N, Chaloner K, Kunz TH, Butler JE. The little brown bat, M. lucifugus, displays a highly diverse VH, DH and JH repertoire but little evidence of somatic hypermutation. Developmental & Comparative Immunology. 2011;35: 421–430. doi:10.1016/j.dci.2010.06.004

414. Friedrichs V, Toussaint C, Schäfer A, Rissmann M, Dietrich O, Mettenleiter TC, et al. Landscape and age dynamics of immune cells in the Egyptian rousette bat. Cell Reports. 2022;40: 111305. doi:10.1016/j.celrep.2022.111305

Publications

1) **Aicher SM**, Streicher F, Chazal M, Planas D, Luo D, Buchrieser J, Nemcova M, Seidlova V, Zukal J, Serra-Cobo J, Pontier D, Pain B, Zimmer G, Schwartz O, Roingeard P, Pikula J, Dacheux L, Jouvenet N. Species-Specific Molecular Barriers to SARS-CoV-2 Replication in Bat Cells. J Virol. 2022 Jul 27;96(14):e0060822. doi: 10.1128/jvi.00608-22. Epub 2022 Jul 5. PMID: 35862713; PMCID: PMC9327701.

2) Mac Kain A, Maarifi G, **Aicher SM**, Arhel N, Baidaliuk A, Munier S, Donati F, Vallet T, Tran QD, Hardy A, Chazal M, Porrot F, OhAinle M, Carlson-Stevermer J, Oki J, Holden K, Zimmer G, Simon-Lorière E, Bruel T, Schwartz O, van der Werf S, Jouvenet N, Nisole S, Vignuzzi M, Roesch F. Identification of DAXX as a restriction factor of SARS-CoV-2 through a CRISPR/Cas9 screen. Nat Commun. 2022 May 4;13(1):2442. doi: 10.1038/s41467-022-30134-9. PMID: 35508460; PMCID: PMC9068693.

3) Szachnowski U, Bhargava A, Chazal M, Foretek D, **Aicher SM**, Pipoli da Fonseca J, Jeannin P, Beauclair G, Monot M, Morillon A, Jouvenet N. Transcriptomic landscapes of SARS-CoV-2-infected and bystander lung cells reveal a selective upregulation of NF-κB-dependent coding and non-coding proviral transcripts. *bioRxiv*. 2022 March doi: https://doi.org/10.1101/2022.02.25.481978

Identification of DAXX as a restriction factor of SARS-CoV-2 through a CRISPR/Cas9 screen

Mac Kain A, Maarifi G, **Aicher SM**, Arhel N, Baidaliuk A, Munier S, Donati F, Vallet T, Tran QD, Hardy A, Chazal M, Porrot F, OhAinle M, Carlson-Stevermer J, Oki J, Holden K, Zimmer G, Simon-Lorière E, Bruel T, Schwartz O, van der Werf S, Jouvenet N, Nisole S, Vignuzzi M, Roesch F.

Interferon restricts SARS-CoV-2 replication in cell culture, but only a handful of Interferon Stimulated Genes with antiviral activity against SARS-CoV-2 have been identified. Here, we describe a functional CRISPR/Cas9 screen aiming at identifying SARS-CoV-2 restriction factors. We identify DAXX, a scaffold protein residing in PML nuclear bodies known to limit the replication of DNA viruses and retroviruses, as a potent inhibitor of SARS-CoV-2 and SARS-CoV replication in human cells. Basal expression of DAXX is sufficient to limit the replication of SARS-CoV-2, and DAXX over-expression further restricts infection. DAXX restricts an early, post-entry step of the SARS-CoV-2 life cycle. DAXX-mediated restriction of SARS-CoV-2 is independent of the SUMOylation pathway but dependent on its D/E domain, also necessary for its protein-folding activity. SARS-CoV-2 infection triggers the re-localization of DAXX to cytoplasmic sites and promotes its degradation. Mechanistically, this process is mediated by the viral papain-like protease (PLpro) and the proteasome. Together, these results demonstrate that DAXX restricts SARS-CoV-2, which in turn has evolved a mechanism to counteract its action.

I performed the sorting of SARS-CoV-2 infected A549-ACE2 cells transduced with the ISG CRISPR/Cas9 library (Figure 1). I also assisted with transduced cell expansions, infections and processing for sorting (Figure 1). I performed the experiments with YFV and MeV to evaluate the potential broad-spectrum activity of DAXX against viral infections (Figure 2E). Finally, I performed the VSV-pseudovirus infections and flow cytometry analysis to determine at which step DAXX inhibited SARS-CoV-2 replication (Figures 3A and 3D).

Transcriptomic landscapes of SARS-CoV-2-infected and bystander lung cells reveal a selective upregulation of NF-κB-dependent coding and non-coding proviral transcripts

Szachnowski U, Bhargava A, Chazal M, Foretek D, **Aicher SM**, Pipoli da Fonseca J, Jeannin P, Beauclair G, Monot M, Morillon A, Jouvenet N.

Detailed knowledge of cellular networks that are modulated by Severe acute respiratory syndrome coronavirus 2 (SARS-CoV-2) is needed to understand viral replication and host response. So far, transcriptomic analyses of interactions between SARS-CoV-2 and cells were performed on mixed populations of infected and uninfected cells or using single-cell RNA sequencing, both leading to inaccurate or low-resolution gene expression interpretations. Moreover, they generally focused on annotated messenger RNAs (mRNAs), ignoring other transcripts, such as long non-coding RNAs (lncRNAs) and unannotated RNAs. Here, we performed deep polyA$^+$ transcriptome analyses of lung epithelial A549 cells infected with SARS-CoV-2, which were sorted based on the expression of the viral protein spike (S). To increase the sequencing depth and improve the robustness of the analysis, the samples were depleted of viral transcripts. Infection caused a massive reduction in mRNAs and lncRNAs, including transcripts coding for antiviral innate immune proteins, such as interferons (IFNs). This absence of IFN response probably explains the poor transcriptomic response of bystander cells co-cultured with spike positive (S$^+$) ones. NF-κB and inflammatory response were among the pathways that escaped the global shutoff in S$^+$ cells. In agreement with the RNA-seq analysis, inflammatory cytokines, but not IFNs, were produced and secreted by infected cells. Functional investigations revealed the proviral function of the NFkB subunit p105/p50 and some of its known target genes, including IL32 and IL8, as well as the lncRNA ADIRF-AS1, which we identified as a novel NFkB target gene. Thus, analyzing the polyA$^+$ transcriptome of sorted populations of infected lung cells allowed unprecedented identification of cellular functions that are directly affected by infection and the recovery of coding and non-coding genes that contribute to SARS-CoV-2 replication.

I optimized the RNA extraction protocol from cells fixed with PFA. Subsequently, I performed the initial SARS-CoV-2 infections of A549-ACE2 cells, the cell sorting and RNA extraction for the samples submitted for RNA-Seq analysis (Figure 1).